

## **General Disclaimer**

### **One or more of the Following Statements may affect this Document**

- This document has been reproduced from the best copy furnished by the organizational source. It is being released in the interest of making available as much information as possible.
- This document may contain data, which exceeds the sheet parameters. It was furnished in this condition by the organizational source and is the best copy available.
- This document may contain tone-on-tone or color graphs, charts and/or pictures, which have been reproduced in black and white.
- This document is paginated as submitted by the original source.
- Portions of this document are not fully legible due to the historical nature of some of the material. However, it is the best reproduction available from the original submission.

Final  
Report

NASA CR-

144412

August 1975

**SS/RCS Surface  
Tension Propellant  
Acquisition/  
Expulsion Tankage  
Technology**

(NASA-CR-144412) SS/RCS SURFACE TENSION  
PROPELLANT ACQUISITION/EXPULSION TANKAGE  
TECHNOLOGY Final Report (Martin Marietta  
Corp.) 278 p HC \$8.75

CSCI 22B

N75-30244

G3/18

Unclass  
34309



**MARTIN MARIETTA**



## FOREWORD

---

This document is submitted by Martin Marietta Aerospace, Denver Division, to the National Aeronautics and Space Administration, Lyndon B. Johnson Space Center, in accordance with the reporting requirements of Contract NAS9-13709.

The work was administered under the technical direction of Mr. Dale L. Connelly, NASA-JSC Technical Monitor. Mr. Dale A. Fester, Aerothermal and Propulsion, was the Martin Marietta Program Manager.

The following Martin Marietta personnel made significant contributions to the program:

James R. Tegart	Technical Lead, Tasks I and II
Preston E. Uney	Technical Lead, Tasks III and V
Ashton J. Villars	Technical Lead, Task IV
James D. Carpenter	Computer Program
K. C. Lunden	Similitude Testing, Full-Scale Tankage
E. Robert Wilson	Hardware Design
John S. Marino	Hardware Fabrication

## ABSTRACT

---

A program was conducted to provide the technology and insight needed for the flight hardware reaction control system (RCS) tankage program. The specific objective was to analyze, design, fabricate, and test surface tension propellant tankage that satisfies the requirements of the Space Shuttle/RCS (SS/RCS). This mission presents very stringent and sometimes conflicting requirements that include high-g boost with off-loaded tanks, gas-free propellant outflow with high expulsion efficiency for both low-g on-orbit conditions and high-g reentry conditions, maximum outflow during high-g boost abort, starting reentry with full aft tanks, 100-mission life, and simple servicing and checkout either on or off the orbiter.

A compartmented-tank device was developed for this application and various ground and drop tower test techniques were employed to verify the design using both subscale and full-scale hardware. Performance was established with 1/3-scale hardware and further substantiation was obtained with the full-scale tankage. Fabrication, acceptance, fill and drain, inspection, and other ground handling procedures were developed.

## CONTENTS

---

	<u>Page</u>
I. INTRODUCTION . . . . .	I-1 thru I-5
II. DESIGN CRITERIA . . . . .	II-1
A. RCS Description . . . . .	II-1
B. Mission Criteria . . . . .	II-3
C. Requirements . . . . .	II-8
D. Revised Criteria . . . . .	II-11 thru II-14
III. CANDIDATE SYSTEM ANALYSIS . . . . .	III-1
A. Candidate Concepts . . . . .	III-1
B. Analysis of Concepts . . . . .	III-5
C. Concept Selection . . . . .	III-14 thru III-17
IV. SUPPORTING TESTS . . . . .	IV-1 thru IV-20
V. PRELIMINARY DESIGN AND SIMILITUDE TESTING . . . . .	V-1
A. Recommendation of Preferred Concept . . . . .	V-1
B. Preliminary Design . . . . .	V-2
C. Test System Fabrication . . . . .	V-11
D. Verification Testing . . . . .	V-23
E. Design Impact . . . . .	V-112
VI. FULL-SCALE TANKAGE . . . . .	VI-1
A. System Design . . . . .	VI-1
B. System Fabrication . . . . .	VI-42
C. Test Program . . . . .	VI-57 thru VI-95
VII. CONCLUSIONS AND RECOMMENDATIONS . . . . .	VII-1
A. Conclusions . . . . .	VII-1
B. Recommendations . . . . .	VII-4
VIII. REFERENCES . . . . .	VIII-1 thru VIII-5
APPENDIX	
TANK PRESSURE AND FLUID EXPOSURE LOG . . . . .	A-1

# Figure

I-1	Program Schedule . . . . .	I-3
II-1	Orbiter Reaction Control Subsystem Modules . . . . .	II-2
II-2	Shuttle Orbiter Load Factors during Typical Boost and RTLS Abort . . . . .	II-9
II-3	Reentry Acceleration and Attitude . . . . .	II-10
II-4	Tank and Orbiter Axes . . . . .	II-14
III-1	Map of Surface Tension Device Applicability . . . . .	III-2
III-2	Total-Communication Device . . . . .	III-4
III-3	Compartmented Tank Device . . . . .	III-4
III-4	Total-Communication Channels with Buffers . . . . .	III-6
III-5	Compartmented Tank Device, Aft Outlet . . . . .	III-7
III-6	Compartmented Tank Device, Forward Outlet . . . . .	III-8
III-7	Effect of Barrier Location on Pressurization Compartment Expulsion . . . . .	III-12
IV-1	Density of $N_2O_4$ as a Function of Temperature . . . . .	IV-2
IV-2	Density of MMH as a Function of Temperature . . . . .	IV-3
IV-3	Density of $N_2O_4$ as a Function of Temperature . . . . .	IV-4
IV-4	Viscosity of $N_2O_4$ as a Function of Temperature . . . . .	IV-5
IV-5	Viscosity of MMH as a Function of Temperature . . . . .	IV-6
IV-6	Viscosity of $N_2O_4$ as a Function of Temperature . . . . .	IV-7
IV-7	Comparison of Published and Measured Surface Tension Data for MIL-P-26539C $N_2O_4$ . . . . .	IV-8
IV-8	Comparison of Published and Measured Surface Tension Data for MIL Specification MMH . . . . .	IV-9
IV-9	Comparison of Published and Measured Surface Tension Data for Purified $N_2O_4$ . . . . .	IV-10
IV-10	Comparison of Published and Measured Surface Tension Data for MIL Specification $N_2H_4$ . . . . .	IV-11
IV-11	Comparison of Published and Measured Surface Tension Data for MIL Specification $N_2H_4$ (IR&D) Data . . . . .	IV-17
IV-12	Density Data Selected for RCS Design . . . . .	IV-18
IV-13	Viscosity Data Selected for RCS Design . . . . .	IV-19
IV-14	Surface Tension Data Selected for RCS Design . . . . .	IV-20
V-1	Computer Program Results for 8-Channel System . . . . .	V-4
V-2	Computer Program Results for 4-Channel System . . . . .	V-5
V-3	Channel Configuration . . . . .	V-5
V-4	Quality Requirements for Propellant Flow from Upper to Lower Compartment . . . . .	V-7
V-5	Geometry for Barrier Angle Determination . . . . .	V-9
V-6	Preliminary Design . . . . .	V-12
V-7	Subscale RCS Model . . . . .	V-15
V-8	Assembly View of 1/3-Scale Model . . . . .	V-17
V-9	Subscale Model Components . . . . .	V-18
V-10	RCS 1/3-Scale Model . . . . .	V-19
V-11	Top View of Subscale Model . . . . .	V-21
V-12	Preliminary Design, Channel Wall-Spacing Configuration . . . . .	V-24

V-13	Transparent Channel Model . . . . .	V-25
V-14	Channel/Wall Spacing Test Article . . . . .	V-26
V-15	Channel/Wall Spacing Test System Schematic . . . . .	V-28
V-16	Channel/Wall Spacing Test Geometry . . . . .	V-30
V-17	Channel/Wall Spacing Test Results . . . . .	V-31
V-18	Flow Loss Factor as a Function of Flow Rate . . . . .	V-34
V-19	Low-g Test Model . . . . .	V-38
V-20	Drop Tower Test System . . . . .	V-39
V-21	Liquid Reorientation during Test 5 . . . . .	V-42
V-22	Liquid Reorientation during Test 8 . . . . .	V-44
V-23	Subscale Test Schematic . . . . .	V-58
V-24	Complete Test System . . . . .	V-59
V-25	One-Third Scale Model Coupled to Test System . . . . .	V-60
V-26	Trapped Gas Volume as a Function of Fill Rate for Isopropyl Alcohol . . . . .	V-63
V-27	Expulsion Efficiency as a Function of Flowrate with Isopropyl Alcohol . . . . .	V-63
V-28	Expulsion Efficiency as a Function of Flowrate with Isopropyl Alcohol . . . . .	V-68
V-29	Expulsion Efficiency as a Function of Flowrate with Isopropyl Alcohol . . . . .	V-69
V-30	Expulsion Efficiency as a Function of Flowrate with Isopropyl Alcohol . . . . .	V-70
V-31	Predicted Full-Scale Performance . . . . .	V-73
V-32	Predicted Full-Scale Performance . . . . .	V-73
V-33	SS/RCS Subscale Model Pulsed-Flow Test Valve Duty Cycle . . . . .	V-76
V-34	Pulsed Flowrate vs Total Flow Rate for Isopropyl Alcohol Pulsed Flow Tests . . . . .	V-77
V-35	Expulsion Efficiency as a Function of Flow- rate for Isopropyl Alcohol . . . . .	V-79
V-36	Expulsion Efficiency as a Function of Flow- rate for Isopropyl Alcohol . . . . .	V-80
V-37	Expulsion Efficiency as a Function of Flow- rate for Isopropyl Alcohol . . . . .	V-81
V-38	RTLS Centrifuge Test Schematic . . . . .	V-85
V-39	Tank Orientation for Reentry Simulation . . . . .	V-86
V-40	Centrifuge Test System . . . . .	V-88
V-41	Third Scale Model Centrifuge Test Results . . . . .	V-90
V-42	On-Orbit Vibration Level for RCS Aft Tanks . . . . .	V-92
V-43	Vibration Test Schematic . . . . .	V-94
V-44	Subscale Model Vibration Attachment Fixture . . . . .	V-95
V-45	Vibration Test Setup . . . . .	V-96
V-46	Vibration Test Results . . . . .	V-99
V-47	Tank Mounted on Slosh Test Apparatus with Barrier Horizontal . . . . .	V-102
V-48	Tank Mounted on Slosh Test Apparatus with Barrier Vertical . . . . .	V-102
V-49	Harmonic Frequencies, Barrier Horizontal . . . . .	V-105
V-50	Harmonic Frequencies, Barrier Vertical . . . . .	V-106



V-51	Damping Ratio, Barrier Horizontal . . . . .	V-109
V-52	Damping Ratio, Barrier Vertical . . . . .	V-109
V-53	Force Response . . . . .	V-110
VI-1	SS/RCS Propellant-Acquisition Device Design Detail . .	VI-3
VI-2	Flightweight Tank Design . . . . .	VI-5
VI-3	Surface Tension Device, Schematic . . . . .	VI-6
VI-4	Entrance Loss as a Function of Screen Bubble Point . . . . .	VI-11
VI-5	Effect of Temperature on Entrance Loss for 325 x 2300 Screen . . . . .	VI-15
VI-6	Critical Mission Event Liquid Orientation . . . . .	VI-16
VI-7	Reentry and RTLS Minimum Volume Puddle Locations . . .	VI-18
VI-8	On-Orbit Vibration Level for RCS Aft Tanks . . . . .	VI-20
VI-9	Failure Modes of Surface Tension Devices . . . . .	VI-29
VI-10	Acquisition System Block Diagram . . . . .	VI-31
VI-11	Channel Structure . . . . .	VI-43
VI-12	Manifold Frame Structure and Manifold Bubble Filter . . . . .	VI-45
VI-13	Completed Ring Manifold . . . . .	VI-45
VI-14	Reentry Sump . . . . .	VI-47
VI-15	Reentry Sump, Another View . . . . .	VI-47
VI-16	Manifold Bubble Filter . . . . .	VI-48
VI-17	Reentry Collector Structure . . . . .	VI-49
VI-18	Reentry Collector . . . . .	VI-50
VI-19	Heavyweight Tank . . . . .	VI-52
VI-20	Lower Compartment Channel Subassembly . . . . .	VI-52
VI-21	Manifold Added to Lower Compartment Channel Subassembly . . . . .	VI-54
VI-22	Lower Compartment Channel Subassembly, Top View . . .	VI-55
VI-23	Upper Compartment Channel Subassembly . . . . .	VI-55
VI-24	Completed Device . . . . .	VI-56
VI-25	Full-Scale Acquisition Test Device, Schematic . . . . .	VI-59
VI-26	Full-Scale RCS Tank Support Stand . . . . .	VI-59
VI-27	General Test Installation Schematic . . . . .	VI-60
VI-28	Full-Scale Tank Test System . . . . .	VI-61
VI-29	Full-Scale Tank Test System, Another View . . . . .	VI-61
VI-30	IPA Bubble Point Trace for Lower Channel System ( $\Delta P_2$ ) . . . . .	VI-70
VI-31	$N_2O_4$ Bubble Point Trace for Lower Channel ( $\Delta P_2$ ) and Reentry Sump ( $\Delta P_1$ ) . . . . .	VI-74
VI-32	Typical $\Delta P$ History for Lower Channels and Sump during Outflow . . . . .	VI-77
VI-33	Vertical Expulsion with Isopropyl Alcohol, Liquid Remaining . . . . .	VI-80
VI-34	Horizontal Expulsion with Isopropyl Alcohol, Liquid Remaining . . . . .	VI-81
VI-35	Mass Flow History for MMH RTLS Expulsion Test . . . . .	VI-82
VI-36	Mass History for MMH RTLS Expulsion Test . . . . .	VI-83
VI-37	Pressure History for MMH RTLS Expulsion . . . . .	VI-83
VI-38	Reentry Collector $\Delta P$ Trace for MMH RTLS Expulsion Test . . . . .	VI-84

VI-39	Mass History, N <sub>2</sub> O <sub>4</sub> Minus 1-g Expulsion Test . . . . .	VI-85
VI-40	Mass History for N <sub>2</sub> O <sub>4</sub> Nominal Reentry Expulsion Test . . . . .	VI-89
VI-41	Mass History for N <sub>2</sub> O <sub>4</sub> Off-Nominal Reentry Expulsion Test . . . . .	VI-89
VI-42	Mass History for IPA, Reentry Expulsion Test . . . . .	VI-91
VI-43	Mass Flow History of MMH Reentry Expulsion Test . . . . .	VI-91
VI-44	Mass History for MMH Reentry Expulsion Test . . . . .	VI-92
VI-45	Pressure History for MMH Reentry Expulsion Test . . . . .	VI-92

# Table

II-1	RCS Tankage Requirements . . . . .	II-4
II-2	Accelerations, Flow Rates, and Liquid Position . . . . .	II-5
II-3	Acceleration Environment and RCS Flow- rate Requirements . . . . .	II-7
II-4	Critical Mission Events . . . . .	II-12
III-1	Device Parameters . . . . .	III-13
III-2	Evaluation of Concepts . . . . .	III-16
IV-1	Measured Contact Angles . . . . .	IV-13
IV-2	Metal Sample Cleaning Procedures . . . . .	IV-16
V-1	Reentry Expulsion Efficiency for Various Barrier Angles . . . . .	V-8
V-2	RCS Preliminary Design Performance . . . . .	V-11
V-3	Channel/Wall Spacing Text Matrix . . . . .	V-29
V-4	Loss Factor . . . . .	V-32
V-5	Gas Pull-through Test Results . . . . .	V-35
V-6	Drop Tower Test Matrix . . . . .	V-40
V-7	Nomenclature for Scaling Analysis . . . . .	V-46
V-8	Low-g Acceleration Scaling for RCS Subscale Model . . . . .	V-48
V-9	High-g Acceleration Scaling for Subscale Model . . . . .	V-48
V-10	Scaled Flowrates Based on Pressure Differentials for Subscale Model . . . . .	V-51
V-11	Scaled Flow Rates for Centrifuge Tests with Freon TF at 21°C (70°F) . . . . .	V-52
V-12	Relative Magnitude of Pressure Terms for Full-Scale System as Determined by Computer Analysis . . . . .	V-53
V-13	Bench Test Scaled Flowrates . . . . .	V-56
V-14	Subscale Fill and Drain Test Results . . . . .	V-65
V-15	RCS Oxidizer Tank Requirements during RTLS and Reentry . . . . .	V-84
V-16	Centrifuge Scaling Results . . . . .	V-84
V-17	Centrifuge Test Matrix . . . . .	V-89
V-18	RCS Requirements during On-Orbit Vibration . . . . .	V-93
V-19	Vibration Test Matrix . . . . .	V-98
V-20	Hydrostatic Test Results . . . . .	V-98
V-21	Slosh Test Matrix . . . . .	V-103
V-22	Force Response for Actual Propellants . . . . .	V-111

VI-1	Screen Bubble Point . . . . .	VI-10
VI-2	Influences of Critical Mission Events on Full-Scale Design . . . . .	VI-17
VI-3	Lower Compartment Residuals . . . . .	VI-21
VI-4	Upper Compartment Residuals . . . . .	VI-23
VI-5	Failure Mode Effects of SS/RCS Capillary Propellant System Components . . . . .	VI-34
VI-6	RCS Tank Test Instrumentation List . . . . .	VI-62
VI-7	Trapped Gas Quantities during IPA Tank Fills . . . . .	VI-65
VI-8	Outflow Test Sequence . . . . .	VI-78
VI-9	+Z Orbital Maneuver Test Predictions . . . . .	VI-86

Surface tension propellant acquisition/expulsion devices have been flight-proven on several earth-orbital and interplanetary vehicles for both monopropellant and bipropellant systems. Many others have been built and tested or are in the conceptual stage (Ref I-1). Each of these devices was designed to perform to a unique set of operational requirements and environmental conditions; a universal design that will satisfy all mission criteria for all applications has not been devised. This is particularly true for the SS/RCS where a new design is needed to meet a completely new and demanding set of requirements and conditions.

The SS/RCS components have as requirements/goals: (1) 30-day operation for 100-mission life with minimum maintenance, (2) capability for servicing, loading, and unloading both on or off the orbiter, (3) simple and insensitive checkout and servicing procedures, and (4) liquid propellant supply to the engines without pressurant gas ingestion. With its passive nature, all-metal surface tension tankage was the most promising acquisition/expulsion method to meet these requirements/goals and it was selected as the baseline system. This is also true for the orbital maneuvering system (OMS).

This orbiter RCS application presents the most stringent requirements ever placed on a surface tension system. In addition to the requirements noted above, the sometimes conflicting requirements include high-g boost with off-loaded tanks, maximum flow rate during high-g boost abort, high expulsion efficiency under either low-g orbital or high-g reentry operations, and the capability of starting reentry with a full tank. Further, the high-g boost and reentry acceleration vectors differ widely (up to 119 deg). The result is a situation that is at least an order of magnitude more difficult than any previously encountered.

Because of the difficult nature of the requirements, a program was undertaken to provide the technology and insight needed for the flight hardware RCS surface tension tankage program. The specific objective of this technology program was to analyze, design, fabricate, and test surface tension propellant acquisition/expulsion tankage that satisfies the requirements of the SS/RCS.

This objective was accomplished in performing the five tasks, as shown by the program schedule (Fig. I-1). Tasks I, II, and III were begun simultaneously at the start of the program in November 1973. The initial effort in Task I was to gather and define the RCS design requirements. This was followed by a continuous update through November 1974 as the requirements changed and became firm. As a result, a marked shift occurred in the requirements used for the first part of the program (Tasks II thru IV) and those applied to the full-scale tankage activity (Task V). The design criteria used for this technology program are presented in Chapter II.

Task II was a five-month effort to analyze and compare various surface tension concepts for meeting the design criteria. Several candidate concepts representing all known capillary techniques were defined, their sensitivity to mission requirements was evaluated, and a tradeoff study was conducted to select the three most promising concepts. A failure mode effects analysis (FMEA) and cost evaluation of these three concepts was then made. During this activity, the tank geometry changed from cylindrical to spherical, necessitating an iteration of the selection and evaluation processes. During Task II, a computer program was developed for analyzing the performance of surface tension tankage. The program, developed under a Martin Marietta-sponsored task (Ref I-2), was refined for use in this program. Additional changes and refinements were made throughout this study as the computer program was used in Tasks IV and V. A computer program manual describing the model and its use was prepared (Ref I-3). This analysis activity is discussed in Chapter III.

The Task II analysis and the Task IV preliminary design was supported by selected fine-mesh screen bubble point testing (Task III). This effort consisted of gathering available data on propellant physical properties of interest (density, viscosity, and surface tension) and evaluating suitability. This was followed by measuring the bubble point of a variety of fine-mesh screen samples in hydrazine ( $N_2H_4$ ), monomethylhydrazine (MMH), and nitrogen tetroxide ( $N_2O_4$ ) as a function of dissolved pressurant gas content, temperature, and purity of the propellant. The results were compared to values that should have been obtained based on published surface tension data. Good agreement was obtained with MMH and  $N_2O_4$ . The variations observed for hydrazine were resolved by a detailed investigation conducted under another Martin Marietta-sponsored task (Ref I-4). All results were subsequently compiled into an interim report published in August 1974 (Ref I-5). Because of this prior publication and distribution, only a summary of the Task III activity is presented in Chapter IV.



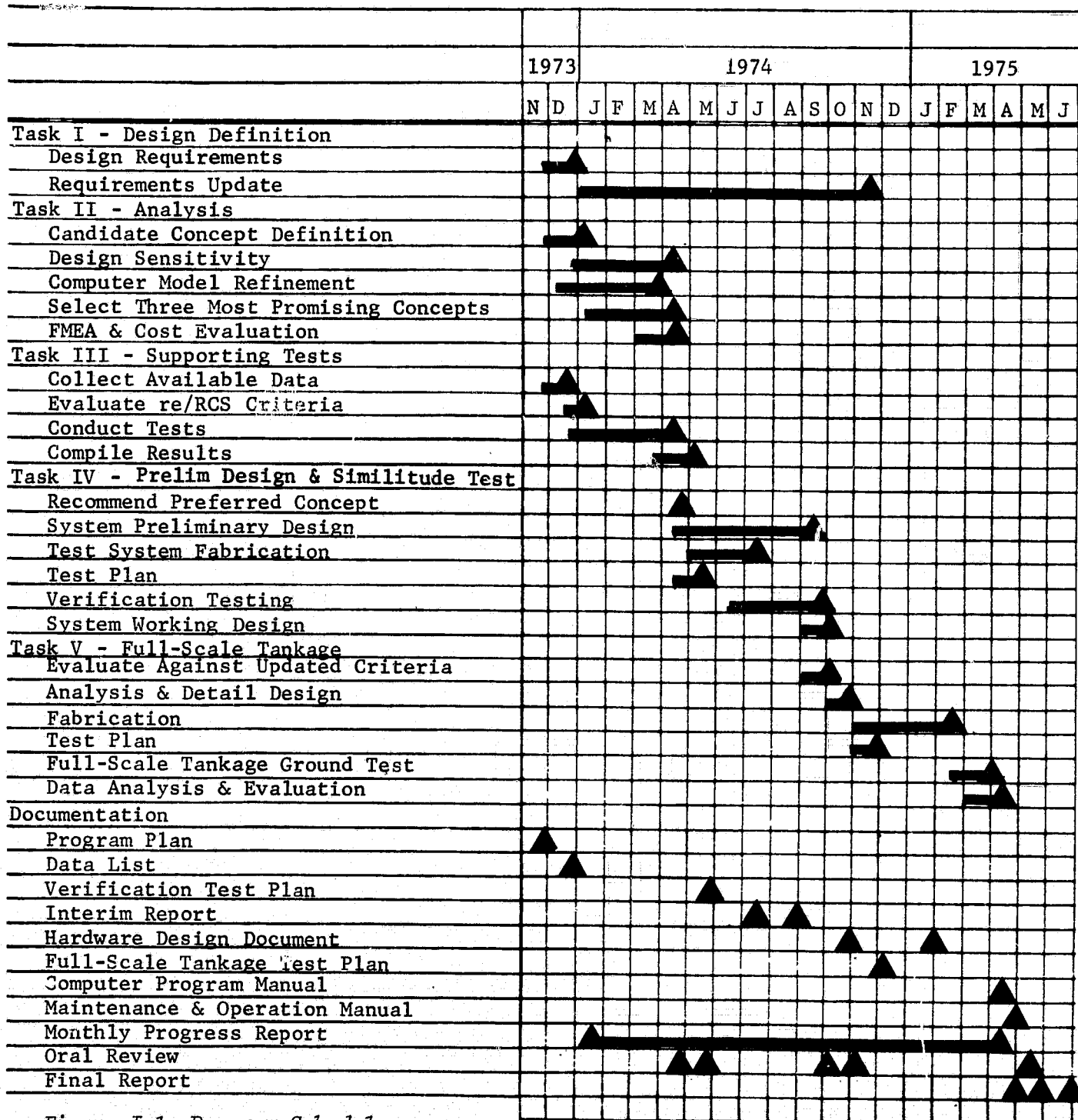


Figure I-1 Program Schedule

Based on the Task II evaluations of the three most promising concepts, the preferred compartmented-tank concept was recommended and subsequently selected by NASA-JSC to begin Task IV (Ref I-6). A preliminary design was made for the acquisition/expulsion system and the similitude/verification test fixtures were designed and fabricated. A scale of one-third was selected for design verification. A 1/3-scale model designed and constructed under Martin Marietta-sponsored task D-14D, Capillary Device Fabrication, to develop and assess specific design/fabrication techniques was used in the Task IV tests. A test plan was published in May 1974 to direct the experimental effort (Ref I-7). It was reviewed and approved by NASA-JSC and the Task IV test effort was initiated in mid-June 1974.

The scaled-test results showed that the system performed essentially as expected with good agreement between predicted and measured performance. Fill and drain are easily accomplished, but gas bleed lines are needed when filling against wetted screens. High-g return-to-launch-site (RTLS) abort outflow was conducted to the 35% of load level. Vibration and pulsed outflow had little effect and the device exhibited good high-g slosh damping and favorable low-g liquid reorientation/slosh damping characteristics. Outflow under scaled high-g reentry conditions verified the need for a bubble filter within the channels and an enlarged channel screen area in the reentry puddle to prevent suction dip and gas pullthrough into the outlet. Preliminary tests with a screen channel had shown this to be a problem. In particular, the tests showed the desirability of the compartmented-tank concept using a tilted, solid barrier with any penetration located on the +Z axis reentry side of the tank and with the propellant outlet located beneath the barrier. Details of the tests and the results obtained are presented in Chapter V.

Task V, the full-scale tankage activity, was a seven-month effort conducted from September 1974 to April 1975. This task is discussed in Chapter VI. Revised criteria were defined, as mentioned previously, based on the Rockwell International RCS specification (Ref I-8) to maximize the benefits accruing to the RCS flight tank program from the technology study. An in-depth analysis and redesign was then accomplished to meet these revised criteria and incorporate modifications indicated by the Task IV tests. An on-orbit and reentry expulsion efficiency of 98% became mandatory at this time but the need for high-mode depletion was eliminated (these are conflicting requirements). The design was evaluated with respect to acceptance testing, cleaning, inspection, and fill and drain procedures. Both flightweight and ground testing (ASME code) tank shells of 38-in. ID spherical geometry were designed. A detailed design review of the full-scale tankage was held at NASA-JSC at the beginning of November 1974 and approval of the design was received (Ref I-9). A hardware design document was prepared to establish the ground test hardware configurations (Ref I-10).

The full-scale ground test tankage (tank and surface tension acquisition/expulsion system) was fabricated and acceptance tested. A test plan was prepared and submitted in December 1974 (Ref I-11). Following review and approval by NASA-JSC and completion of fabrication, the full-scale tankage ground test program was conducted to verify cleaning, fill and drain, and inspection procedures. In addition, 1-g outflow tests were conducted to simulate RTLS abort and reentry operations and an adverse 1-g expulsion test simulated a +Z orbital maneuver. These tests were conducted with isopropyl alcohol (IPA), MMH, and  $N_2O_4$ .

Excellent results were obtained from the Task V full-scale tankage activity. Information was obtained concerning (1) detail parts design and fabrication, (2) acceptance of screen material, parts and subassemblies, and (3) the completed system. A method for, and the suitability of, a welded tank/barrier assembly was demonstrated, together with barrier penetration mechanical sealing. Assembly in a careful manner to meet system cleanliness requirements was demonstrated. Procedures were verified for vertical fill and vertical and horizontal drain. An expulsion efficiency of 98% was demonstrated during drain in either orientation. The need for bleed lines to purge gas from the various compartments during tank fill was shown, particularly when filling against wetted screens. This is required to assure filling the aft compartment beneath the barrier.

The tank was successfully outflowed to the 65% of load level during the RTLS abort outflow demonstration. An expulsion efficiency of 98% was repeatedly demonstrated during the reentry outflow tests. Even following breakdown and gas ingestion during the adverse one-g outflow, the tank was oriented for reentry and liquid feed was again established to the 98% expulsion level. Finally, considerable progress was made in establishing inspection/check-out procedures. More testing is required to establish the final techniques, however. At test completion, the full-scale tankage was shipped to NASA-JSC for further ground testing. A maintenance and operation manual was prepared for this tank system (Ref I-12).

Conclusions and recommendations resulting from the program are presented in Chapter VII. Considerable technology and pertinent information from this study have influenced the RCS flight tankage program, e.g., the solid welded barrier with penetrations only on the +Z side of the tank and one aft compartment outlet. Further testing is required, however, with particular attention given to inspection, assessment of screen dryout, and system performance in low-g.

References for this report are contained in Chapter VIII. An appendix is also included. This comprises the full-scale tankage pressure and fluid exposure histories accumulated during the full-scale ground test program.

## II. DESIGN CRITERIA

---

The purpose of the first task of this program (Task I, Design Definition) was to collect and compile the mission criteria and guidelines applicable to the design of a surface tension propellant acquisition system for the RCS. These criteria were specifically defined by the NASA Lyndon B. Johnson Space Center for this technology study (Ref II-1). While they are based on the Space Shuttle concept, they represent the worst-case operating conditions for the spacecraft. For example, it was initially assumed that the full maneuvering capability of the RCS would be used when the acceleration environment and the propellant flow rates were determined. Therefore, these criteria imposed the worst-case requirements on the propellant acquisition system.

Throughout the study these criteria were updated as the actual requirements for the Space Shuttle became more firmly established. One of the first major revisions involved the change from cylindrical to spherical tankage. Since cylindrical tanks are no longer of interest for this application, only the criteria for spherical tanks are presented. Other revisions that occurred during the early phases of the study have been incorporated. These changes had little impact on the preliminary design and the selection of the preferred system since they always relaxed the requirements. The analysis of the candidate concepts, selection of the preferred concept and its preliminary design, and the similitude testing (Tasks II and IV of the program) were performed using the design criteria defined in the first part of this chapter. Prior to designing and fabricating the full-scale tankage (Task V) a major revision to the design criteria took place. These revised criteria are presented in Section D of this chapter.

### A. RCS DESCRIPTION

The orbiter RCS bipropellant propulsion system, using  $N_2O_4$  and MMH, performs attitude control and small  $\Delta V$  translational maneuvers. It consists of a single forward module and two aft modules as depicted in Figure II-1. The forward module contains two propellant tanks (one oxidizer and one fuel), a pressurization system, and 22 thrusters (eight primary and three vernier on each side) mounted in the nose of the orbiter. These forward thrusters are used for on-orbit operation only. The vernier thrusters are used by themselves and not in combination with the primary

PRECEDING PAGE BLANK NOT FILMED

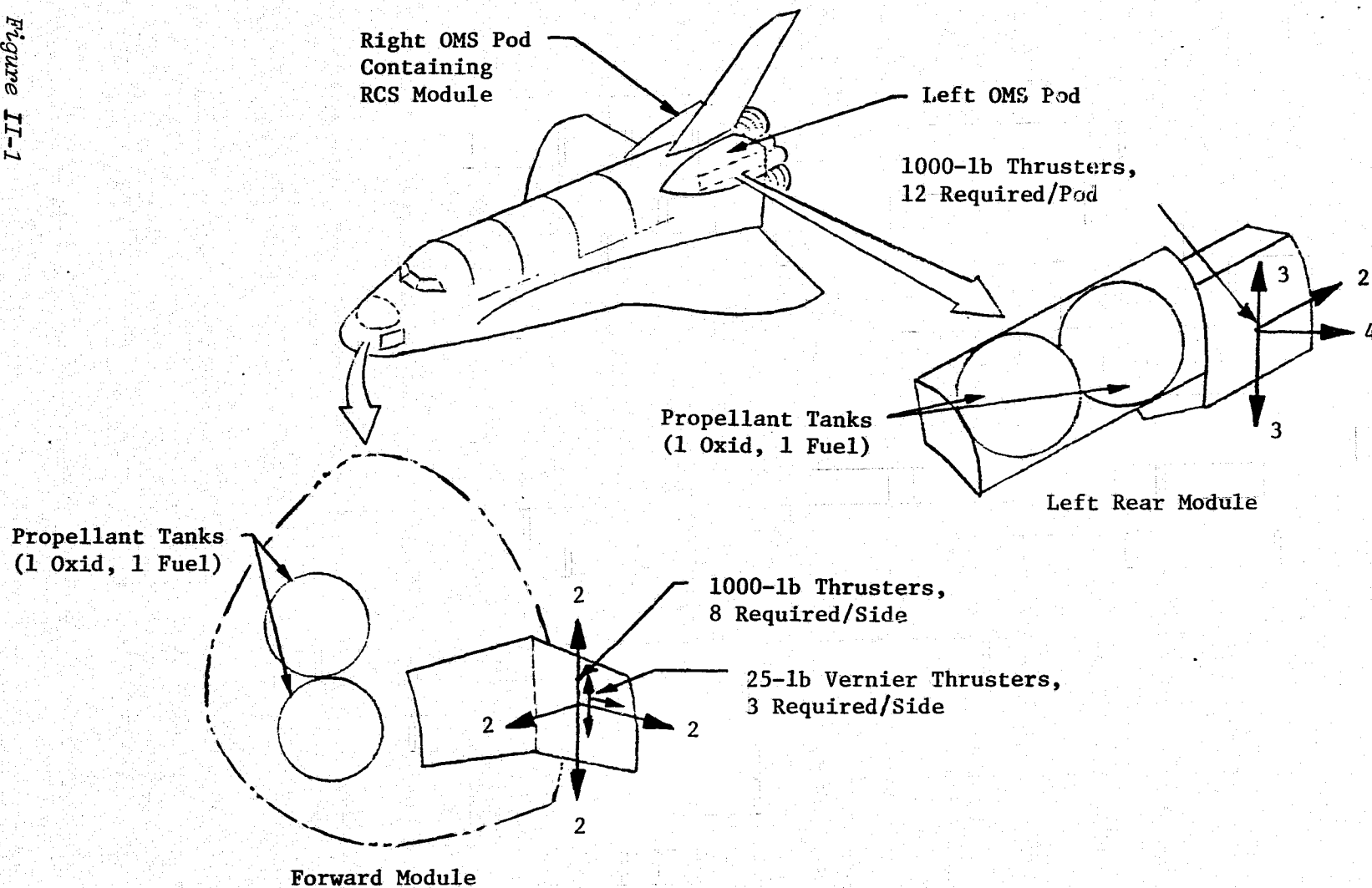


Figure II-1 Orbiter Reaction Control Subsystem Modules



thrusters. The flow rates and thrust levels resulting from vernier thruster operation are very small compared to the primary thrusters and do not affect surface tension device design.

Twelve thrusters are supplied by each aft module at the rear of orbiter. These thrusters are used on orbit and also provide all RCS accelerations in the +X direction and supply all RCS demands during reentry. The total quantity of propellant required for reentry is thus contained in the rear tanks. Each aft module also contains two propellant tanks, one oxidizer and one fuel. A description of the RCS tankage and propellant load requirements are presented in Table II-1.

## B. MISSION CRITERIA

A specific mission duty cycle cannot be specified for the RCS because of the diverse acceleration and flow rate requirements of each mission. In addition, RCS usage during boost abort and reentry depends on the specific mission and trajectory flown. By using typical conditions, the environment for specific mission events such as boost, abort, and reentry can be defined. The environmental conditions on orbit are determined by operation of the orbital maneuvering system (OMS) and the RCS. Although OMS can only produce translational maneuvers, many possible maneuvers can be performed by the RCS. Table II-2 lists the mission events and maneuvers that can occur during a Shuttle mission.

For each RCS maneuver the maximum acceleration was determined by assuming that the maximum number of thrusters that could produce the maneuver were firing, with a minimum orbiter mass of 71,000 kg (156,000 lbm). Angular rotation rates and angular accelerations were also considered. The accelerations, as sensed at each RCS tank, were determined and only the tank with the largest acceleration for a given maneuver is listed. This approach also establishes the maximum flow rates for each maneuver. The typical position of the propellant within a tank is also shown.

This information is summarized in Table II-3, showing only the worst-case conditions for each mission event. The most significant source of acceleration while coasting on orbit is aerodynamic drag, with values on the order of  $10^{-6}$  to  $10^{-5}$  g. Docking, crew movement, and other extraneous sources of acceleration may be on the order of  $10^{-5}$  to  $10^{-4}$  g. By designing the acquisition system to satisfy the worst-case operational conditions, the system will perform satisfactorily throughout any mission.

## TANKAGE

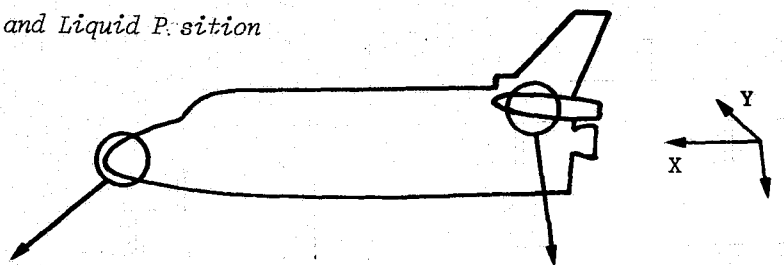
## PROPELLANTS

## PROPELLANT LOADS

## PRESSURIZATION

II-4

Table II-2 Accelerations, Flowrates, and Liquid Position



Mission Phase	Forward Module						Aft Module					
	Maximum RCS Flow rate, lbm/s		Maximum Acceleration, g			Typical Liquid Position	Maximum RCS Flow rate, lbm/sec		Maximum Acceleration, g			Typical Liquid Position
	Fuel	Oxid	X	Y	Z		Fuel	Oxid	X	Y	Z	
<u>Boost</u>												
	0	0	3.0	0	0.5		0	0	3.0	0	0.5	
RTLS Abort	0	0	-0.3	0	-2.5		15.9	26.2	-0.3	0	-2.5	
AOA Abort	0	0	3.0	0	0.5		2.7	4.4	3.0	0	0.5	
<u>On-Orbit</u>												
OMS	0	0	0.077	0	0		0	0	0.077	0	0	
RCS -X	5.3	8.7	-0.026	0	-0.005		0	0	-0.026	0	-0.001	
+X	0	0	0.026	0	0.007		2.7	4.4	0.026	0	0.003	
+Y	2.7	4.4	0	0	0.041		4.0	6.6	0.001	0.040	-0.009	
-Y	2.7	4.4	0	0	-0.041		4.0	6.6	-0.001	-0.040	0.009	
+Z	5.3	8.7	0.001	0	0.083		4.0	6.6	-0.004	0	0.057	

FOLDOUT FRAME

+Y	2.7	4.4	0 0	0.041	-0.002	X		4.0	6.6	0.001	0.040	-0.009	X		
-Y	2.7	4.4	0 0	-0.041	0.002	X		4.0	6.6	-0.001	-0.040	0.009	X		
+Z	5.3	8.7	0.001	0	0.083	X		4.0	6.6	-0.004	0	0.057	X		
-Z	5.3	8.7	0.009	0	-0.081	X		4.0	6.6	0.005	0	-0.054	X		
+Roll	0	0	0.005	-0.021	0.007	X		4.0	6.6	0.007	0.052	-0.027	X		
-Roll	0	0	0.005	0.021	0.007	X		4.0	6.6	0.007	-0.052	-0.027	X		
+Pitch	5.3	8.7	-0.022	0	-0.170	X		4.0	6.6	0.049	0	0.083	X		
-Pitch	5.3	8.7	-0.016	0	0.171	X		4.0	6.6	-0.026	0	-0.074	X		
+Yaw	2.7	4.4	-0.018	0.088	0	X		4.0	6.6	0.031	-0.038	0	X		
-Yaw	2.7	4.4	-0.019	-0.088	0	X		4.0	6.6	-0.031	0.038	0	X		
+X,+Y,+Z	8.0	13.1	0.024	0.041	0.092	X		10.6	17.5	0.031	0.040	0.070	X		
-X,-Y,-Z	13.2	21.9	-0.034	-0.041	-0.088	X		8.0	13.1	-0.039	-0.040	-0.063	X		
+Pitch, +Yaw,+X	8.0	13.1	-0.015	0.152	-0.166	X		11.9	20.0	0.057	-0.021	0.105	X		
Reentry	0	0	-0.4	0	-1.3	X		11.9	19.7	-0.4	0	1.3	X		

Table II-2

Table II-3 Acceleration Environment and RCS Flow Rate Requirements

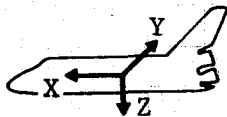
Mission Phase	Acceleration Source	Maximum Acceleration			Flow Rate, kg/s (lbm/s)		
					N <sub>2</sub> O <sub>4</sub>	MMH	
		X	Y	Z			
Boost							
	Normal Insertion	Solid Rocket Motors, Main Engines	3.0	0	0.5	----	----
	RTLS Abort	Main Engines, OMS, RCS	3.3	0	0.5	11.9 (26.2)	7.2 (15.9)
	AOA Abort	Main Engines, OMS, RCS	3.0	0	0.5	2.0 (4.4)	1.2 (2.7)
On-Orbit							
	Unpowered Coast	Drag	-3.0x10 <sup>-6</sup> axial (0° angle of attack) -1.6 x 10 <sup>-5</sup> lateral (90° angle of attack)			----	----
	ΔV Translation	OMS	0.077	0	0	----	----
	Random, Omnidirectional Maneuvers	RCS Forward	+0.027	0.231	0.231	9.9 (21.9)	6.0 (13.2)
		RCS Aft	-0.035	0.117	0.117	8.9 (19.7)	5.4 (11.9)
		+0.047	-0.039				
Reentry	Aerodynamic Drag	-0.68	0	-2.1	8.9 (19.7)	5.4 (11.9)	

Table II-3



RCS operation is not required during a normal boost sequence. However, various abort modes may be required during a boost sequence because of loss of thrust from the main engines. Operation of the RCS is required during portions of these aborts. If one main engine is lost during the first phase of ascent following separation from the solid boosters, the powered return to launch site (RTL) abort mode is used. After staging, the orbiter is rotated 180 deg about the Y axis (tail into the wind) and the remaining main engines, OMS, and RCS aft engines are burned to return to the launch site. All aft module engines are fired to deplete all but 340 kg (750 lbm) of propellant [210 kg (463 lbm) oxidizer, 132 kg (290 lbm) fuel as noted in Table II-1]. The propellant flow rates during the RTL abort are the highest encountered in the mission, as indicated in Table II-3. Axial acceleration (X axis) reaches +3.3-g before burnout of the main propulsion system and then drops to 0.25-g for 400 s, as shown in Figure II-2. During the main propulsion system burn, the Z-axis acceleration starts at a value of +0.2-g and reaches +0.5-g at burnout. After burnout, it increases to -2.5-g briefly and then eventually becomes -1.0-g. The acceleration profile during a normal boost sequence is also shown for reference in Figure II-2.

The abort-once-around (AOA) mode is used if one engine is lost during the later phases of ascent but prior to external tank separation. The RCS is used to provide additional  $\Delta V$  so the orbiter can achieve orbit. Only the +X thrusters on the aft pods are burned. The X acceleration reaches a value of +3.0-g and the Z acceleration a value of +0.5-g during this burn. Prior to entry, all RCS propellant not required for reentry maneuvering is burned on orbit.

The magnitude and direction of the reentry acceleration vector as a function of time is presented in Figure II-3. The propellant required during entry is between 13 and 34.5% of the tank capacity depending on the particular mission and trajectory flown. The capillary system must have the capability to expel a completely full aft tank during reentry. During the first vertical launches, the aft tanks will not be used on orbit to allow the full load to be used for reentry if necessary.

## C. SYSTEM REQUIREMENTS

The basic requirement placed on the propellant acquisition system is that it continue to provide gas-free propellant to the thrusters throughout the mission under the conditions previously specified. Further, the Space Shuttle concept places emphasis on

Figure II-2

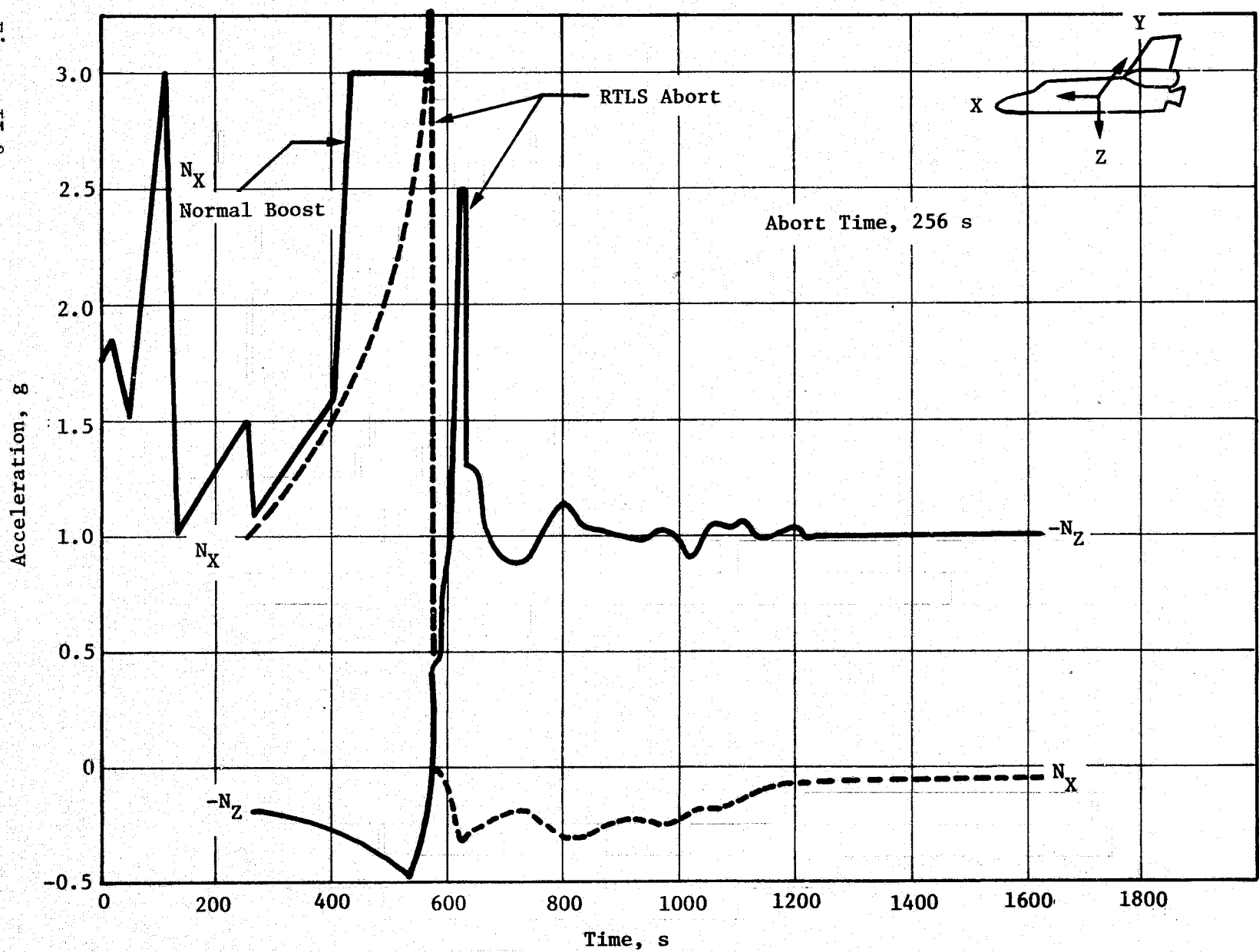


Figure II-2 Shuttle Orbiter Load Factors during Typical Boost and RTLS Abort

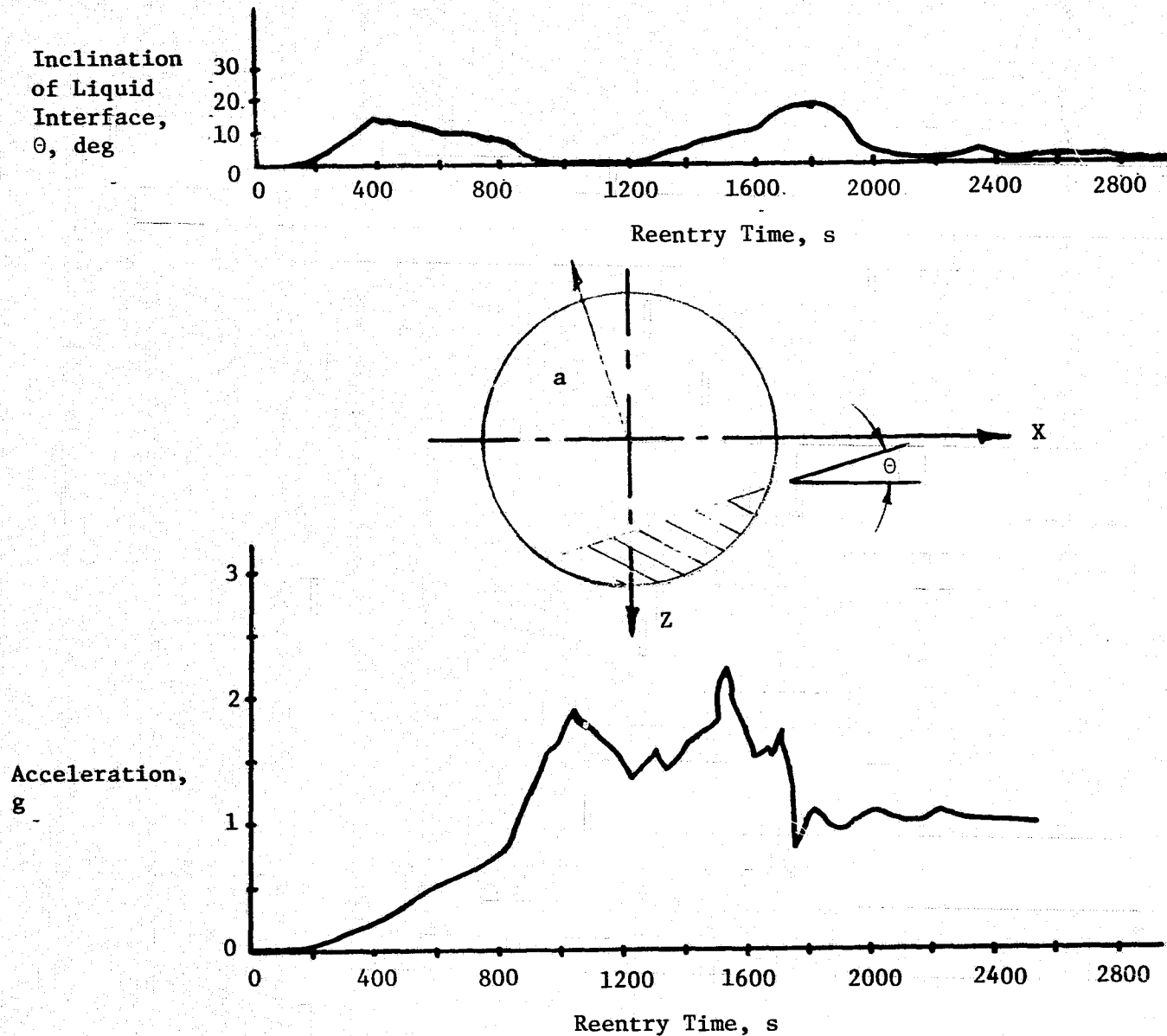


Figure II-3 Reentry Acceleration and Attitude

reusability. As a result, the acquisition device for the RCS is intended to be reused for up to 100 missions over a 10-year period with a minimum of servicing. In addition, man-rated reliability must be maintained. Also, the propellant acquisition device must be compatible with operations involved in servicing the orbiter before and after each flight. The tanks will be loaded when the orbiter is vertical, but they must be capable of being drained in either the vertical or horizontal orientation.

#### D. REVISED CRITERIA

Before starting design and fabrication of the full-scale tankage (Task V), a major revision in the design criteria took place. At this point, the criteria defined in Section B were changed to more closely align the tankage with the newly established criteria for the Space Shuttle. Only changes to the criteria defined in the first part of this chapter will be identified here.

##### 1. Expulsion Efficiency

A requirement for 98% expulsion efficiency was established. This applies to the expulsion of the forward tanks on orbit and to the aft tanks during reentry.

##### 2. Safety Factor

A design safety factor of 1.15 applied to the screen bubble point was established.

##### 3. Mission Events

The accelerations and flow rates specified by Rockwell International for the RCS (Ref II-2 and II-3) were used to define the worst-case operating conditions. The specific design conditions derived from the criteria are listed in Table II-4.

The accelerations and flow rates for RTLS have been changed. Two conditions are listed, one for boost and the other for the reentry phase of the abort. The minimum propellant level for RTLS has been changed from 34.5 to 65% of loaded propellant.

Previously the maximum capability of the RCS was always assumed as being used on orbit. Now the full-capability "high-mode" is not used when the volume of propellant remaining is less than 13% of that loaded. A "low-mode" operation is also defined in which only part of the RCS capability is used. The criteria

Table II-4 Critical Mission Events

Mission Event	Maximum Flow Rate, kg/s (lbm/s)		Maximum Acceleration, g			Tanks Affected	Propellant Temperature °C (°F)	Minimum Propellant Volume %
	Fuel	Oxidizer	X	Y	Z			
1. RTLS	6.8 (15.0)	10.9 (24.0)	3.3	0	0	Aft	18 (65)	65
	6.8 (15.0)	10.9 (24.0)	2.42	0	0.47	Aft	18 (65)	65
2. On-Orbit								
a) Low Mode (Event 14)	2.9 (6.3)	4.5 (10.0)	-0.032	0.015	0.064	Fwd	4-52 (40-125)	2 (residual)
b) High Mode	5.1 (11.3)	8.2 (18.0)	-0.013	0.032	-0.017	Fwd	4-52 (40-125)	13
	4.5 (10.0)	7.3 (16.0)	0.022	0.019	0.013	Aft	4-52 (40-125)	13
c) OMS Roll Control	2.3 (5.0)	3.6 (8.0)	0.039	0	0	Aft	4-52 (40-125)	13
d) Deorbit	0	0	0.077	0	0	Aft	4-52 (40-125)	13
3. Reentry	2.3 (5.0)	3.6 (8.0)	-0.68	0	-2.1	Aft	4-52 (40-125)	2 (residual)

define 15 low-mode and 6 high-mode events, of which the most critical are listed in the table.

Two other on orbit mission events were identified as critical due to the vibration environment. The OMS engines produce random vibrations of 1.93-g rms. In one OMS engine is not operating, the RCS must maintain the orbiter attitude. The RCS must function in the environment defined as "OMS roll control" with the vibration present. While the RCS is not operating when the OMS accomplishes the deorbit burn, the effect on the static retention of the acquisition device with less than 13% of the propellant remaining must be considered.

The flow rates and accelerations for reentry were also changed slightly.

#### 4. Tank Orientation

The axes of the RCS tanks are rotated with respect to the orbiter axes as defined in Figure II-4.

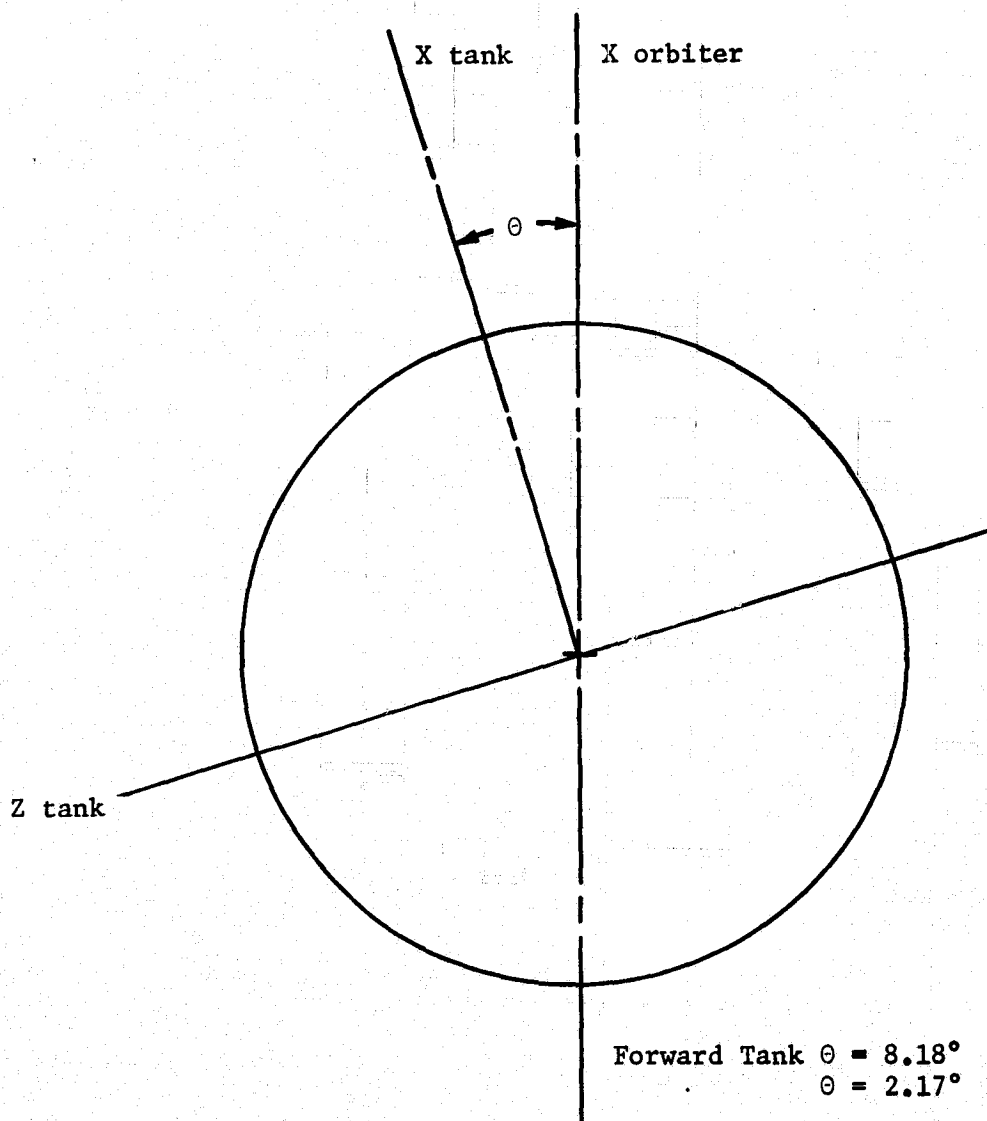


Figure II-4 Tank and Orbiter Axes

### III. CANDIDATE SYSTEM ANALYSIS

---

The purpose of the second task in this contract (Task II. Analysis) was to select the preferred surface tension propellant acquisition concept for the Space Shuttle RCS. A number of candidate acquisition systems were identified. The ability of these concepts to satisfy the mission criteria was analyzed and evaluated. This evaluation weighed heavily the requirements for reusability and servicing. The number of candidate concepts was reduced to the most promising and, through further evaluation, the preferred concept was identified. A failure mode and effects analysis and a cost evaluation were part of the final evaluation.

When this task began, the design criteria specified cylindrical tankage. After the concept was selected, the criteria were changed, including the specification of spherical tankage. The rationale for selection of the preferred concept was repeated with the new criteria and little change was found in the conclusions. Tank shape had very little effect on the relative evaluation of the concepts. Therefore, only the results of the selection process for the spherical tank, which are the most pertinent, are presented here.

The performance analysis of the candidate concept was accomplished with a computer model developed under this contract. The capabilities and operation of this model are completely described in a separate report (Ref III-1).

#### A. CANDIDATE CONCEPTS

The number of forms surface tension propellant acquisition systems can take can be divided into two categories--concepts that use capillary pumping, which usually have a relatively open, sheet-metal structure, and concepts that use fine-mesh screen. An example of a capillary pumping device is the vane-like system developed and qualified for the Viking orbiter '75 (Ref III-2). Screen devices are further subdivided into trap devices (hold a volume of propellant at the tank outlet) and liner, or total-communication devices (always in contact with the bulk propellant regardless of its location). The applicability of these devices can be established based on the more significant operational parameters, as shown in Figure III-1.



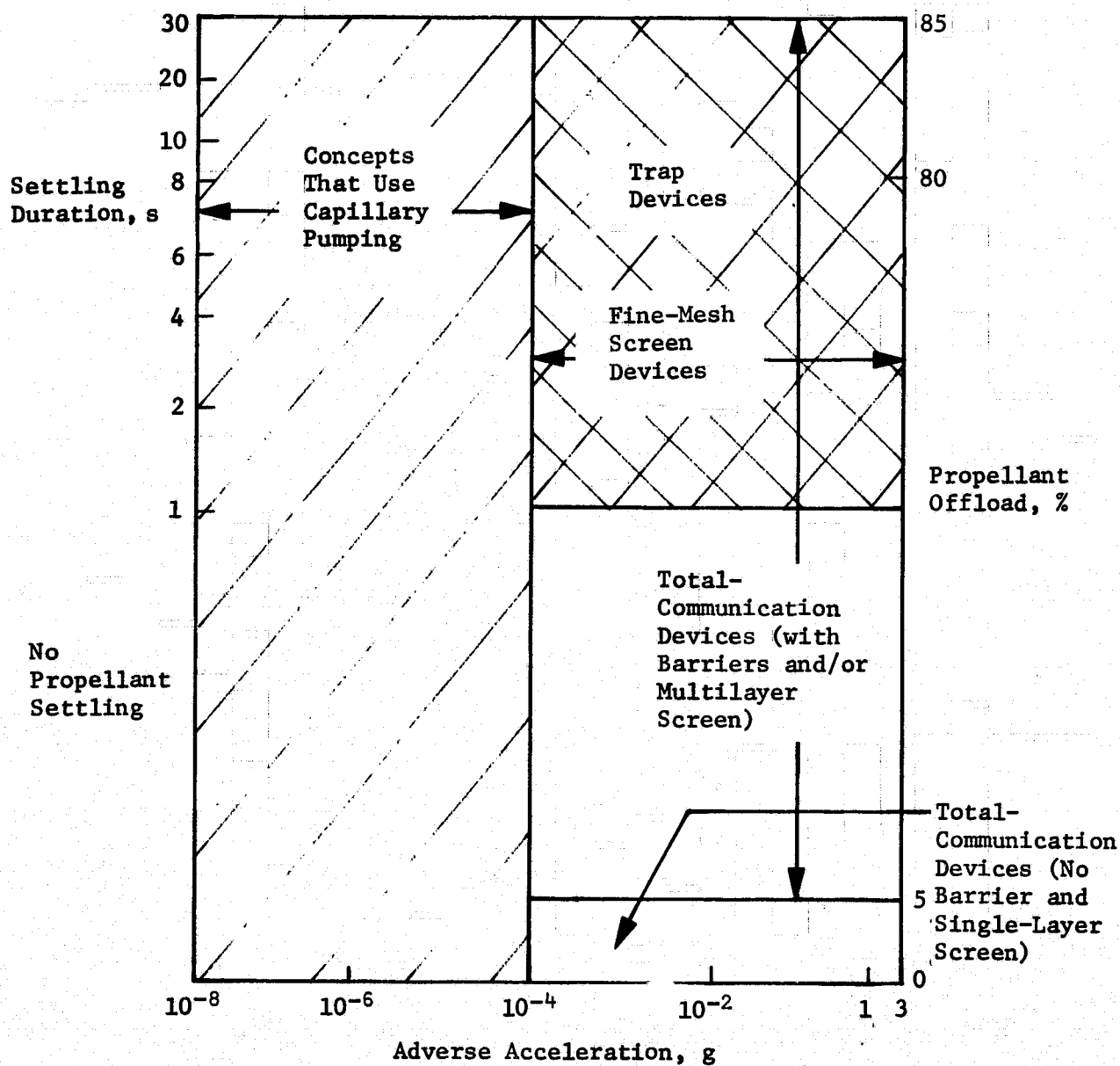


Figure III-1 Map of Surface Tension Device Applicability

Considering the mission criteria, i.e., adverse accelerations on the order of  $10^{-1}$  g, burn durations too short to produce propellant settling, and propellant off-loads up to 40%, the figure indicates that only total-communication devices with barriers and/or multilayer screen would be applicable. Although the low-g conditions present during coast periods are conducive to using capillary pumping to preferentially orient the propellant, the coast periods will be randomly interrupted by firing of the RCS so these systems could not be depended on to function reliably in such an acceleration environment. Trap devices are not applicable since they depend on propellant settling to continue feeding gas-free liquid. For these reasons, variations in the total-communication concept were considered as the candidate concepts to be evaluated and are discussed further.

## 1. Total-Communication Devices

The basic device is a screen barrier that is concentric with the tank wall (Fig. III-2). An annular gap, formed by the screen and the tank wall is kept full of liquid so it acts as a flow passage to transfer propellant from the bulk region to the tank outlet. When the volume of liquid in the tank is small, the screen must be capable of maintaining the annulus full of liquid. While this is not a problem in the relatively low-g environment on orbit, the accelerations experienced during boost with a partial propellant load, pose a problem. Since a single layer of the finest mesh screen cannot retain the liquid under such conditions, some means of increasing the retention capability of the liner device is needed.

It has been shown (Ref III-3) that screens can be layered to increase their retention capability. Another method developed for certain applications (Ref III-4) is to add a gas buffer annulus between the liquid flow annulus and the bulk liquid region. The device is not stable under a high, steady acceleration and the buffer annulus ingests and traps gas at a finite rate. Thus for transient high-g periods on the order of a few minutes, the buffer protects the primary liquid flow annulus from breakdown.

## 2. Compartmented-Tank Devices

If barriers are added to a total-communication device, the tank is divided into compartments (Fig. III-3). The compartments feed from one to another, bringing the propellant to the tank outlet. By adding the barriers, the length of the annulus is reduced and stability is increased over a broader range of applied acceleration. The number of barriers used and the relative size of the compartments are variables in the design.

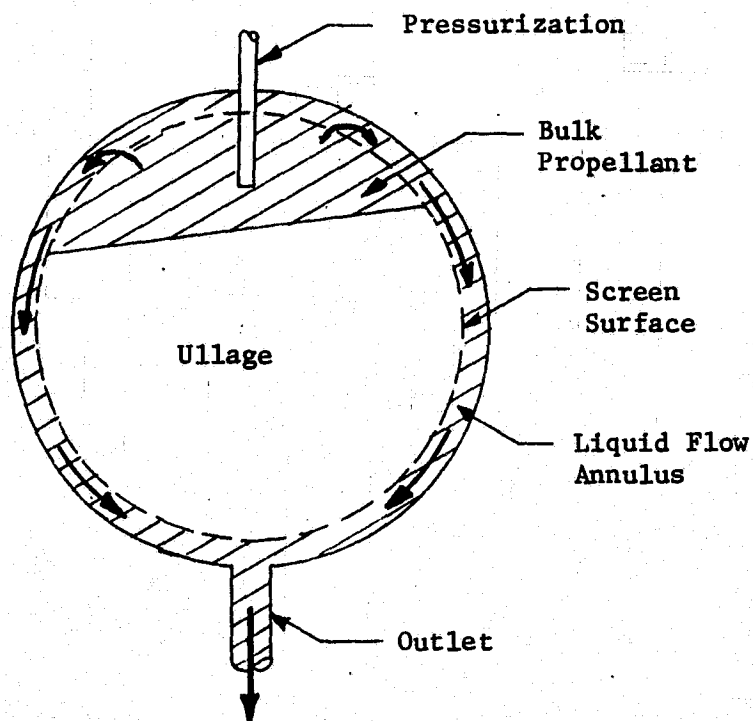


Figure III-2 Total-Communication Device

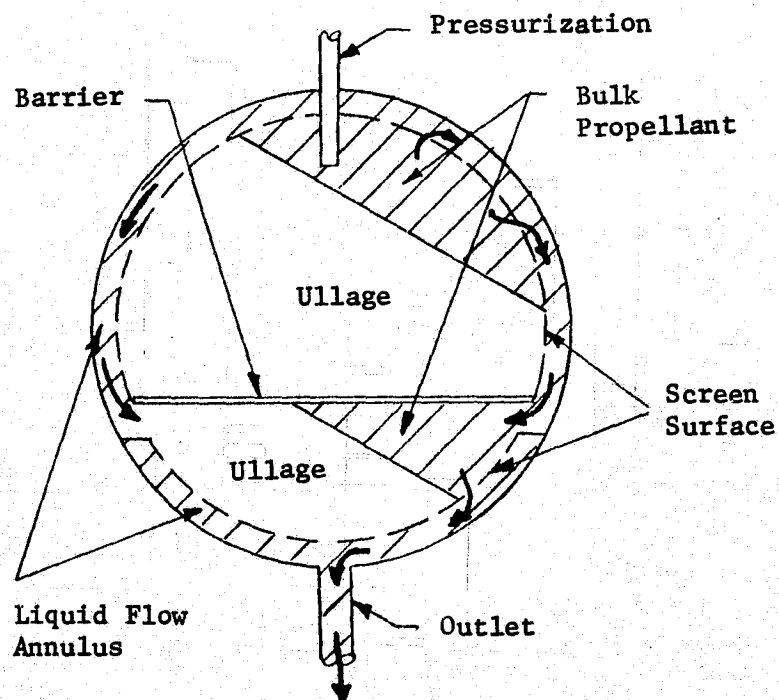


Figure III-3 Compartmented Tank Device

### 3. Concept Variations

Numerous variations exist in the total-communication and compartmented-tank devices. The liquid flow annulus can be formed by either a complete or partial screen liner. A full screen liner forms an annulus with the tank wall, encircling the entire tank, while a partial liner device is usually composed of screen or screen-and-plate flow channels connected to the tank outlet. Both function in essentially the same manner. Channels can be positioned along the tank wall, on barriers, or through the center of the tank. Their cross section is usually rectangular and one or more of the surfaces is formed by fine-mesh screen. The number of channels required is a variable. Location of the tank outlet with respect to the vehicle coordinate axes is also a variable. Many other more subtle variations that can be considered in the design of a surface tension device will be discussed in detail in later chapters of this report. However such variations are not pertinent to the present objective of selecting the best concept.

## B. ANALYSIS OF CONCEPTS

The candidate concepts were analyzed to provide comparative information for selection of the best concept. Numerous concepts were defined and evaluated, and the three most promising concepts were identified and analyzed in detail. A sensitivity study was also conducted as part of the analysis.

### 1. Selection of Most Promising Concepts

All of the previously mentioned concept variations were evaluated and compared in reducing the candidate systems to those appearing most promising. In general it was found that a channel system provided advantages over a full liner. A liner is heavier and holds a larger volume of residual liquid at tank depletion (lower expulsion efficiency,  $\eta_e$ ) than the channels.

Three concepts illustrated in Figures III-4, III-5, and III-6 were selected for further evaluation. These were the channel with gas buffer region total-communication device and two variations of the compartmented-tank device using channels in both compartments. One of the compartmented devices has the outlet at the aft end of the tank, while the other has the outlet at the forward end of the tank.

Figure III-4  
III-6

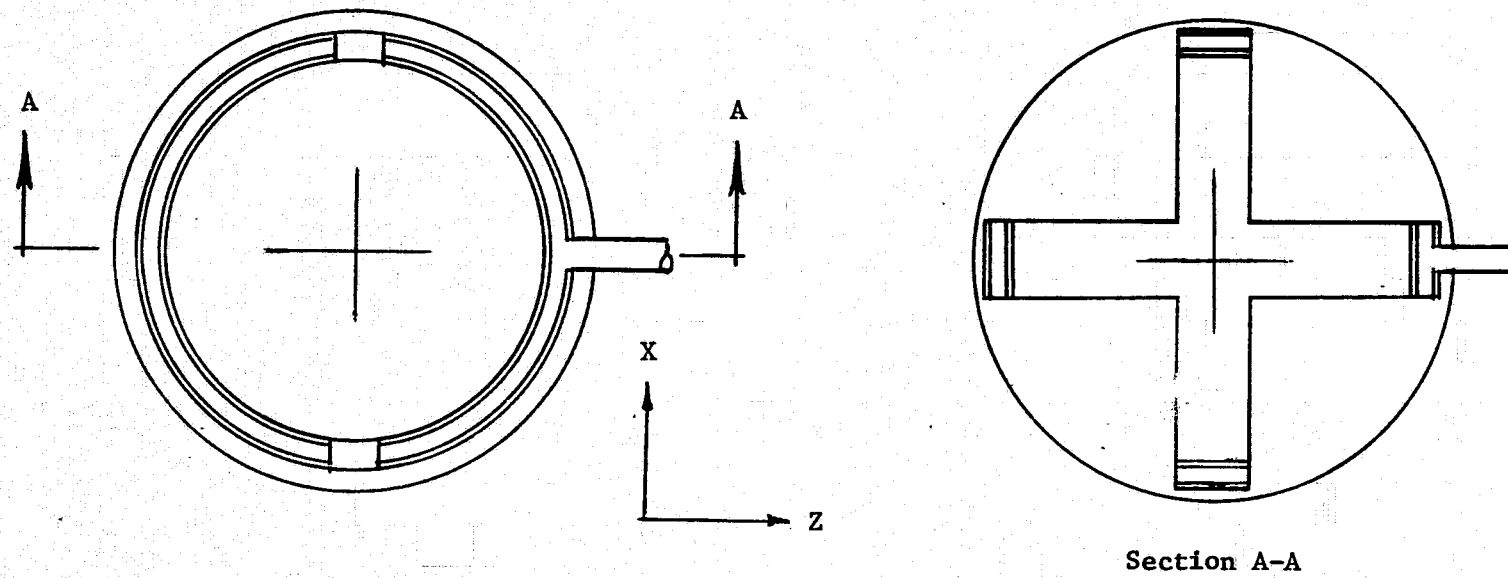


Figure III-4 Total-Communication Channels with Buffers

Figure III-5

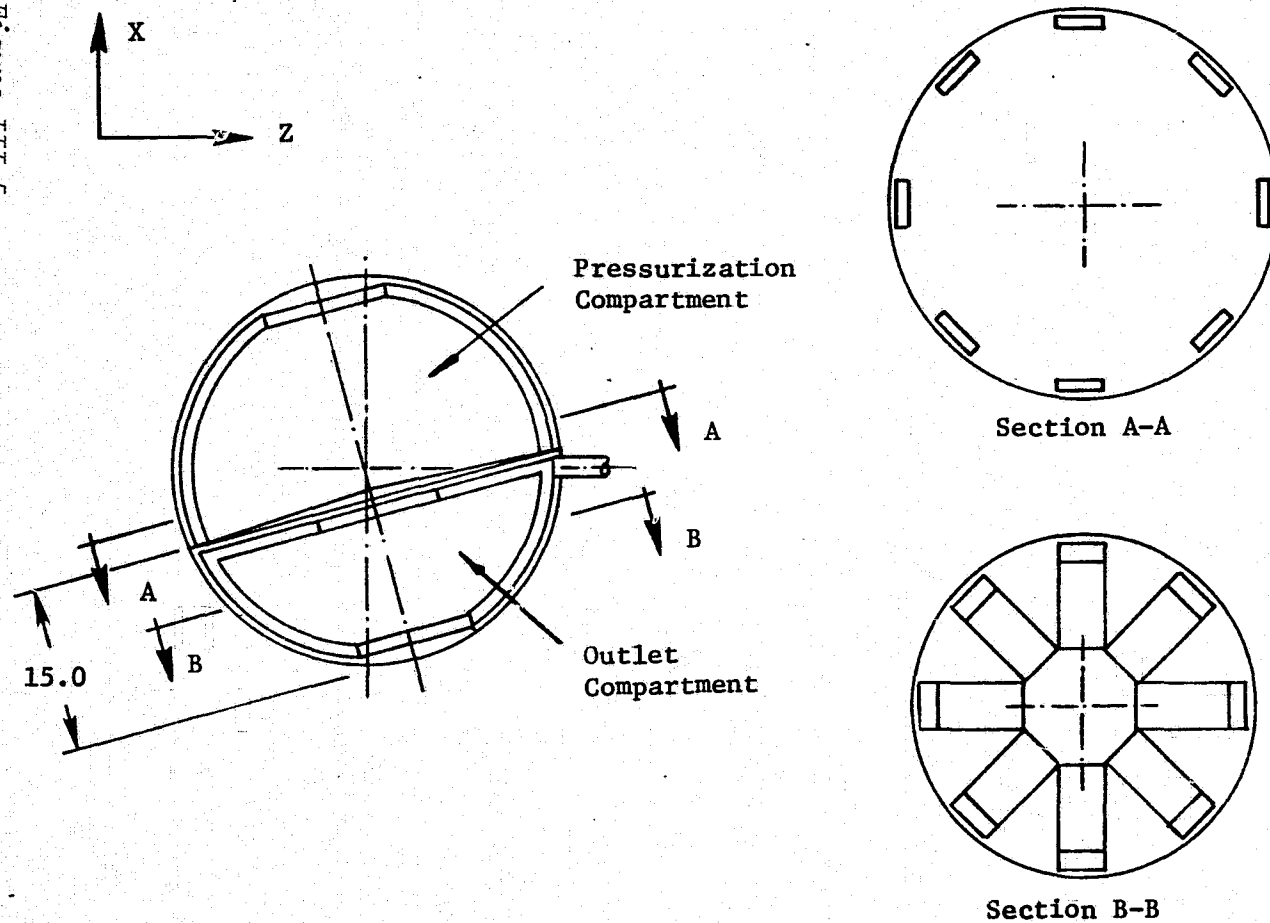
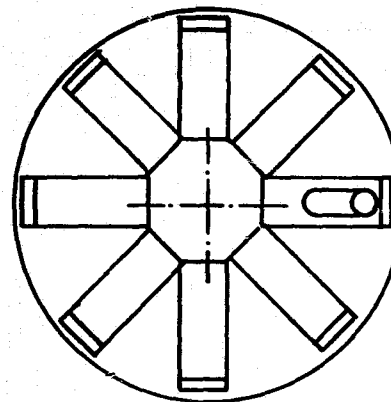
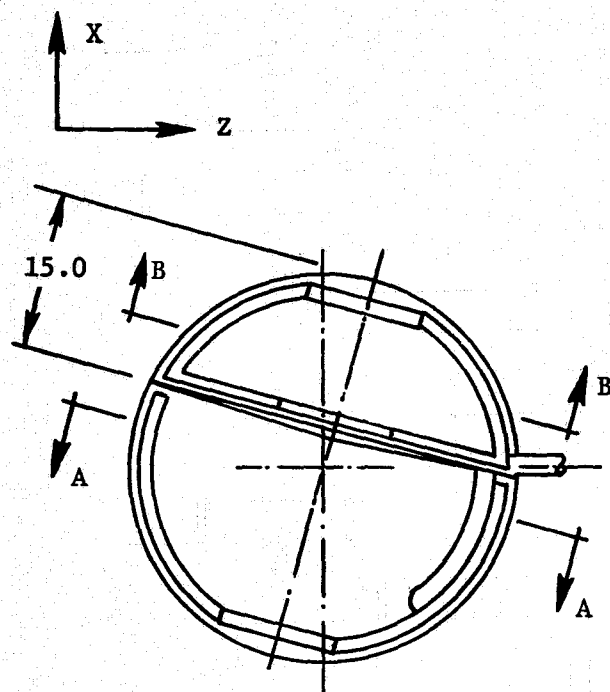
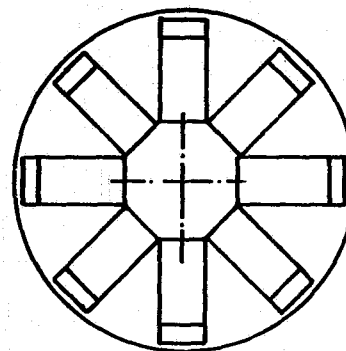


Figure III-5 Compartmented Tank Device, Aft Outlet

Figure III-6



Section A-A



Section B-B

Figure III-6 Compartmented Tank Device, Forward Outlet

a. *Channels with Buffers* - The primary advantage of a total-communication device, whether it includes a full liner or channels, is that it maintains direct contact with the bulk propellant. Buffers are preferred as a means of increasing the retention capability of the flow annulus. Multiple screen layers are less attractive since they result in a more costly system that requires a larger amount of screen. The buffer region enables the flow channels to remain stable, full of liquid, throughout the boost phase of the mission, including the abort modes. During reentry the propellant is positioned over the outlet so it will feed independent of the surface tension device.

b. *Compartmented Device, Aft Outlet* - A single barrier divides the tank into two compartments, designated the pressurization and outlet compartments. The outlet compartment is located on the aft end of the tank. Propellant is fed through the channels of the pressurization compartment to the bulk region of the outlet compartment. The channels of the outlet compartment are connected to the tank outlet. With this arrangement, the channels of the pressurization compartment can feed two-phase fluid to the outlet compartment. The only requirement is that the pressurization compartment be depleted before the outlet compartment so no liquid will be left behind in the pressurization compartment. This is dictated by the on-orbit depletion requirements of the forward module. A device with three or more compartments was considered but was eliminated because of increased mass and reduced performance.

During the boost phase of the mission, the outlet compartment is submerged even at the minimum load and during an abort. Gas may enter the channels of the pressurization compartment but it will be purged into the bulk region of the outlet compartment once outflow is initiated. The channels in the lower compartment will continue to supply gas-free propellant to the thrusters throughout the mission. During reentry, the propellant is settled over the tank outlet.

To position the outlet on the Z axis of the tank without having a large outlet compartment, the barrier of the device was tilted as shown. The outlet compartment holds the volume of propellant required for reentry (34.5%).

c. *Compartmented Device, Forward Outlet* - Both compartmented devices are very similar in configuration and operation. Locating the tank outlet on the forward end of the tank is better for reentry. The reentry acceleration vector has a -X component, tending to orient the liquid towards the front end of the tank. A tube is required to transfer propellant from the pressurization compartment to the outlet compartment during boost abort.



## 2. Design Sensitivity

General sensitivities of the RCS propellant acquisition system and the sensitivity of specific aspects of the two candidate concepts were evaluated.

*a. Commonality* - Since the properties of the fuel and oxidizer are different, the performance of a given surface tension device will vary with the propellant. A device designed for the fuel could be different than one designed for the oxidizer, e.g., different screen mesh size and different annulus flow area. Analysis of the candidate concepts showed little difference between fuel and oxidizer performance for this application. Because of this, a common device was selected for both fuel and oxidizer since the savings in cost far exceed any performance increase.

Commonality of design for the forward and aft tanks was another consideration. Since the forward RCS thrusters are not operational during boost or reentry while the aft thrusters are, a somewhat simplified device could be used in the forward tanks. Again, the slight improvement in performance would not warrant the cost of developing and qualifying two different surface tension devices. As a result the same device should be used in all six tanks, both forward and aft, of the RCS.

*b. Impact of Mission Criteria* - As discussed in Chapter II.B, mission criteria, the approach taken in defining the criteria for this effort was to assume that the full capability of the RCS would be used, i.e., the accelerations experienced and flow rates are worst case. This acquisition system was designed to operate reliably under such conditions. If the RCS will only operate at some fraction of its full capability, however, the size, weight, and complexity of the device could be reduced accordingly.

The boost phase imposes the most stringent requirements on the system, especially the aft tanks; the system must remain stable under the high boost acceleration with off-loaded tanks and must supply propellant during the aborts. This phase establishes the mesh size of the screen material and the number of screen layers required. Conversely, on-orbit operation determines the channel flow area and cross section (aspect ratio) because of the high outflow rates during this mission phase. Reentry has a lesser impact since the tank outlet can be positioned to take advantage of the propellant orientation although gas pullthrough must be precluded.

*c. Compartmented-Tank Device Sensitivity* - A prime factor in establishing the performance of a compartmented device is how effectively the propellant will be emptied from the pressurization compartment. Propellant within the outlet compartment

enters the channels and is fed directly to the tank outlet, while propellant in the pressurization compartment must first be transferred to the outlet compartment. A low on-orbit propellant residual can only be provided if essentially all the propellant is expelled from the pressurization compartment. This is possible because the channels of the pressurization compartment can continue to scavenge propellant as it comes into contact with the channels, transferring a gas-liquid mixture to the outlet compartment. However, the pressurization compartment must be depleted before the outlet compartment. Once gas begins to enter the channels of the outlet compartment, gas-free propellant expulsion is no longer possible and the residual in both pressurization and outlet compartments determines performance of the device.

The barrier location, and therefore the relative volumes of the two compartments, is a significant factor influencing the capability to deplete the pressurization compartment prior to the outlet compartment. An estimate of the effect of the barrier location, based on a fully loaded tank, is provided by Figure III-7. The average liquid quality that must pass through the barrier over the entire mission to ensure that both compartments are depleted simultaneously is shown as a function of barrier location. In reality, the liquid quality will be near 100% throughout most of the mission. After the screens in the pressurization compartment break down, the quality will begin to decrease. If the channel system of the pressurization compartment can be shown to have an expulsion capability greater than that given by Figure III-7, the pressurization compartment will empty prior to the outlet compartment.

### 3. Performance of the Concepts

The three most promising concepts were analyzed in detail to provide data for selection of the preferred concept. Three parameters were calculated for each device:

- 1) Weight - Dry weight is the total mass of the device and wet weight includes dry weight and residual propellant;
- 2) Expulsion efficiency is the percentage of the loaded propellant that can be expelled by the device;
- 3) Volumetric efficiency is the percentage of the tank volume that is usable with the surface tension device installed.

Channel size and number of channels were evaluated to optimize the expulsion efficiency of the device while keeping weight to a minimum. The configuration of the device and the calculated parameters are listed in Table III-1 for both forward and aft tanks.

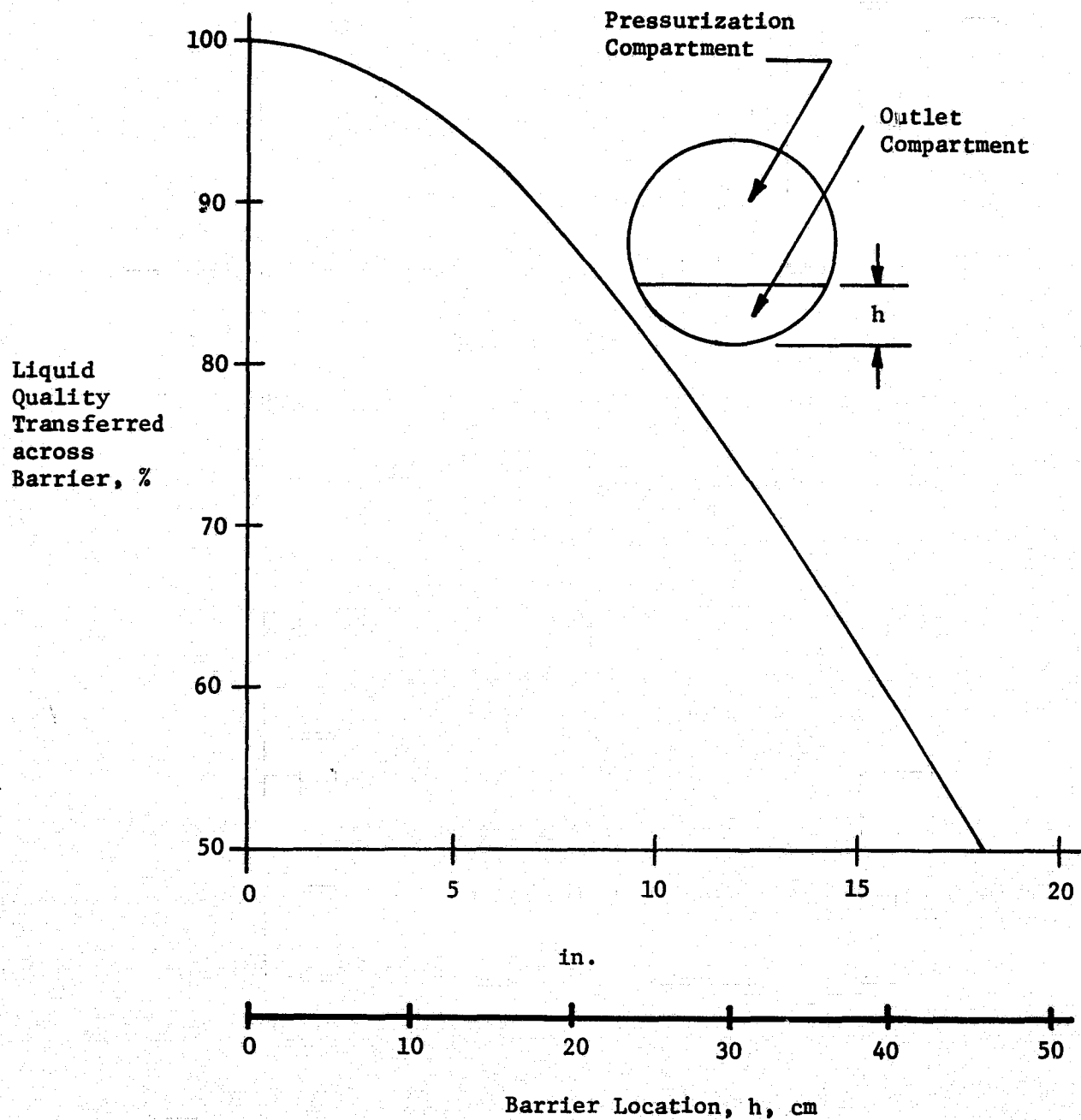


Figure III-7  
Effect of Barrier Location on Pressurization Compartment Expulsion

Table III-1 Device Parameters

Design	Tank Location	Number of Channels	Number of Screen Layers		Channel Size, cm (in.)	Weight, kg (lb <sub>m</sub> )			Expulsion Efficiency, %	Volumetric Efficiency, %
			Channel	Buffer		Dry	Wet (N <sub>2</sub> O <sub>4</sub> )	Wet (MMH)		
Channels with Buffers	Forward	4	2	2	12.7 x 2.5 (5.0 x 1.0)	9.3 (20.5)	51.5 (113.5)	33.0 (72.6)	93.8	99.7
	Aft	4	2	2	12.7 x 2.5 (5.0 x 1.0)	9.3 (20.5)	11.8 (26.0)	10.9 (23.9)	99.6	99.7
Compartmented Device, Aft Outlet	Forward	8	1	-	13.3 x 1.8 (5.25 x 0.7)	12.3 (27.2)	39.8 (87.6)	29.5 (65.0)	95.5	99.7
	Aft	8	1	-	13.3 x 1.8 (5.25 x 0.7)	12.3 (27.2)	14.8 (32.6)	13.9 (30.6)	99.6	99.7
Compartmented Device, Forward Outlet	Forward	8	1	-	13.3 x 1.8 (5.25 x 0.7)	12.7 (27.9)	40.1 (88.3)	29.8 (65.7)	95.5	99.7
	Aft	8	1	-	13.3 x 1.8 (5.25 x 0.7)	12.7 (27.9)	15.1 (33.3)	14.2 (31.3)	99.6	99.7

Table III-1

All of the devices use 325 x 2300 Dutch-twill screen. The influence of various screen meshes was analyzed using the computer program. It was found that the expulsion efficiency was decreased if a coarser mesh screen was used. While the finer mesh increases the resistance to liquid flow through the screen, there is a significant increase in retention capability of the screen. Using a finer screen mesh also permitted a smaller channel flow area, thereby decreasing the residual propellant at tank depletion and increasing the expulsion efficiency.

A computer model was the primary means of analyzing the candidate concepts. This model was initially developed under an IR&D task. It was modified and refined under this program so it could analyze the specific geometry of the candidate concepts in the Space Shuttle operational environment. The model determines the expulsion efficiency of the input surface tension device configuration for a specified propellant acceleration environment and flow rate. Pressure differentials within the flow passages of the device are calculated as a function of the volume of liquid in the tank. The point at which the sum of the pressure differentials will cause breakdown of the screen surface, allowing gas to leave the tank outlet, is established.

#### C. CONCEPT SELECTION

The surface tension concept found to best satisfy the Shuttle RCS propellant acquisition requirements was selected as the preferred approach. All factors influencing the development, fabrication, and operation of the device were considered, using the following evaluation factors:

- 1) Flexibility included the sensitivity of the device to mission duty cycle during orbit and reentry and the sensitivity to off-loading and aborts during boost;
- 2) Performance considered the ability to provide gas-free liquid on demand, expulsion efficiency, and volumetric efficiency;
- 3) System mass was the dry weight of the device;
- 4) Structural design and fabrication evaluated the difficulty of designing the device to withstand applied loads and the ease of fabrication;
- 5) Reliability was determined by FMEA;

- 6) Compatibility with the propellant and ease of cleaning were considered;
- 7) Loading and handling included the sensitivity to all ground operations;
- 8) Reusability assessed the ability to meet the 100-mission requirements;
- 9) Development status evaluated the need for developing new technology;
- 10) Cost assessed the relative cost of the devices, including development, qualification, and production.

An operations research process, developed and successfully used in selecting preferred propellant acquisition/expulsion systems for previous NASA contracts (Ref III-5 and III-6), was used in rating the candidate concepts. The evaluation factors were assigned weighting factors considering relative importance. Values from one to five were used, with five indicating the most importance. At least one evaluation factor received a weighting of five and another a weighting of one; the others were then weighted on a relative basis. Following this, each candidate device was rated with respect to the other for each of the evaluation factors, using a rating number between one (poorest) and five (best). At least one device was given a rating of five.

A figure of merit for each device was established by multiplying the weighting by the rating for each evaluation factor and summing the products. The entire process is summarized by Table III-2, which shows the weighting, rating, and figure of merit for each of the devices.

Based on the evaluation, the most significant differences between the three candidates can be identified. The device using channels with buffers has greater flexibility during on-orbit operation because it is always in direct communication with the bulk liquid.

The direction of the acceleration, the duration of each on-orbit burn, and the total number of burns have very little influence on the design of this device. The barrier of the compartmented-tank devices interrupts the communication between propellant in the pressurization compartment and the outlet, so the engine duty cycle must be considered in ensuring that the pressurization compartment empties before the outlet compartment. Hydrostatic heads acting on the channels are reduced due to the barrier, so the compartmented devices are less sensitive to the high-g boost.

Table III-2 Evaluation of Concepts

Evaluation Factors	Weighting	Rating			Figure of Merit		
		Total Communication	Compartmented Tank, Aft Outlet	Compartmented Tank, Fwd Outlet	Total Communication	Compartmented Tank, Aft Outlet	Compartmented Tank, Fwd Outlet
Flexibility							
Mission Duty Cycle	5	5	4	4	25	20	20
Off-Loading, Boost Abort	4	4	5	4	16	20	16
Performance							
Gas-Free Liquid on Demand	5	5	5	5	25	25	25
Expulsion Efficiency	5	3	5	5	15	25	25
Volumetric Efficiency	2	5	5	5	10	10	10
System Mass	5	5	4	4	25	20	20
Structural Design & Fabrication	4	4	5	4	16	20	16
Reliability	5	4	5	3	20	25	15
Compatibility	3	4	5	5	12	15	15
Loading and Handling	4	3	5	3	12	20	12
Reusability	3	5	5	5	15	15	15
Development Status	1	5	5	5	5	5	5
Cost	3	4	5	5	12	15	15
Overall Figure of Merit					212	235	209

Essentially only the liquid within the outlet-compartment channels of the compartmented devices cannot be expelled, so they have a higher on-orbit expulsion efficiency. The total-communication device must use multiple layers of screen to prevent the channels from breaking down, which increases its entrance loss, cost, and weight, makes it difficult to clean, and reduces its reliability.

It is easier to load a compartmented device if the outlet is on the aft end of the tank. For the compartmented device with the forward outlet, some means of filling only the outlet compartment would be necessary if the tanks were off-loaded. Boost abort would require that the propellant flow against a large hydrostatic head if the outlet is forward. With respect to the other evaluation factors, the three systems are equally attractive. While the three candidate devices are capable of meeting the RCS requirements, the evaluation indicates that the compartmented-tank device is the preferred system. The device is configured with the outlet compartment in the aft end of the tank and the tank outlet within that compartment. In arriving at the preferred concept, the volume of the outlet compartment was determined by the maximum volume of propellant required for reentry. The tank outlet was located on the +Z axis side of the tank so it is favorably positioned for reentry. To satisfy the outlet location and outlet compartment volume requirements, the barrier was tilted at an angle to the tank axes. The barrier is solid, with a single penetration in the vicinity of the tank outlet. This device was recommended to NASA and approved as the selected concept.



#### IV. SUPPORTING TESTS

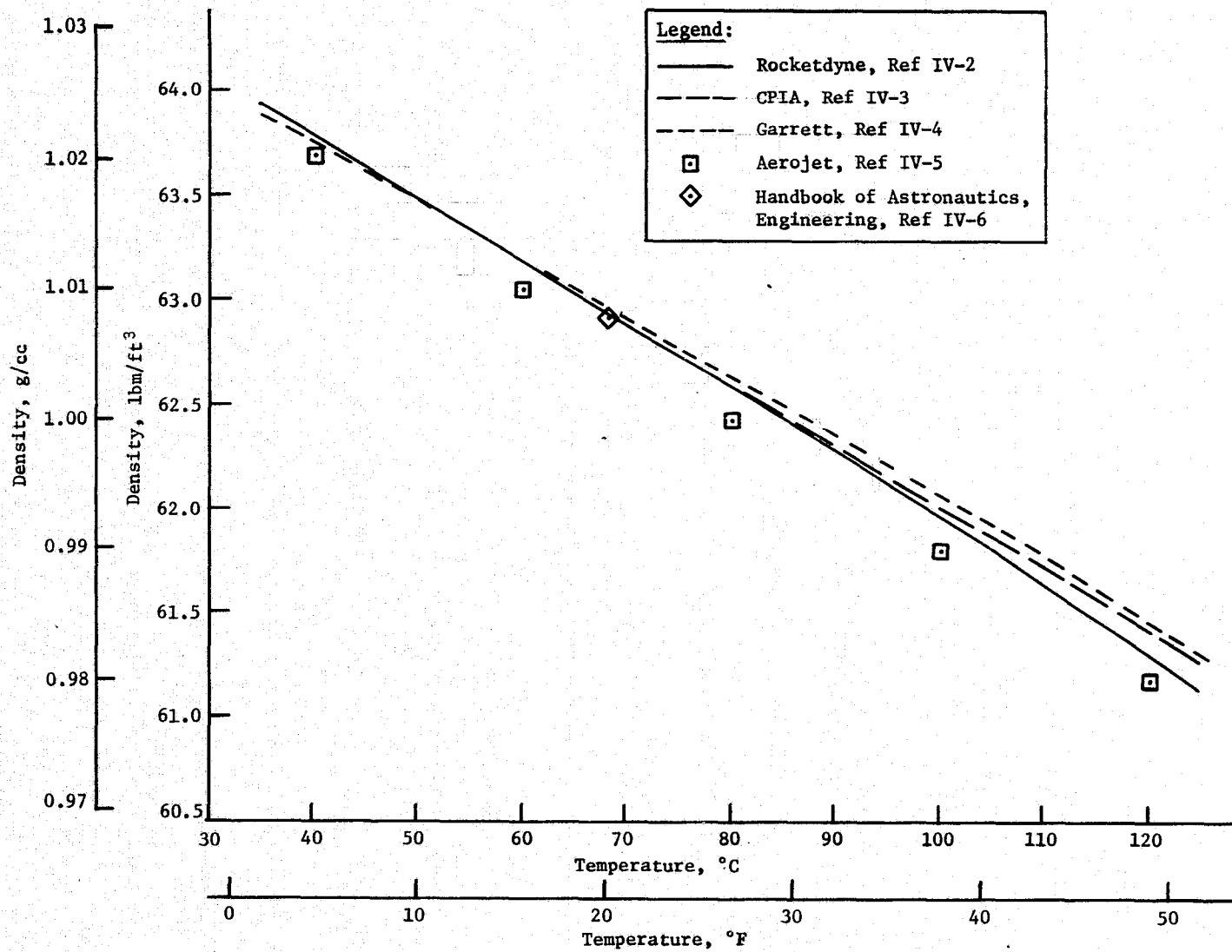
---

An evaluation of published propellant physical property data, together with bubble point tests of fine-mesh screen in propellants, was conducted under Task III. The effort consisted of (1) collection and evaluation of pertinent physical property data for hydrazine ( $N_2H_4$ ), monomethylhydrazine (MMH), and nitrogen tetroxide ( $N_2O_4$ ), (2) testing to determine the effect of dissolved pressurant gas, temperature, purity, and system cleanliness or contamination on system bubble point, and (3) compilation of both the literature and test results. The results of this task were published in a separate interim report under the contract (Ref IV-1). Because of this only a brief summary of Task III results are presented here. For a more detailed presentation of the data obtained under Task III, the reader is directed to Reference IV-1.

Information on propellant density, viscosity, surface tension, and contact angle was collected, compiled, and evaluated. Both NASA and DOD literature searches plus personal contacts were employed. With the exception of contact angle, the data were obtained as a function of propellant temperature. Some data were obtained showing the effects of pressure on propellant viscosity and density. The density and viscosity data for the three propellants investigated are presented in Figures IV-1 thru IV-6.

Screen bubble point was chosen as the parameter to be measured in the test program. The propellant acquisition systems proposed for the SS/RCS employ fine-mesh screen in their design. For these fine-mesh screen systems, screen bubble point in the propellant rather than propellant surface tension is the primary design parameter (Ref IV-13). Therefore the bubble points of three fine-mesh screen, Dutch-twill weaves (325 x 2300, 200 x 1400, and 165 x 800) in propellant-grade  $N_2O_4$ , MMH, and  $N_2H_4$  were measured as a function of propellant temperature and system pressure. Tests were also conducted with purified  $N_2H_4$  to investigate the effect of propellant purity. Contamination and screen cleaning effects were also evaluated. Excellent agreement between measured and predicted screen bubble points was obtained with  $N_2O_4$  and MMH. However anomalous and inconsistent bubble point data were obtained with screens in the two grades of hydrazine. Figures IV-7 thru IV-10 show some of the test data obtained.

Figure IV-1

Figure IV-1 Density of  $N_2H_4$  as a Function of Temperature

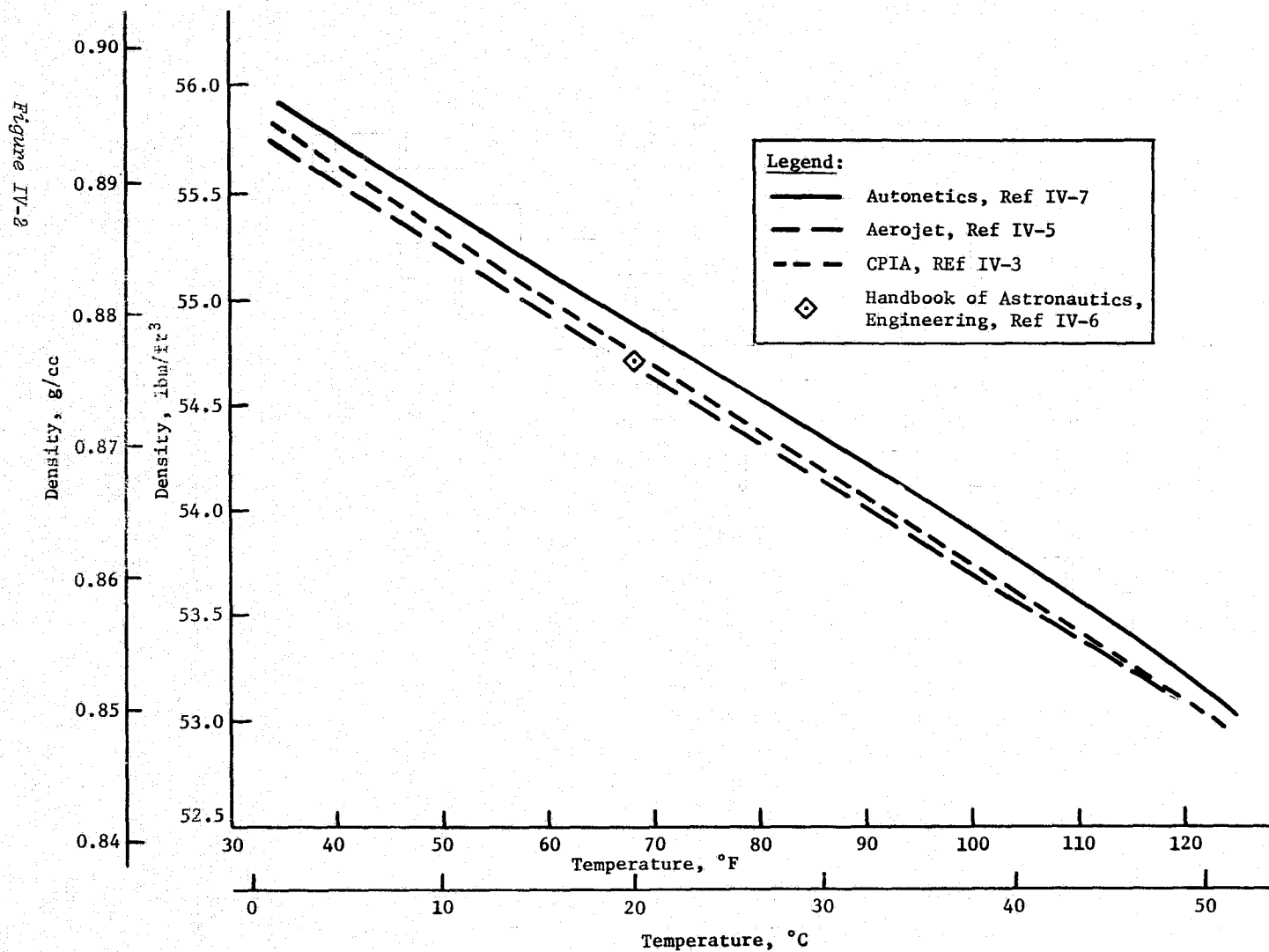


Figure IV-2 Density of MMH as a Function of Temperature

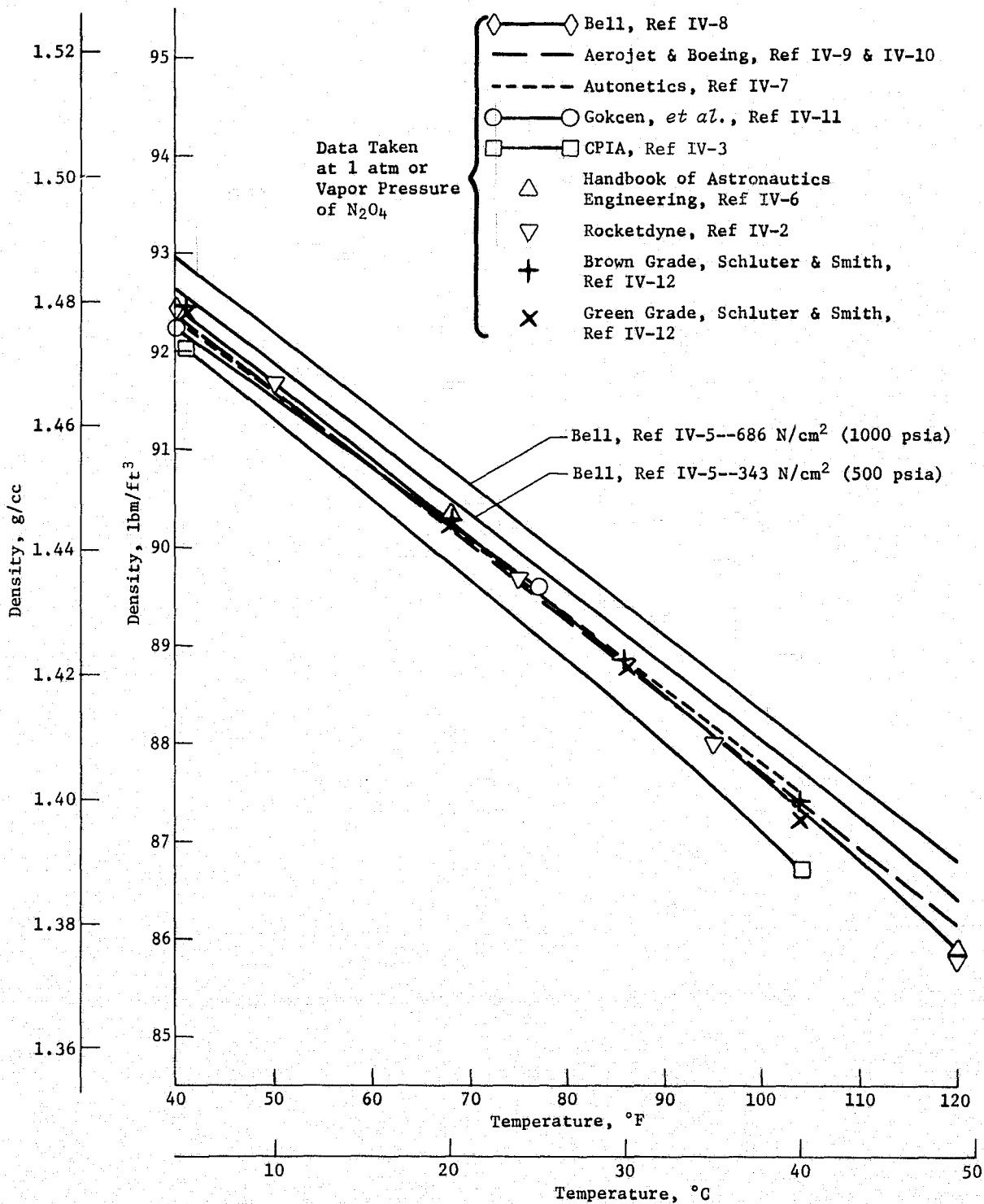


Figure IV-3 Density of  $N_2O_4$  as a Function of Temperature

Figure IV-4

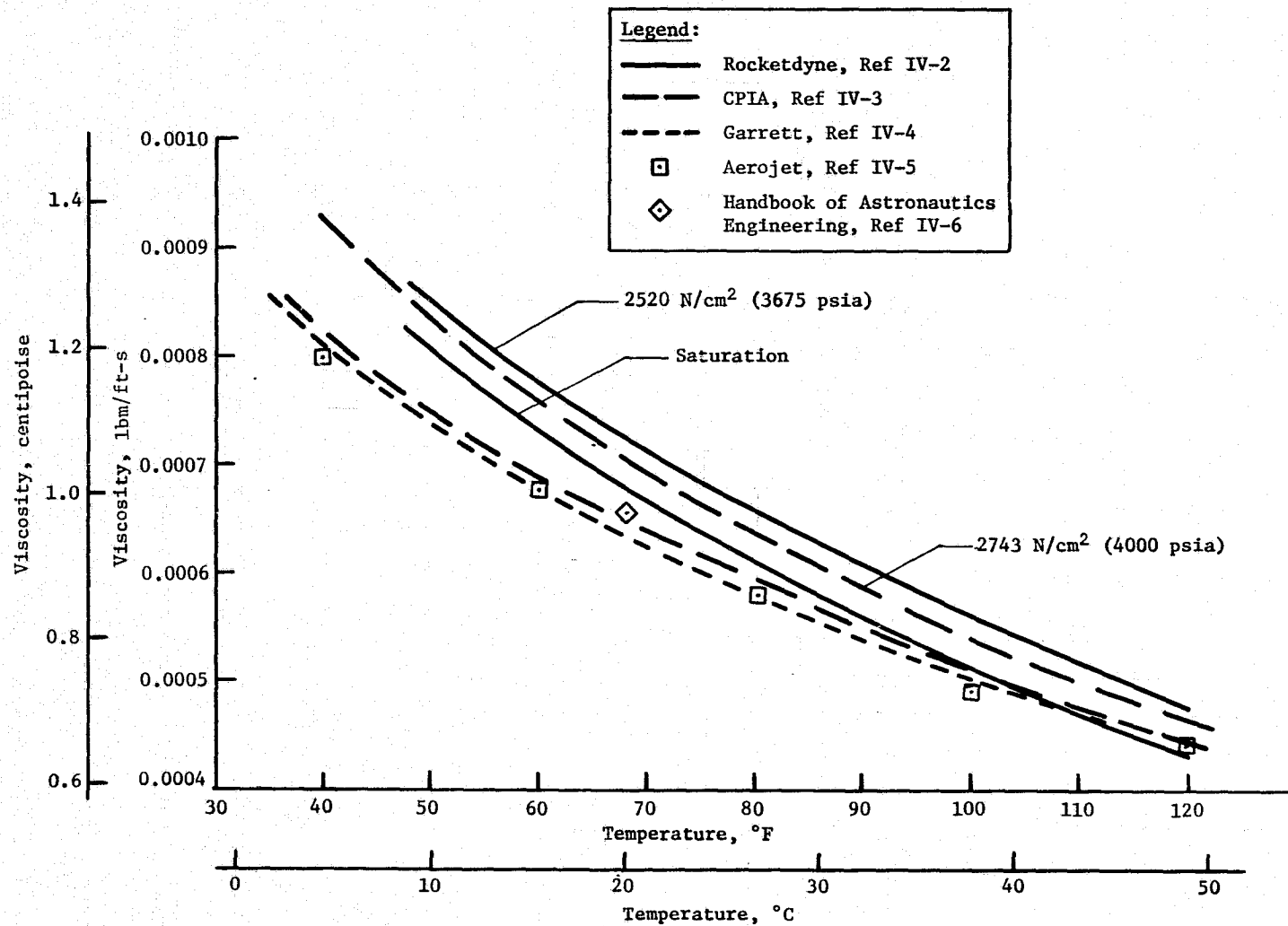


Figure IV-4 Viscosity of N<sub>2</sub>H<sub>4</sub> as a Function of Temperature

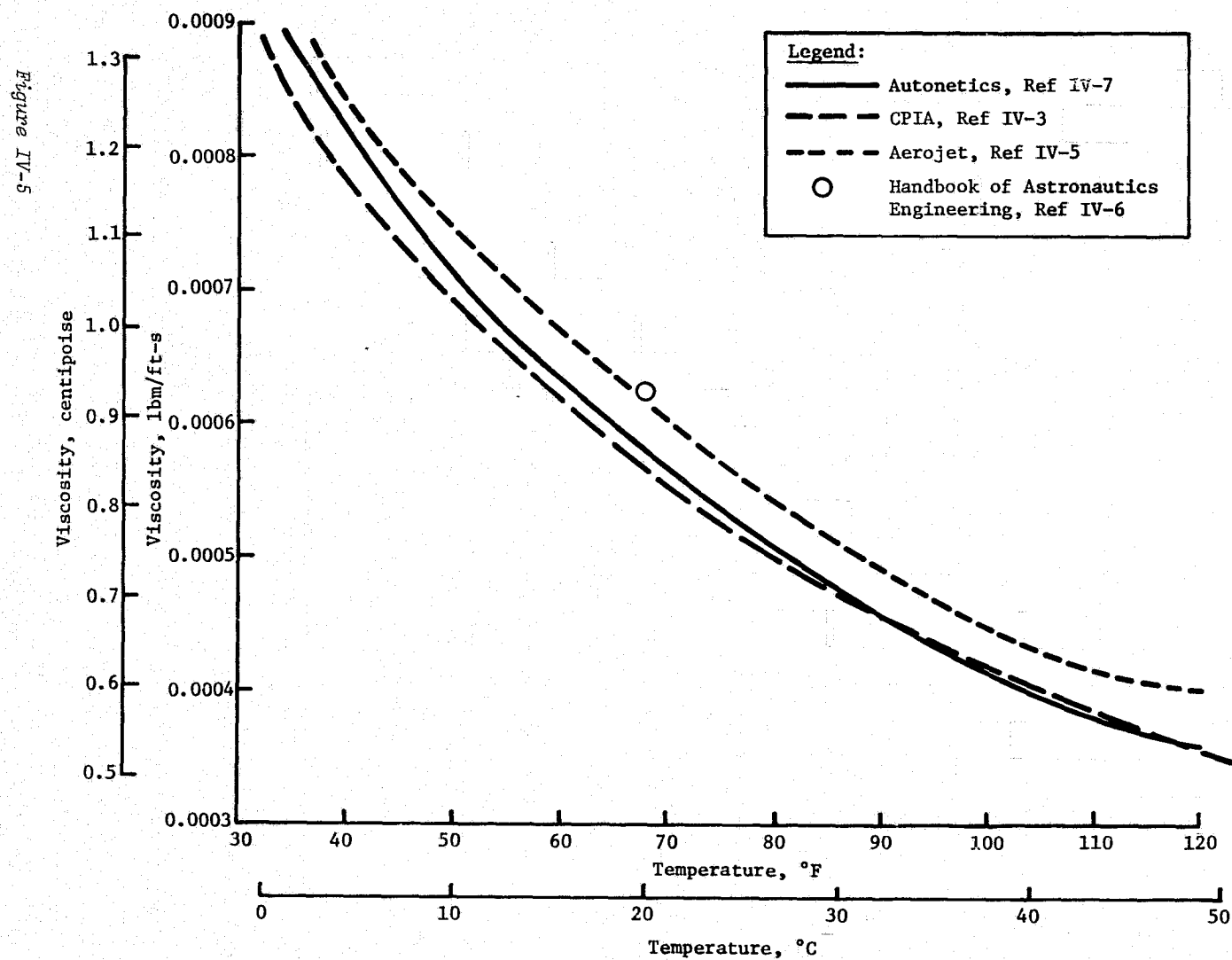


Figure IV-5 Viscosity of MMH as a Function of Temperature

Figure IV-6

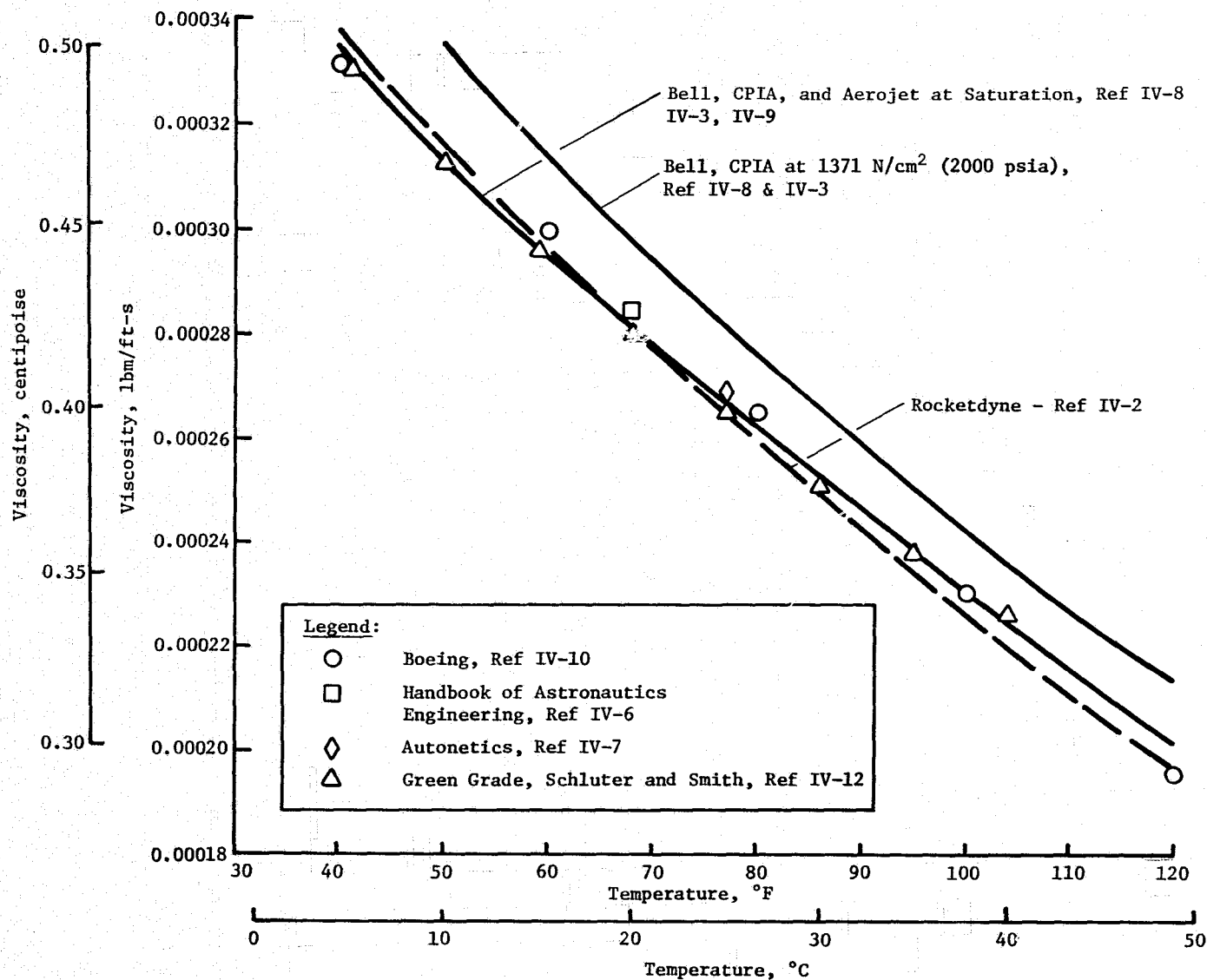


Figure IV-6 Viscosity of  $N_2O_4$  as a Function of Temperature

Figure IV-7

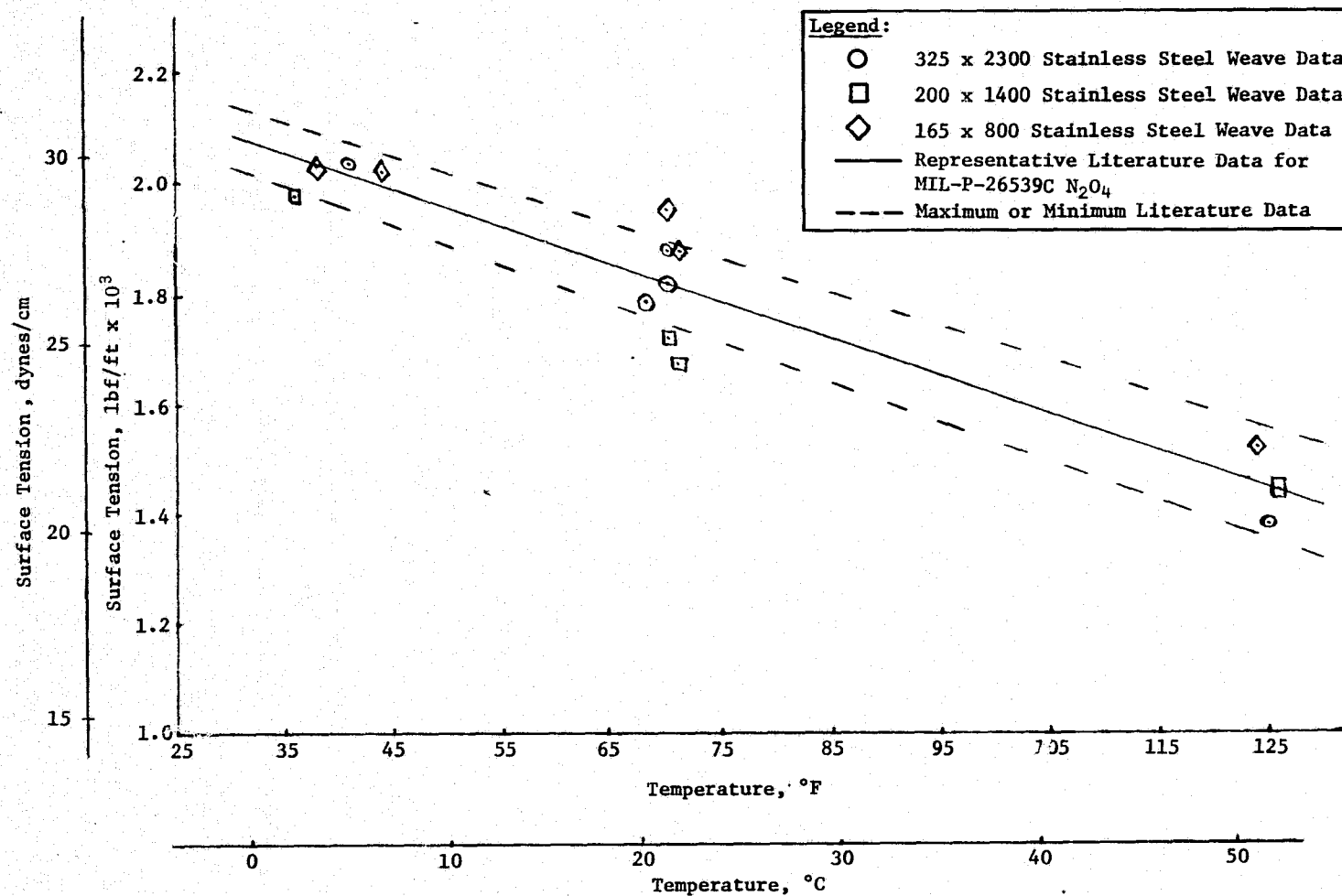


Figure IV-7  
Comparison of Published and Measured Surface Tension Data for MIL-P-26539C  $N_2O_4$



Figure IV-8

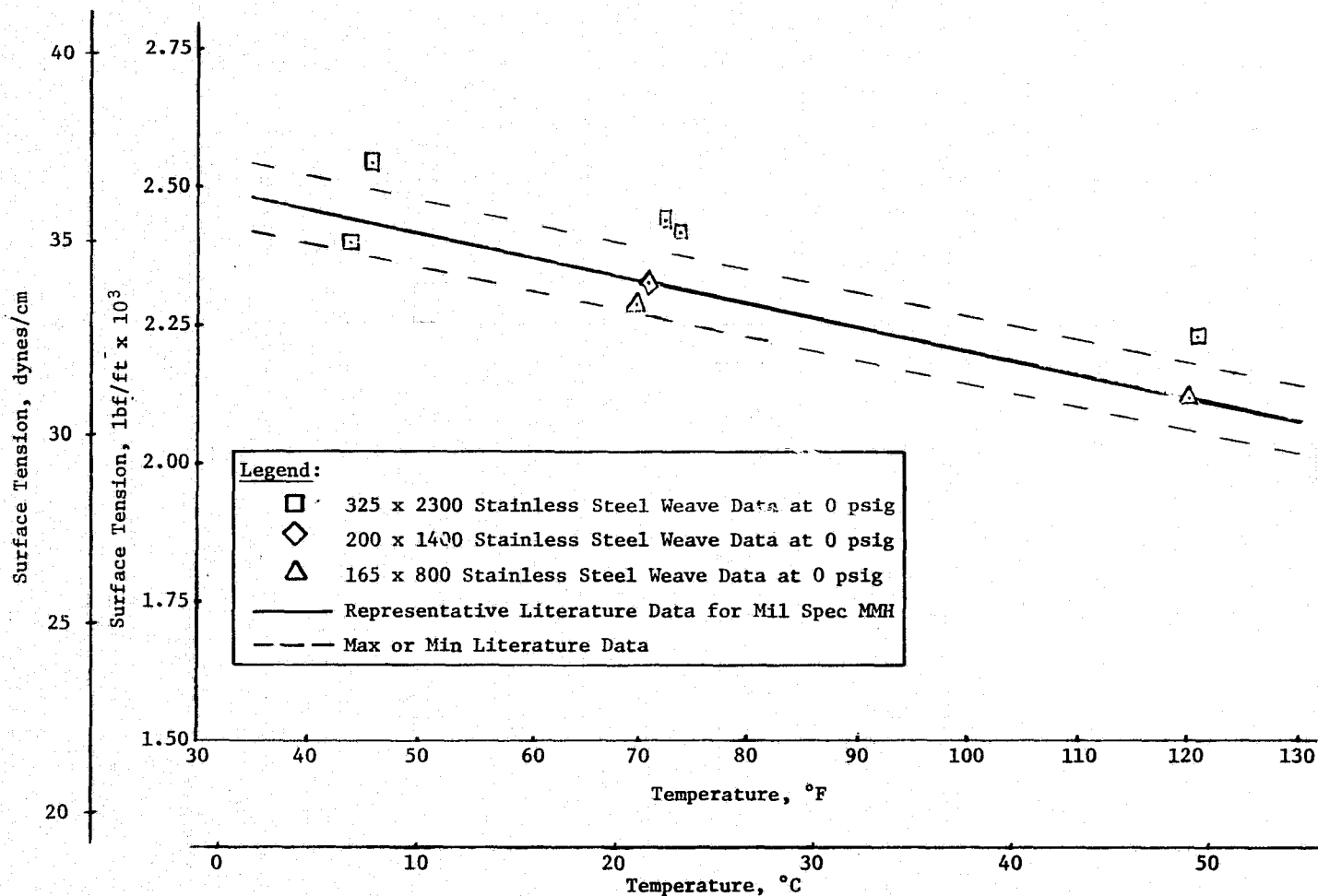


Figure IV-8 Comparison of Published and Measured Surface Tension Data for MIL Spec MMH

IV-10

Figure IV-9

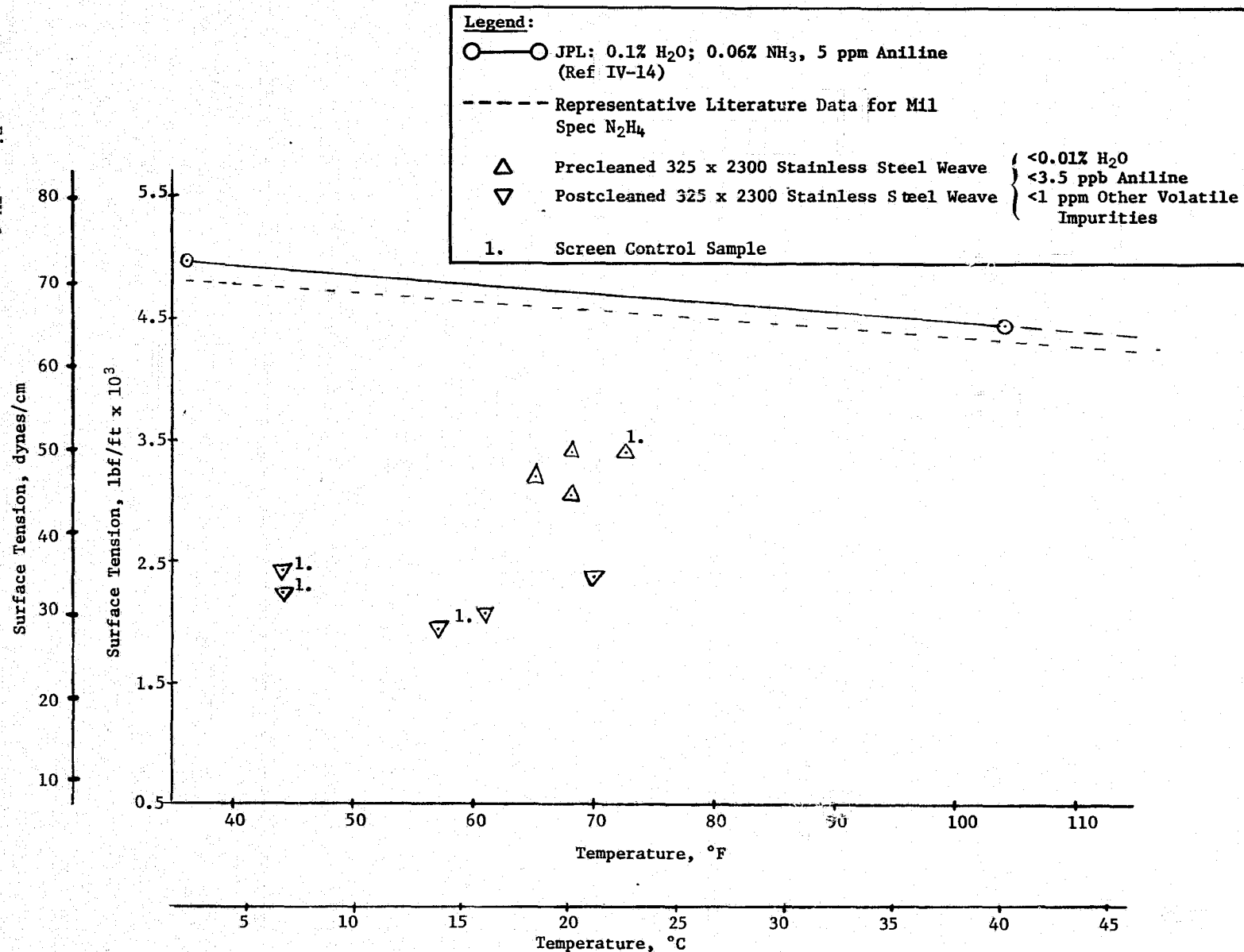


Figure IV-9

Comparison of Published and Measured Surface Tension Data for Purified N<sub>2</sub>H<sub>4</sub>

Figure IV-10

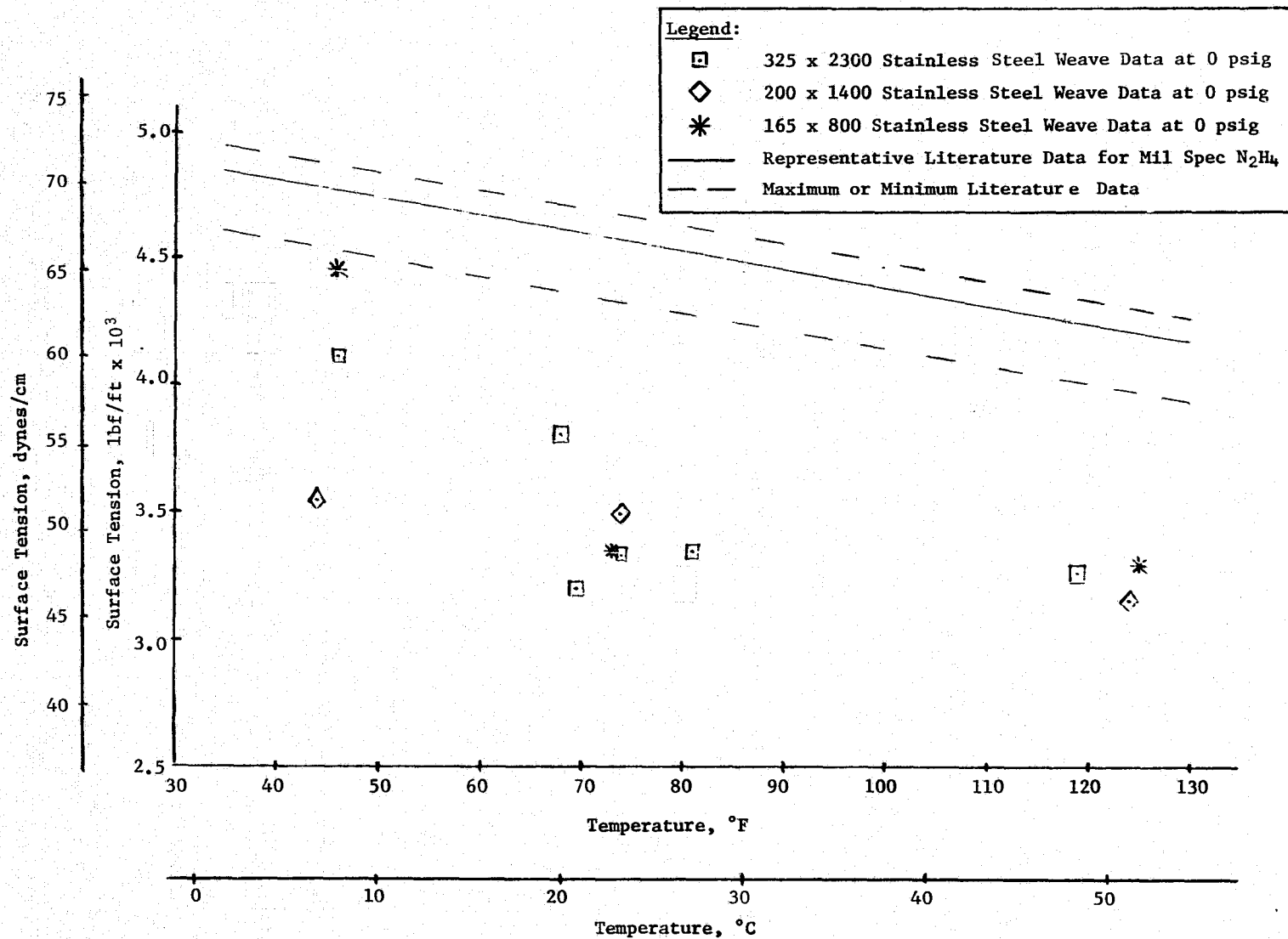


Figure IV-10 Comparison of Published and Measured Surface Tension Data for MIL Spec  $N_2H_4$

The test data are presented in terms of propellant surface tension. The standard conversion equation

$$\sigma_{\text{propellant}} = \sigma_{\text{referee fluid}} \times \frac{\text{bubble point in propellant}}{\text{bubble point in referee liquid}}$$

was used to calculate the surface tension of the propellant from the measured bubble points with the referee liquid and the propellant and the known surface tension of the referee liquid.

As a result of the anomalous data on screen bubble point in hydrazine, additional testing was conducted under a Martin Marietta IR&D test program to evaluate the surface tension of  $\text{N}_2\text{H}_4$ , its contact angle with metals, and its bubble point with 325 x 2300 fine-mesh stainless steel screen (Ref IV-15). The IR&D tests showed that high contact angles will be obtained with  $\text{N}_2\text{H}_4$  unless special metal surface cleaning methods are employed. Bubble point is a function of both surface tension and contact angle; increasing the contact angle decreases the bubble point.

The contact angle test data are presented in Table IV-1. The various cleaning procedures used on the test sample are listed in Table IV-2. The methods found to be most effective in reducing the contact angle were flame cleaning and chromic acid cleaning. These cleaning methods were used to clean 325 x 2300 fine-mesh screen and excellent bubble point data were obtained. These IR&D bubble point data are presented in Figure IV-11.

As a result of the Task III effort, representative propellant physical property data were selected for use with the subscale testing (Task IV) and full-scale design and testing (Task V) activities. These selected physical property data are presented in Figures IV-12 thru IV-14.

Table IV-1 Measured Contact Angles

Sample	Stainless Steel Surface	Propellant	Cleaning Procedure	Test No.	Drop No. on Surface	$\theta$ , deg
AA	304L	MIL Spec $N_2H_4$	I	1	1	18
					2	14
				2	1	38
				3	1	15
				4	1	15
BB	304L	MIL Spec $N_2H_4$	II	1	1	31
				2	1	33
				3	1	26
				4	1	16
			I		2	26
CC	304L	MIL Spec $N_2H_4$	III	1	1	4
				2	1	7
1	304L	MIL Spec $N_2H_4$	VI	1	1	44
				2	1	21
				3	1	31
				4	1	14
				5	1	11
					2	11
2	304L	MIL Spec $N_2H_4$	V	1	1	20
3	304L	MIL Spec $N_2H_4$	VII	1	1	13
				2	1	10
4	304L			3	1	17
				4	1	14
5	304L			5	1	14
6	304L			6	1	13
					2	12
7	304L	MIL Spec $N_2H_4$	X	1	1	7
					2	6
8	304L			2	1	8
					2	7
9	304L			3	1	9
					2	6

Table IV-1 (cont)

Sample	Metal Surface	Propellant	Cleaning Procedure	Test No.	Drop No. on Surface	$\theta$ , deg
10	304L SS	MIL Spec $N_2H_4$	VIII	1	1	42
				2	1	55
			IX		2	45
				3	1	37
					2	50
M1	304L SS	MIL Spec MMH	IX	1	1	3
					2	3
				2	1	1
					2	2
					3	5
			VIII		4	2
				3	1	6
					2	7
					3	5
H1	304L SS	MIL Spec $N_2H_4$	IX	1	1	35
					2	35
				2	1	46
					2	39
H2	6Al-4V Ti	MIL Spec $N_2H_4$	IX	1	1	34
					2	34
				2	1	26
					2	29
				3	1	25
					2	27
H3	6Al-4V Ti	MIL Spec $N_2H_4$	III	1	1	4
					2	4
				2	1	4
H4	6061 Al	MIL Spec $N_2H_4$	IX	1	1	17
					2	32
				2	1	7
					2	13
H5	6061 Al	MIL Spec $N_2H_4$	III	1	1	3
					2	1

Table IV-1 (concl)

Sample	Metal Surface	Propellant	Cleaning Procedure	Test No.	Drop No. On Surface	$\theta$ , deg
H6	6Al-4V Ti	MIL Spec N <sub>2</sub> H <sub>4</sub>	X	1	1	4
					2	4
					3	4
H7	6Al-4V Ti			2	1	4
					2	8
H8	6Al-4V Ti			3	1	7
					2	4
H9	6Al-4V Ti			4	1	7
H10	6061 Al	MIL Spec N <sub>2</sub> H <sub>4</sub>	X VIII	1	1	6
				2	1	19
H11	6061 Al			3	1	4
			X		2	4

Table IV-2 Metal Sample Cleaning Procedures

<p><u>Procedure 1</u></p> <ol style="list-style-type: none"> <li>1) Concentrated <math>\text{HNO}_3</math>, 12°C (70°F)</li> <li>2) Tap <math>\text{H}_2\text{O}</math> Rinse</li> <li>3) Isopropanol Rinse</li> <li>4) <math>\text{GN}_2</math> Dry in Air</li> </ol> <p><u>Procedure III</u></p> <ol style="list-style-type: none"> <li>1) Concentrated <math>\text{HNO}_3</math>, 21.1°C (70°F)</li> <li>2) Tap <math>\text{H}_2\text{O}</math> Rinse</li> <li>3) <math>\text{GN}_2</math> Dry in Air</li> </ol> <p><u>Procedure III</u></p> <ol style="list-style-type: none"> <li>1) Soap/<math>\text{H}_2\text{O}</math> Solution, 21.1°C (70°F)</li> <li>2) Tap <math>\text{H}_2\text{O}</math> Rinse</li> <li>3) Concentrated <math>\text{HNO}_3</math>, 21.1°C (70°F)</li> <li>4) Tap <math>\text{H}_2\text{O}</math> Rinse</li> <li>5) Isopropanol Rinse</li> <li>6) Propane/Air Flame</li> <li>7) Air Cool</li> </ol> <p><u>Procedure IV</u></p> <ol style="list-style-type: none"> <li>1) Diversey 909 Alkaline Cleaner, 21.1°C (70°F)</li> <li>2) Tap <math>\text{H}_2\text{O}</math> Rinse</li> <li>3) Isopropanol Rinse</li> <li>4) Heat in Air to Dry</li> </ol> <p><u>Procedure V</u></p> <ol style="list-style-type: none"> <li>1) 100°C (212°F) Diversey 909 Solution</li> <li>2) 100°C (212°F) Distilled <math>\text{H}_2\text{O}</math> Rinse</li> <li>3) Air Dry</li> </ol>	<p><u>Procedure VI</u></p> <ol style="list-style-type: none"> <li>1) 100°C (212°F) Diversey 909 Solution</li> <li>2) 20°C (68°F) Distilled <math>\text{H}_2\text{O}</math> Rinse</li> <li>3) Concentrated <math>\text{HNO}_3</math>, 21.1°C (70°F)</li> <li>4) 100°C (212°F) Distilled <math>\text{H}_2\text{O}</math> Rinse</li> <li>5) Air Dry</li> </ol> <p><u>Procedure VII</u></p> <ol style="list-style-type: none"> <li>1) Procedure VI</li> <li>2) Soak 3 to 4 Days in Propellant To Be Tested</li> <li>3) <math>\text{GN}_2</math> Dry in Air</li> </ol> <p><u>Procedure VIII</u></p> <ol style="list-style-type: none"> <li>1) Concentrated <math>\text{HNO}_3</math>, 21.1°C (70°F)</li> <li>2) 100°C (212°F) Distilled <math>\text{H}_2\text{O}</math> Rinse</li> <li>3) Freon TF Rinse</li> <li>4) Air Dry</li> </ol> <p><u>Procedure IX</u></p> <ol style="list-style-type: none"> <li>1) Concentrated <math>\text{HNO}_3</math>, 21.1°C (70°F)</li> <li>2) 100°C (212°F) Distilled <math>\text{H}_2\text{O}</math> Rinse</li> <li>3) Isopropanol Rinse</li> <li>4) Heat in Air to Dry</li> </ol> <p><u>Procedure X</u></p> <ol style="list-style-type: none"> <li>1) 100°C (212°F) Chromic Acid Cleaning Solution (<math>\text{K}_2\text{CrO}_4/\text{H}_2\text{O}</math> Solution Dissolved in Concentrated <math>\text{H}_2\text{SO}_4</math>)</li> <li>2) Distilled <math>\text{H}_2\text{O}</math> Rinse and Soak, 20°C (68°F)</li> <li>3) Heat in Air to Dry</li> </ol>
---	---



Figure IV-11

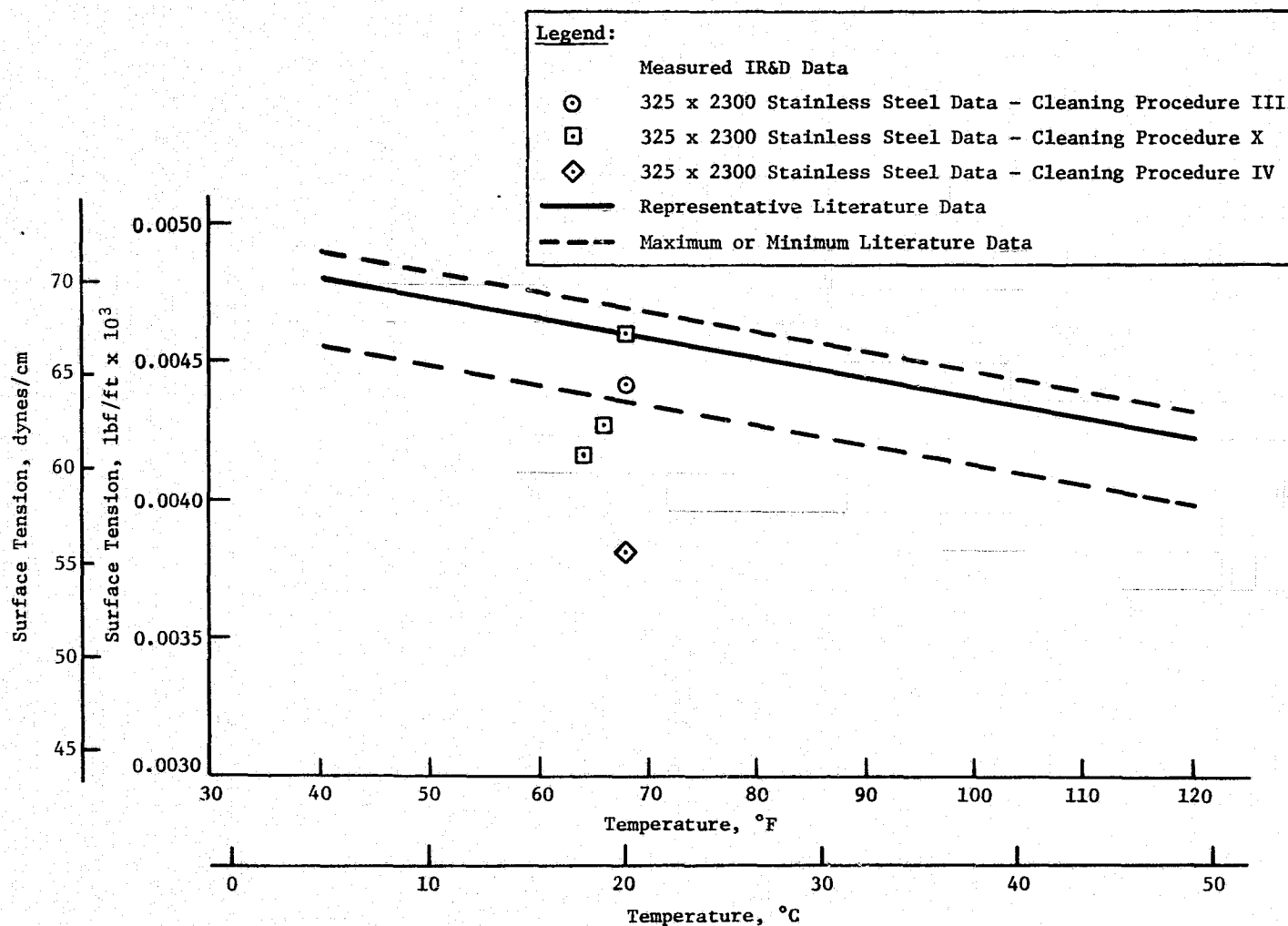


Figure IV-11  
Comparison of Published and Measured Surface Tension Data for MIL Spec  $N_2H_4$  (IR&D Data)

Figure IV-12

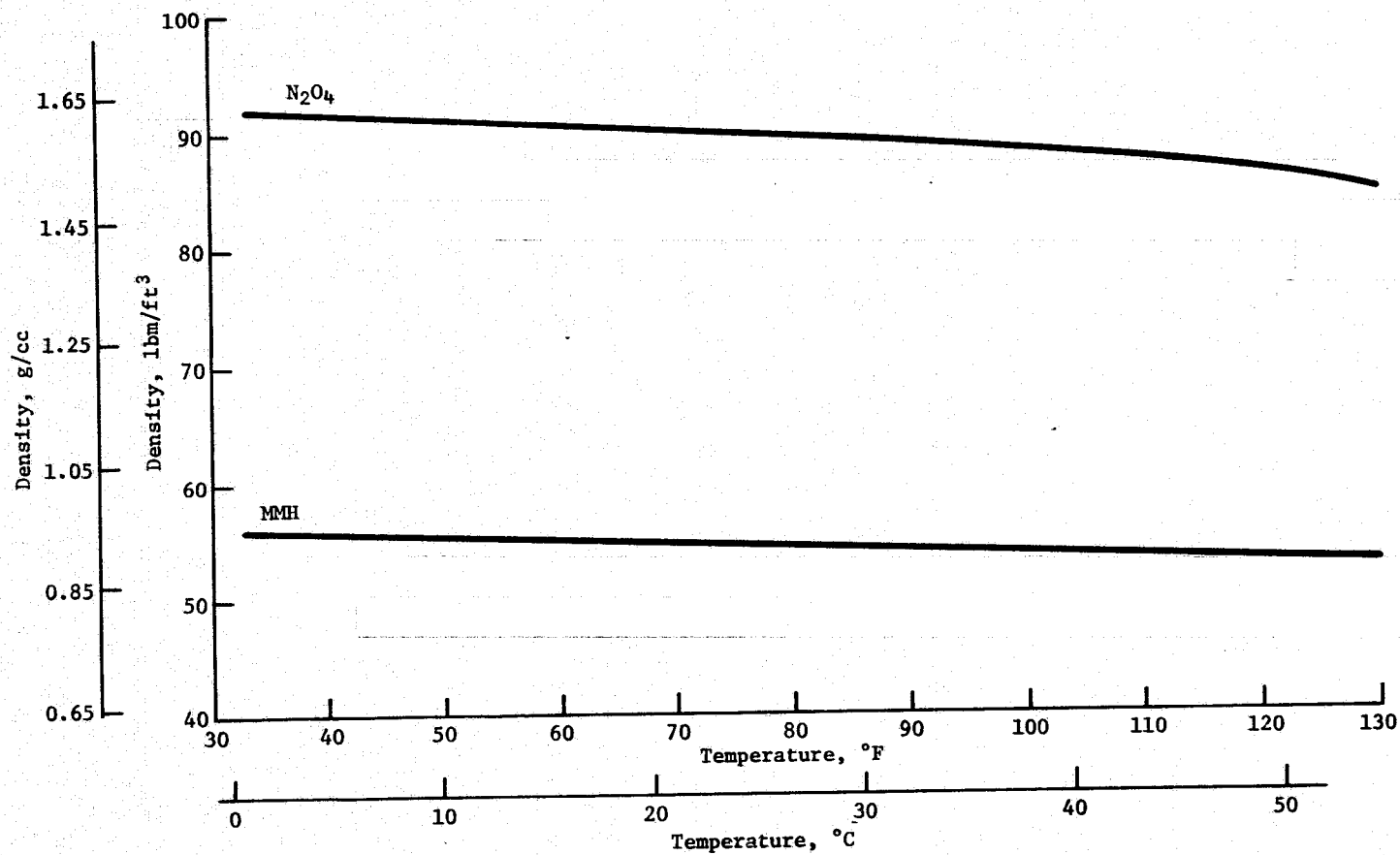


Figure IV-12 Density Data Selected for RCS Design

Figure IV-13

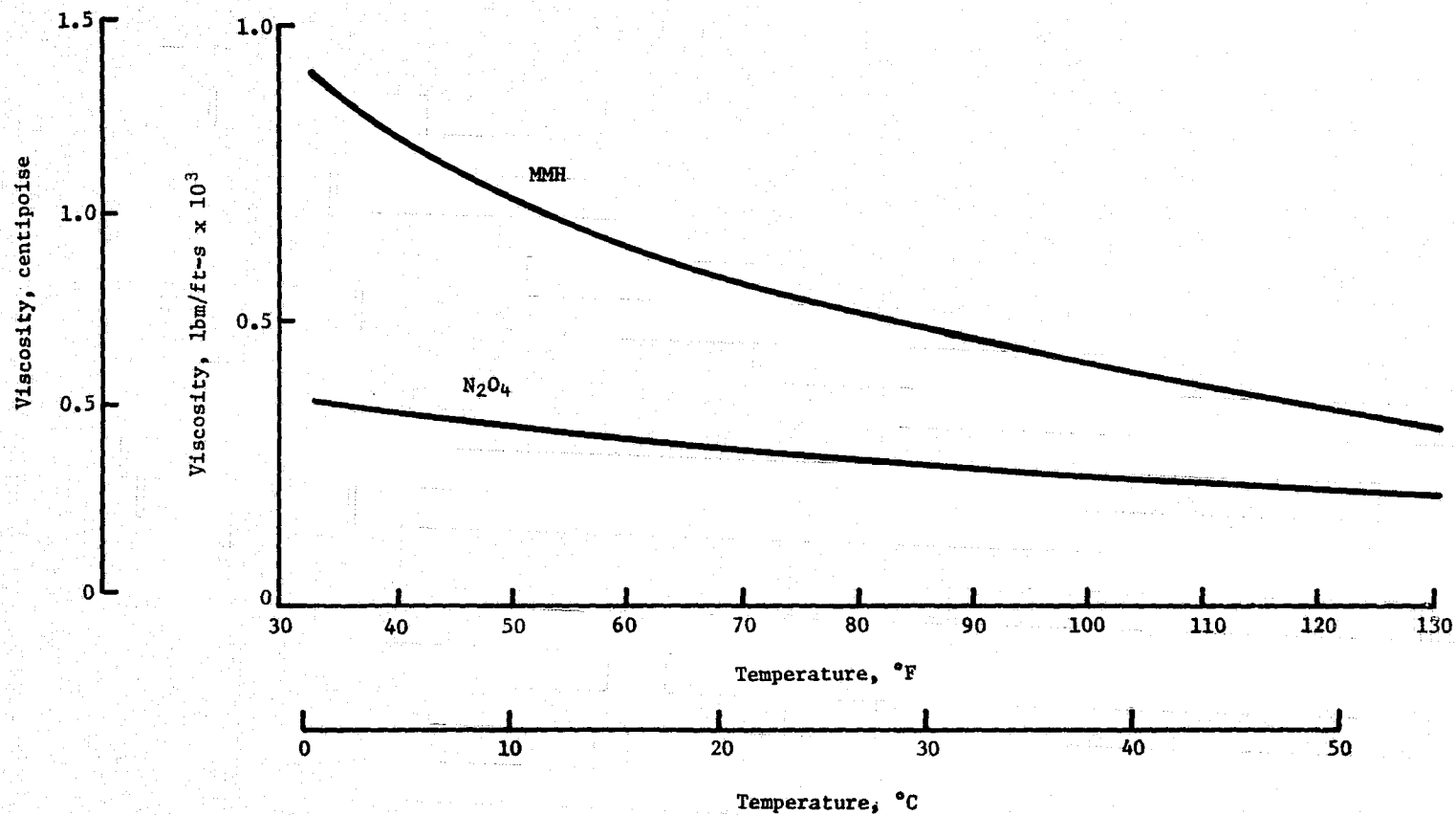


Figure IV-13 Viscosity Data Selected for RCS Design

Figure IV-14

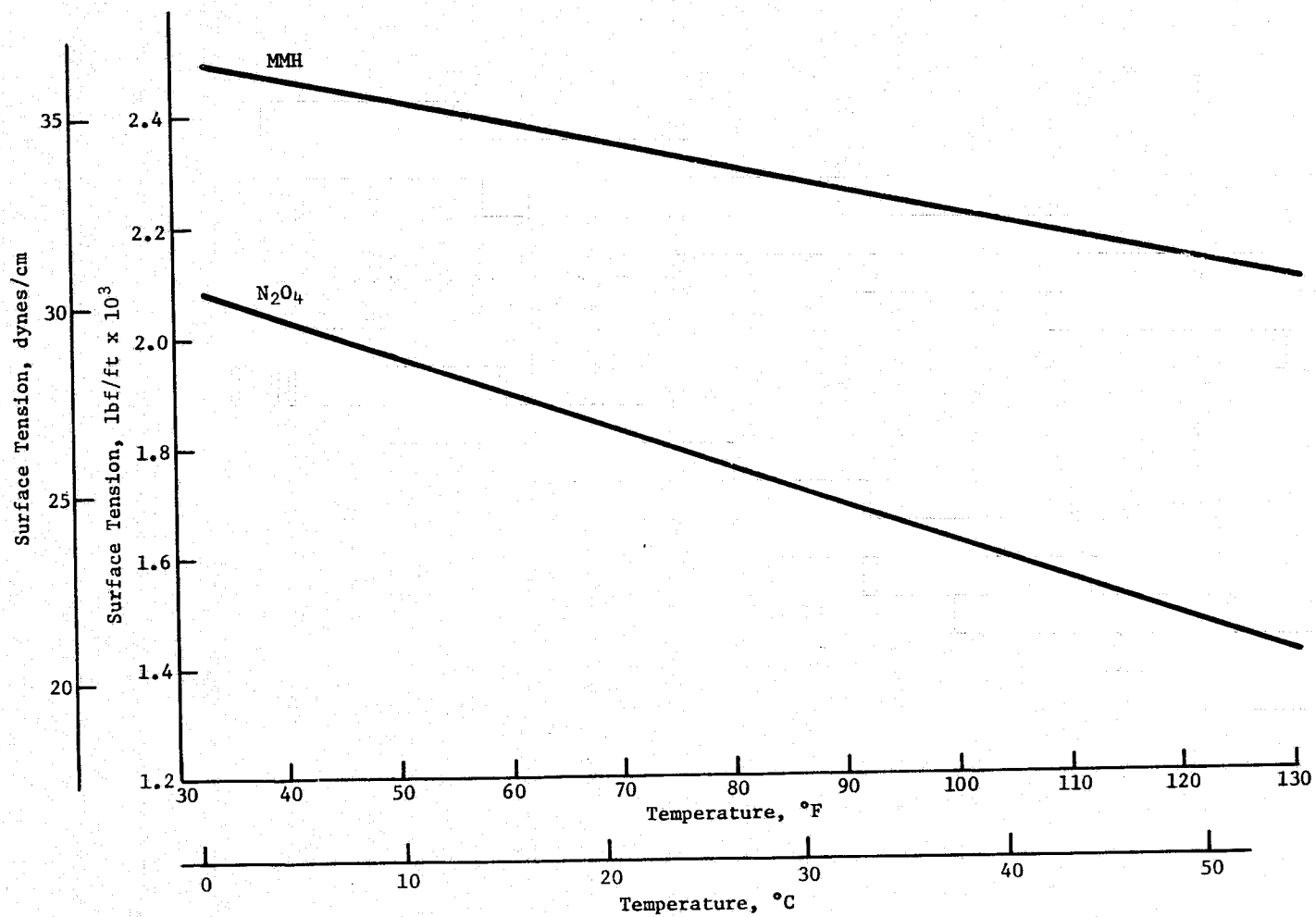


Figure IV-14 Surface Tension Data Selected for RCS Design

## V. PRELIMINARY DESIGN AND SIMILITUDE TESTING

At the beginning of this task (Task IV), the selected acquisition concept was recommended to and approved by NASA. A preliminary design of the selected concept was accomplished to specifically define the device configuration. A one-third scale model of the preliminary design was fabricated and tested. Expulsion under one-g and high-g acceleration, with vibration and with pulsed flow, was performed with this model. Slosh tests were conducted. Other tests using special models were also accomplished. The preliminary design was then updated based on the results of these tests.

### A. RECOMMENDATION OF PREFERRED CONCEPT

The analysis of Task II compared many different acquisition/expulsion system designs for the SS/RCS. Results of this comparison indicated that a compartmented tank with single-layer fine-mesh screen channels was the preferred concept. Also, a single design was recommended for forward and aft, and fuel and oxidizer tanks since additional development and qualification cost could not be justified.

The concept recommended to and approved by NASA-JSC is shown in Figure III-5. At this point it was only an acquisition system concept; the number of channels and the barrier location are not indicative of a detailed design.

## B. PRELIMINARY DESIGN

The recommended concept was a compartmented tank with a channel system in the upper and lower compartments. The selected concept was optimized to establish a preliminary design capable of meeting the RCS requirements. The design parameters established were:

- 1) Number of channels;
- 2) Channel size and shape;
- 3) Barrier position;
- 4) Barrier angle;
- 5) Size and number of screen windows;
- 6) Position of pressurization and outflow lines.

The computer program optimized items one, two, and three listed above. Hand analysis was required to determine the remaining design parameters.

The design approach included:

- 1) Safety factor of 1.5 on bubble points;
- 2) A common design for forward and aft tanks;
- 3) Propellant temperature of 21°C (70°F);
- 4) Complete draining of the upper compartment in low-g;
- 5) Common channel cross section in upper and lower compartments;
- 6) Single-layer 325 x 2300 Dutch-twill screen.

The following subsections discuss in more detail the preliminary design and how it evolved.

### 1. Channel Geometry and Barrier Position

The important mission phase for defining channel geometry and barrier position is low-g on-orbit depletion. The computer model was used to define these parameters by optimizing on-orbit expulsion efficiency. The study encompassed 4-, 6-, and 8-channel systems with different cross-sectional flow areas and channel aspect ratios. The computer analysis considered only

the outlet compartment of the tank and assumed the pressurization compartment was completely drained of propellant. Channel optimization was performed with a barrier height of 34.5%, and the effect of decreased barrier height was determined once the channel size and number of channels were selected. Both +X axial and +Z lateral accelerations were considered; however, lateral depletion under 0.231 g proved to be the worst design condition.

Two cases were considered with lateral depletion: (1) liquid puddled over one channel,  $\theta = 0$ , and (2) liquid puddled between two channels,  $\theta = \pi/4$ ,  $\pi/6$ , or  $\pi/8$ , depending on the number of channels. Designing for both these orientations assured that the system will perform as required under the worst possible liquid orientation. For a given tank geometry, channel number, and channel size, the point of intersection on an expulsion efficiency versus propellant mass flow rate curve, as shown in Figure V-1, represents an optimum design point since expulsion efficiency is maximized for both orientations ( $\theta = 0$  and  $\theta = \pi/n$ ).

Computer results are shown in Figures V-1 and V-2 for an 8-channel and 4-channel system, respectively. Each graph represents a constant cross-sectional area that was optimized for each number of channels by computer analysis. Two sets of curves are shown, corresponding to barrier positions of 34.5% and 16.5% respectively. Curves A, B, and C represent different aspect ratios for  $\theta = 0$  and  $\theta = \pi/8$  or  $\pi/4$  (liquid puddled over a single channel or between two channels) at a barrier position of 34.5%. Curve D shows performance for the same channel geometry as Curve B, but at a barrier position of 16.5%. Note that the locus of intersection points (dashed lines) is close to the design flow rate represented by the dotted line. This determined the optimum channel cross-sectional area for a given number of channels. Other significant trends indicated by these graphs are the decrease in residual propellant with increasing aspect ratio and decreased barrier level (Curve D). Analysis of this type of data for varying cross-sectional flow areas and 4-, 6-, and 8-channel systems produced the following conclusions:

- 1) For a given number of channels, the optimum cross-sectional area is determined when the locus of the intersection points ( $\theta = 0$ ,  $\theta = \pi/n$ ) for varying aspect ratios is nearest the design flow rate;
- 2) For low liquid volumes near tank depletion, positioning the channel along the tank wall, configuration A, gave higher expulsion efficiency than orienting the channel toward the tank center, configuration B (Fig. V-3);
- 3) For a constant channel cross-sectional area, increasing channel aspect ratio yielded increased expulsion efficiency;

V-4

Figure V-1

Residual Propellant at Breakdown, % Tank Volume

**Note:** 8 channels, 325 x 2300 Dutch-twill,  
0.231-g lateral acceleration,  
Barrier level = 34.5%,  
Channel cross section = 3.67 in.<sup>2</sup>,  
Channel dimensions, in.

Curve	Width	Depth
A	7.35	0.5
B	5.25	0.7
C	4.08	0.9
D*	5.25	0.7

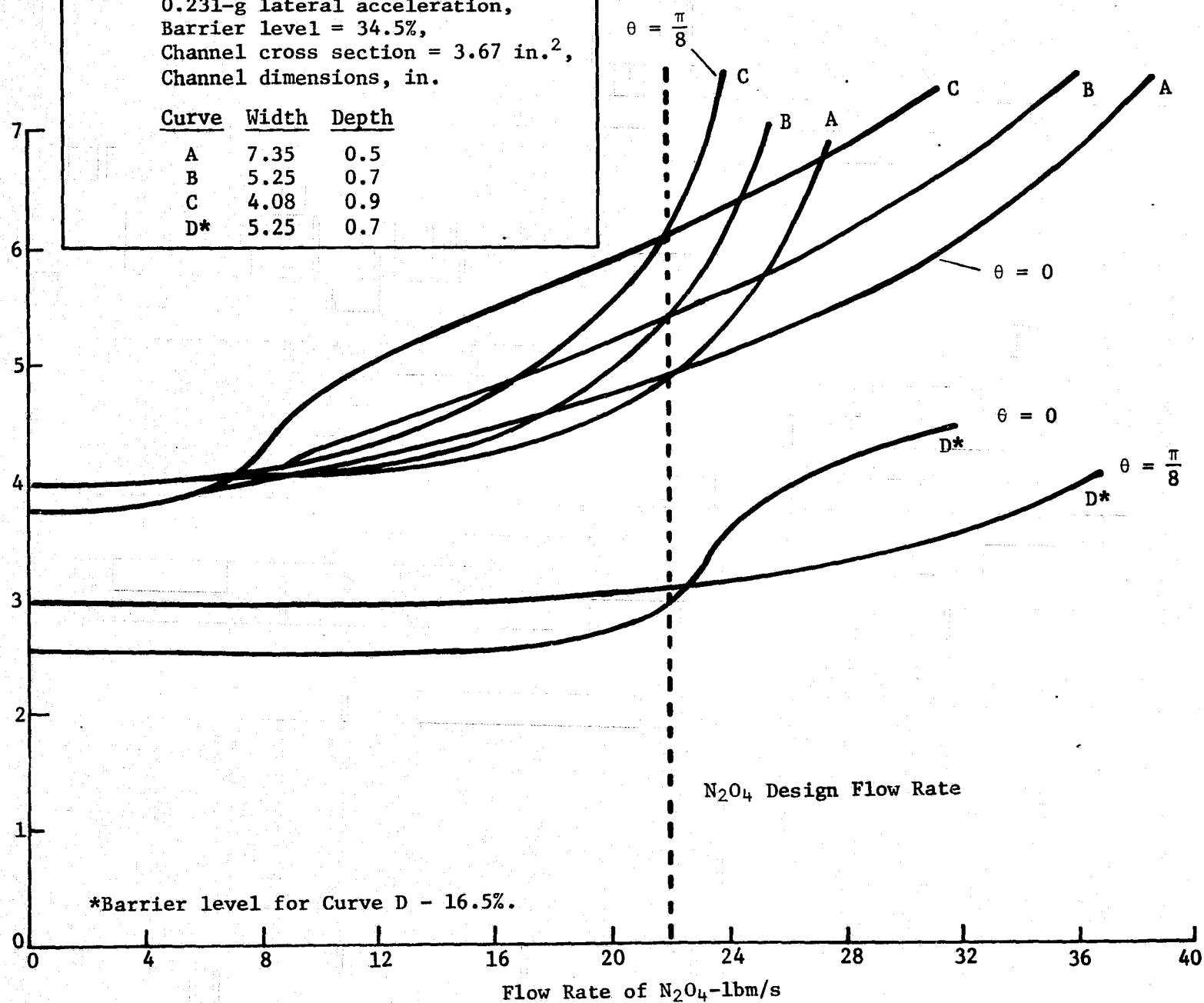


Figure V-1 Computer Program Results for 8-Channel System



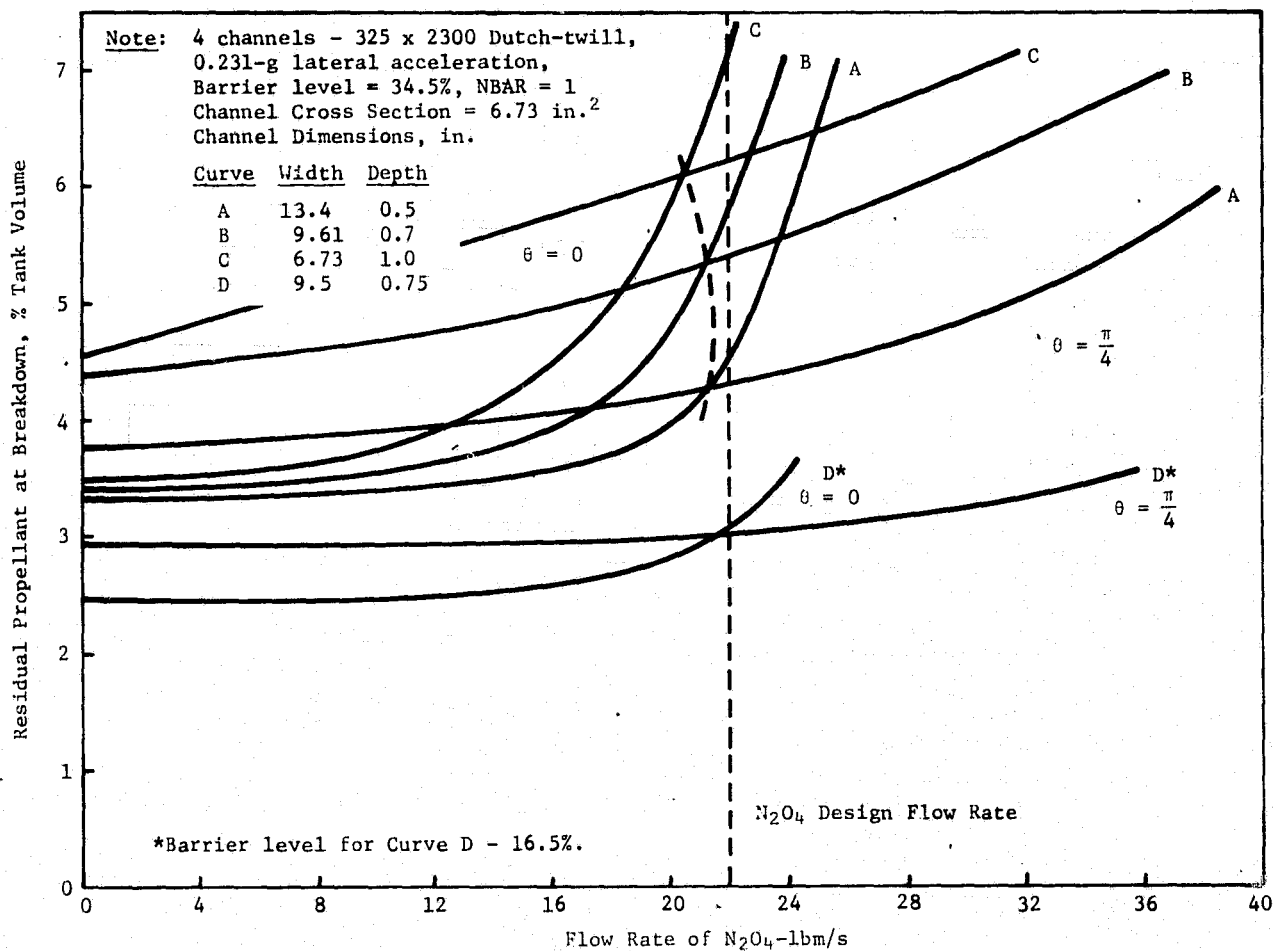


Figure V-2 Computer Program Results for 4 Channel System

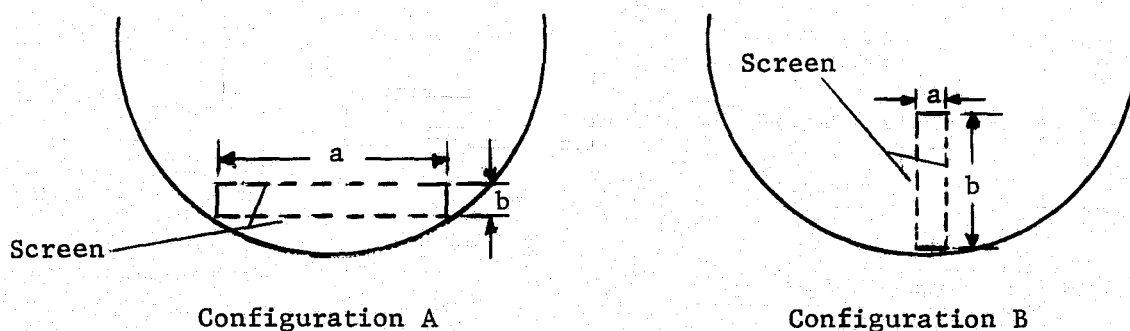


Figure V-3 Channel Configuration

- 4) Optimized 4- and 8-channel systems gave about the same expulsion performance and were better than a 6-channel system;
- 5) Lowering the barrier from the 34.5% to 16.5% level increased the low-g expulsion efficiency approximately 2%;
- 6) The optimum channel geometry is not sensitive to barrier position over the range of channel sizes and barrier heights considered.

As a result of this study a 4-channel system with 22.9 x 1.9 cm (9 1/2 x 3/4 in.) (a x b) channels was selected over the 8-channel design due to weight and fabrication considerations. In selecting channel geometry, conflicting effects on aspect ratio were noted due to performance and fabrication considerations. Increased aspect ratio increased performance. However, wider and thinner channels became more difficult to fabricate and adequately support to prevent a reduction in channel flow area as the screen surfaces are displaced toward the center of the channel when pressurized. Additional support also incurs additional structural material mass. A screen deflection analysis was conducted for the channel sizes of interest based on the work of References V-1 and V-2. Results indicated that a minimum thickness of 1.8 cm (0.7 in.) could be tolerated for a 4-channel system. Therefore, a 24.4 cm (9.6 in.) by 1.8 cm (0.7 in.) channel cross section was selected for the preliminary design.

Barrier positioning was dictated by three considerations: (1) outlet compartment expulsion efficiency, (2) ability to completely drain the upper (pressurization) compartment, and (3) vibration effects on liquid/vapor interface stability at the screen. Items 1 and 3 suggest a lower barrier position, while item 2 tends to increase the barrier height. With an initial barrier position of 34.5%, the channels below the barrier were not stable in the on-orbit environment. Assuming a minimum depletion level of 13% of loadable propellant for the aft tank, a barrier position at a level corresponding to 14% of the tank volume assures the channels are hydrostatically stable with an omnidirectional vibration input of 1.9 g rms (2.4% ullage in outlet compartment). The effect on forward tank expulsion efficiency is an increase of approximately 2.5% over that with the barrier at the 34.5% level. The impact of lowering the barrier on requirements for draining the upper compartment is shown in Figure V-4. This figure shows the quality of flow required from the upper compartment to the lower compartment as a function of channel size (barrier level of 34.5%). For the selected channel size, a quality of only 9% is required after the upper channels breakdown. By decreasing the barrier level to 14%, the quality required is increased to 22.5%

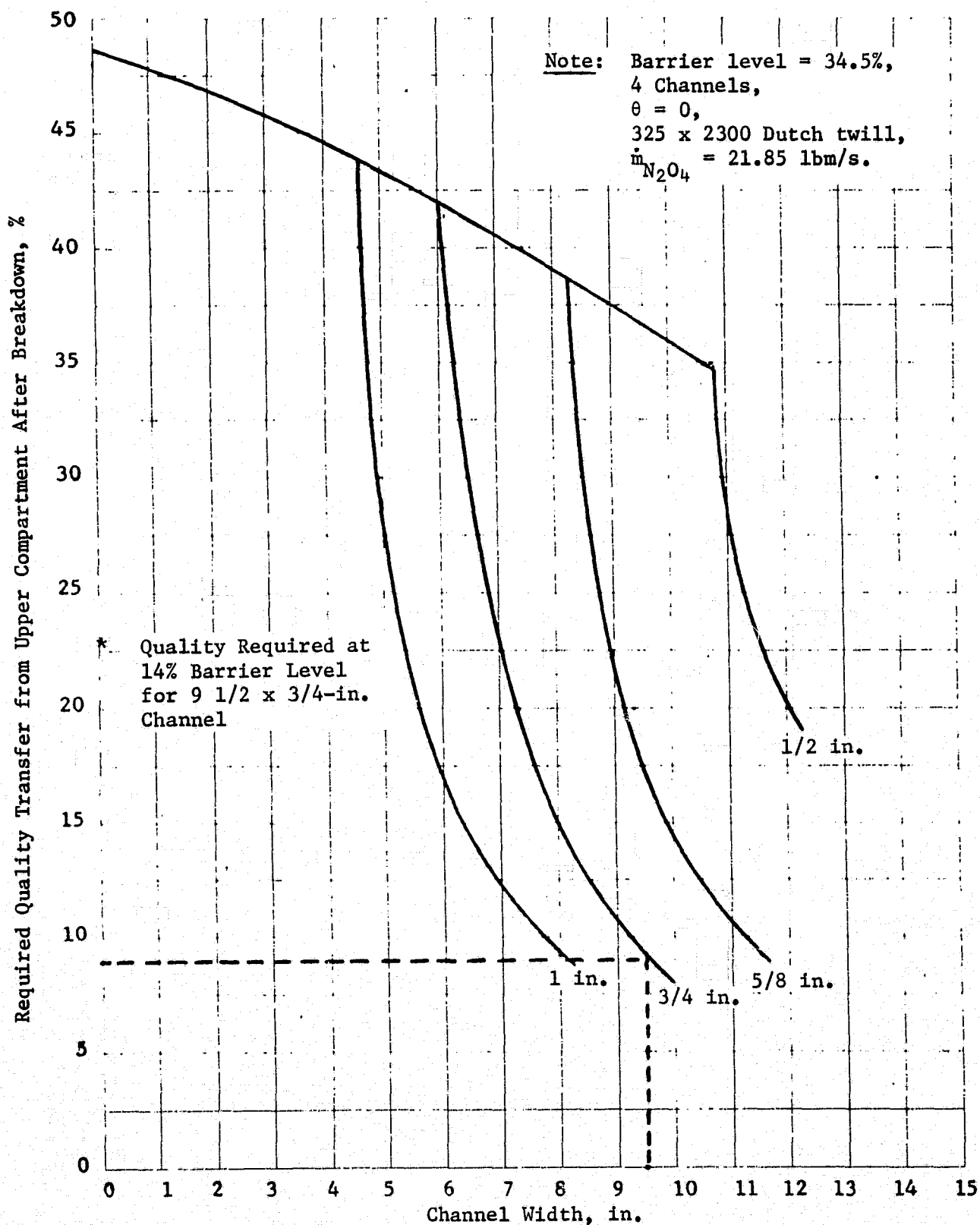


Figure V-4  
Quality Requirements for Propellant Flow from Upper to Lower  
Compartment

for the design configuration. Since this requirement does not appear to be a problem, the barrier level of 14% of tank volume was chosen.

## 2. Barrier Angle and Outlet Positioning

The barrier inclination angle  $\theta$  was chosen on the basis of reentry terminal drain, +1-g vertical drain, and RTLS requirements. Increasing  $\theta$  increases reentry expulsion efficiency but makes +1-g vertical draining and RTLS draining more difficult.

Since a reentry expulsion efficiency of 98% (independent of the device) was desired, the smallest angle that achieved this performance was chosen. Figure V-5 shows a sketch of the geometry considerations for barrier angle calculation. The analysis assumed the reentry acceleration puddled liquid 18 deg above the +Z axis and the device was not in the tank except for the outlet positioned on the +Z side of the barrier. The lower compartment volume was assumed to be 14%, as determined by vibration analysis, with a height of 22.9 cm (9 in.). Results are tabulated in Table V-1 for several values of  $a$ , defined as the distance of the barrier-tank intersection point below the +Z axis (Fig. V-5). For an expulsion efficiency of 98%, an angle of 16.5 deg or greater was required. This angle was not considered too large to make +1-g draining performance unacceptable. Analysis of RTLS draining indicated that part of the screen window, described in the following section, would be exposed. However, considering that the window was internal to the upper screen system and screens could be relied on during RTLS abort, RTLS was not considered a problem for the barrier design.

*Table V-1 Reentry Expulsion Efficiency for Various Barrier Angles*

$a$ , cm (in.)	Barrier Angle $\theta$ , deg	Reentry Expulsion Efficiency, %
10.2 (4)	19.5	98.4
12.7 (5)	16.5	98.0
15.2 (6)	13.2	97.1
20.3 (8)	6.7	94.6
25.4 (10)	0	90.6

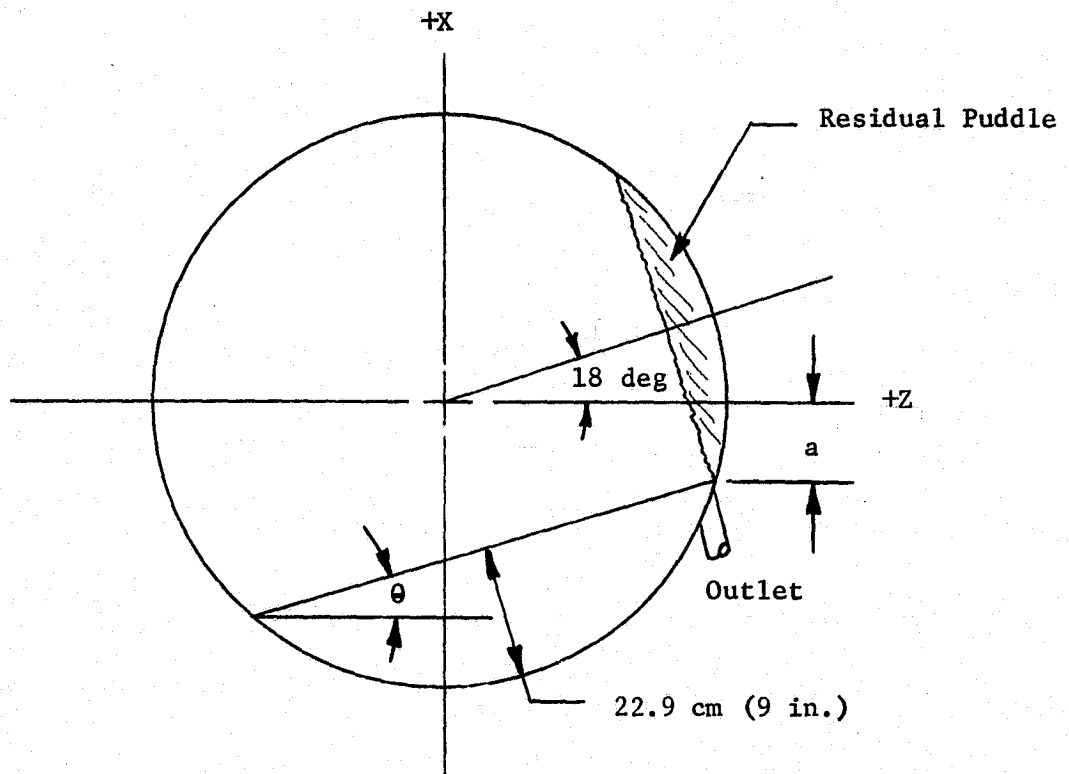


Figure V-5 Geometry for Barrier Angle Determination

The foregoing analysis did not consider the channel/tank outlet geometry. Design of the tank outlet/channel interface revealed that additional liquid would be left during reentry drain since the entrance to the outlet protruded inside the tank wall. With the outlet coming directly out of the +Z side of the tank, the reentry expulsion efficiency was reduced to 96.5%. To help reduce residual propellant during reentry and increase on-orbit performance when liquid is settled against the barrier, a spherical rather than flat barrier was chosen. This was also advantageous from a structural standpoint. A barrier with a radius of 5 times the tank radius resulted in reentry performance of 97.2% for a constant compartment volume and angle.

### 3. Screen Window

One or more penetrations through the barrier were required for flow of liquid from the top to bottom compartment. The openings in the barrier must be covered with screen to provide stability in the on-orbit environment, however. Screen on multiple penetrations may dry out during certain mission events and reduce the ability of the system to deplete the upper compartment. This is especially true during reentry terminal drain, where any loss of pressure differential between the two compartments by dry out of a screen window away from the outlet would cause the bottom compartment to drain before the top compartment was depleted, because the window near the outlet would require a finite pressure differential to pass liquid through the screen. Consequently, a single window design was chosen.

Placement of the window was dictated by the requirement that reentry be accomplished independent of the screen device. This necessitated placing the barrier window as near to the tank outlet as possible. The resulting location was on the +Z axis, adjacent to the tank wall. This allowed the window to be covered by liquid on both sides until the tank was almost depleted of liquid during reentry. Considerations that dictated the detail design of the window follow.

- 1) Barrier structural considerations because of pressure differential associated with flow through the window;
- 2) Sufficient area to allow for some screen clogging;
- 3) Hydrostatic stability during low-g phases of the mission.

Because of the high ratio of bubble point to flow loss through the screen, 165 x 800 Dutch-twill screen was used for the window. A total window area of  $516 \text{ cm}^2$  ( $80 \text{ in.}^2$ ) gave a pressure drop of  $0.14 \text{ N/cm}^2$  (0.2 psi) and  $0.28 \text{ N/cm}^2$  (0.4 psi) for  $\text{N}_2\text{O}_4$  and MMH, respectively. These low pressure differentials had a high safety

factor for structural and clogging considerations. The maximum window dimension was 38.1 cm (15 in.), which met the stability requirements for fuel and oxidizer at 0.231 g.

#### 4. Acquisition System Design

The RCS preliminary design is shown in Figure V-6. Single layer 325 x 2300 Dutch-twill screen is used throughout the design with the exception of the screen window. The same size and number of channels are used in the lower and upper compartments. Channel manifolds that measure 24 cm (9.5 in.) x 24 cm (9.5 in.) also employ fine mesh screen to gain additional entrance area into the channel systems. The mass of the entire capillary acquisition/expulsion device, including the barrier, was calculated as 10.0 kg (22 lbm).

The 1/3-scale model fabricated and tested during Task IV was geometrically scaled to simulate the design presented there. A summary of performance for various mission phases is contained in Table V-2.

*Table V-2 RCS Preliminary Design Performance*

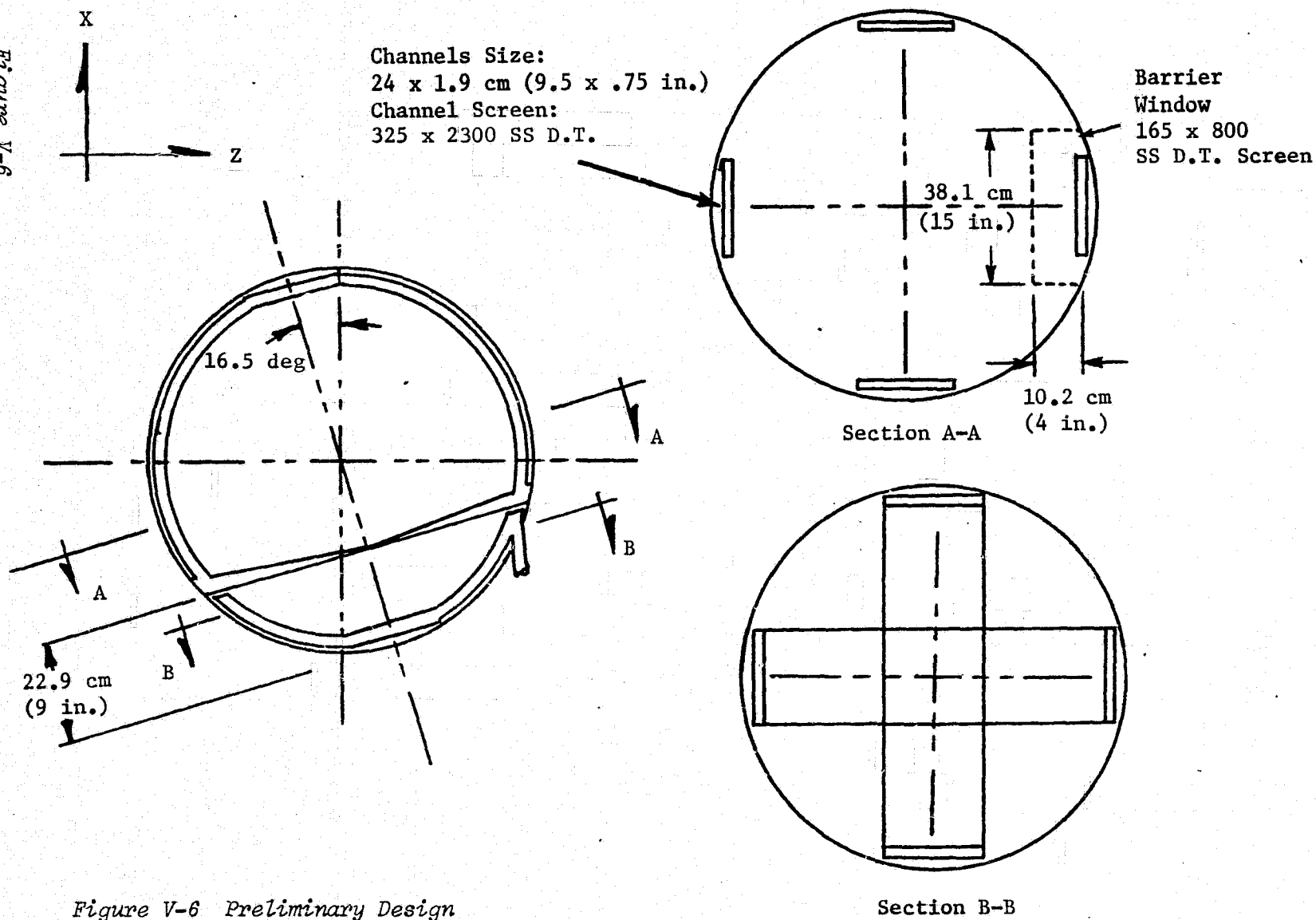
Tank	EXPULSION EFFICIENCY, %		
	On-Orbit Depletion	Reentry	
		With Device	Without Device
Oxidizer Forward Aft	96.6	98	97.2
Fuel Forward Aft	96.6	98	97.2

#### C. TEST SYSTEM FABRICATION

Test hardware to support the verification test program may be divided into two categories: subscale model and test systems support. The subscale model was fabricated as part of Martin Marietta IR&D Task D-14D, Capillary Device Fabrication, to assess specific design/fabrication techniques associated with a surface tension design of this complexity. The model was used

V-12

Figure V-6





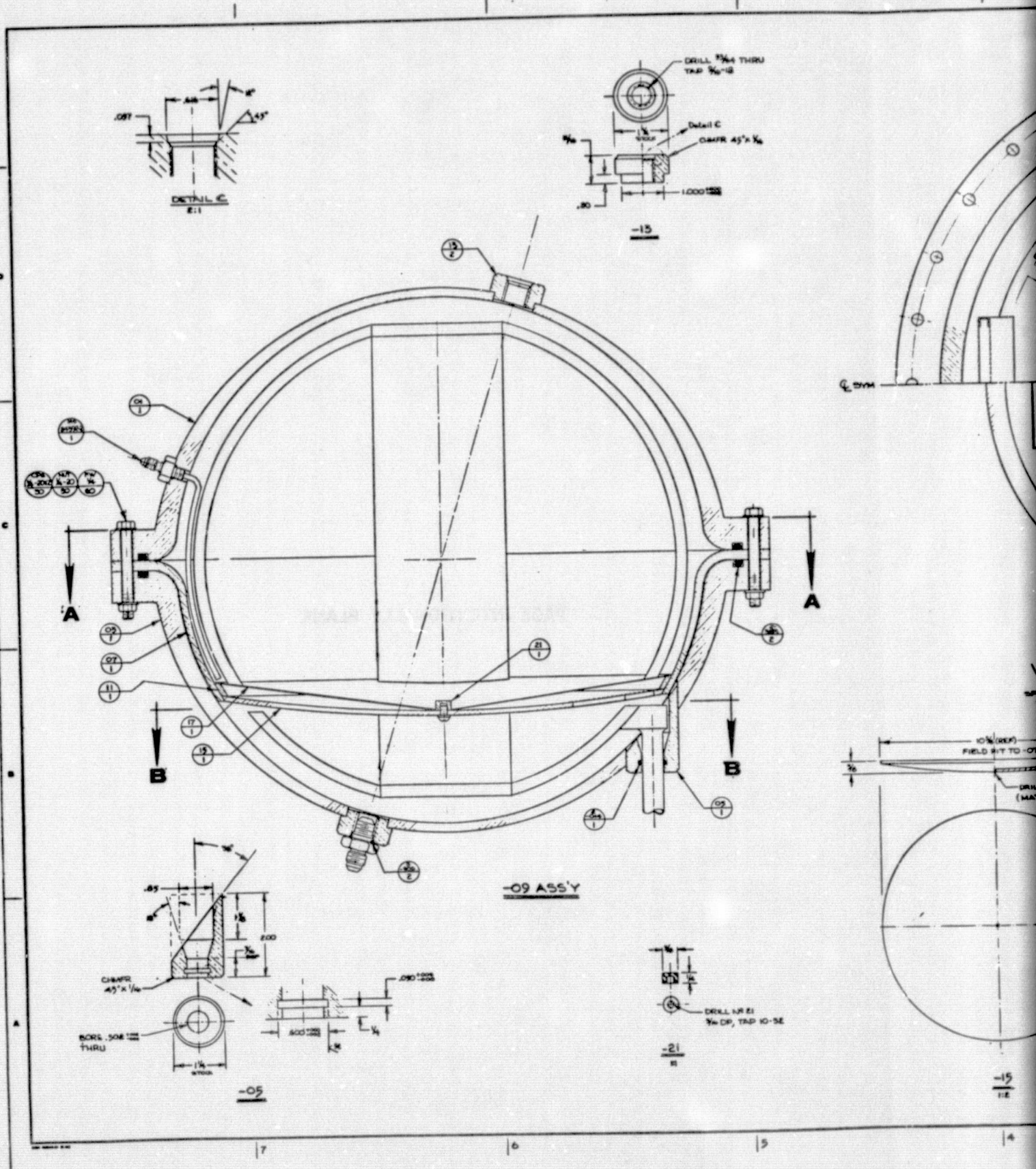
in the scaled-test series of the verification program. The major fabrication effort involved modification of existing models for use in supporting tests, and the fabrication of test systems. A more detailed discussion of the hardware fabricated, including the subscale model, follows.

## 1. Subscale Model

The subscale model was constructed per the preliminary design discussed in Section B of this chapter. Based on the preliminary design and a scale of 1/3, the tank I.D. was 32.2 cm (12.67 in.) and the channel dimensions were 8.04 cm (3.17 in.) by 0.64 cm (0.25 in.). The barrier was curved with a radius of 81.3 cm (32 in.). A drawing of the model is shown in Figure V-7. The tank and barrier were constructed of plexiglass to allow visual observation of the liquid during testing. All other hardware in the tank was stainless steel, including fine mesh screens used on the capillary acquisition/expulsion system.

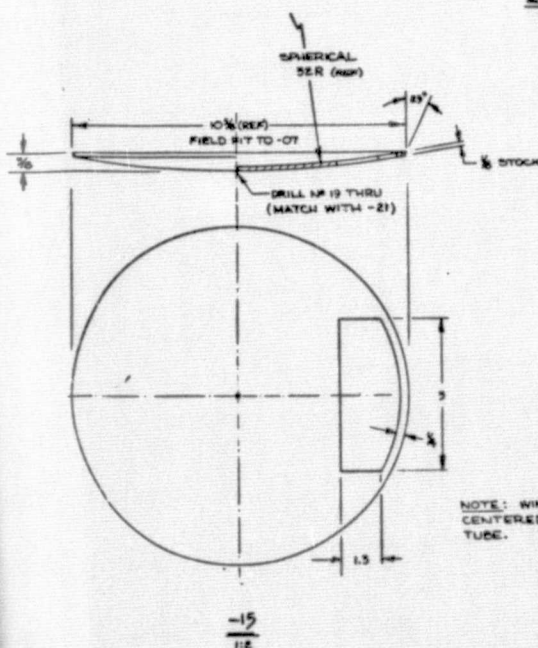
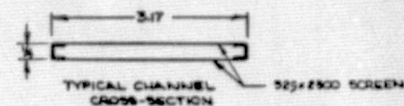
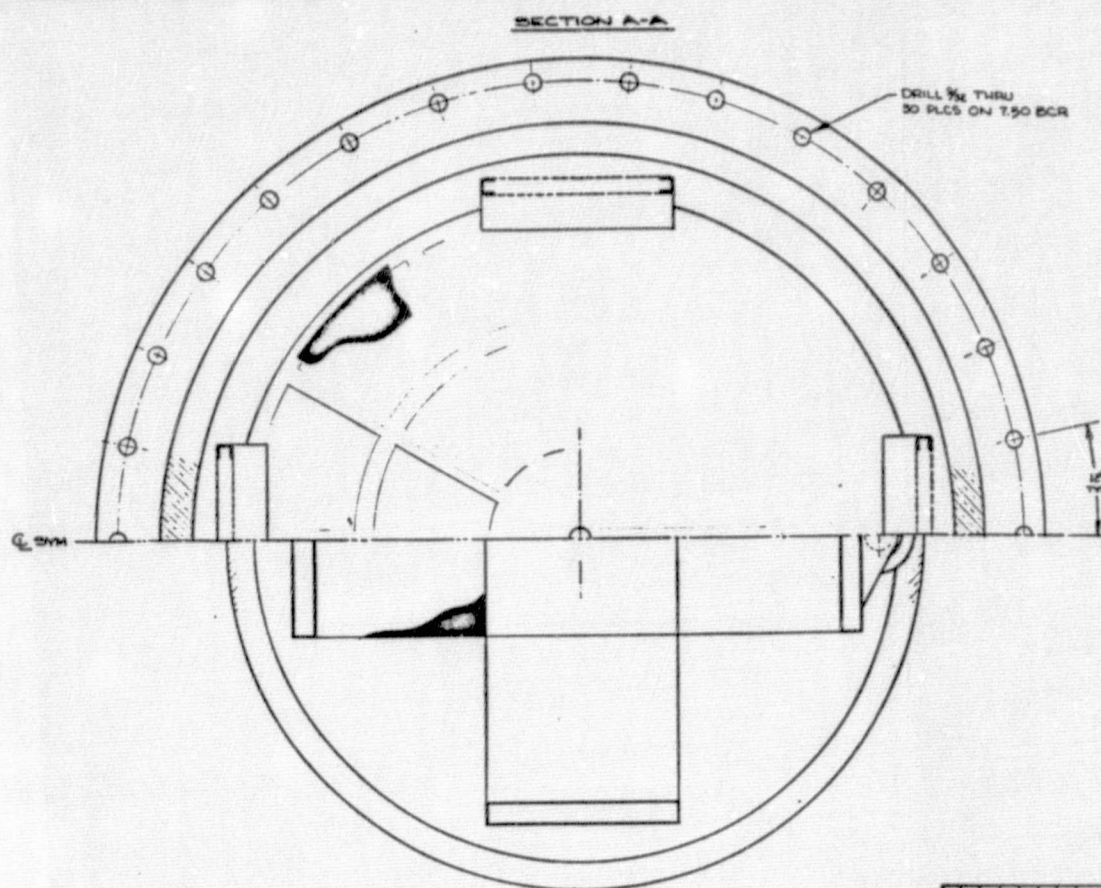
Figures V-8 and V-9 show the various components of the tank at different stages of fabrication. Figure V-8 shows the three major components of the tank: (1) the upper and lower hemispheres, (2) the lower channel assembly, and (3) the barrier and upper channel assembly. The right hand tank dome includes a vent port that allowed the tank to be loaded in the reentry attitude. The only other tank dome penetrations were the outflow and pressurization lines and a bottom compartment pressure sensing line located at the tank -X axis. Figure V-9 shows the lower channel and barrier assembly in more detail. The lower channel system was composed of four channels manifolded together and connected to the outlet. These were all covered by 325 x 2300 Dutch-twill screen. The 1.27 cm (0.5 in.) stainless steel outflow tube was attached to the end of one of the channels by a plenum. The plexiglass barrier plainly shows the screen window and attachment of the upper channel system and barrier manifold to the barrier. This attachment and the attachment of the screen window to the barrier was made with epoxy cement. The single bolt shown in the center of the barrier pulled the barrier manifold snug with the barrier and gave the system rigidity. The screen on the barrier window was 80 x 700 mesh Dutch-twill instead of the planned 165 x 800 because of material availability.

Figure V-10 shows the assembled model mounted on the support stand used for bench testing. All components of the acquisition/expulsion device are clearly visible. Wicking barriers were installed on all four of the lower assembly channels. These included small sections of 325 x 2300 Dutch-twill screen to allow venting of gas from inside the channels during filling. The pressurization and outflow penetrations are shown at the top and bottom left of the tank.



PRECEDING PAGE BLANK NOT FI

FOLDOUT FRAME



NOTE: WINDOW TO BE  
CENTERED OVER OUTLET  
TUBE.

QTY	PART NO.	DESCRIPTION	QTY	PART NO.	DESCRIPTION	QTY	PART NO.	DESCRIPTION
1	-21	A5 1	BOSS	3/16 X 1/4				
1	-17		CONE	1/16 X 1/8 X 1/8				
1	MS-2450-2		UNION	1/8 TUBE				STL
2	2-583		O-RING					BUNA-N
2	2-529		O-RING					BUNA-N
1	2-014		O-RING					STL-KN-12
50	EW 1/4		FLAT WASHER	1/4				STL-KN-12
50	NUT 1/4-20		HEX NUT	1/4-20				STL-KN-12
50	CPB 1/4-20 X 2		CAPSCREW	1/4-20 X 2				STL-KN-12
1	-15	A4 1	BULKHEAD	1/16 X 1/8				ACRYLIC
2	-15	D6 1	BOSS	1/16 X 1/8				
1	-11		RTB	1/16 X 1/8				
1	-07	D5 2	SKIRT	1/16 X 1/8				
1	-09	A7 1	FITTING	1/16 X 1/8				
1	-05	B7 2	DOME LOWER	1/16 X 1/8				
1	-01	D7 2	DOME UPPER	1/16 X 1/8				ACRYLIC
1	-09	C7 1	TANK ASSY					

Figure V-7 Sub-Scale RCS Model

V-15 and V-16

GE BLANK NOT FILMED

DOUT FRAME



Figure V-8

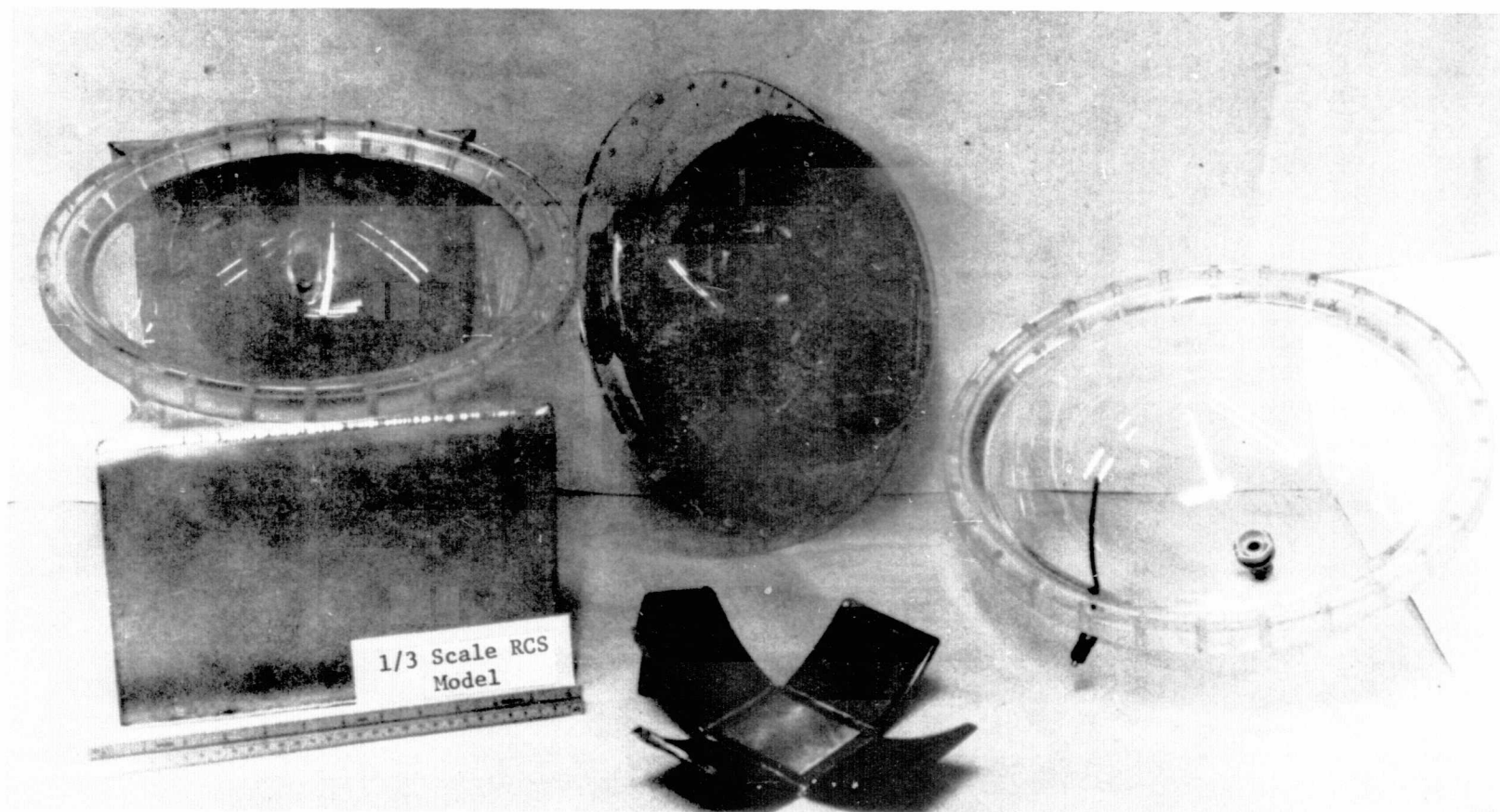
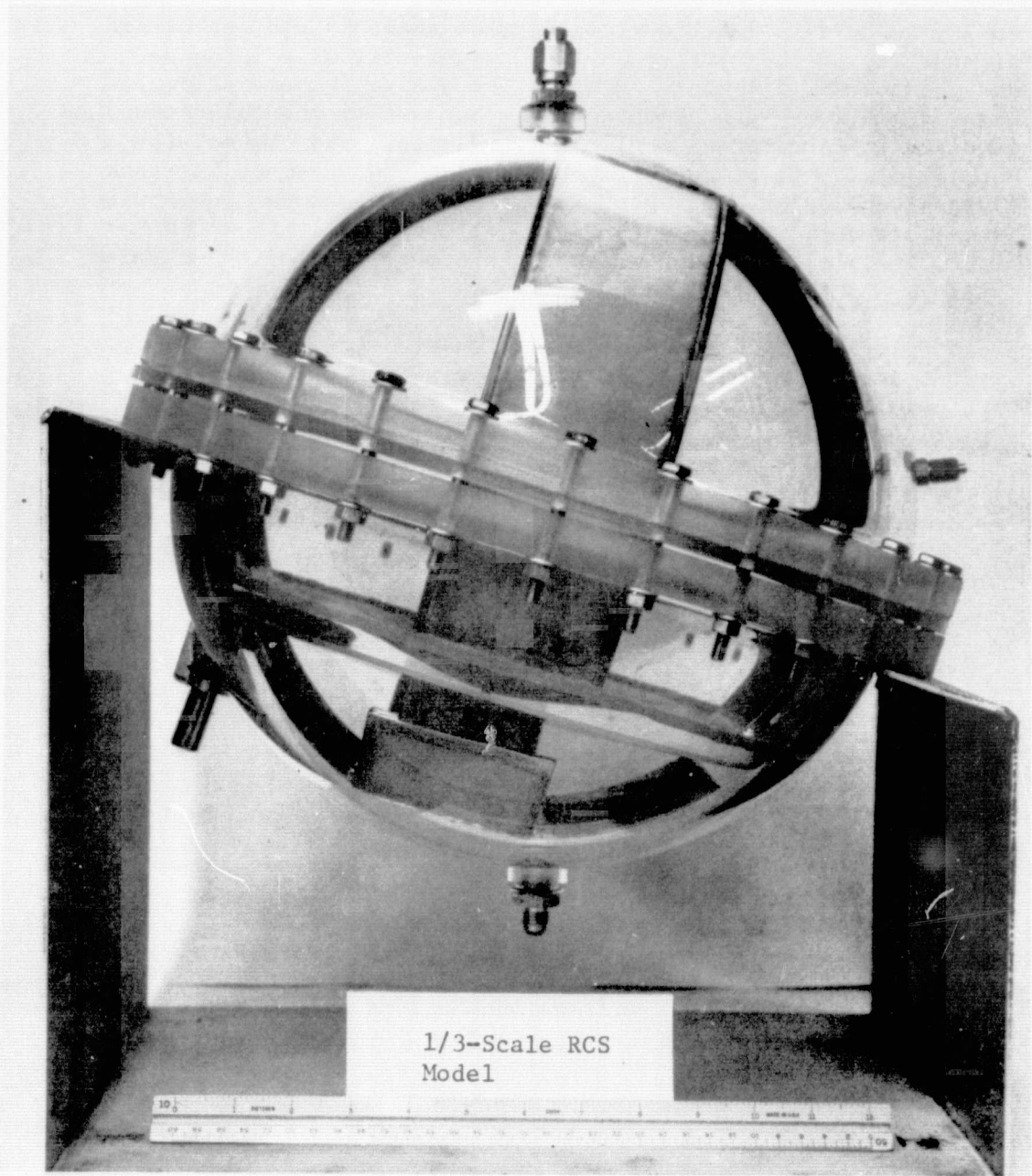


Figure V-8 Assembly View of 1/3 Scale Model

Figure V-9



Figure V-9 Subscale Model Components



*Figure V-10 RCS 1/3-Scale Model*

This picture of the system is of particular significance for it shows one of the most important deviations of the model from scaled geometry. The lower compartment channels did not extend all the way to the barrier as the design originally intended, and channel-to-wall clearances were excessive in some places. These deviations were uncontrollable because of the tolerances involved in fabricating a plexiglass device. The channel-to-barrier distance, although not as large as shown since the tank flanges were not drawn together, was enough to affect performance in certain attitudes. Another view of the tank is shown in Figure V-11. This top view shows the screen area of the barrier manifold and the upper channel system.

The model, as fabricated, deviated from scaled conditions in various areas that affected performance. Some of these areas were briefly discussed in the foregoing text. The significant deviations follow.

- 1) Barrier window screen was 80 x 700 instead of 165 x 800 mesh screen. This would tend to decrease performance slightly during RTLS because the ratio of entrance loss to bubble point is greater than for 165 x 800.
- 2) Barrier volume was 13% of tank volume instead of design value of 14%. Any increase in performance for this deviation is negligible compared to experimental error.
- 3) Lower compartment channel-to-wall spacing was larger than design value. This tended to decrease the expulsion efficiency during on-orbit simulation tests.
- 4) Lower compartment channel-to-barrier distance was larger than design value. This had an adverse effect on performance when liquid was puddled against the barrier.
- 5) Decreased outlet channel screen area. Because of model size and outlet configuration, the screen area available when liquid was puddled over the outlet was reduced from design levels and reduced performance in attitudes such as reentry.
- 6) Barrier manifold screen area to volume ratio not optimized. The volume of the barrier manifold was larger than required to reduce flow losses to an acceptable value. This tended to increase upper compartment residuals.

These items were taken into account in the computer model that predicted subscale performance and should be kept in mind in analyzing test results presented in the following sections, and in assessing full-scale performance in light of these results.



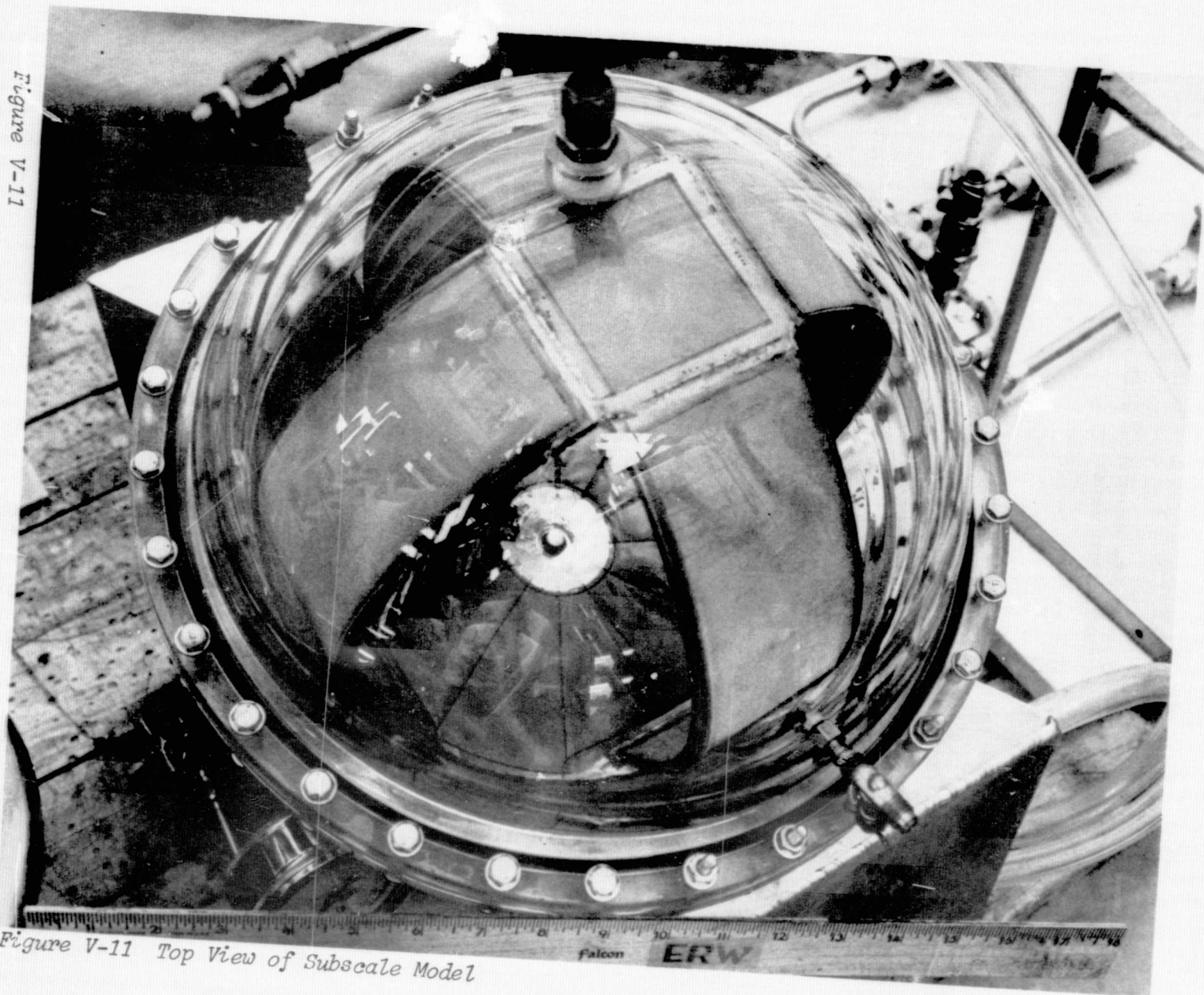


Figure V-11

Figure V-11 Top View of Subscale Model



### Test System Fabrication

The individual test systems are described with each test in Section D. The items fabricated were:

- 1) bench test system;
- 2) centrifuge test apparatus;
- 3) vibration shaker attachment fixture;
- 4) slosh test apparatus;
- 5) drop tower model;
- 6) transparent model test system.

All of the above items were fabricated specifically for this test program. Equipment that was required but is not listed here includes the drop tower test apparatus and the transparent channel model. These items were available from other programs. Details of each system are discussed in Section D.

#### D. VERIFICATION TESTING

The objective of the similitude test program was to verify the operational performance of the selected passive surface tension design for the SS/RCS propellant acquisition/expulsion system. The test program evaluated the operational characteristics of the propellant tank/acquisition device assembly over a range of mission sequences, including ground, high-g boost, low-g orbital, high-g reentry operations.

Testing was divided into supplemental model tests and scale model tests. Supplemental model tests investigated key functional items of the design isolated from the complexity of a full system. Scale model tests were run to verify design capability through computer correlation and test scaling. Although exact scaling of flow rates was not possible, an approach was used that gave good results. Methanol, water, isopropyl alcohol, and Freon TF referee fluids were used throughout the test program.

Scale model testing included fill and drain 1-g expulsion tests, centrifuge tests, slosh tests, and vibration tests to determine the effect of oscillatory motion on the system.

Test results were analyzed and design impact determined. These were incorporated into redesign effort resulting from a significant change in criteria.

##### 1. Supplemental Model Tests

Supplemental model testing was conducted to verify functional capability of the design in specific areas of concern in contrast to the systems related experiments discussed in subsection D.2. This series of experiments used existing models and hardware where possible, and consisted of the following tests: (1) channel-wall spacing tests; (2) gas pull-through tests; and (3) drop tower tests. The specific problems investigated were:

- 1) pressure loss due to propellant flow between a wall and a screen flow channel;
- 2) expulsion efficiency of a surface tension device in a plus 1-g attitude;
- 3) Low-g fluid behavior in a compartmented spherical tank.

These items are important to the performance of the RCS propellant tanks and were isolated from the system to obtain specific data.

a. *Channel Wall Spacing Tests*

1) Objective - The preliminary channel configuration is shown in Figure V-12. This channel geometry has half of the screen surface facing the tank wall to provide large screen-liquid contact areas at small liquid volumes as the tank is drained. With this configuration, however, the wall influences the flow of liquid into the channel as the wall spacing  $t$  becomes small. Analysis determined the additional pressure loss because of this phenomenon, assuming a constant loss factor for incompressible flow around the channel edges. This resulted in determination of a minimum spacing  $t$ , which had no appreciable effect on channel flow capability.

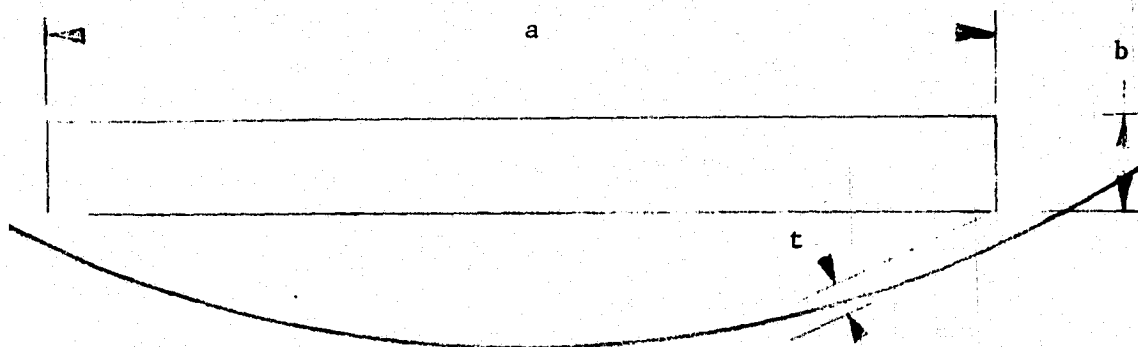
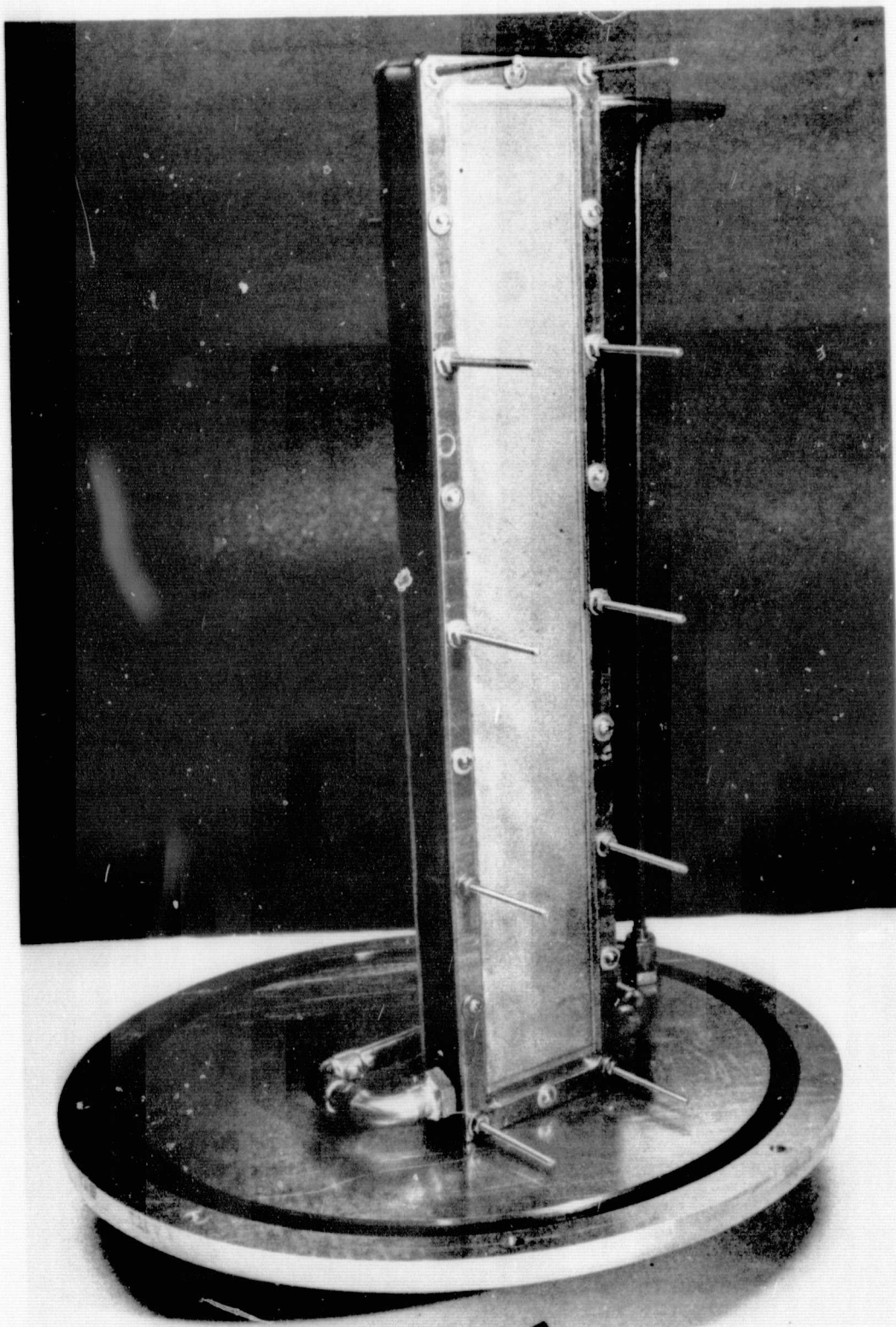


Figure V-12 Preliminary Design, Channel Wall-Spacing Configuration

The objective of this series of tests was to provide experimental data to verify the design analysis and determine an effective loss factor  $K$  to be used in further design of the optimum channel wall spacing.

2) Apparatus and Procedure - The test article used was an existing transparent channel with a screen and perforated plate combination on one side and a solid plate on the other. This configuration allowed liquid flow into the channel from one side only. The channel, shown in Figure V-13, used 325 x 2300 Dutch-twill stainless steel screen 38.75-cm (15.25-in.) high and 5.72-cm (2.25-in.) wide. The 1.25-cm (0.5-in.) outflow line connected through a tee to both sides of the channel, imposing little restriction to flow. Also shown is the channel vent tube, which allowed the channel to be filled completely full of liquid. The tube runs from the top of the channel through the baseplate where it is vented to atmosphere by a hand valve.

Figure V-14 shows another view of the test channel with the aluminum plate used to provide the desired channel/wall spacing. A linear scale with 0.64-cm (0.25-in.) graduations was engraved on the aluminum wall plate for measuring bulk liquid level, liquid-screen contact area, and screen hydrostatic head.



*Figure V-13 Transparent Channel Model*

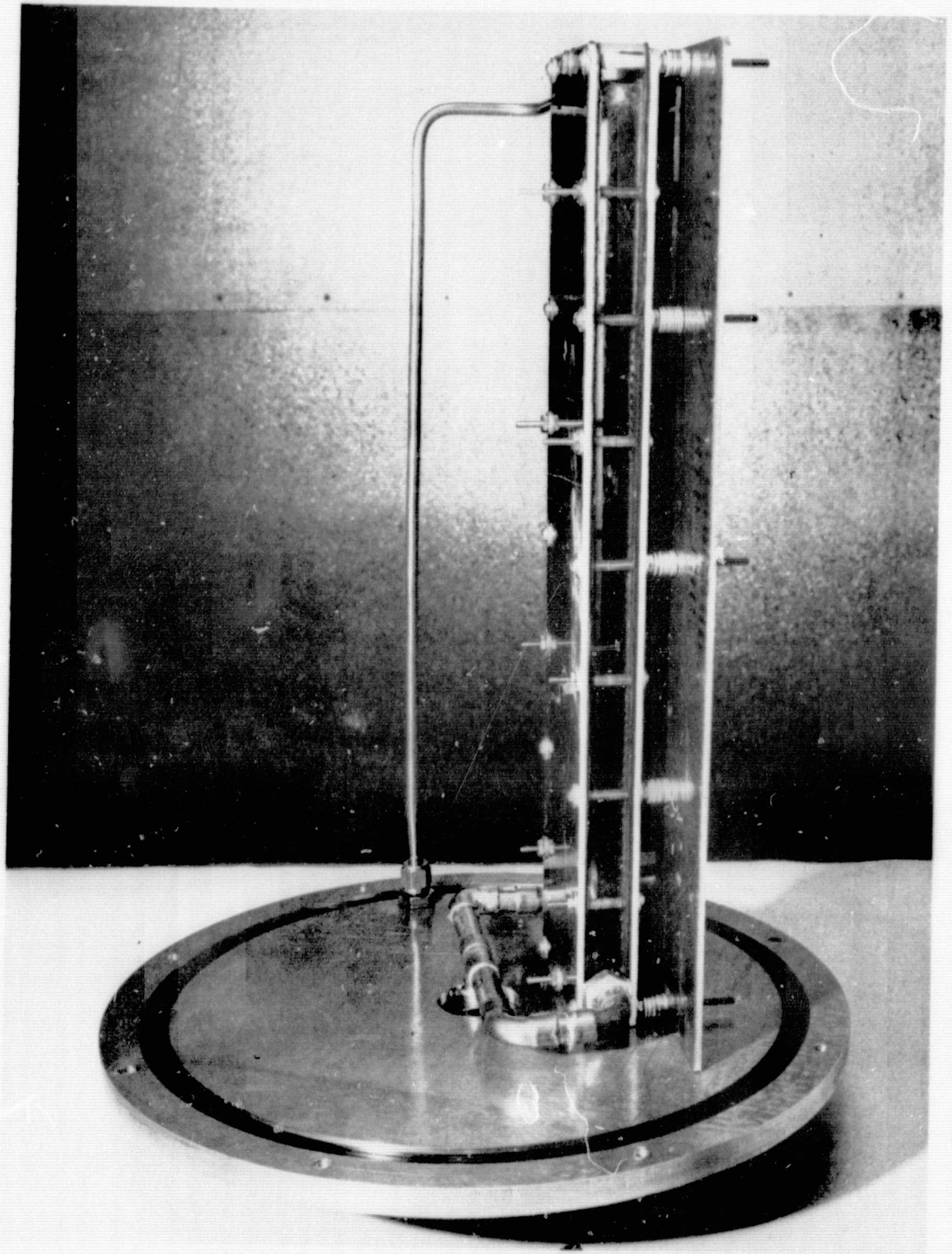


*Figure V-14 Channel/Wall Spacing Test Article*

The test article was inserted into a 29.2-cm (11.5-in.) diameter by 43-cm (17-in.) long plexiglass cylinder mounted vertically in a plus 1-g outflow configuration for all tests. A schematic of the test system is shown in Figure V-15. Main components of the system were the pressurization source, test article, receiver tank with graduated sight glass, and associated hardware.

The test fluid was methanol at ambient temperature and the pressurant was ambient  $\text{GN}_2$ . The procedure for running each test was the same. Before filling the tank with liquid, the aluminum plate was adjusted to give the desired wall spacing,  $t$ . With the test tank assembled, the model was filled with methanol through the outflow line by pressurizing the receiver tank. During fill, the channel was vented using valve 3 to assure no ullage was present at the start of the test. After fill was completed, the tank was pressurized to the desired pressure and the test initiated by opening valve 4. Flow rate was determined periodically during the test by timing the discharge between two points on the graduated sight glass with a stop watch. End of the test was signified by gas ingestion into the channel determined from visual observation. At this point outflow was stopped and the bulk liquid level was recorded.

This procedure was repeated for different flow rates and channel/wall spacings. Twenty-one tests were run, as denoted by the test matrix in Table V-3. Five different wall spacings, including no wall, were evaluated. Each test shown in the table was repeated at least once for purposes of reproducibility. The bubble point of the 325 x 2300 mesh screen was measured before and after testing and found to be 65.0-cm (25.6-in.) of water or  $0.637 \text{ N/cm}^2$  (0.924 psi).

The data was analyzed on the basis of the pressure differential equation for fine-mesh screens during a plus 1-g outflow. With no wall effects, the pressure differential across the screen is equal to the hydrostatic head and entrance losses. At breakdown, the following equation applies:

$$[V-1] \quad BP = \rho gh + \Delta P_e$$

where:

BP = screen bubble point

$\rho$  = liquid density

$h$  = height of liquid supported

$\Delta P_e$  = pressure loss due to flow of liquid across the screen.

Figure V-15

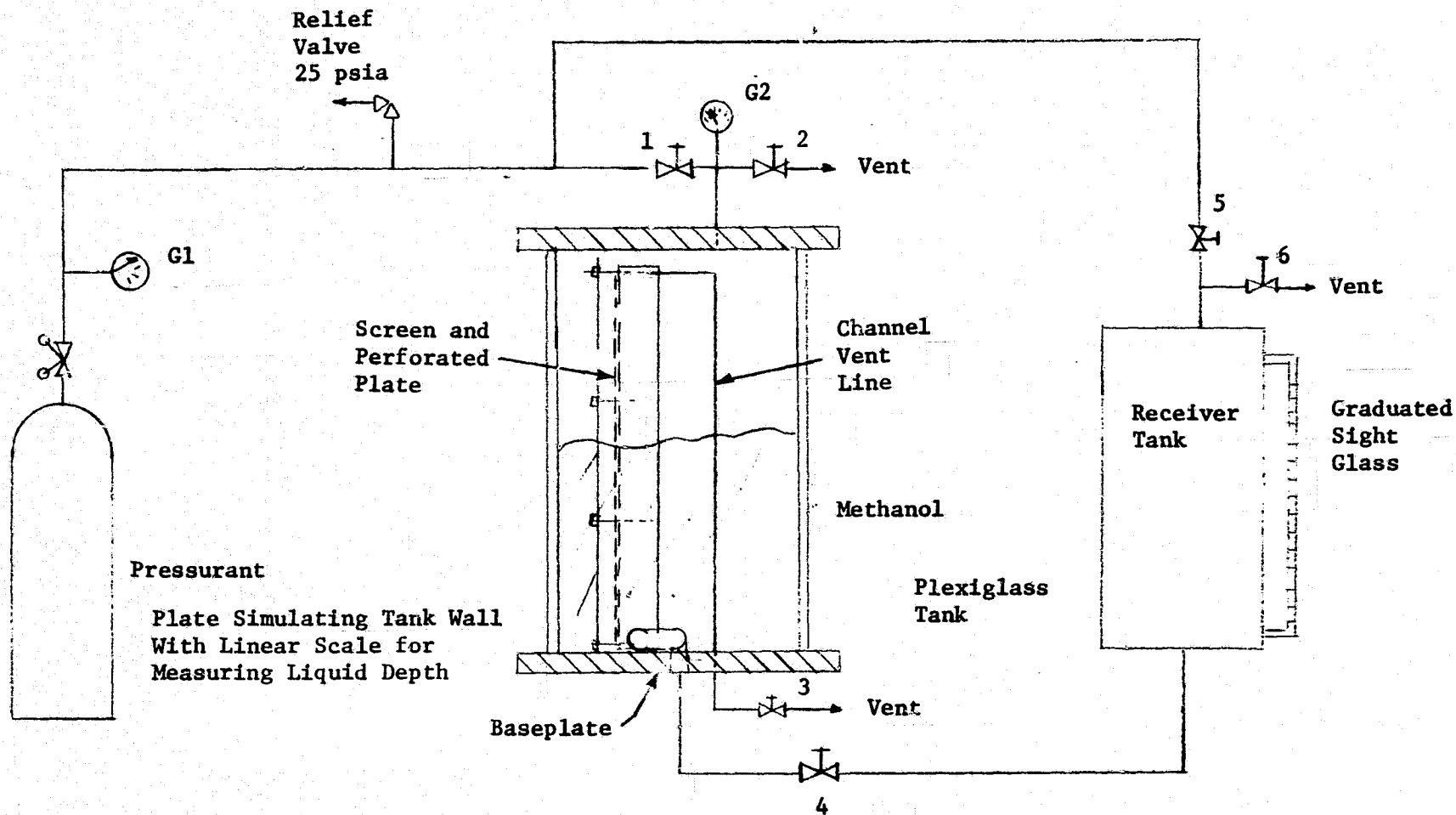


Figure V-15 Channel/Wall Spacing Test System Schematic



Table V-3 Channel/Wall Spacing Test Matrix

Test No.	Test Fluid and Temperature	Channel/Wall Spacing, t, in cm (in.)	Flow Rate	GN <sub>2</sub> Pressure, N/cm <sup>2</sup> (psig)	
1	Methanol at 21-27°C (70-80°F)	No Wall	A	1.4	(2.0)
2		↓	B	2.8	(4.0)
3			C	3.6	(5.3)
4			D	4.5	(6.5)
5			E	6.6	(9.5)
6			F	9.1	(13.3)
7			G	15.5	(21.0)
8		0.635 (0.25)	A	5.0	(7.3)
9		↓	B	9.3	(13.5)
10			C	11.7	(17.0)
11			D	13.8	(20.0)
12		0.381 (0.15)	A	4.1	(6.0)
13		↓	B	6.9	(10.0)
14			C	13.8	(20.0)
15		0.165 (0.065)	A	2.9	(4.3)
16		↓	B	6.9	(10.0)
17			C	13.8	(20.0)
18		0.076 (0.030)	A	1.3	(1.8)
19		↓	B	2.1	(3.0)
20			C	6.9	(10.0)
21			D	13.8	(20.0)

With the presence of a wall, an additional pressure loss is incurred such that Equation [V-1] becomes:

$$[V-2] \quad BP = \rho gh + \Delta P_e + \Delta P_w$$

where:

$\Delta P_w$  = pressure loss due to flow of liquid around the edge of the channel

From the experimental data, BP,  $\rho gh$ , and the velocity of liquid through the screens were determined. Because the flow loss through the screen/perforated plate combination is higher than that for the screen alone, the value of  $\Delta P_e$  is the only known term in Equation [V-1] and may be solved for as a function of liquid approach velocity. In this manner the flow loss caused by wall effects,  $\Delta P_w$ , was determined from Equation [V-2].



The loss term,  $\Delta P_w$ , was assumed to follow the standard description of incompressible minor losses, i.e., the product of the dynamic head and a loss coefficient, K. In equation form:

$$[V-3] \quad \Delta P_w = K \frac{\rho V^2}{2g_c}$$

where  $\rho$  = liquid density

V = fluid velocity

K = constant loss factor

$g_c$  = gravitational constant

This equation was used to determine the effective loss factor, K.

The actual channel-wall geometry tested exactly modeled the preliminary design shown in Figure V-12. The test configuration more closely simulated flow through a sudden contraction and sudden expansion, as shown in Figure V-16. Pressure losses for this configuration should be higher than for the preliminary design with a limiting value of 1.5 for K at small values of t.

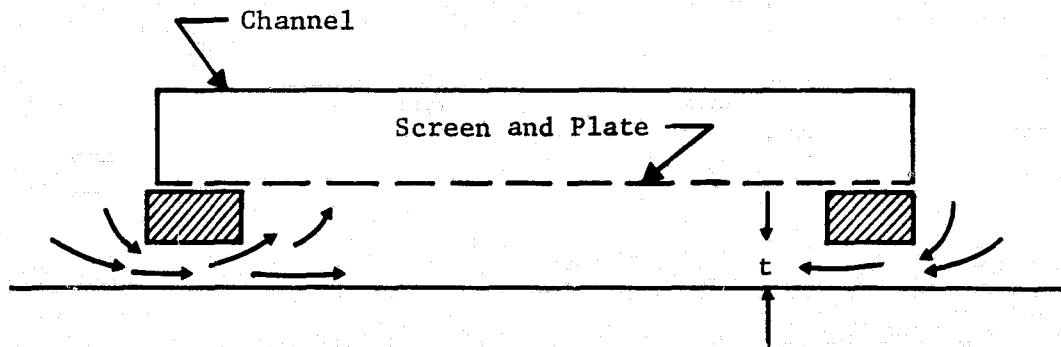


Figure V-16 Channel/Wall Spacing Test Geometry

3) Results - Test results are plotted in Figure V-17. Flowrate is plotted as a function of channel hydrostatic head at screen breakdown. Smaller hydrostatic heads indicate less liquid expelled from the tank and larger liquid-screen contact areas. Experimental data are shown for  $t = \infty$ , (no wall effects) and four values of wall spacing, t. No trends are evident with the  $t = \infty$ ,  $t = 0.635$  cm (0.25 in.), and  $t = 0.381$  cm (0.15 in.) data, indicating negligible wall effects. However at  $t = 0.164$  cm (0.065 in.), a definite effect is seen. At a given flowrate, channel hydrostatic head is less at breakdown indicating increased pressure losses. An even greater effect is noted at  $t = 0.076$  cm (0.030 in.). This added loss is due to the constricting flow passage between the channel and the wall.

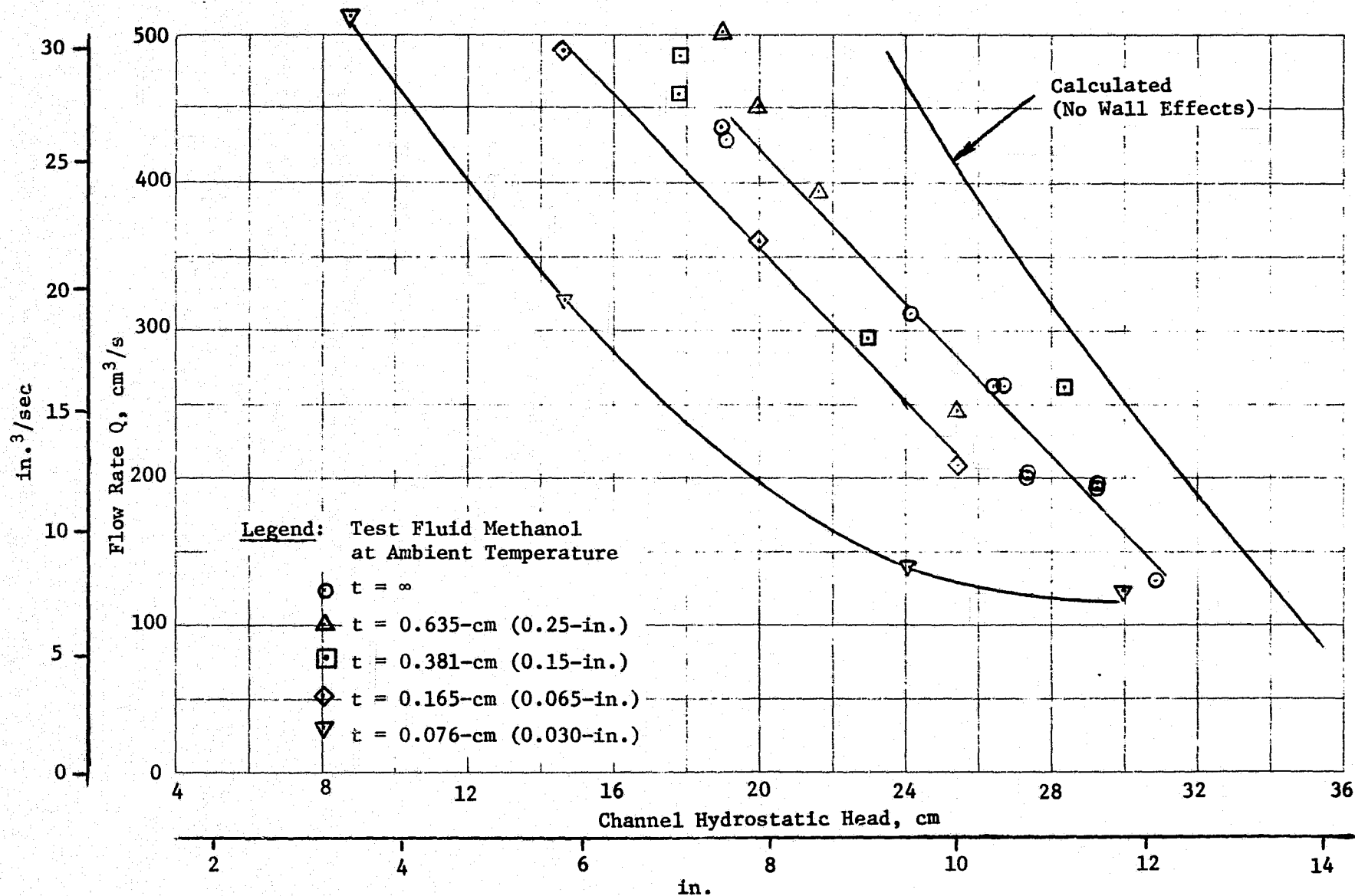


Figure V-17 Channel/Wall Spacing Test Results

Loss factors calculated for the two wall spacings of 0.635 cm (0.25 in.) and 0.381 cm (0.15 in.) are shown in Table V-4. Four points are shown for each spacing, which correspond to the data points shown in Figure V-16. The loss factor, K, was calculated from the relationship:

$$[V-4] \quad K = \frac{\Delta P_w \text{ test}}{\Delta P_w \text{ calc}}$$

where

$\Delta P_w \text{ test}$  = Pressure differential due to wall spacing losses from test data.

$\Delta P_w \text{ calc}$  = Calculated pressure loss due to wall spacing from dynamic head  $\left( \frac{\rho v^2}{2g_c} \right)$ .

The loss factor, K, ranges from 0 to a value of 28.4 for these two spacings and shows no consistency in value. The small pressure differentials associated with these two sets of data are within the accuracy of the tests. Flow losses appear.

Table V-4 Loss Factor

Flowrate, cm <sup>3</sup> /sec (in. <sup>3</sup> /sec)	Wall Spacing, t, cm (in.)	$\Delta P_w \text{ test},$ N/cm <sup>2</sup> (psi)	$\Delta P_w \text{ calc},$ N/cm <sup>2</sup> (psi)	Loss Factor, K
246 (15)	0.635 (0.25)	0.033 (0.0483)	0.001 (0.0017)	28.4
393 (24)	0.635 (0.25)	0 (0)	---	0
451 (27.5)	0.635 (0.25)	0 (0)	---	0
500 (30.5)	0.635 (0.25)	0 (0)	---	0
262 (16)	0.381 (0.15)	0 (0)	---	0
311 (19)	0.381 (0.15)	0.039 (0.051)	0.003 (0.0052)	11.1
459 (28)	9.381 (0.15)	0.050 (0.072)	0.004 (0.0067)	10.7
492 (30)	0.381 (0.15)	0.038 (0.012)	0.005 (0.0077)	1.56

4) Conclusions - Test results indicated a constant loss factor of 3.5 for tests that yielded pressure differentials large enough for measurement. However, the pressure differentials during these tests,  $t = 0.76 \text{ mm}$  (0.030 in.) and  $1.65 \text{ mm}$  (0.065 in.), were small enough to question the accuracy of the data and the loss factors calculated. This is indicated by the large differential in constant loss factor between theory and test calculations. Pressure differentials for spacings of  $t = 0.635 \text{ cm}$  (0.25 in.) and  $0.381 \text{ cm}$  (0.15 in.) were so small that consistent measurement was impossible

and no change in performance was evident as compared to an infinite spacing  $t$ . A variation in calculated loss factor from 0 to 28.4 supports this conclusion.

As a result, it was concluded that values of wall spacing,  $t$ , in the design range of 0.318 cm (0.125 in.) to 0.635 cm (0.25 in.) had little effect on system performance. A value of 0.476 cm (0.1875 in.) was chosen for the full-scale design based on expulsion efficiency and pressure loss considerations.

A similar analysis of the two smallest wall spacings,  $t = 0.1651$  cm (0.065 in.) and 0.0762 cm (0.030 in.), resulted in the data shown in Figure V-18. Correlation is somewhat better since the pressure differentials involved are greater but still small enough so that accurate measurement is difficult. The loss factor is approximately constant with flowrate at a value of 3.55. This is significantly higher than the 1.5 value estimated from theory based on a sudden contraction and sudden expansion analysis.

#### *b. Transparent Channel Positive-g Expulsion Tests*

Positive-g expulsion capabilities of a capillary acquisition/expulsion device may be predicted analytically in a manner similar to negative-g expulsions. However, since liquid is puddled over the outlet, and gas away from the outlet, gas-free liquid may be expelled for some period following initial breakdown of the screen channel, giving increased expulsion capability. The point at which the entrance loss caused by flow of bulk liquid into the channels equals the pressure drop due to flow of gas into the channel denotes the expulsion capability of the system. The pressure drop caused by flow of gas into the channel is the bubble point of the screen unless some dry out has taken place. The amount of dryout, if any, and its effect on the added expulsion capability is dependent upon flow rate, and is important to the design of capillary acquisition/expulsion devices.

1) Objective - The objective of these tests was to verify expulsion capability of a capillary device during a +1-g expulsion. The effect of screen dryout, and gas pull-through (that point at which liquid is completely drained from the channel while bulk liquid remains) on system performance is of interest.

2) Apparatus and Procedure - The test system used was identical to that described for the channel wall spacing tests. A 325 x 2300 Dutch-twill screen channel mounted in a cylindrical Plexiglas tank was tested using methanol at ambient temperature. The channel was completely filled by outflow of liquid through the channel vent/bleed line to assure no gas was present at the start of each test. The tank was outflowed by pressure discharge.

Figure V-18

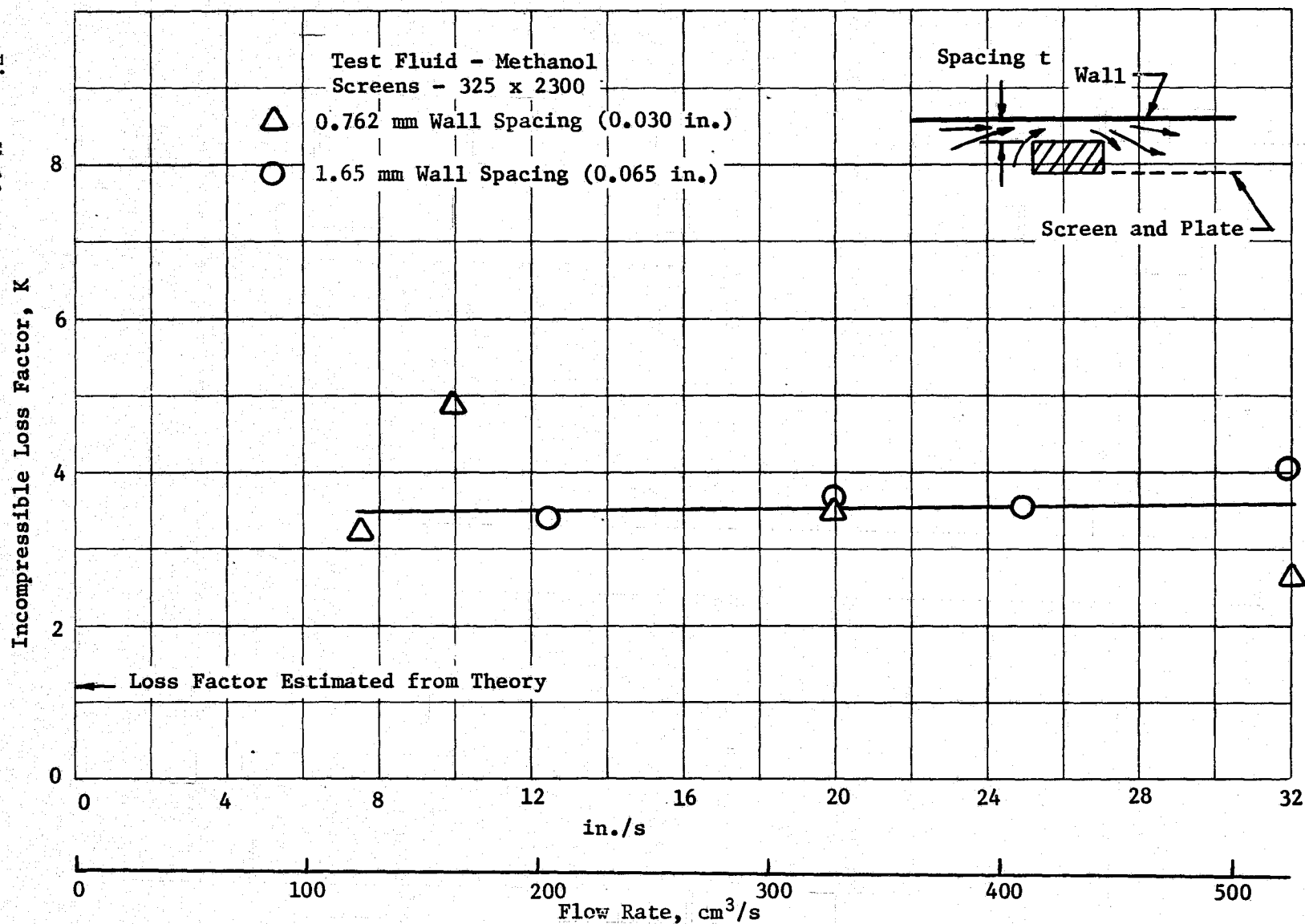


Figure V-18 Flow Loss Factor as a Function of Flow Rate

Flowrate was measured by timing the discharge at various points during the test. During outflow, the upper section of the channel was monitored for the presence of gas, indicating the bubble point of the screen was exceeded. The height of liquid in the tank was recorded at screen breakdown. Outflow was then continued until gas was ingested into the outlet of the system, where bulk liquid height was again recorded.

3) Results - Results of the gas pull-through tests are shown in Table V-5. Two different values of bulk liquid height are presented, as discussed previously. Flowrate varied from 0.12 l/sec (7.5 in.<sup>3</sup>/sec) to 0.31 l/sec (19 in.<sup>3</sup>/sec). The difference in liquid levels indicates that additional liquid was expelled from the system after the bubble point of the screen channel was exceeded. This differential liquid height,  $\Delta H$  varied from 4.1 cm (1.6 in.) to 6.4 cm (2.5 in.) as flowrate increased. It appeared that more liquid was expelled at higher flowrates before screen dryout occurred than at lower flowrates. At a flowrate of 0.256 l/sec. (15.6 in.<sup>3</sup>/sec), an additional 5.1 cm (2 in.) of liquid was expelled after breakdown before gas entered the outlet. This amounts to 13% of the channel length for a screen height of 38.75 cm (15.25 in.). Although these results may not be quantitatively applied to an actual system, they indicate that a significant amount of gas-free liquid may be expelled from a screen channel system in a positive-g attitude after the bubble point of the screen is exceeded.

Table V-5 Gas Pull-Through test Results

Test	Flowrate, l/sec (in. <sup>3</sup> /sec)	Bulk Liquid At Screen Breakdown	Height, cm (in.) Gas In Outflow Line	$\Delta H$ cm (in.)
1	0.123 (7.5)	9.8 (3.9)	5.7 (2.3)	4.1 (1.6)
2	0.180 (11.0)	11.4 (4.5)	7.6 (3.0)	3.8 (1.5)
3	0.180 (11.0)	11.4 (4.5)	7.6 (3.0)	3.8 (1.5)
4	0.188 (11.5)	13.3 (5.3)	8.9 (3.5)	4.4 (1.75)
5	0.213 (13.0)	13.3 (5.3)	8.4 (3.3)	5.0 (1.95)
6	0.241 (14.7)	14.0 (5.5)	8.9 (3.5)	5.1 (2.0)
7	0.256 (15.6)	14.2 (5.6)	9.1 (3.6)	5.1 (2.0)
8	0.306 (18.7)	16.5 (6.5)	10.9 (4.3)	5.6 (2.2)
9	0.311 (19.0)	16.5 (6.5)	10.9 (4.3)	5.6 (2.2)
10	0.311 (19.0)	18.4 (7.3)	12.1 (4.8)	6.4 (2.5)

4) Conclusions - The following conclusions may be drawn from these tests and may be qualitatively applied to surface tension devices of a similar geometric nature when in a positive-g attitude with liquid puddled over the outlet.

- a) A significant amount of gas-free liquid may be expelled from a screen channel after the bubble point has been exceeded.
- b) The amount expelled after breakdown of the channel varied from 10.4% of the channel height at the lowest flowrate to 16.4% at the highest flowrate.
- c) The additional amount of liquid expelled increased with flowrate.
- d) Additional work is required to characterize the phenomena involved before the results can be quantitatively applied to designing systems.

#### *c. Drop Tower Tests*

1) Objective - To maintain a gas-free supply of liquid from the tank, sufficient screen area of the surface tension device must always be in contact with the bulk liquid. Since the liquid tends to attach itself to the tank walls in low-g, positioning the channels along the walls should enable them to maintain contact with the liquid. However, acceleration of the Space Shuttle on-orbit due to RCS engines firing may reorient the bulk liquid within the tank. If the motion of the interface during the reorientation is such that most of the liquid travels through the center of the tank, the amount of bulk liquid in contact with the device could fall below the required minimum.

The objective of the drop tower test program was to simulate the reorientation of propellant within the RCS tank, due to typical on-orbit mission accelerations, and determine if sufficient contact was maintained between the surface tension device and the bulk propellant.

2) Approach - When the surface tension device is functioning on-orbit, the motion of the propellant within the RCS tank is essentially random. Almost any manner of liquid motion can be produced by the firing of the RCS thrusters. Only the worst case liquid motion that could move the liquid out of contact with the device was considered in the test program. The initial interface shape and the direction of the applied acceleration with respect to the tank have been shown to be significant factors affecting the liquid motion (Ref V-3). Based on that information, all the tests were accomplished with the liquid initially oriented against the tank wall with a flat interface. An acceleration

was continuous, so significant liquid motion was produced. A small lateral acceleration was added in certain tests to establish the effect of the direction of the acceleration.

Martin Marietta's Drop Tower Test Facility provides a low-g acceleration of sufficient duration so that the reorientation of the propellant within an RCS tank can be simulated. The actual conditions can be scaled to the drop tower test conditions. Scaling was accomplished using the approach presented in detail in Reference V-3. To summarize the scaling, dimensional analysis indicates that liquid reorientation can be parametrized as a function of the Froude, Reynolds and Bond numbers. If the Bond number is greater than 10 and Reynolds number is greater than 50, the Froude number is a constant. The test model and test liquid can be selected so that both Bond number and Reynolds number are large. Scaling of the acceleration, tank size, and test time is then provided by the Froude number, resulting in:

$$[V-5] \quad \frac{t_m}{t_p} = \sqrt{\frac{a_p r_m}{a_m r_p}}$$

where

t = time

r = tank radius

and the subscript m refers to the model and the subscript p refers to the prototype.

3) Apparatus and Procedure - A model RCS tank, 12.7 cm (5 in.) in diameter, was built. The barrier of the surface tension device, the only part of the device that has a significant effect on the liquid motion, was included in the model. The tank was mounted in a test module, shown in Figure V-19, which allows the tank to be oriented at various angles with respect to the axial acceleration. The module, slider (for the lateral acceleration), and camera are shown in Figure V-20, as mounted on the drop capsule. The entire drop capsule is axially accelerated, relative to a drag shield, with a spring motor.

Test conditions are noted in Table V-6. The orientation of the tank with respect to the axial acceleration and the magnitude of the lateral acceleration were varied with each test. A single liquid volume that filled each compartment to 30% of its volume was used. The 133 N (30 lbf) axial force produced accelerations of 0.084 g and the maximum lateral acceleration was on the order of 0.02 g. In some cases, the slider mechanism did not function as expected and only a lateral acceleration pulse was applied to the model at the beginning of the test.



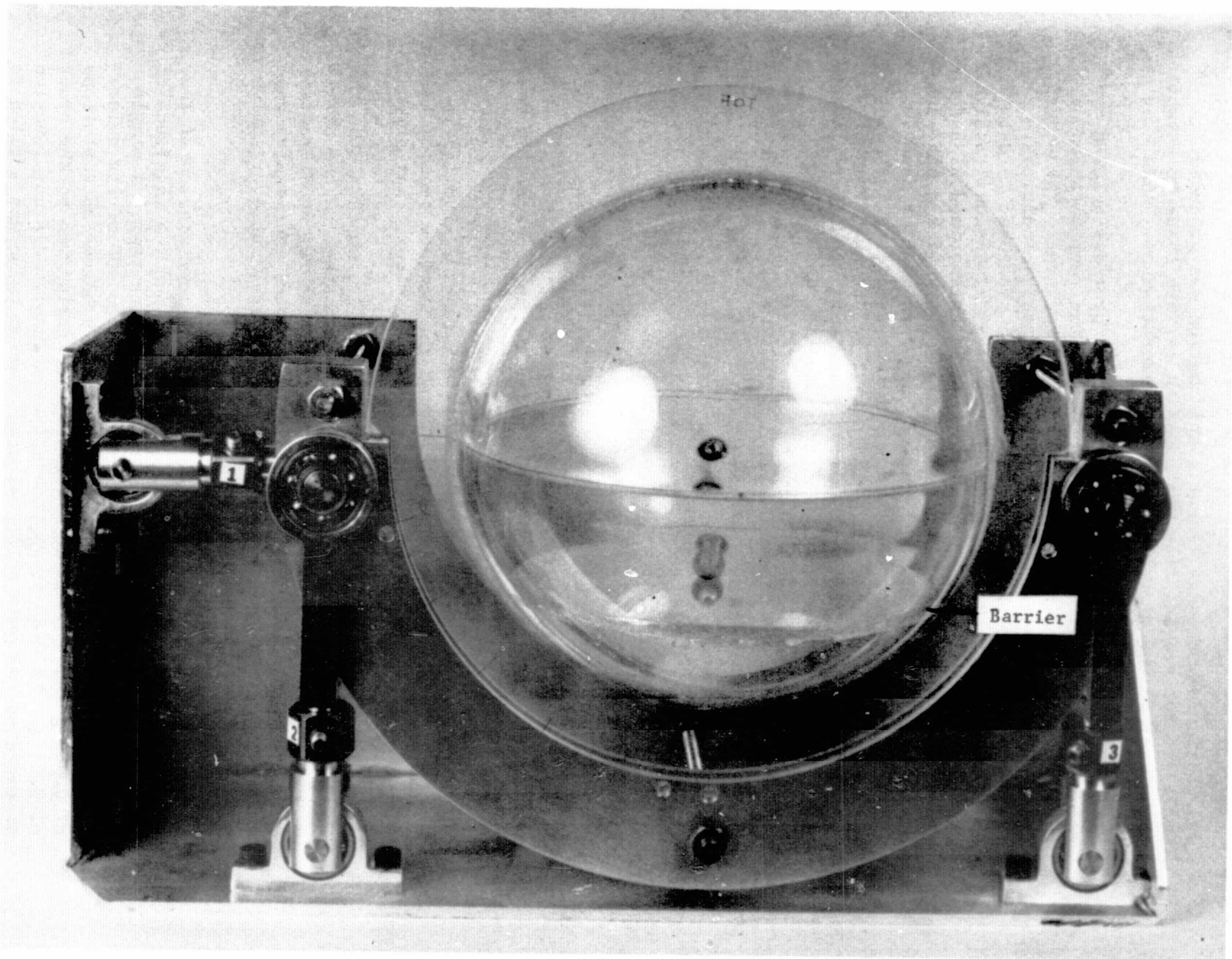
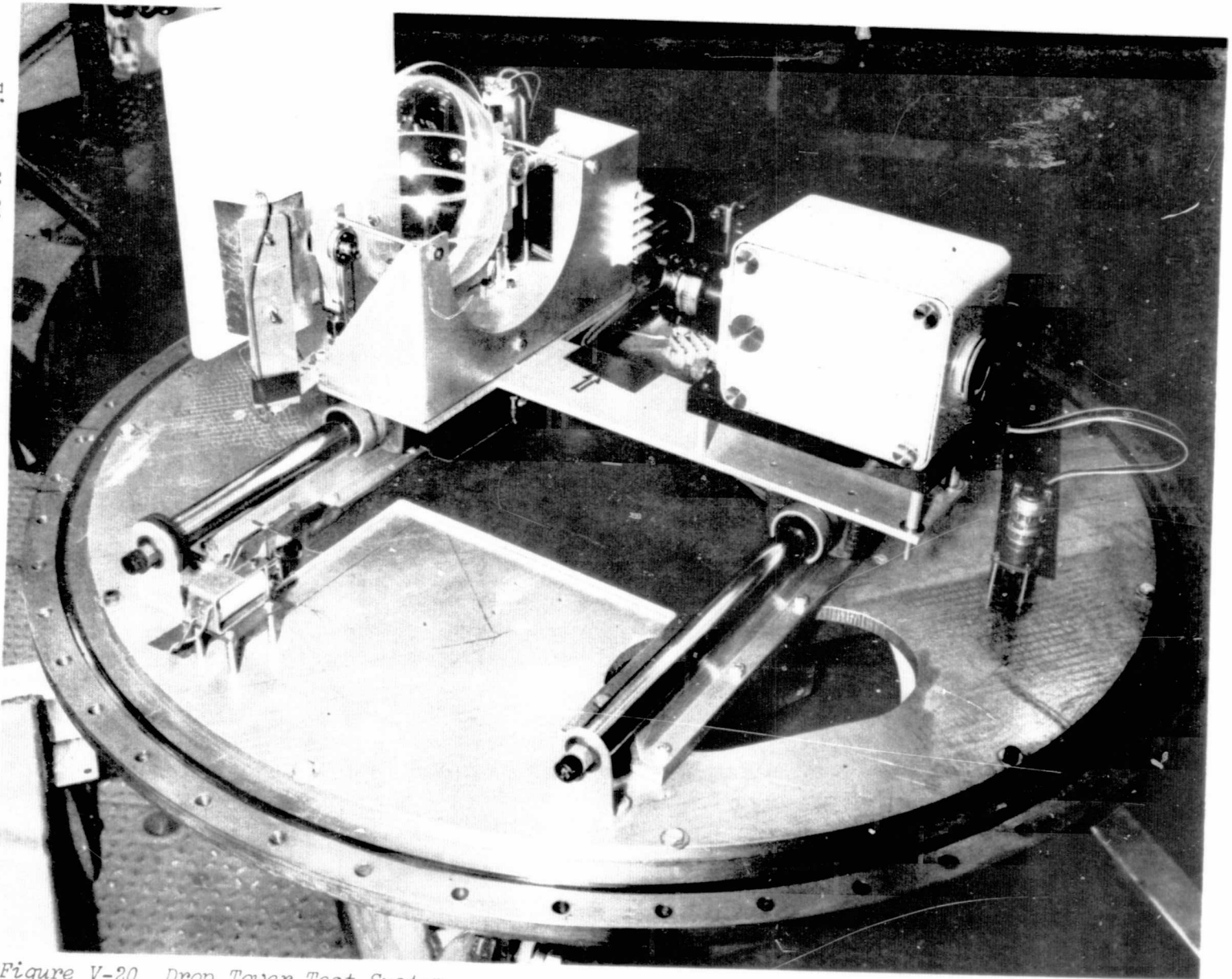


Figure V-19 Low-g Test Model

Figure V-19

V-38

*Figure V-20*

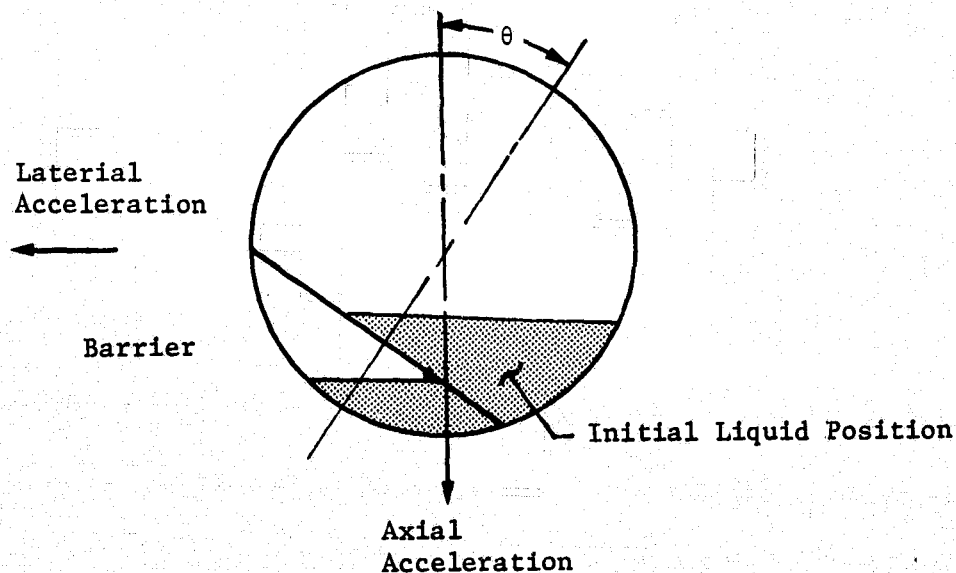


*Figure V-20 Drop Tower Test System*

Table V-6 Drop Tower Test Matrix

Test Number	Liquid Volume (Percentage of Compartment Volume)	Tank Orientation, $\theta^*$ (deg)	Spring Motor Force, N, (lbf)	
			Axial	Lateral
1	30%	0	133 (30)	3.3 (0.75)
2	30%	45	133 (30)	3.3 (0.75)
3	30%	90	133 (30)	3.3 (0.75)
4	30%	0	133 (30)	1.67 (0.375)
5	30%	45	133 (30)	1.67 (0.375)
6	30%	90	133 (30)	1.67 (0.375)
7	30%	0	133 (30)	0
8	30%	45	133 (30)	0
9	30%	90	133 (30)	0

\*The angle is defined as shown below.



A fluorocarbon solvent, FC-43, was selected as the test liquid. It has a high density and low surface tension, to aid in satisfying the scaling requirements. FC-43 has a density of 1.9 gm/cc (119 lbm/ft<sup>3</sup>) and a surface tension of 16.7 dynes/cm ( $1.14 \times 10^{-3}$  lbf/ft) (Ref V-4). Based on the selected accelerations, tank size, and liquid, the Froude number scaling indicates that the available 1.7 seconds of test time is equivalent to 4.9 seconds in a full-size tank being accelerated at 0.077 g.

4) Results - The results of the drop tests can be combined because the liquid motion was similar for each lateral acceleration.

a) Tests 1, 2, and 3 - In drop tests 1 through 3 a significant lateral acceleration was applied during the test. At the beginning of the test there is flow of the liquid along the tank walls and a hump of liquid also forms in the center of the tank. There is a tendency for some of the liquid to move through the center of the tank. However, the lateral acceleration causes the hump to quickly join the wall flow, and throughout the remainder of the test the motion of the liquid is predominantly along the wall. Most of the liquid flow is along one side of the tank, because of the lateral acceleration.

Some splashing of the liquid occurs when the barrier is vertical (Test 3). The liquid has a high velocity when it reaches the barrier and some of it is deflected as it hits the barrier. At the end of the test, collection of the liquid is nearly complete in the upper compartment. The center of mass of the liquid has overshot its final equilibrium position and is in the process of returning. Since the distance the liquid must move in the lower compartment is much less, reorientation is complete at the end of the test.

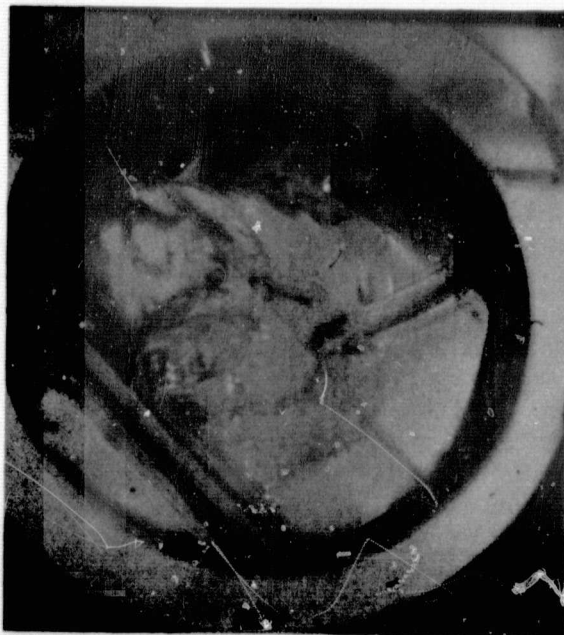
b) Tests 4, 5, and 6 - In these tests the lateral acceleration was only a short duration pulse that was applied at the very beginning of the test. The slider only moves a short distance and then stops. Regardless, the motion of the liquid was essentially the same as that observed in tests 1, 2, and 3. The liquid moved up one side of the tank, following the wall. The initial central hump of liquid was slightly larger, but it quickly joined the wall flow. The liquid position at the end of the test was the same as observed in tests 1, 2, and 3. Figure V-21 is a sequence of photos from test 5 to illustrate a typical reorientation.



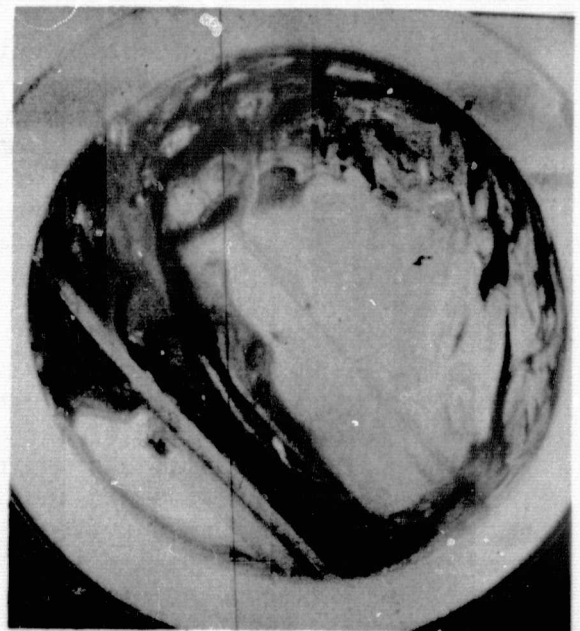
(a)



(b)



(c)



(d)

*Figure 7-21 Liquid Reorientation during Test 5*



c) Tests 7, 8, and 9 - No lateral acceleration was applied during these tests. The initial hump of liquid becomes a column that travels through the center of the tank and impacts the other end of the tank. An effect due to the barrier was noticed. When the barrier is inclined at 45 deg (Test 8), the column was displaced so that it joined the wall flow. Apparently, surface tension is the force causing the displacement of the column. The barrier makes the curvature of the surface different on opposite sides of the column, so a net lateral force acts on the column.

Even though some liquid is moving through the center of the tank, there is always a significant area and volume of liquids in contact with the tank wall. Some liquid still flows along the wall during the reorientation, and the column of liquid is still in contact with the bottom of the tank when the column reaches the top of the tank. A small column formed within the lower compartment during Test 7, but the effect is much less pronounced in this compartment. Figure V-22 illustrates a typical reorientation (Test 8) for this series of tests.

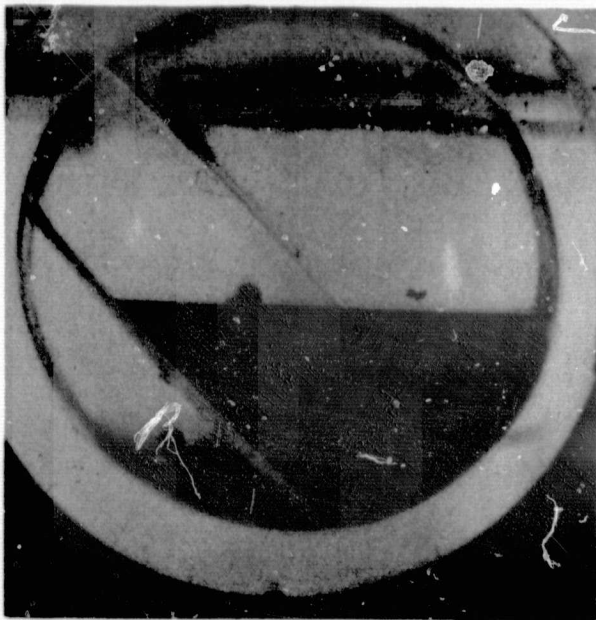
5) Conclusions - The smallest contact area between the liquid and the surface tension device will occur if some of the liquid moves through the center of the tank during reorientation. However, all of the following requirements must be satisfied before a central liquid column will be formed:

a) The liquid interface must initially be flat. Other test programs have shown that if the initial interface is highly curved, as it would be in low-g, the liquid flows along the tank walls during reorientation (Ref V-5). Bond numbers from 3 to 450 were simulated in those tests. The interface was initially flat in all the tests performed during this program;

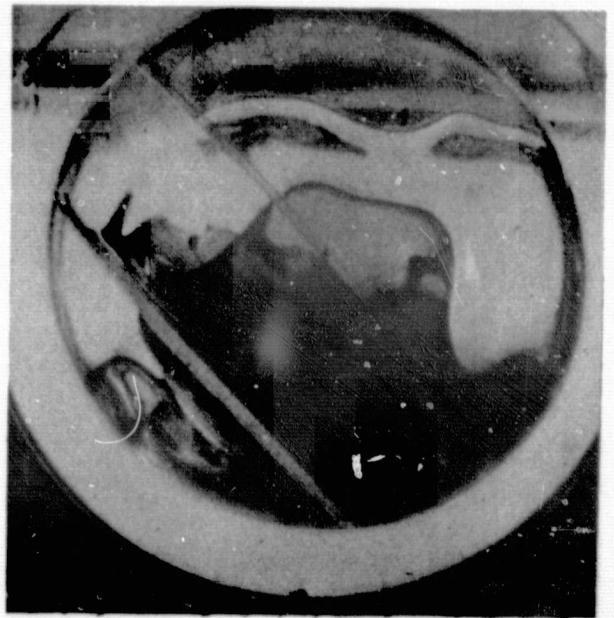
b) Inertial forces must dominate capillary forces. If the Bond number is small (capillary forces dominate), the liquid will reorient along the wall, even if the initial interface is flat. Tests have shown this is true when the Bond number is less than 2.0 (Ref V-6). The Bond number was 380 for these tests;

c) The acceleration must be purely axial. These tests have shown that a small lateral acceleration pulse is all that is required to make the liquid move along the wall of the tank;

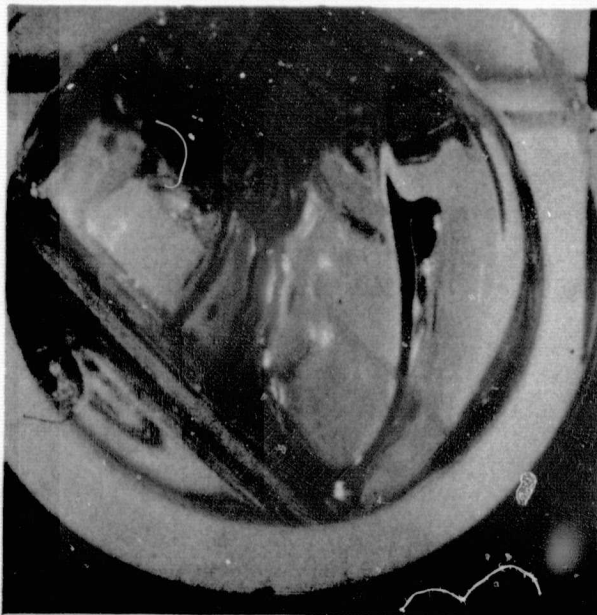
d) The internal geometry of the tank must be symmetrical with respect to the acceleration vector. Previous tests have shown that misalignments as small as one degree will cause the central column of liquid to be deflected into the wall (Ref V-7). These tests have shown that the barrier of the surface tension device can influence the motion of the liquid column.



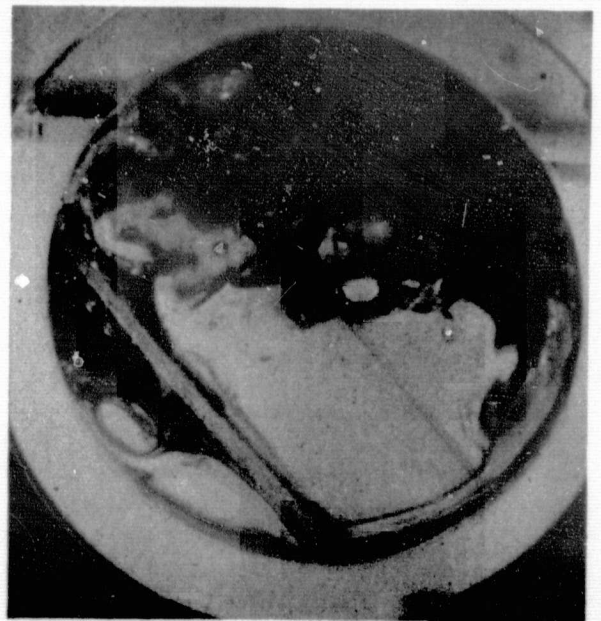
(a)



(b)



(c)



(d)

*Figure V-22 Liquid Reorientation during Test 8*

The chance that all of the requirements could be satisfied within an RCS tank during a Space Shuttle mission is considered remote. At the liquid volume tested, it was found that the column of liquid is always in contact with either the top or bottom of the tank, and there is still some flow of liquid along the tank wall. In the lower compartment, the effects of the liquid column are much less pronounced and very little loss of contact between the liquid and wall occurs.

## 2. Scale Model Tests

All of these tests were performed with the one-third scale model described in Section C. An analysis of the scaling for these tests is presented, followed by a discussion of each test program.

### a. *Scaling Analysis*

A scaling analysis was performed to determine the parameters for the subscale tests. Dimensions, accelerations, flowrates and the screen pressure retention capability were considered in this analysis. Proper scaling of these items, based on propellant and test fluid properties, produced test conditions that should indicate performance of the full-scale system. A discussion of the scaling approach for each of these items follows. Table V-7 defines the symbols used in this section of this report.

1) Dimensional Scaling - A one-third scale was chosen for the subscale model based on handling, cost, fabrication, and test conditions. The full-scale system used a 96.5-cm (38-in.) diameter spherical tank. The subscale tank radius is then  $\frac{1_m}{1_p} = \frac{1_m}{38} = 1/3$ ; and  $1_m = 32.17$  cm (12.67 in.). The dimensional one third scaling was applied to the tank and capillary acquisition/expulsion device.

2) Pressure Differential Scaling - To assure that acquisition device performance of the subscale model is indicative of the full-scale system requires maintaining similarity of the individual pressure drops associated with the system. Since the performance of the system is governed by the capillary retention capability of the screen used, proper scaling requires that

$$[V-6] \quad \frac{\Delta P}{\Delta P_c} \left( \frac{\Delta P}{\Delta P_c} \right)_m = \left( \frac{\Delta P}{\Delta P_c} \right)_p$$



*Table V-7 Nomenclature for Scaling Analysis*

$\Delta P$	- pressure differential across screen
$\Delta P_c$	- capillary pressure retention capability of fine mesh screen
$\sigma$	- liquid surface tension
$r$	- screen pore radius
$\Delta P_h$	- pressure differential caused by hydrostatic head
$\rho$	- liquid density
$g$	- local acceleration in g
$\ell$	- characteristic dimension
$\Delta P_e$	- pressure loss associated with flow of liquid through a screen
$Q$	- volumetric flowrate
$A$	- area of flow - cross-sectional area of screen flow channel
$g_c$	- gravitational constant
$T$	- screen tortuosity factor
$\epsilon$	- screen void fraction
$B$	- screen thickness
$b$	- surface area to unit volume ratio of screen wire
$d$	- screen pore diameter
$\mu$	- liquid absolute viscosity
$A_e$	- liquid/screen contact area
$\Delta P_v$	- velocity head pressure that decreases the static pressure in the capillary system
$V$	- screen channel flow velocity
$\Delta P_f$	- pressure loss caused by frictional flow in a duct
$L$	- length of frictional flow
$D$	- hydraulic diameter of flow duct
$f$	- friction factor
$K$	- empirical correlation factor
$Re$	- Reynolds number of flow
$x$	- Reynolds number exponent
$BP$	- bubble point of capillary system

#### SUBSCRIPTS

$m$	- model
$p$	- prototype
$e$	- entrance loss
$f$	- friction loss
$v$	- velocity head
$s$	- scaled

or:

$$[V-7] \quad \frac{\left( \frac{\Delta P}{\Delta P_c} \right)_m}{\left( \frac{\Delta P}{\Delta P_c} \right)_p} = 1$$

where  $\Delta P$  is the individual differential for entrance loss, velocity head, friction loss, or hydrostatic head. The capillary pressure retention capability of a circular pore having a contact angle of 0 deg is

$$[V-8] \quad \Delta P_c = \frac{2\sigma}{r}$$

This expression was used in scaling each of the individual flow terms.

Acceleration Environment Scaling - Acceleration scaling requires maintaining hydrostatic head similarity between model and prototype. In equation form, the pressure associated with hydrostatic considerations is,

$$[V-9] \quad \Delta P_h = \rho gh$$

For scaling

$$[V-10] \quad \frac{\left( \frac{\Delta P_h}{\Delta P_c} \right)_m}{\left( \frac{\Delta P_h}{\Delta P_c} \right)_p} = 1$$

or:

$$[V-11] \quad \frac{\left( \frac{\rho gh}{2\sigma} \right)_m}{\left( \frac{\rho gh}{2\sigma} \right)_p} = 1$$

The resulting ratio of model acceleration to prototype acceleration is:

$$[V-12] \quad \frac{g_m}{g_p} = \frac{\left( \frac{\sigma}{\rho} \right)_m}{\left( \frac{\sigma}{\rho} \right)_p} \left( \frac{1}{1_m} \right)$$

With a maximum on-orbit acceleration of 0.231 g, the scaling for oxidizer and fuel and the test fluids Freon TF and isopropyl alcohol is shown in Table V-8. Propellant and test fluid temperature was assumed to be 21°C (70°F).

*Table V-8 Low-g Acceleration Scaling for RCS Subscale Model*

Test Fluid	Prototype Acceleration, g	Subscale Acceleration, g	
		Oxidizer	Fuel
Freon TF	0.231	0.45	0.22
Isopropyl Alcohol and Methanol	0.231	1.06	0.51

It is seen that using isopropyl alcohol as the test fluid in a 1-g environment simulates the oxidizer acceleration environment and is a conservative test for fuel.

Table V-9 shows similar results for the high-g phases of a Space Shuttle mission. The subscale accelerations are those required to simulate RTLS and reentry for the propellants and test fluids stated.

*Table V-9 High-g Acceleration Scaling for Subscale Model*

Mission Event	Test Fluid	Prototype Acceleration, g	Subscale Acceleration, g	
			Oxidizer	Fuel
RTLS	Freon TF	3.3	6.67	3.18
	Methanol and IPA	3.3	15.3	7.3
Reentry	Freon TF	2.2	4.44	2.12
	Methanol and IPA	2.2	10.2	4.87

The scaled accelerations are much higher with methanol and isopropyl alcohol than Freon TF. Based on this information and that in the following paragraphs, as well as compatibility considerations, isopropyl alcohol and Freon TF were chosen as the best fluids for the bench and centrifuge tests, respectively.

**Flowrate Scaling** - The scaling of flowrate was based on the pressure differentials caused by entrance loss, velocity head, and friction loss. The equations that govern the required flowrate for each of these terms are based on maintaining the equality defined by Equation [V-6]. These equations are derived here for each pressure term.

Entrance Loss:

The equation for pressure loss caused by flow through a screen is:

$$[V-13] \quad \Delta P_e = \frac{74.88 \text{ TB} \rho}{g_c \epsilon^2 d} \left( \frac{Q}{A} \right)^2 + \frac{8.61 \text{ TB} b^2}{g_c \epsilon^2} \left( \frac{Q}{A} \right)$$

For Scaling:

$$[V-14] \quad \frac{\left( \frac{\Delta P_e}{\Delta P_c} \right)_m}{\left( \frac{\Delta P_e}{\Delta P_c} \right)_p} = 1 = \frac{\left( \frac{74.88 \text{ TB} \rho}{g_c \epsilon^2 d} \left( \frac{Q}{A} \right)^2 + \frac{8.61 \text{ TB} b^2 \mu}{g_c \epsilon^2} \left( \frac{Q}{A} \right) \right)_m}{\left( \frac{74.88 \text{ TB} \rho}{g_c \epsilon^2 d} \left( \frac{Q}{A} \right)^2 + \frac{8.61 \text{ TB} b^2 \mu}{g_c \epsilon^2} \left( \frac{Q}{A} \right) \right)_p} \frac{\frac{2\sigma}{r}}{\frac{2\sigma}{r}}$$

If the same screen is used in the model and prototype and the  $\left( \frac{Q}{A} \right)^2$  term is assumed to be negligible, then the equation reduces to:

$$[15] \quad \left( \frac{\mu}{\sigma} \frac{Q}{A} \right)_m = \left( \frac{\mu}{\sigma} \frac{Q}{A} \right)_p$$

and

$$[V-16] \quad \frac{Q_m}{Q_p} = \left( \frac{1_m}{1_p} \right)^2 \left( \frac{\frac{\mu_p}{\sigma_p}}{\frac{\mu_m}{\sigma_m}} \right)$$

For RTLS simulation of an oxidizer tank with Freon TF as the test fluid and a full-scale flowrate of 11.9 kg/sec (26.2 lbm/sec), the ratio of flowrates is:

$$[V-17] \quad \frac{Q_m}{Q_p} = \left( \frac{1}{3} \right)^2 \left( \frac{0.21}{0.43} \right) = 0.0542$$

and the model flowrate required,  $Q_m$ , is 0.45 l/sec (27.2 in.<sup>3</sup>/sec).

### Velocity Head:

The velocity head associated with flow decreases the static pressure in the channel and adds to the pressure differential across the screen. The equation defining velocity head is:

$$[V-18] \quad \Delta P_v = \frac{\rho V^2}{2g_c} = \frac{\rho Q^2}{2g_c A^2}$$

Solving Equation [V-7] for velocity head pressure differentials results in

$$[V-19] \quad \frac{Q_m}{Q_p} = \sqrt{\left(\frac{\sigma}{\rho}\right) \frac{m}{p}} \left(\frac{1_m}{1_p}\right)^2$$

Again solving this equation for RTLS oxidizer conditions and Freon TF as the referee fluid, we have

$$[V-20] \quad \frac{Q_m}{Q_p} = 0.091 \text{ and } Q_m = 0.75 \text{ l/sec (45.7 in.}^3\text{/sec).}$$

### Friction Loss:

The friction loss associated with flow of an incompressible fluid in a duct reduces the total and static pressure of the system. This added pressure loss must also be supported by the screen pressure retention capability. The equation defining frictional losses in a duct is:

$$[V-21] \quad \Delta P_f = f \frac{L}{D} \frac{\rho V^2}{2g_c} = f \frac{L}{D} \frac{\rho Q^2}{2g_c A^2}$$

The friction factor is a function of the Reynolds number associated with flow and may be defined by:

$$[V-22] \quad f = \frac{K}{Re^x}$$

Substituting into Equation [V-21], the relationship for frictional pressure loss becomes:

$$[V-23] \quad \Delta P_f = \frac{K \mu^x L}{D^{(1+x)}} \left( \frac{\rho^{(1+x)} Q^{(2-x)}}{2g_c A^{(2-x)}} \right)$$

For the range of Reynolds numbers of interest,  $x = 0.1675$  gives a conservative relationship for friction factor. The resulting ratio of flowrates for model and prototype is:

$$[V-24] \quad \frac{Q_m}{Q_p} = \sqrt[1.8325]{\left(\frac{\mu_p}{\mu_m}\right)^{0.1675} \left(\frac{\sigma_m}{\sigma_p}\right) \left(\frac{\rho_p}{\rho_m}\right)^{0.8325} \left(\frac{l_m}{l_p}\right)^{3.825}}$$

For the conditions mentioned previously,  $Q_m = 0.64 \text{ l/sec}$  ( $39.1 \text{ in.}^3/\text{sec}$ ). A list of flowrates required to scale each pressure term for bench tests and centrifuge tests is shown in Table V-10. These numbers are based on isopropyl alcohol and Freon TF as the test fluids for the bench tests and centrifuge tests, respectively.

Table V-10  
Scaled Flowrates Based on Pressure Differentials for Subscale Model

Test	Depletion Mode	Test Fluid	Propel- lant	Propel- lant Temperature, °C (°F)	Scaled Flowrate, l/sec (in./sec)		
					$\Delta P_e$	$\Delta P_v$	$\Delta P_f$
Bench	Low	Isopropyl Alcohol	N <sub>2</sub> O <sub>4</sub>	21 (70)	0.0613 (3.74)	0.423 (25.8)	0.308 (18.8)
			MMH	4.4 (40)	0.115 (7.0)	0.295 (18.0)	0.241 (14.7)
	High		N <sub>2</sub> O <sub>4</sub>	21 (70)	0.125 (7.6)	0.946 (57.7)	0.692 (42.2)
			MMH	4.4 (40)	0.246 (15.0)	0.648 (39.5)	0.528 (32.2)
	Centrifuge RTLS	Freon TF	N <sub>2</sub> O <sub>4</sub>	21 (70)	0.446 (27.2)	0.749 (45.7)	0.641 (39.1)
			Re-Entry	Freon TF	N <sub>2</sub> O <sub>4</sub>	21 (70)	0.336 (20.5)

Data for both propellants, MMH and  $N_2O_4$ , are shown at the worst case temperature. Flowrates for  $N_2O_4$  were calculated at 21°C (70°F) because temperature differentials possible (4.4°C to 51°C) (40°F to 125°F) caused little variation in scaling results. The lowest possible on-orbit temperature of 4.4°C (40°F) is by far the worst case for scaling MMH flowrates.

Analysis of the flowrate data in Table V-10 clearly shows that for a given set of propellant and test conditions, one flowrate will not scale each of the pressure loss terms, i.e., at any given test flowrate the relative magnitude of the pressure loss terms at breakdown will be different for the subscale model than for the full scale tank. The relative magnitude change, caused by variation in fluid properties between propellant and test fluid, is greater for isopropyl alcohol, because of the very high viscosity of isopropyl alcohol which requires lower flowrates to scale the entrance loss term. For Freon TF, the relationship between density, viscosity, and surface tension more closely resembles  $N_2O_4$ , resulting in flowrates that are closer in magnitude for each of the pressure loss terms.

Since the ideal case of exact scaling of each flow loss term cannot be achieved, the question as to what flowrate should be selected to best represent the mission simulation of interest must be addressed. The most reasonable approach is to base the selection of scaled flowrate on the relative importance of the flow losses in the prototype tank. For high-g phases of an RCS mission, and low-g conditions where liquid is puddled over the tank outlet, the entrance loss term  $\Delta P_e$  is the only contributor to the losses that impact device performance. The other flow terms,  $\Delta P_v$  and  $\Delta P_f$ , do not contribute to screen breakdown because the flow channels are either submerged in liquid or contain static liquid. As a result, RTLS and reentry test flowrates may be scaled on the basis of entrance loss alone. The resulting flowrates for centrifuge tests are shown in Table V-11.

Table V-11

*Scaled Flow Rates for Centrifuge Tests with Freon TF  
@ 21°C (70°F)*

Mission Simulation	$N_2O_4$ Flowrate, kg/sec (lbm/s)	Propellant Temperature, °C (°F)	Test Scaled Flowrate, l/sec (in. <sup>3</sup> /s)
RTLS	11.9 (26.2)	21 (70)	0.446 (27.2)
Reentry	8.9 (19.7)	21 (70)	0.336 (20.5)

When the outlet of the channel system, either upper or lower compartment, is not covered by liquid and screen in this area is exposed to the ullage, each flow term will contribute to the gas ingestion into the system. This condition is simulated by on-orbit depletion of the forward tank during various mission events, and in particular event 14. This situation requires consideration of each pressure loss and its relative contribution to the breakdown of the system. The relative importance of these terms at system breakdown was determined by computer runs for the

prototype tank in an orientation that simulated a bench test configuration. These runs were made for both oxidizer and fuel to determine variation in  $\Delta P$  and the worst case condition for scaling.

Four tank attitudes were studied during the subscale bench test program. Two of these attitudes puddled liquid over the tank outlet. The remaining two orientations were with the +X axis up and +Z axis up. The latter tank attitude, +Z axis up, represents a worst-case condition for scaling because the highest friction losses will be incurred with this situation. This orientation was simulated on the computer program and used to determine scaled flowrates for these test orientations.

Table V-12 shows results of the computer analysis. It should be noted that propellant temperature was assumed to be 21°C (70°F), the safety factor on bubble point was 1.0, and the acceleration was 0.231 g in the +Z direction.

Table V-12

*Relative Magnitude of Pressure Terms for Full-Scale System as Determined by Computer Analysis*

Depelction Mode	Propellant	Temperatures, °c (°F)	Bubble Point, N/cm <sup>2</sup> (psi)	Flowrate, Kg/sec (lbm/s)	Pressure Differentials in % of Bubble Point,			
					$\Delta P_h$	$\Delta P_e$	$\Delta P_v$	$\Delta P_f$
Low	N <sub>2</sub> O <sub>4</sub>	21 (70)	0.707 (1.026)	4.5 (10)	30.0	65.0	3.4	1.6
	MMH	21 (70)	0.965 (1.40)	2.84 (6.25)	13.4	84.0	1.7	0.9
High	N <sub>2</sub> O <sub>4</sub>	21 (70)	0.707 (1.026)	9.91 (21.85)	23.3	46.6	22.1	8.0
	MMH	21 (70)	0.965 (1.40)	6.19 (13.65)	10.0	75.0	10.0	5.0

At low mode depletion, the hydrostatic head and entrance loss terms are dominant, accounting for a total of 95% and 97.4% of the bubble point for N<sub>2</sub>O<sub>4</sub> and MMH, respectively. The entrance loss accounts for 92% and 97% of the pressure differential attributable to flow for oxidizer and fuel, respectively. Consequently, low mode depletion may be scaled on the basis of entrance loss terms with negligible error incurred.



During high mode depletion, the entrance loss and hydrostatic head terms account for a total of 70% and 85% of the bubble point of  $N_2O_4$  and MMH, respectively. Although the entrance loss is still dominant at 61% and 85% of the total flow loss for oxidizer and fuel, the remaining terms are of sufficient magnitude to warrant consideration in scaling flowrate, especially for  $N_2O_4$ . This was achieved by weighting the individual pressure loss terms in the equation governing system performance according to the percentages of bubble point shown in Table V-12. The basic equation that dictates performance of a screen-channel network is:

$$[V-25] \quad \Delta P_e + \Delta P_f + \Delta P_v + \Delta P_h = BP$$

Oxidizer simulation at high mode is the worst case presented in Table V-12 for flowrate scaling. Substituting the tabularized values of  $\Delta P$  for this case into Equation [V-25] gives:

$$[V-26] \quad 0.446 BP + 0.080 BP + 0.221 BP + 0.233 BP = BP$$

or

$$0.446 + 0.080 + 0.221 = 0.767$$

This shows the relative importance of each flow term ( $\Delta P_e$ ,  $\Delta P_f$ , and  $\Delta P_v$  in order from left to right) to the bubble point and the total contribution of flow terms to screen pressure retention capability. The values shown on the left are the percentage of bubble point each term would have in the subscale model at system breakdown if the model were outflowed at the flowrate scaled for that term as shown in Table V-12. Because each term requires a different scaled flowrate, scaling one term means an increase or decrease in the other two pressure differentials as compared to the values of Equation [V-26]. The dependency of each term with flowrate is of major importance in order to maintain total flow pressure differential constant. Both  $\Delta P_f$  and  $\Delta P_v$  vary as velocity of flow to the second power. Assuming entrance loss,  $\Delta P_e$ , varies linearly with velocity, we have in terms of volumetric

flowrate  $\Delta P_e \propto \frac{Q}{A_e}$ ,  $\Delta P_f \propto \left(\frac{Q}{A}\right)^2$ , and  $\Delta P_v \propto \left(\frac{Q}{A}\right)^2$ . It should be

noted that  $A$  is the channel duct cross-sectional area of flow for the subscale model and is constant for this analysis. The term  $A_e$  is the entrance area for liquid flow into the surface tension system at breakdown and is dependent on the amount of liquid in the tank for given conditions. If we denote  $Q_m$  as the model volumetric flowrate and  $Q_{m_e}$ ,  $Q_{m_f}$ , and  $Q_{m_v}$  as the model scaled flowrates for each flow term, the variation of each term from scaled conditions is given by

$$[V-27] \quad \Delta P_e \propto \frac{\frac{Q_m}{A_e}}{\frac{Q_{m_e}}{A_{e_s}}} = \frac{Q_m}{Q_{m_e}}$$

$$[V-28] \quad \Delta P_f \propto \left( \frac{\frac{Q_m}{A}}{\frac{Q_{m_s}}{A}} \right)^2 = \left( \frac{Q_m}{Q_{m_f}} \right)^2$$

$$[V-29] \quad P_v \propto \left( \frac{\frac{Q_m}{A}}{\frac{Q_{m_v}}{A}} \right)^2 = \left( \frac{Q_m}{Q_{m_v}} \right)^2$$

The key is to assure a meaningful test that will indicate prototype performance. The liquid level and thereby entrance area in the subscale model must remain scaled so  $A_e = A_{e_s}$ . Substituting

Equation [V-27] thru [V-29] into Equation [V-26] gives:

$$[V-30] \quad 0.466 \frac{Q_m}{Q_{m_e}} + 0.080 \left( \frac{Q_m}{Q_{m_f}} \right)^2 + 0.221 \left( \frac{Q_m}{Q_{m_v}} \right)^2 = 0.767$$

This equation gives a solution for flowrate scaling when each of the flow terms is considered to have a significant effect on system performance. Substituting values for scaled flowrates from Table V-10 results in

$$0.466 \frac{Q_m}{7.6} + 0.080 \left( \frac{Q_m}{42.2} \right)^2 + 0.221 \left( \frac{Q_m}{57.7} \right)^2 = 0.767$$

Solution of this equation gives a value for  $Q_m$  of 0.2 l/sec (12.2 in.<sup>3</sup>/sec). This number is a great deal lower than that dictated by velocity head and friction loss scaling, and somewhat higher than that for  $Q_{m_e}$ . This approach was also used for

scaling MMH at high mode conditions at two different temperatures--4.4°C (40°F) and 51.7°C (125°F).

Bench test scaling results are shown in Table V-13 along with the other scaled flowrates. Flowrates are presented as a function of liquid orientation and propellant temperature. When liquid is puddled over the outlet, -X and -Z axes up, only the entrance term is significant. With outlet channel exposed to ullage, +X and +Z axes up, all terms were considered resulting in higher flowrate at high mode scaling. A variation in flowrate of about two is noted for MMH at the temperatures shown--the low temperature condition of 4.4°C (40°F) requiring much higher flowrates for performance scaling. Since the flowrate variation for N<sub>2</sub>O<sub>4</sub> over this temperature range is insignificant, only data for 20°C (70°F) is shown for N<sub>2</sub>O<sub>4</sub>. The values for scaled flowrates derived in this section were used in analyzing centrifuge and expulsion test results. Actual test data, predicted performance, and scaled performance are discussed separately in the presentation of each test.

Table V-13 Bench Test Scaled Flowrates

Prototype Depletion Mode	Tank Orientation	Scaled Model Flowrates			
		Prototype Flowrate, kg/s (lbm/s)	$\frac{\text{l}}{\text{s}}$ (in. <sup>3</sup> /s)		
			N <sub>2</sub> O <sub>4</sub>	MMH	
			21°C (70°F)	4.4°C (40°F)	51.7°C (125°F)
Low	+X up and +Z up	4.5 N <sub>2</sub> O <sub>4</sub> (10) 2.8 MMH (6.25)	0.0607 (3.7)	0.115 (7.0)	0.0574 (3.5)
	-X up and -Z up	↓	0.0607 (3.7)	0.115 (7.0)	0.0574 (3.5)
High	+X up and +Z up	9.9 N <sub>2</sub> O <sub>4</sub> (21.85) 6.2 MMH (13.65)	0.200 (12.2)	0.287 (17.5)	0.156 (9.5)
	-X up and -Z up	↓	0.125 (7.6)	0.246 (15.0)	0.133 (8.1)

## b. Tests

1) Basic Bench Test Apparatus and Procedure - The same basic test apparatus was used for all of the fill, drain, expulsion, and pulsed flow tests. The test system is shown schematically in Figure V-23, and is pictured in Figures V-24 and V-25. The system consisted primarily of the 1/3-scale model transparent tank, a pressurization system, and a supply/receiver tank with volume calibration and parallel outflow lines. As seen in the figures, the tank was fitted with a flexible, transparent outflow line. This transparent line allowed easy detection of screen breakdown, because the gas ingestion into the lower compartment screen device was readily seen when it entered the transparent line. The parallel outflow lines shown in the schematic were used in the pulsed-flow tests, with one line for steady flow and the other for simultaneous pulsed flow. Not shown in the schematic, but seen in Figure V-25, is the scale on which the test tank rested during the tests. Both the scale and the graduated supply/receiver tank were used to measure the weight and volume, respectively, that was expelled from the tank during a test.

The pressurization system was connected so that it could be used to pressurize either the test tank for an expulsion, or the supply tank for a transfer of liquid into the test tank. The three vents on the test tank, labeled 5, 6, and 7 on Figure V-23, allowed the upper and lower compartments to be vented for filling or drying the tank and screen devices. Vent 6 allowed the upper compartment to be vented when the tank was in a horizontal attitude with the tank outlet on the bottom.

The test tank support fixture was designed in such a way that the tank could be positioned in any of four attitudes for expulsion testing. The normal 1-g attitude is pictured in Figure V-25. In addition, the tank could be completely inverted in the fixture for a -1g test, or the test fixture could rotate 90 deg either clockwise or counterclockwise, and it would rest on one of the other two flat surfaces pictured.

The tank was tested to a proof pressure of  $20.7 \text{ N/cm}^2$  (30 psia) using the standard 1.5 safety factor applied to the maximum working pressure of  $13.8 \text{ N/cm}^2$  (20 psia). A relief valve was placed in the system to assure that the working pressure was not exceeded.

The flow valves in the system were hand-operated ball valves. Valve 2 in the steady flow line was a 1.9 cm (3/4 in.) valve with a bore approximately the same size as the internal diameter of the flow lines. The valve in the pulsed-flow line is discussed in detail in the section on pulsed flow. The flowmeter shown in the schematic was inserted and used only during the pulsed flow tests.

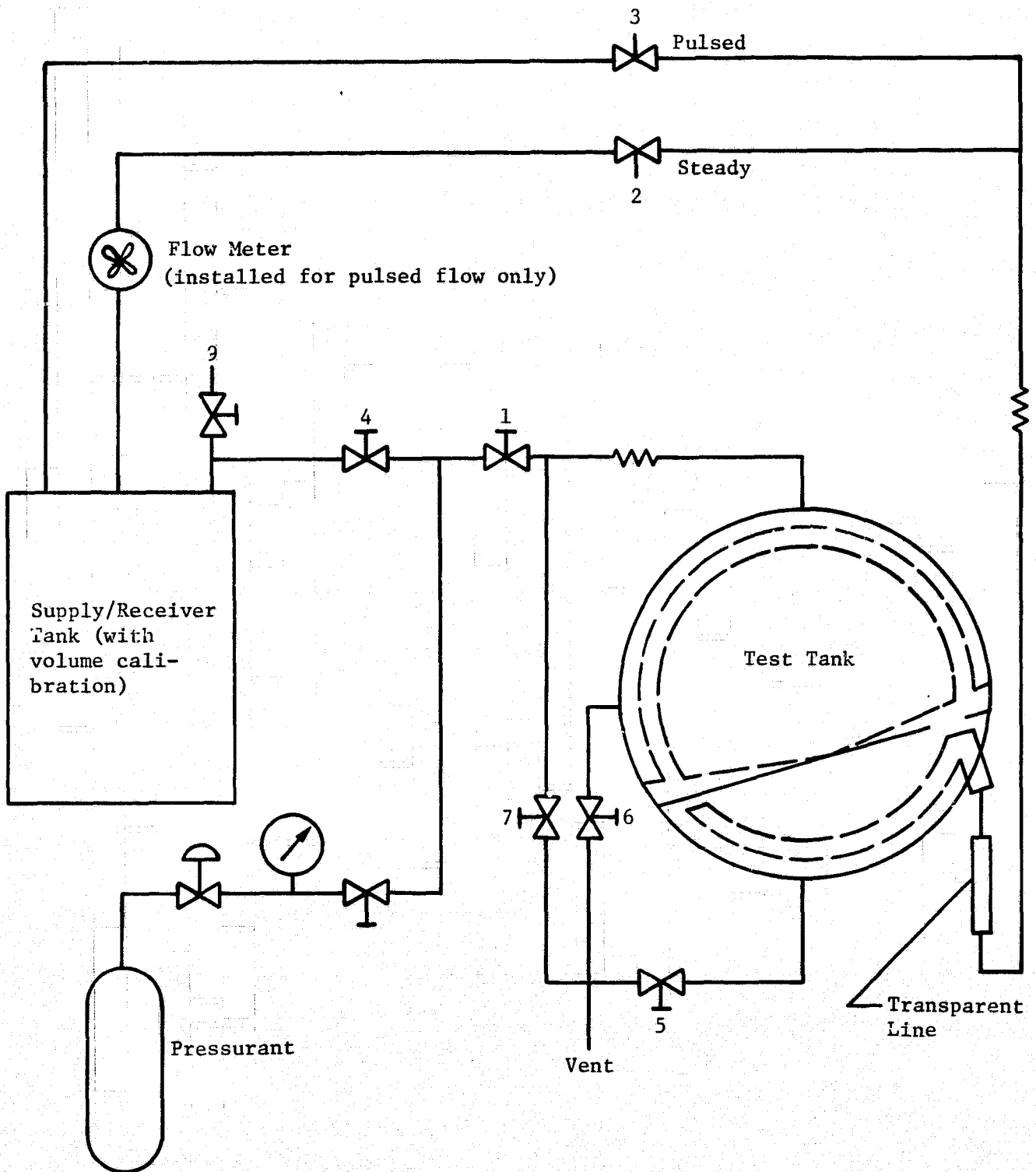


Figure V-23 Subscale Test Schematic

Figure V-24

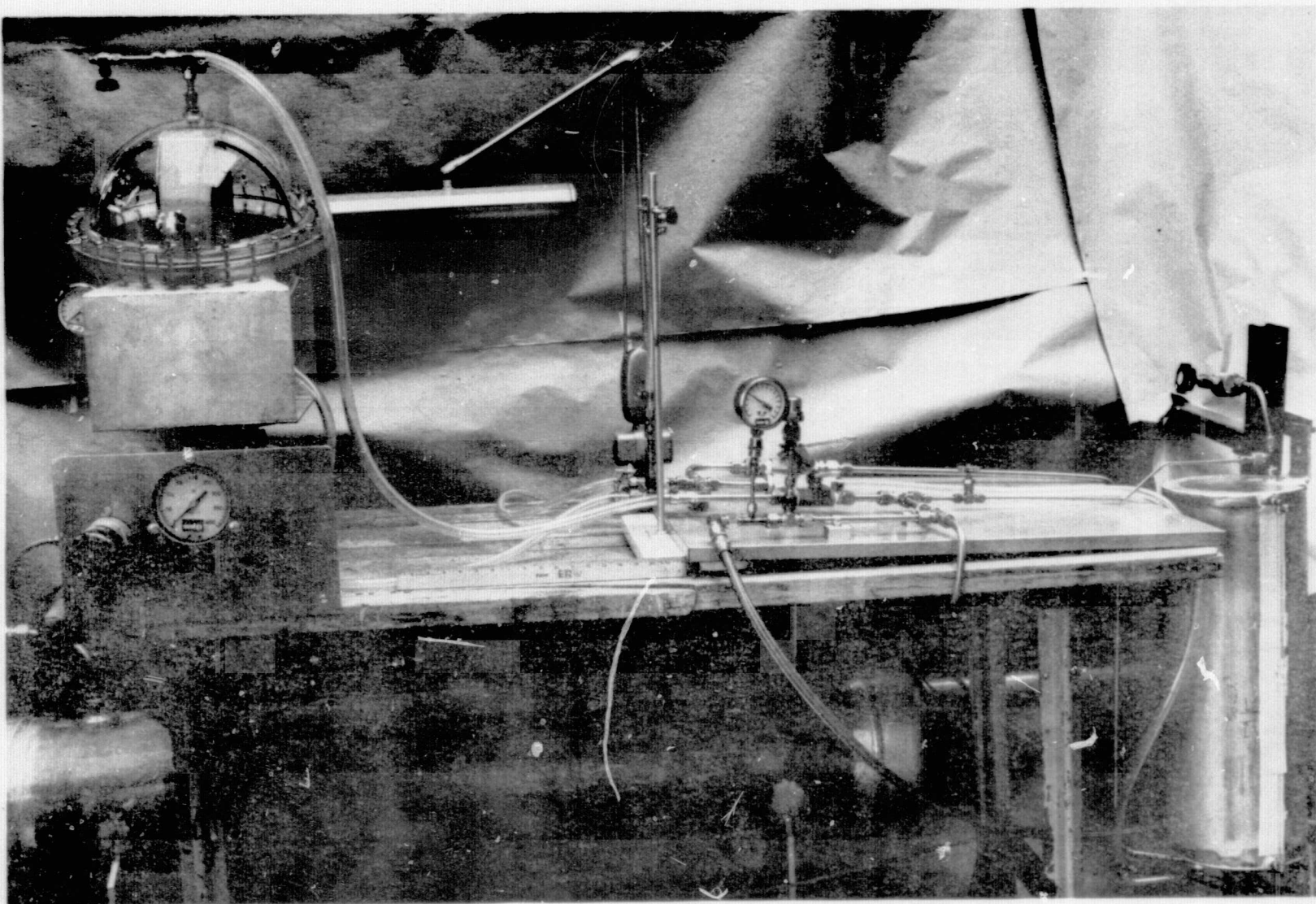
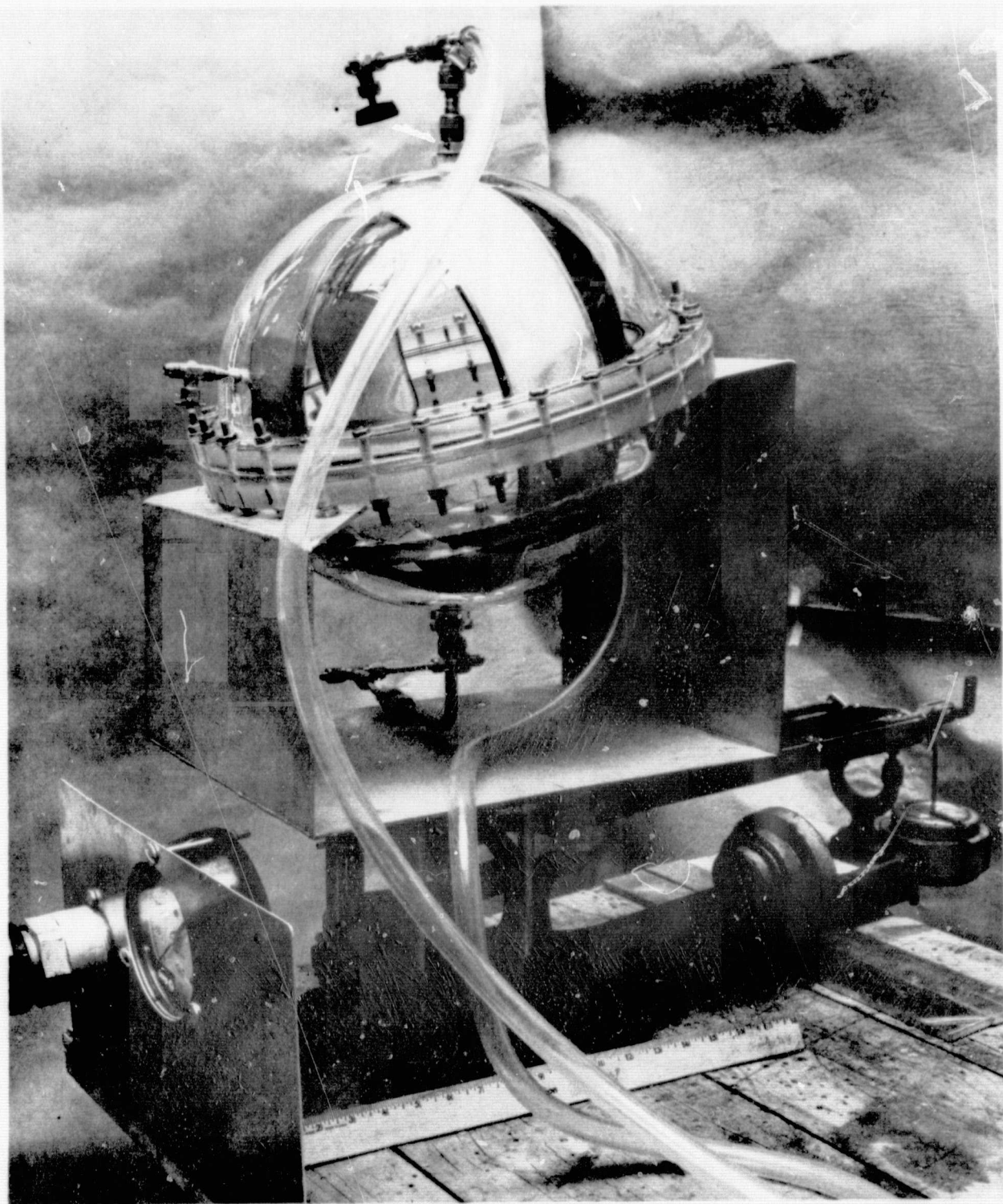


Figure V-24 Complete Test System





*Figure V-25 One-Third Scale Model Coupled to Test System*

The test procedure for all tests (fill and drain, expulsion, and pulsed flow) was essentially the same. The test tank was placed on the scales and the dry weight was recorded. At the same time, the volume of liquid in the supply tank was recorded. The next step was to pressurize the supply tank and allow liquid to be transferred until the transparent flow line was filled just to the level of the tank outlet. Again the test tank weight and supply tank volume were recorded. This technique was used to compensate for the effect on the weight of the tank that the filled flow line would have. The tank was then filled to the appropriate level for the specific test and final test tank weight and supply tank volume were recorded.

After the fill procedure was completed, the supply tank was vented, and the test tank was pressurized. The expulsion test was initiated by actuating the ball valve in the flow line. The instant that bubbles were first observed in the outflow line, the valve was again closed and the final test tank weight and supply tank volume were recorded. The elapsed time between the initiation and the termination of the expulsion was also recorded for use in determining the average flow rate for the test. Breakdown characteristics of the screens and operator reaction times were generally such that when bubbles were first noted in the outflow line and the flow valve was closed, the volume of liquid differed by only a few cubic centimeters. Therefore, very accurate values of the volume and weight expelled could be obtained by subtracting the final data from the filled flow line data. The scales were measured to the nearest 5 grams (0.01 lbm) and the volume level was recorded to the nearest millimeter (0.04 in.). This accuracy resulted in measurement errors, using single sample error analyses, of from 0.28% to 0.96%. (See Error Analysis Summary for the tests.)

## 2) Fill and Drain Tests

a) Objectives - The objectives of this series of tests were to verify the proposed loading and draining techniques in both the vertical and horizontal positions and to develop procedures for accurate and repeatable loading of the full scale tank.

The criteria used were that the tank be fillable to a minimum 3% ullage, that the flow channels in the lower compartment be free of vapor or noncondensable gas bubbles after loading, and that the tank be capable of draining most of the liquid not trapped in the screen device.

b) Approach - For the fill test, the tank was loaded through the normal tank outlet while venting the tank through the pressurization line. For the draining tests the test liquid was expelled at flow-rates lower than the nominal scaled orbital demand. Both isopropyl alcohol and water were used as test fluids for this series of tests.



c) Procedures - The basic procedures for acquiring data were discussed previously. By comparing the data with the known value of the tank volume, the quantity of gas trapped during a fill sequence could be assessed; by comparing the final weight of the drained tank with its dry weight, the amount of liquid remaining after a drain sequence could be determined.

Several techniques for both filling and draining were investigated for a wide range of low rates. Fill tests were conducted with the screens in both wet and dry initial conditions.

d) Data and Results - Fill Tests - The technique found to give the best results involved filling the lower compartment at a low fill rate until liquid began to flow through the barrier window, and then increasing the fill rate to any desired level greater than the initial rate. The lower channels had wicking barriers approximately 6.4 mm (0.25 in.) square for a total area of 40 mm<sup>2</sup> (0.063 in.<sup>2</sup>). Because of their small size, any splashing of the liquid would immediately wet the screen on the wicking barrier, trapping any remaining gas in the channels. Therefore, a slow initial flow rate, with a quiescent liquid surface proved to be the most effective in allowing the lower channels to vent any internal gas before the lower compartment was filled.

The upper channels did not have a wicking barrier, as such. However, because of the fabrication techniques used, the screen covering the exterior surface of the upper channel manifold was isolated from the remainder of the channel screens. This screen [approximately 40 cm<sup>2</sup> (6.25 in.<sup>2</sup>)] acted as a very effective wicking barrier, allowing all the gas in the upper channel assembly to be purged even at the highest fill rates.

With the screens initially in the dry condition, most of the trapped gas was in the lower compartment channels. Some small volume was trapped at the screen window, and probably less than 33 cc (2 in.<sup>3</sup>) total was trapped in the upper manifold and channel system. The amount trapped was functionally related to the fill rate, and for the isopropyl alcohol tests this relationship is shown in Figure V-26. The curve shows that from essentially no trapped gas at a 0.16 l/s (10 in.<sup>3</sup>/s) fill rate, the trapped volume increased to approximately 98 cc (6 in.<sup>3</sup>) at a fill rate of 330 cc/s (20 in.<sup>3</sup>/s). These same tests were also run with demineralized deionized water; however, whereas screens wetted with isopropyl alcohol were easily dried out, such was not the case for screens wetted with water. As a result the amount of trapped gas was variable from a low of 82 cc (5 in.<sup>3</sup>) when the screens were obviously dry, to a high of 660 cc (40 in.<sup>3</sup>) for screens that were thought to be dry but apparently were not. All these water fill tests were conducted at a low flowrate, so no variation due to flowrate can be imparted to the data.

Figure V-26

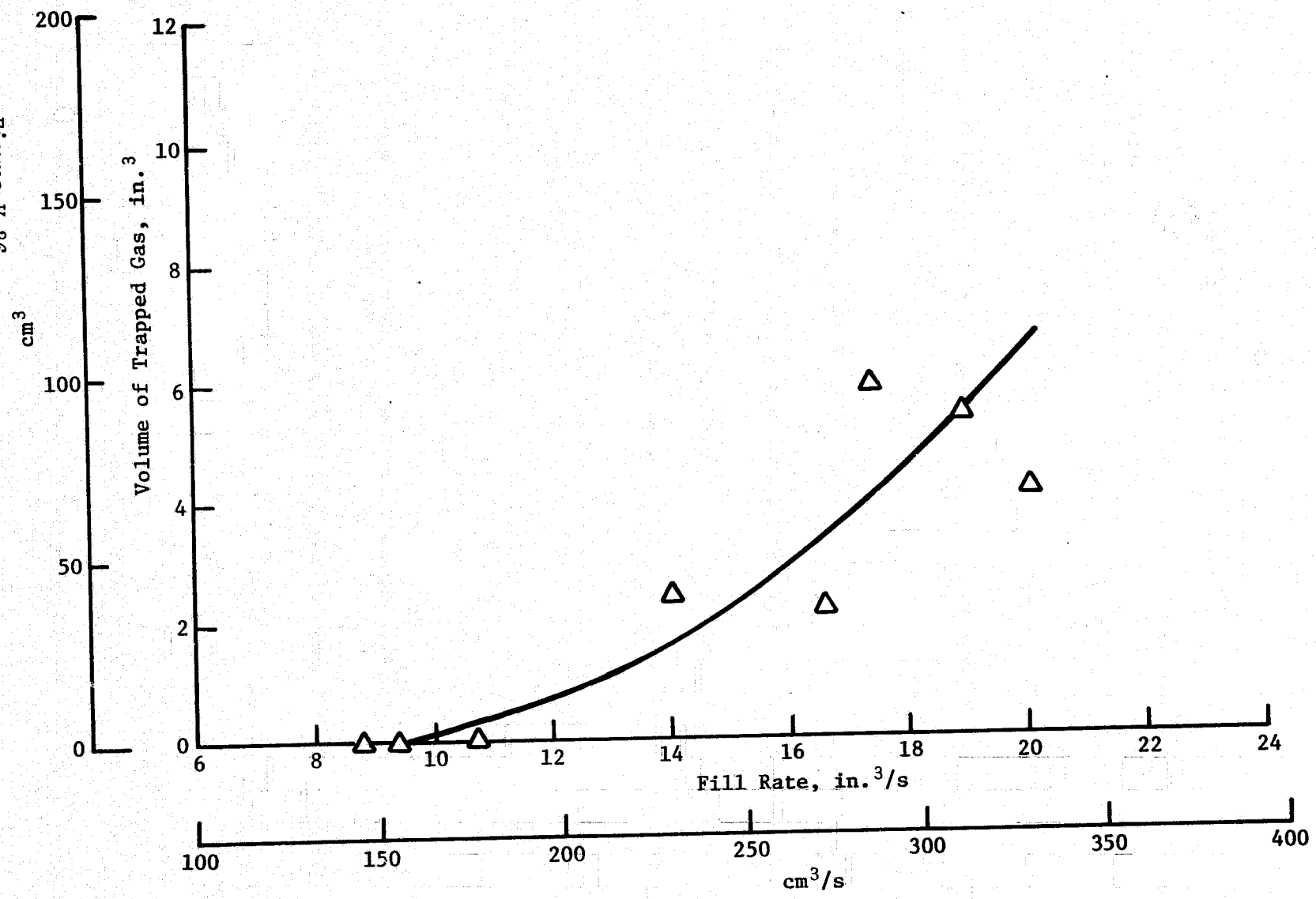


Figure V-26 Trapped Gas Volume as a Function of Fill Rate for Isopropyl Alcohol

Wet screen fill tests were conducted with water only because the upper channel screens could not be consistently maintained in a wet condition with isopropyl alcohol after the bulk liquid had been drained from the compartment. This implied screen dry out and the inability of the upper channel manifold to remain wet with the alcohol. The average volume of trapped gas for these wet screen tests was 610 cc (37 in.<sup>3</sup>). The barrier manifold was always filled, but a substantial portion of the upper channel volume contained gas as well as half of the lower channel assembly. This 610 cc (37 in.<sup>3</sup>) volume represents nearly 4% of the total tank volume.

The fill tests also revealed that the tank had to be completely filled to fill the upper channels. From that point, the tank could be off-loaded to any desired level. But to simply fill the tank to the desired level would not fill the upper channels.

A brief summary of the important results of the filling tests follows.

- 1) The tank was successfully filled to the desired level with dry screens.
- 2) Wicking barriers in the lower compartment were not totally effective.
- 3) The channel manifold screen in the upper compartment acted as an effective wicking barrier.
- 4) For dry screen tests, most gas was trapped in the lower compartment.
- 5) The tank had to be completely filled to fill the upper channels.
- 6) Filling was accomplished in two minutes with essentially no gas trapped and in just under one minute with approximately 0.6% gas trapped.
- 7) Filling with wet screens trapped large quantities of gas - nearly the entire volume of the channels.

The numerical results of the fill tests are summarized along with the drain test results in Table V-14.

Table V-14 Subscale Fill and Drain Test Results

Test	Screen Condition	Fluid	Tank Orientation	Flowrate and Procedure	Gas Trapped or Liquid Residual, cc (in. <sup>3</sup> )
Fill Tests	Dry	Isopropyl	+1g	Filled slowly until -Z channel wicking barrier was covered, and then increased flow rate to test condition	98 at 0.328 l/s (6 at 20 in. <sup>3</sup> /s)
		Water	+1g		82 (5) Dry to 655 (40) Wet
	Wet	Isopropyl	+1g		
		Water	+1g		
					606 (37) Average
Drain Tests		Isopropyl	Vertical	Drained slowly until breakdown occurred, then quickly increased flow rate to blow out all possible liquid	131-147 (8-9)
		Water			
		Isopropyl	Horizontal	Tests not conducted	
		Water			

e) Drain Tests - The procedure developed for the most efficient draining was to expel the fluid in a normal manner at a low flow rate until the channels in the lower compartment broke down. At that point the driving pressure was increased to blow all remaining fluid in the channels out of the tank in a two-phase mixture. The results with this technique were a fairly constant residual volume, in the 130 to 150 cc (8 to 9 in.<sup>3</sup>) range. This occurred because of the inclined barrier with the window at the upper edge.

During the drain, the volume in the upper bulk region would be expelled completely. As soon as the upper bulk was depleted, the upper channels would begin to drain. When the channels had drained, the barrier manifold would begin to drain and as soon as the barrier window was uncovered, transfer of liquid across the barrier would stop and the lower compartment would begin to drain. This compartment would be completely drained except for the small amount of liquid in the bottom of the compartment not in contact with the screens. When breakdown occurred in the lower compartment, increasing the pressure would blow out the contents of the lower channels. Therefore, the liquid that could not be drained from the tank was essentially that volume trapped in the barrier manifold. This volume represented less than 1% of the tank volume. The results of these tests are also summarized in Table V-14.

f) Conclusions - The tank can be filled successfully to any level independent of fill rate and with little trapped gas if the screens are initially dry. Wicking barriers can be effective if properly designed. Filling with wet screens does not appear feasible without additional venting capability being provided.

The tank can be successfully drained to less than 1% residual in the inclined barrier configuration; a noninclined barrier design could be drained to nearly 100%.

### 3) Expulsion Tests

a) Objective - The objective of these tests was to demonstrate the capability of the propellant management device to deliver gas-free propellant during simulated on-orbit mission events. An additional objective was to compare the results with estimates provided by the computer to verify ability to predict performance in both 1-g and other gravitational environments.

b) Approach - In excess of 175 expulsion tests were conducted on the subscale tank. Tests were run in four different tank attitudes starting with the nominal 1-g attitude and rotating the tank in 90 deg increments around its Y-axis for each of the other three attitudes. Isopropyl alcohol was used as the test fluid because of its more favorable compatibility with the Plexiglas tank shell.

The design philosophy considered that any liquid in the upper compartment during the orbital phase of the mission could eventually be fed across the barrier into the lower compartment because of changes in tank attitude and acceleration levels. Therefore, attention was concentrated on tests that depleted the lower compartment while leaving the upper compartment free of liquid. These tests are more representative of an orbital type of depletion. Some testing of a full tank was done despite the more limited usefulness of the results, however. In addition, computer predictions were available only for the lower compartment depletion. The approach for all the tests was to determine expulsion efficiency as a function of flowrate.

c) Procedures - The basic procedures were outlined previously. Because of the difficulty encountered in loading the device when the screens were wet, it was necessary to manually rotate the tank after loading so that any trapped gas could migrate to the exit. This was followed by a brief expulsion to purge the gas from the system into the supply tank. This expulsion was terminated and the tank was again loaded to the required level. This method assured that no gas was in the system and made accurate and repeatable data acquisition possible. For tests in other than the 1-g attitude, the tank was filled in the 1-g attitude and then manually rotated. Flowrates were controlled by varying the test tank pressure.

d) Data and Results - The results of the expulsion tests conducted in the 1-g attitude are shown in Figure V-27. The expulsion efficiencies, based on the nominal propellant load, ranged from 98% to 96% for the lower compartment over the flowrate range tested. Data for full tank expulsions are also shown. The difference between the full tank data and the lower compartment only data, a roughly constant value of 3.5%, is the amount trapped in the upper compartment because of the inclined barrier. Also shown is the computer performance prediction, which falls slightly below the actual data but is in very good agreement.

At the bottom of the figure, the range of scaling to actual propellants is indicated. As is shown, the low mode flowrates are lower than any flowrate actually tested and would have expulsion efficiencies in excess of 98%. An expulsion efficiency of approximately 98% was also obtained at the scaled high mode flowrate for  $N_2O_4$ . A range of flowrates for MMH is also shown. The comparison for this test is a conservative one (See Scaling Analysis.); however, the data indicate an expulsion efficiency of about 98% for this case also.

The results for expulsion tests from the lower compartment, in the attitude with the tank outlet down, are shown in Figure V-28. This attitude is also representative of the reentry attitude. Outflow rates ranged from less than 0.15 l/s (9 in.<sup>3</sup>/s) to greater than 0.36 l/s (22 in.<sup>3</sup>/s) and the corresponding expulsion efficiencies ranged from a high of 97.7% to a low of 94.2%. Also shown is the computer prediction, which is in excellent agreement with experimental results. The data show expulsion efficiencies in the 98% or greater range for low mode depletion with both propellants and high mode depletion with  $N_2O_4$ .

Expulsion test results with the tank inverted, outlet compartment up, are presented in Figure V-29. For the range of isopropyl flowrates tested, expulsion efficiencies varied from 92% to 89%. In this case, the computer predictions were approximately 3.5% higher than the actual test data. This difference results from the difficulty encountered in modeling this particular tank attitude and the fact that the channel-to-barrier distance was greater than the design value. The expulsion efficiency results for this attitude are several percentage points less than those at comparable flowrates in the positive 1-g attitude. Much of this can be explained by the fact that the same amount of liquid wets significantly more of the lower channel screens in the 1-g attitude than in the attitude discussed here. Therefore, for any given volume of liquid, the entrance losses will be higher in the minus 1-g attitude, and breakdown will of necessity occur sooner, reducing expulsion efficiency. Again, the scaled flowrates are shown at the bottom of the figure.

V-68

Figure V-27

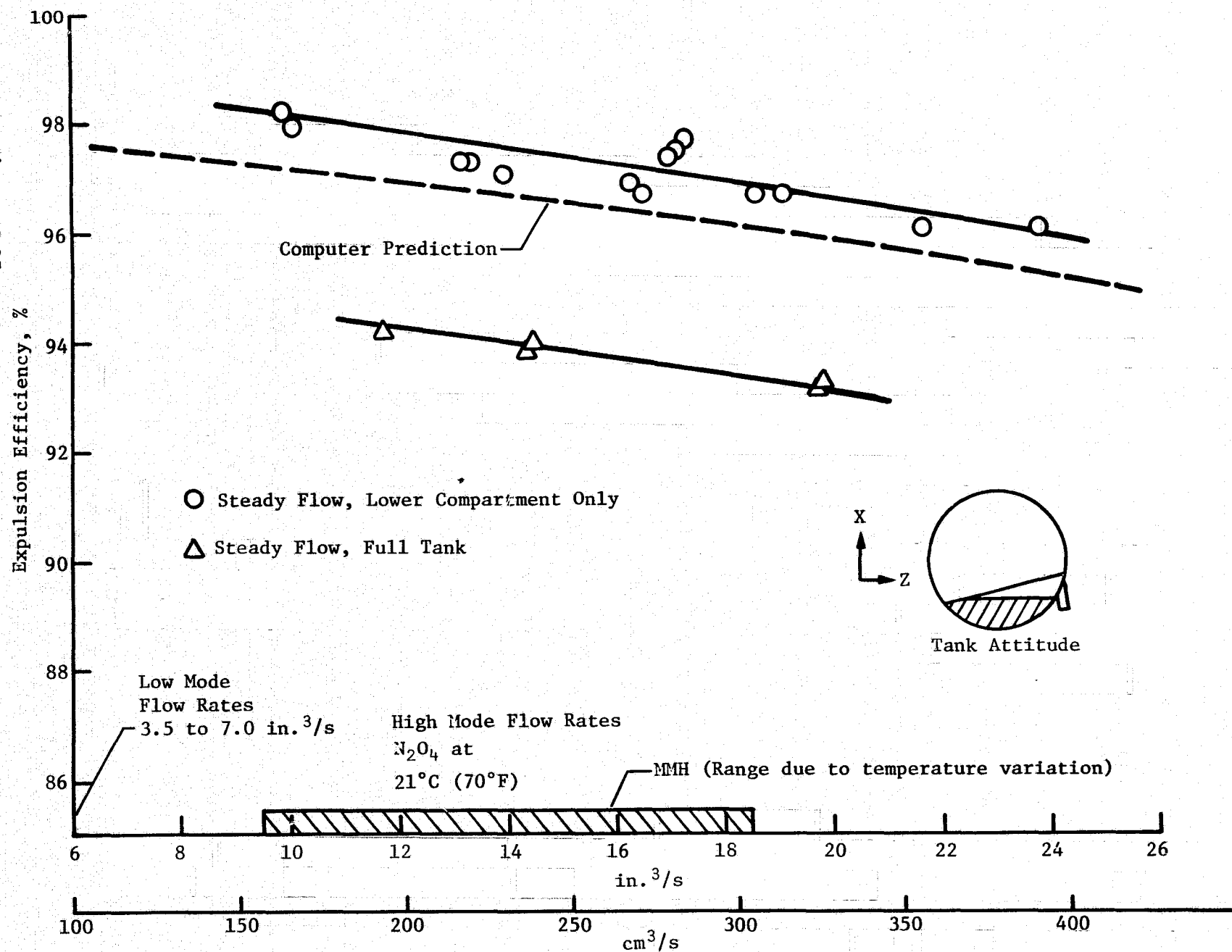


Figure V-27 Expulsion Efficiency as a Function of Flowrate with Isopropyl Alcohol

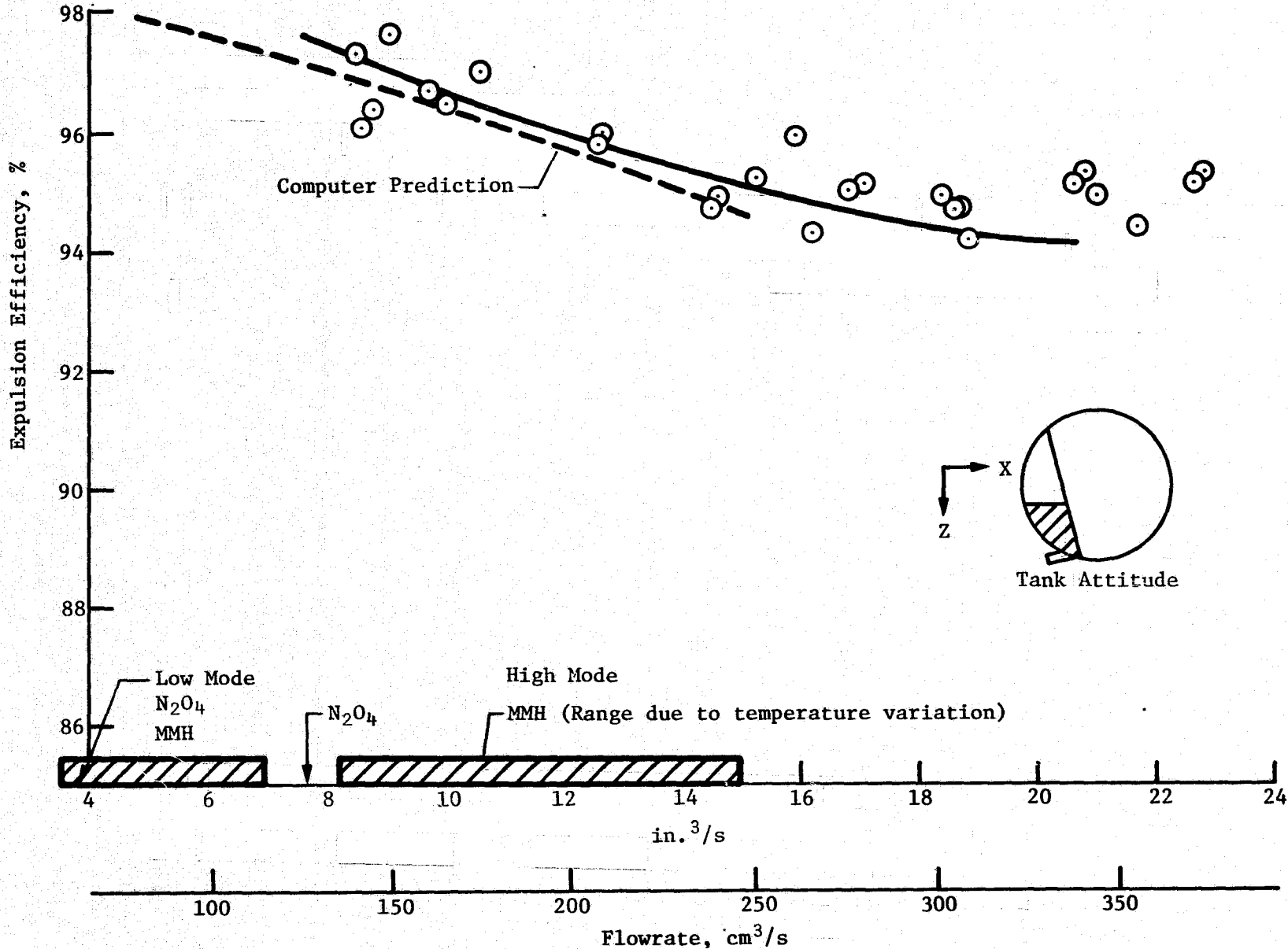


Figure V-28 Expulsion Efficiency as a Function of Flowrate with Isopropyl Alcohol



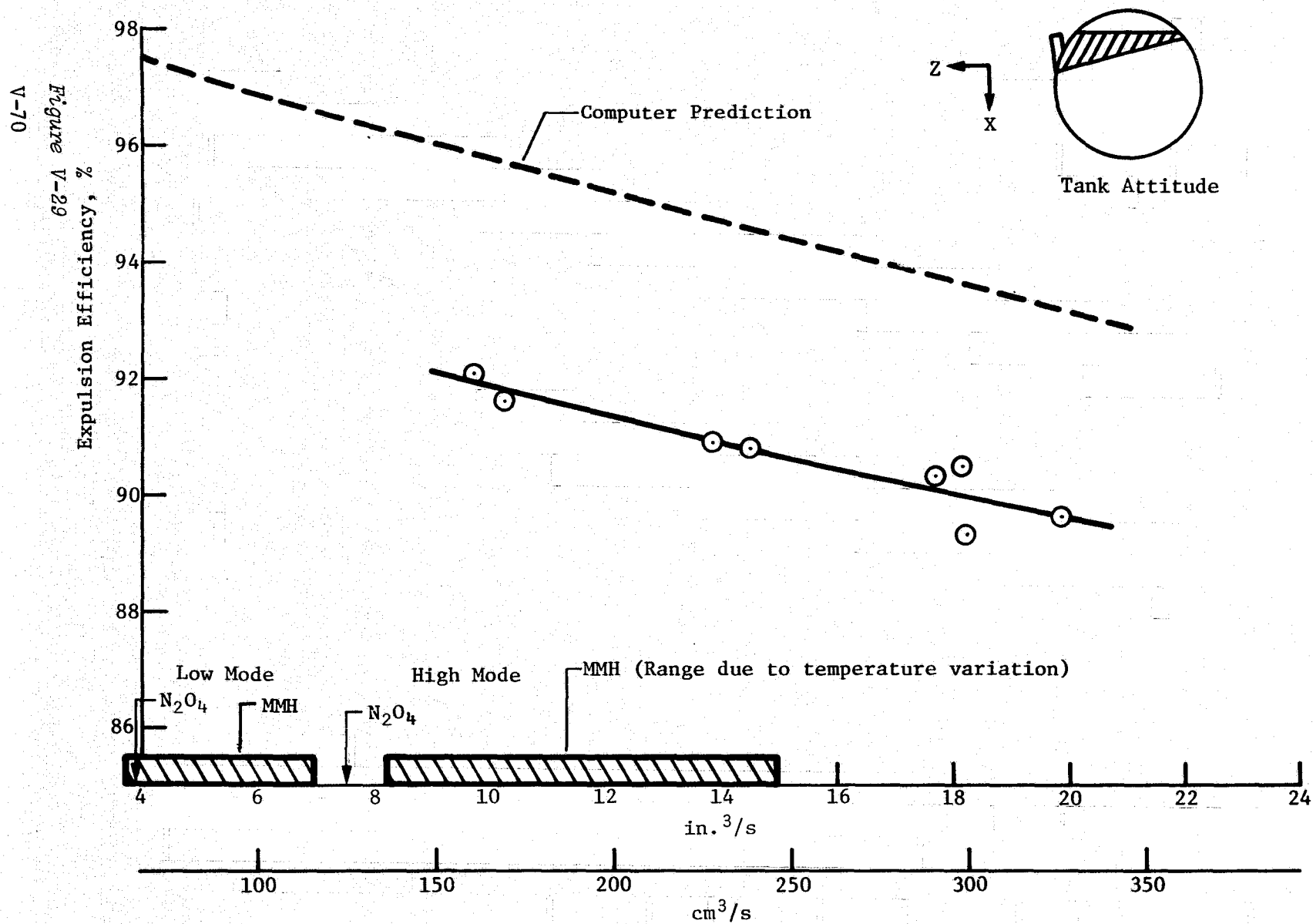


Figure V-29 Expulsion Efficiency as a Function of Flowrate with Isopropyl Alcohol

Results for the final attitude, with the tank outlet nearly at the top and the tank barrier close to a vertical position, are shown in Figure V-30. Expulsion efficiencies ranged from 94% to 92%. The computer predictions fall roughly 1% above the actual data and the scaled flowrates are generally lower than the flowrates tested. This attitude is representative of an orbital maneuver that would settle propellant away from the outlet. At breakdown only one of the four channels in the bottom compartment remained in the bulk liquid. Some additional testing was done with water, including testing of the expulsion efficiency of a full tank. The data from these tests indicated that the expulsion efficiency for full tanks differed from the expulsion efficiency for a lower compartment test in the same tank attitude by a nearly constant value of about 3% through the entire range of test flowrates.

In the attitude with the outlet down and the barrier in a near vertical plane (Figure V-28), the difference was a nearly constant 1.5%, and in the minus 1-g attitude (Figure V-29), the difference was again approximately 3%. The difference in the 1-g case (Figure V-27) represents the volume trapped in the channels, manifold, and bulk area of the upper compartment at the time of breakdown. Because of the large screen areas in the upper compartment, this volume was affected very little by changes in test flowrate, and explains the constant difference between upper and lower compartment performance. The 1.5% differential for the attitude representative of reentry (Figure V-28) is the volume that could not be expelled from the upper compartment after the screen barrier window was uncovered. In the negative 1-g attitude (Figure V-29), most of the barrier manifold was drained to the lower compartment because the window was on the low side of the barrier; but as before, as soon as the barrier window was uncovered, transfer stopped and a nearly constant 3% was trapped in the upper compartment.

e) Full-Scale and Subscale Performance Comparison - A comparison of computer predicted full-scale performance and measured subscale performance at scaled flowrates was conducted to determine the accuracy of the scaling approach for design verification purposes. Discussion of the scaling analysis indicated that flowrates were based on orientations where liquid was puddled away from the outlet; namely +X and +Z axes up. Full-scale computer predictions for these orientations are shown in Figures V-31 and V-32, respectively. A safety factor of 1 on bubble point and a barrier position comparable to the subscale model were used in the analysis. Oxidizer is of primary interest for evaluation purposes since hydrostatic head during subscale testing was not scaled for MMH.

V-12

Figure V-30

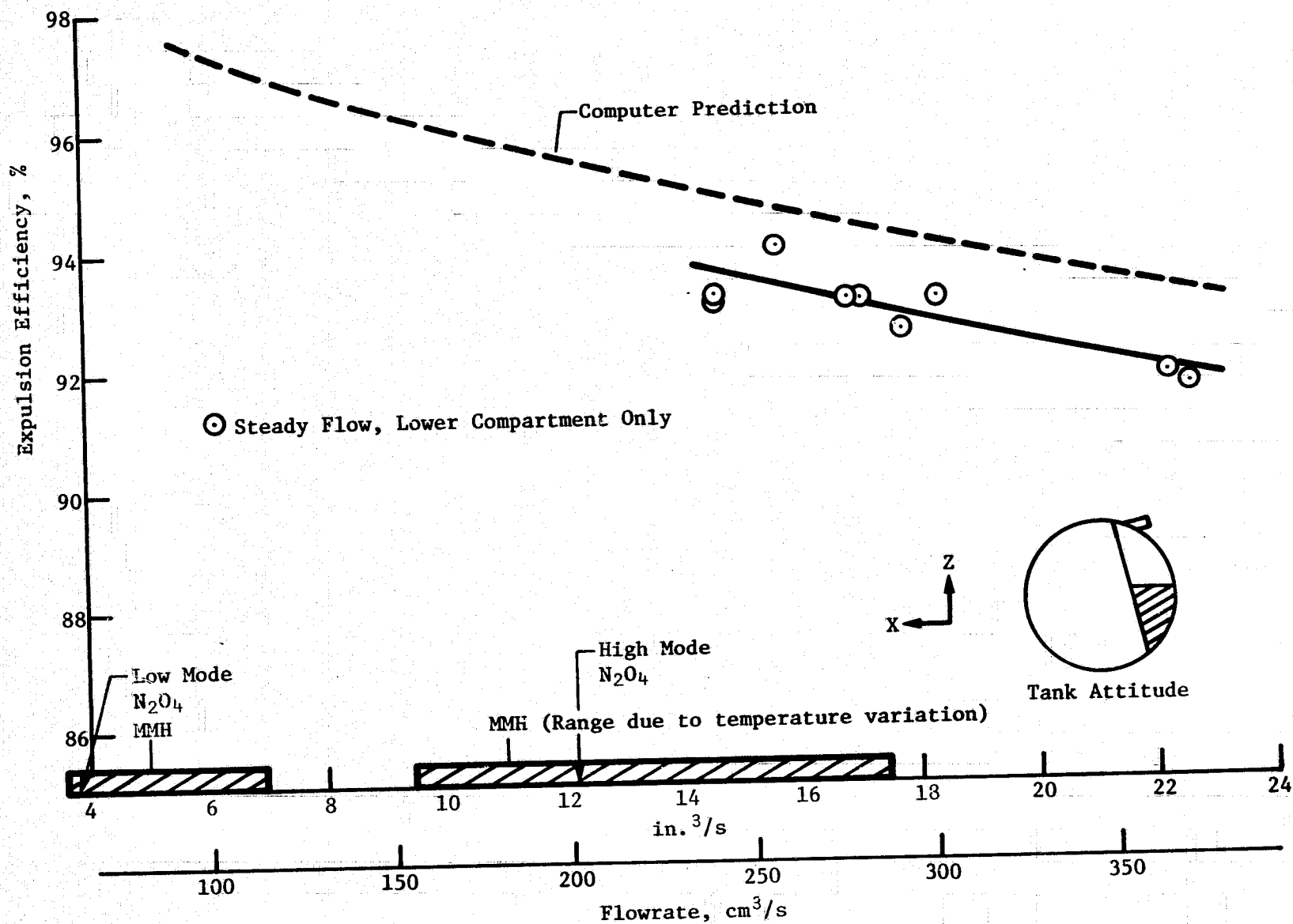


Figure V-30 Expulsion Efficiency as a Function of Flowrate with Isopropyl Alcohol

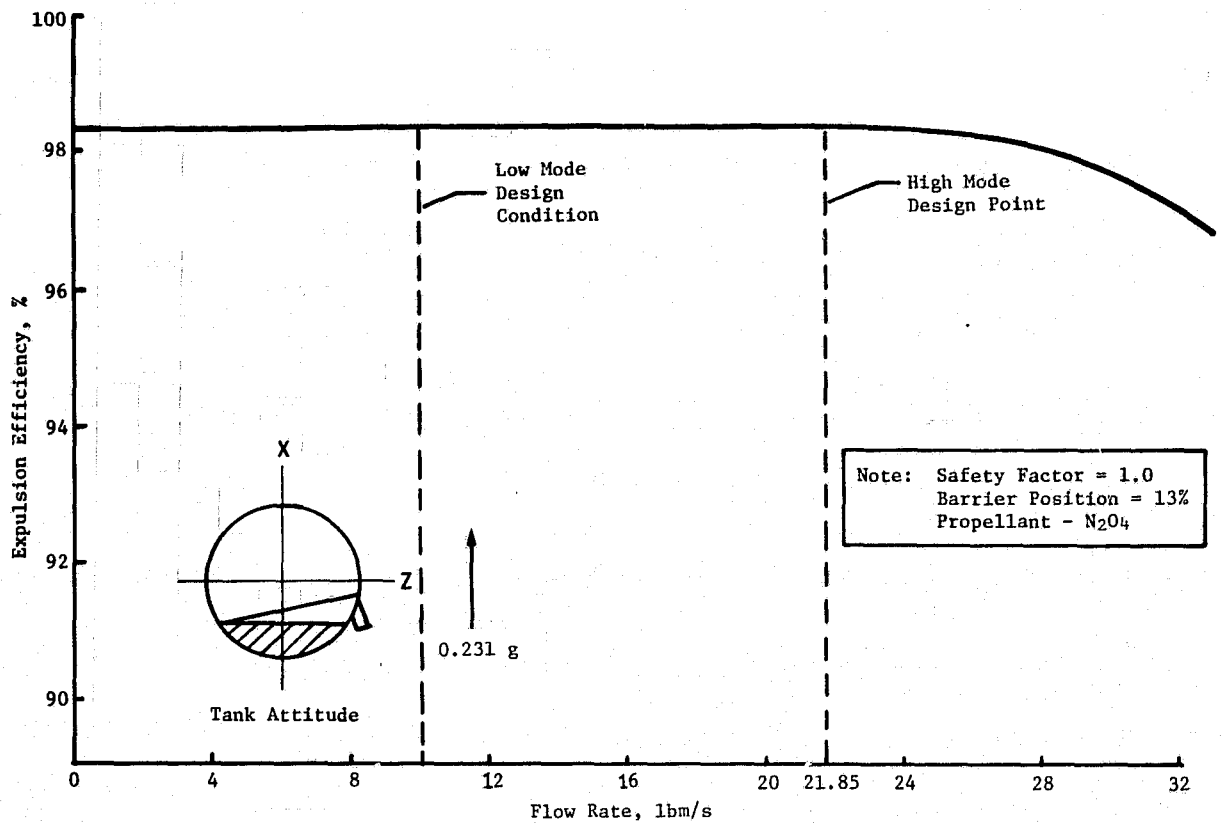


Figure V-31 Predicted Full-Scale Performance

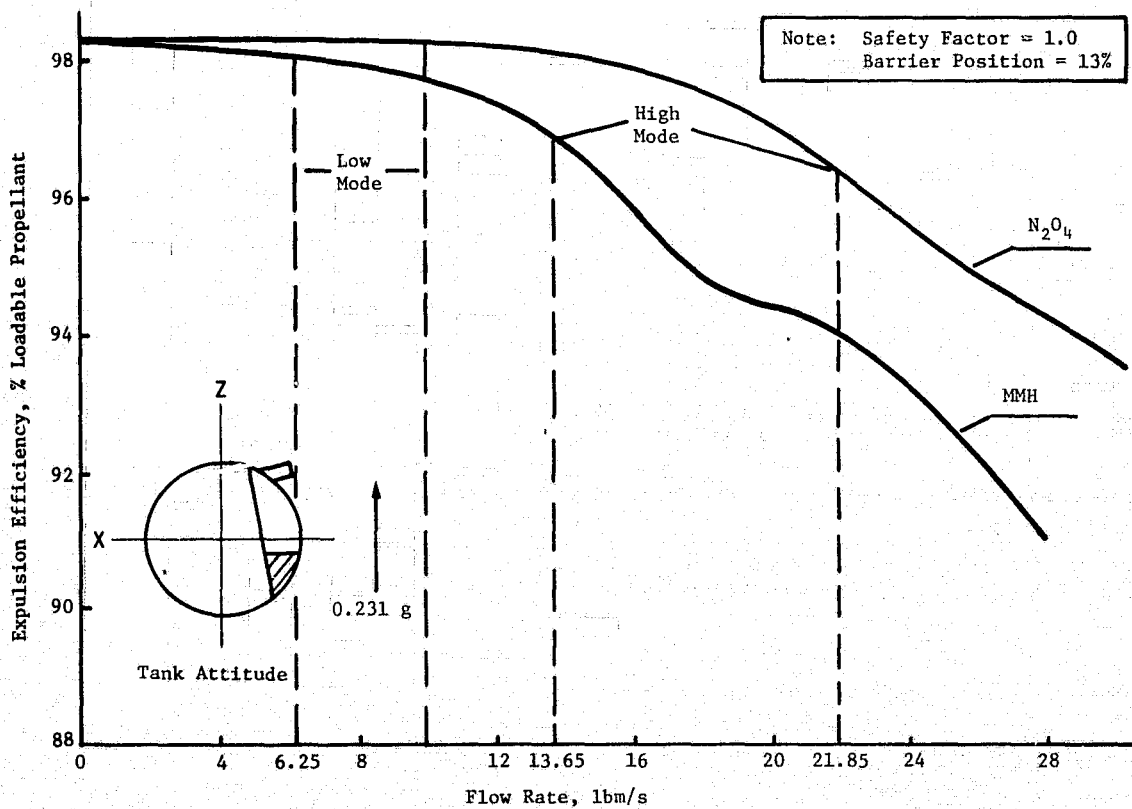


Figure V-32 Predicted Full-Scale Performance

Predicted performance for the full-scale system with  $N_2O_4$  propellant at  $21^\circ C$  ( $70^\circ F$ ) and a design flowrate of  $9.91 \text{ kg/s}$  ( $21.85 \text{ lbm/s}$ ) was 98.3% expulsion efficiency with the +X axis up. Test data in Figure V-27 show model performance was 97.8% at scaled conditions. With the +Z tank axis vertical, full-scale predicted and subscale measured performance was 96.3% and 94.6%, respectively. The differences noted are attributed to geometric differences between the model and the preliminary design.

f) Conclusions - The simulated on-orbit performance of the subscale tank was satisfactory and generally showed very good agreement with pretest computer predictions. Some discrepancy was noted for the minus one-g outflow tests, but the difference can probably be attributed to the difficulty encountered in modeling this case. Performance at scaled flowrates indicated acceptable expulsion efficiencies can be expected. Correlation of predicted full-scale system and measured subscale model performance showed that flowrate scaling is an acceptable approach for verification purposes in certain applications where hydrostatic scaling between full-scale and subscale is preserved. Performance deficiencies revealed by the tests are treated in Section E of this Chapter.

#### 4) Pulsed-Flow Tests

a) Objective - The objective was to evaluate the effects of startup and shutdown transients on the retention capability of the fine-mesh screen acquisition system during the minimum impulse burns of the RCS thrusters.

b) Approach - The tests were conducted in the tank attitudes used for the previously discussed expulsion tests. Liquid was expelled either in a pulsed mode or in a combined mode of pulsed flow plus steady flow in parallel (Figure V-23). Previous analysis had shown that a combined pulsed and steady flow provides the worst-case condition for pressure transients in the system (Ref V-8). This combined mode represents a case where RCS thrusters supplied from a single tank are fired in both a steady and pulsed manner. The approach for the test series was to again investigate a range of flowrates and to compare the resulting expulsion efficiencies with those achieved at the same flowrate in a steady-flow-only operational mode. Isopropyl alcohol was the test fluid.

c) Criteria - The valve duty cycle criteria established for the pulsed mode operation were:

Nominal valve opening and closing time	20 msec
Minimum on-time	40 msec
Minimum off-time	40 msec

d) Apparatus - The basic test apparatus was used. A standard ball valve was selected for use in the pulsed system, both for its ease of operation and for its low flow restriction. The valve was actuated by a variable speed electric motor and synchronized with a stroboscope at the appropriate speed. Therefore, as the valve was turned through 360 deg, it completed two open and closed cycles. The valve duty cycle, as determined by flow tests, is shown in Figure V-33 for a valve frequency of 8.5 Hz.

The valve was placed in the pulsed-flow line and another ball valve was placed downstream to initiate or terminate flow during a test. A turbine flowmeter was placed in the steady-flow line to determine the portion of the flow in a combined mode that was flowing through that line.

e) Procedures - After the test tank was pressurized, the pulsing valve was actuated. Then either the pulsed-flow line valve was actuated or both the pulsed-flow line valve and the steady-flow line valve were actuated simultaneously, depending on the nature of the test. When breakdown occurred, the process was repeated for closing the valves. Data were taken as previously described for the expulsion tests; the flowmeter output was recorded on a strip chart.

f) Data and Results - Several tests were conducted with pulsed-mode operation only. The maximum flowrate achieved was approximately 0.10 l/s (6 in.<sup>3</sup>/s). For the duty cycle tested, this is the approximate equivalent of 0.16 l/s (9.5 in.<sup>3</sup>/s) during the time the valve was open. None of the pulsed mode only tests yielded expulsion efficiencies different from those previously obtained with steady flow at the same flowrate. However, because of flow restrictions and limits on test tank pressurization levels, high flow rates in this mode were not possible.

For tests in the combined pulsed and steady modes, some initial tests were conducted to determine if the ratio of pulsed flowrate to steady flowrate changed as the total flowrate increased. Tests were conducted over a range of 0.16 l/s (10 in.<sup>3</sup>/s) to 0.39 l/s (24 in.<sup>3</sup>/s) combined flowrate with isopropyl alcohol. The results of these tests are shown in Figure V-34. The line of best fit was obtained by regression analysis. The line appears to have a slight slope, suggesting that as flowrate increased the fraction of the flow attributable to the pulsed system increased slightly. However, further statistical analysis indicated that at the 90% confidence level, the confidence interval for the curve shown included a slope of zero. Therefore, the zero slope could not be ruled out at a 90% confidence level, and it was therefore assumed that the mean value of 0.25 for the ratio was, in fact, constant throughout the tested range.

Figure V-33

Fraction of Maximum Flow Rate

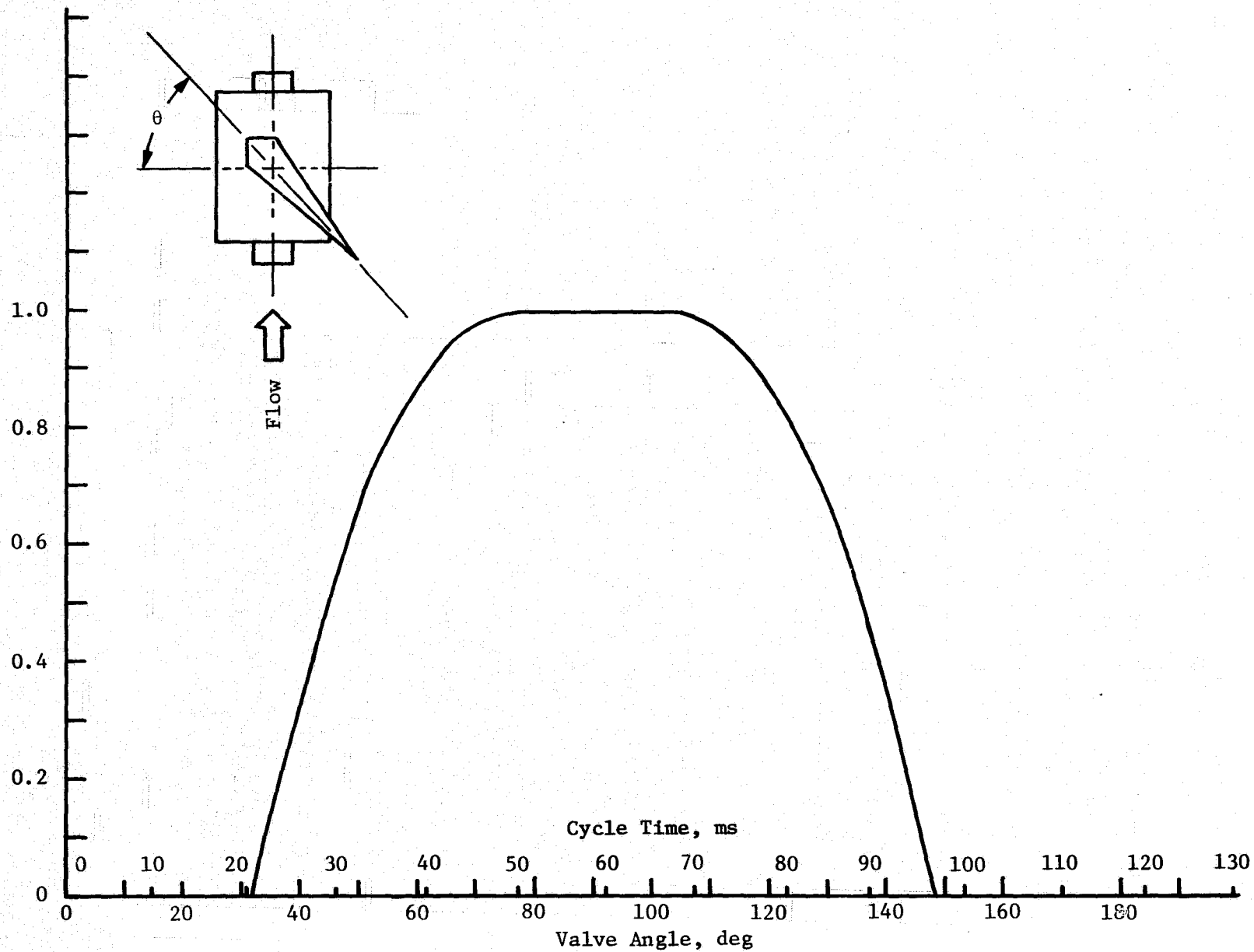


Figure V-33 SS/RCS Subscale Model Pulsed-Flow Test Valve Duty Cycle

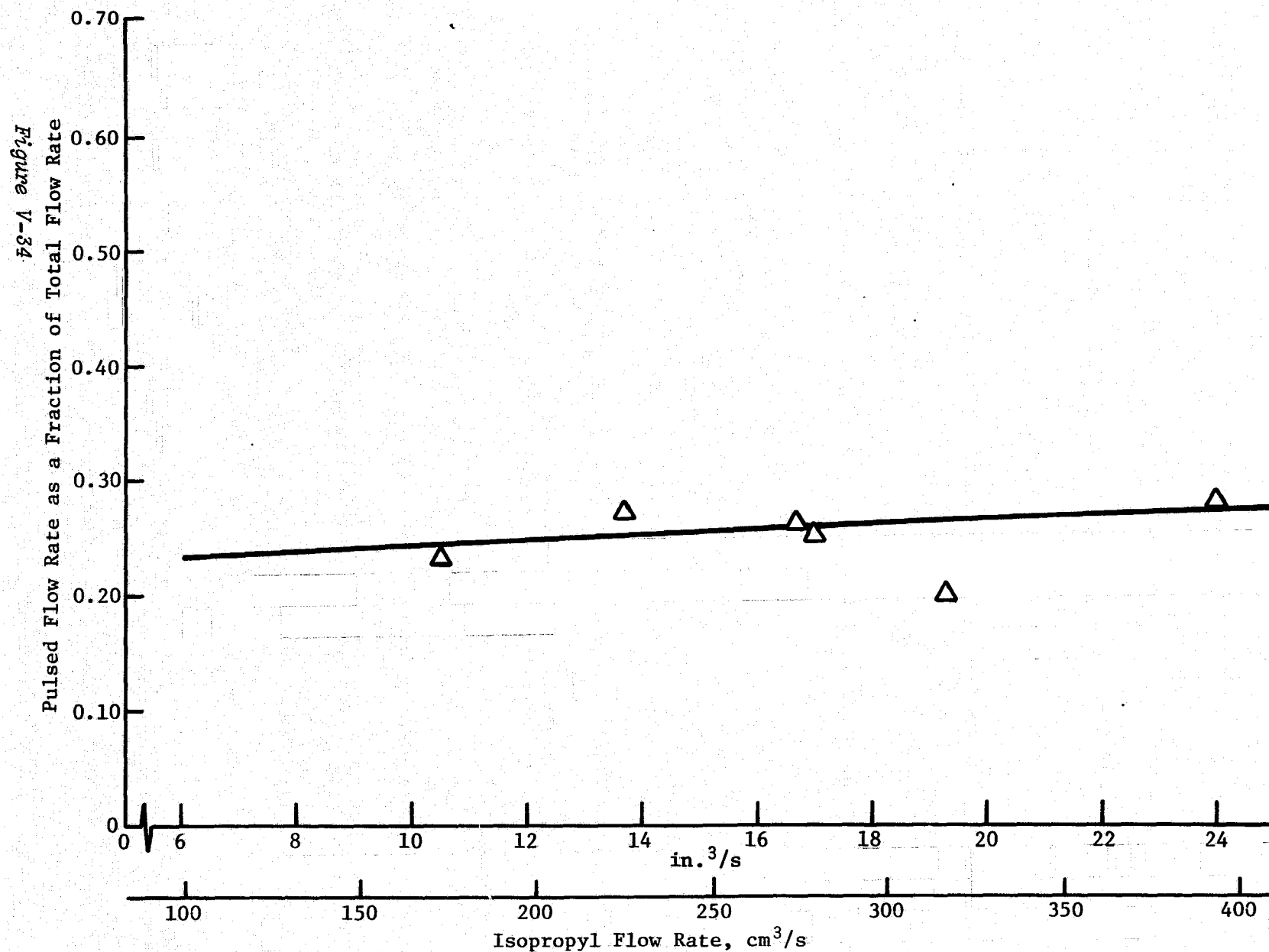


Figure V-34 Pulsed Flowrate vs Total Flow Rate for Isopropyl Alcohol Pulsed Flow Tests



The results of the pulsed flow tests for the 1-g tank attitude are shown in Figure V-35, together with the results of the steady flow expulsion from the previous section for comparison. Curves of best fit are shown for all four tests conditions, as noted. The scaled flowrates are shown at the bottom of the figure. Some degradation of the pulsed plus steady flow curves is noted when compared to the steady-flow-only curves. At the highest flowrates tested, well beyond the range of interest, this difference is about 5%. However, below flowrates of about 0.23 l/s (14 in.<sup>3</sup>/s) where the majority of the scaled flowrates occur, the difference is not significant or is not distinguishable.

Figure V-36 shows the results of tests for the tank in the attitude with the outlet at the bottom and the barrier in a nearly vertical position. Data for both lower compartment tests and full tank tests are shown. There is no discernible difference between the data for the combined flow mode tests and the steady-flow-only tests for either the lower compartment or the full tank tests.

The comparison of steady flow versus pulsed plus steady flow for the test with the tank in a minus 1-g attitude is shown in Figure V-37. Again, when the data were treated with statistical analysis, no significant difference existed between the two flow modes.

One additional result was noted during the pulsed flow tests. For the same driving pressure, the flowrate through the pulsed flow line in the combined mode tests was slightly greater than flowrate through the pulsed flow line during pulsed only tests. This suggests that the impedance for the pulsed flow line was in some way reduced by the presence of the steady flow line in the system.

g) Conclusions - Of the tank attitudes tested, only the plus 1-g test (Figure V-35) exhibited any degradation of performance when subjected to pulsed mode operation. It should be noted that this is the only tank attitude that requires liquid to be flowed against an exposed hydrostatic head during the terminal drain stages. For both the minus 1-g attitude and the attitude similar to that experienced during reentry, the tank outlet is submerged during all phases of the terminal drain. These results substantiate the fact that outflow against an adverse acceleration presents a worst case for screen systems. The results are in accord with recent testing to evaluate flow transient effects on screen device performance (Ref V-9). That program showed that lower pressure differentials caused by pulsing were obtained across a screen device in a plus-g orientation than in a minus-g orientation. Considering the specific SS/RCS application, no significant performance declines were observed over the flowrate range of interest. From these results, it is concluded that pulsed flow presents no problems to RCS performance.

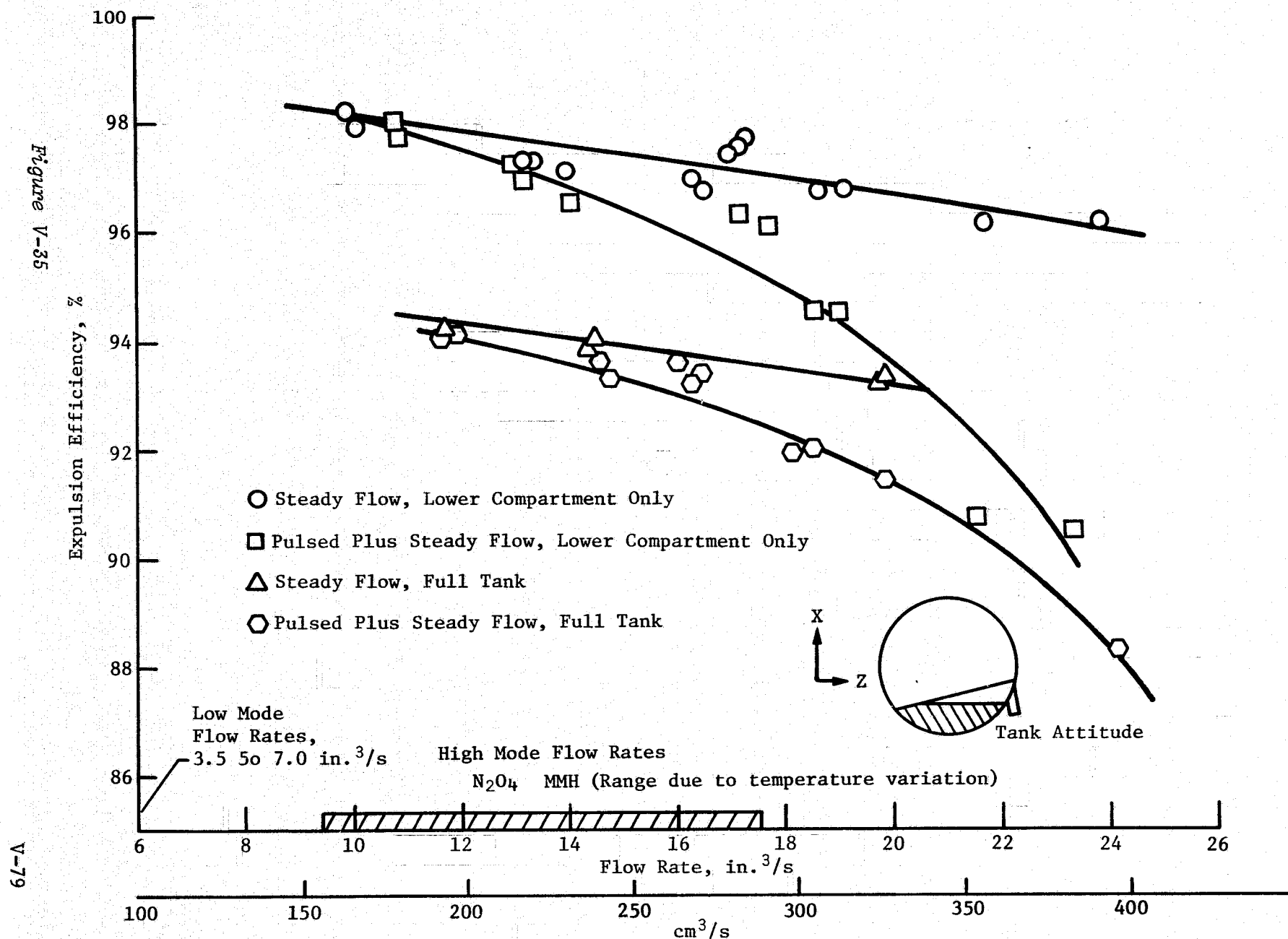


Figure V-35 Expulsion Efficiency as a Function of Flowrate for Isopropyl Alcohol

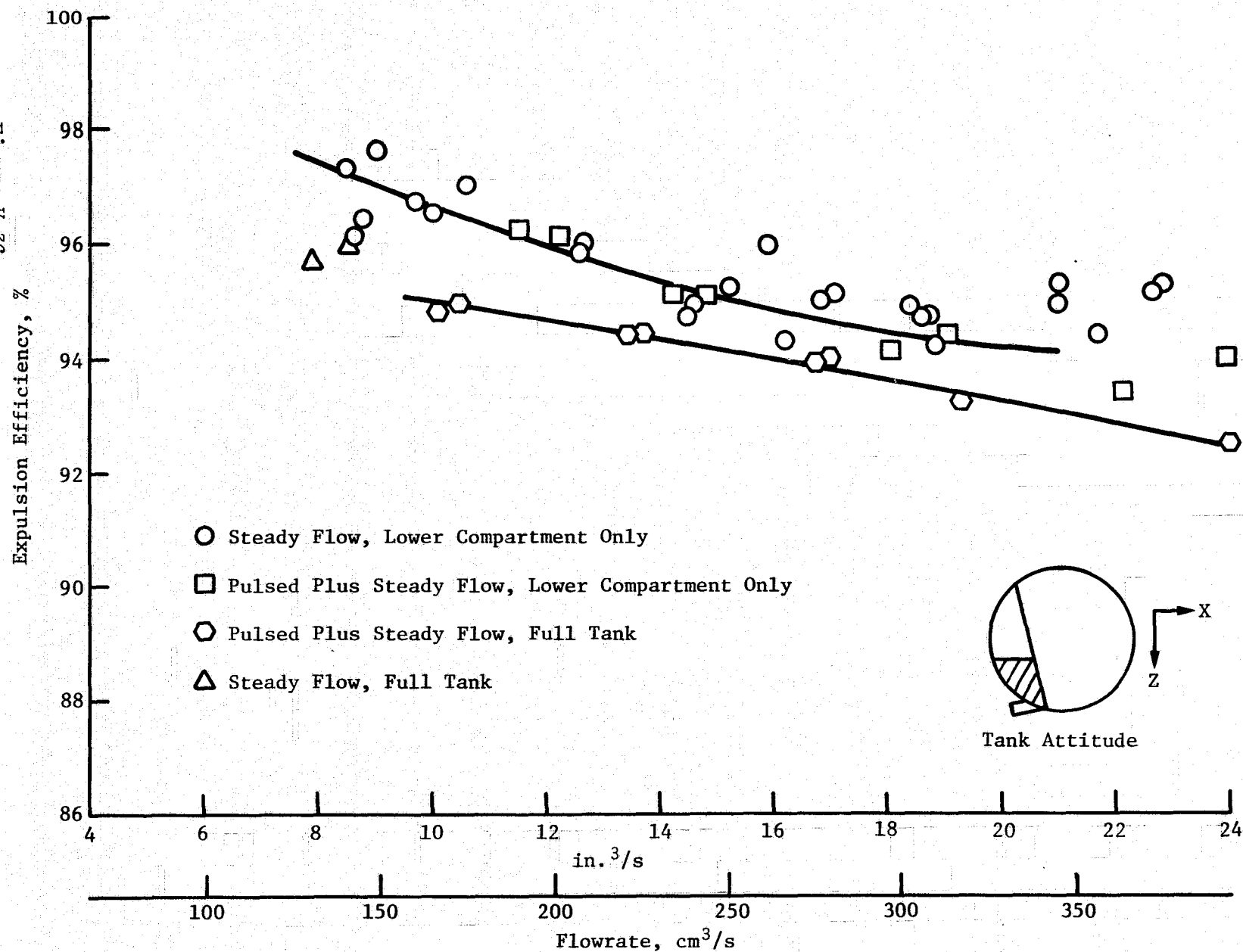


Figure V-36 Expulsion Efficiency as a Function of Flow Rate for Isopropyl Alcohol

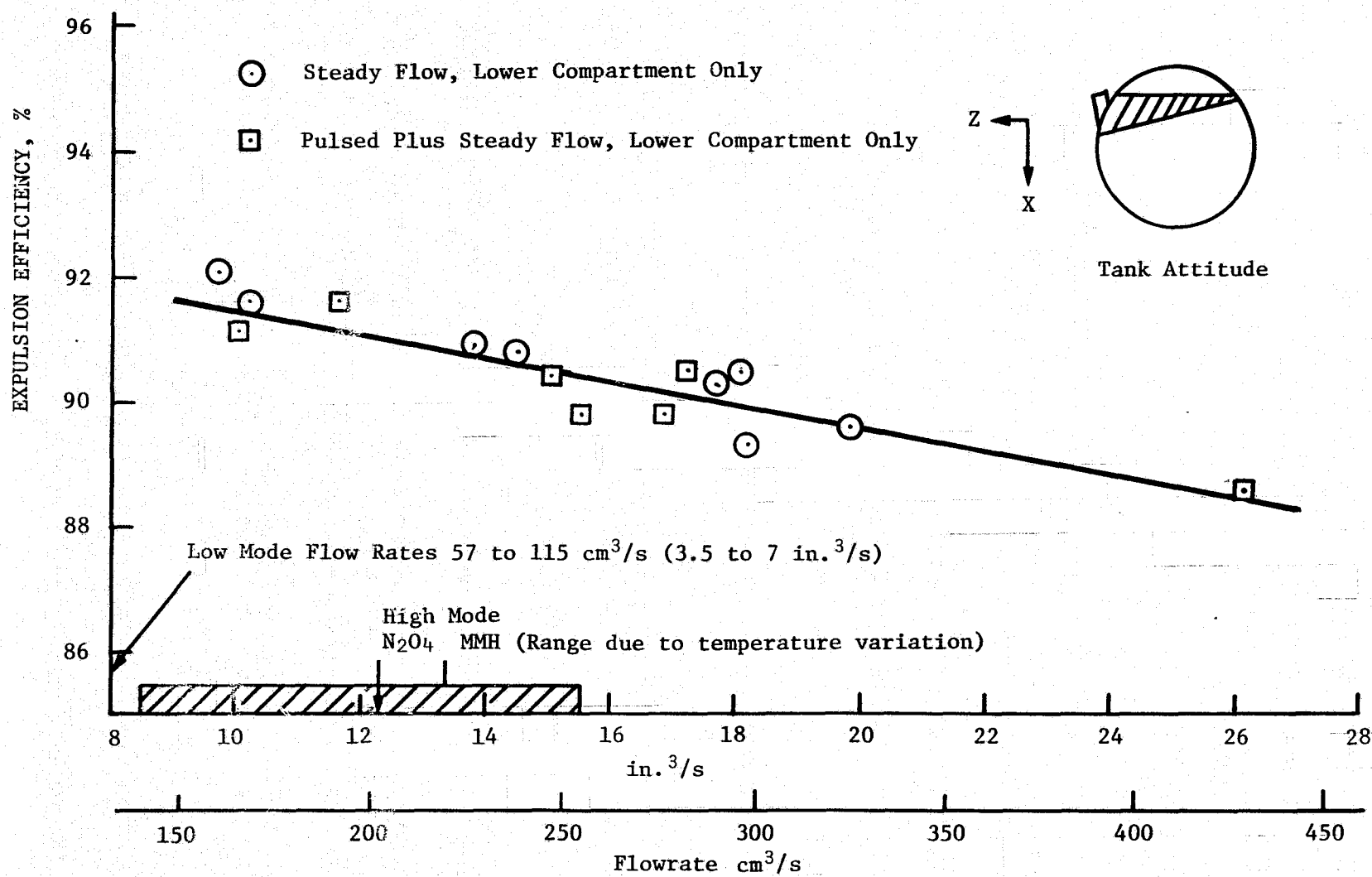


Figure V-37 Expulsion Efficiency as a Function of Flow Rate for Isopropyl Alcohol

## 5) Error Analysis for Fill, Drain and Expulsion Tests

A single sample error analysis was performed on the data for the fill and drain tests, the expulsion tests, and the pulsed flow tests using the method suggested by Kline and McClintock (Ref V-10).

The equations used were:

for load ( $\ell$ ) uncertainty limits:

$$[V-31] \quad \frac{\omega_{\ell}}{\ell} = \left[ \left( \frac{\omega_{w_i}}{w_i} \right)^2 + \left( \frac{\omega_{w_f}}{w_f} \right)^2 + \left( \frac{\omega_{\rho}}{\rho} \right)^2 \right]^{\frac{1}{2}}$$

and for expulsion efficiency ( $\eta_e$ ) uncertainty limits

$$[V-32] \quad \frac{\omega_{\eta_e}}{\eta_e} = \left[ \left( \frac{\omega_{w_i}}{w_i} \right)^2 + \left( \frac{\omega_{w_f}}{w_f} \right)^2 + \left( \frac{\omega_{\rho}}{\rho} \right)^2 + \left( \frac{\omega_{\ell}}{\ell} \right)^2 \right]^{\frac{1}{2}}$$

The terms in the equations together with their uncertainty values follow. The uncertainty values are based on equal odds of each measurement occurring no more than 5% of the time.

$w_i$  = Initial weight of test tank;  $\omega_{w_i} = \pm 25 \text{ g } (\pm 0.055 \text{ lbm})$

$w_f$  = Final weight of test tank;  $\omega_{w_f} = \pm 25 \text{ g } (\pm 0.055 \text{ lbm})$

$\rho$  = Density of test liquid;  $\omega_{\rho} = \text{for water } \pm 0.0016 \text{ g/cc } (\pm 0.1 \text{ lbm/ft}^3)$

$\omega_{\rho} = \text{for isopropanol } \pm 0.0048 \text{ g/cc } (\pm 0.3 \text{ lbm/ft}^3)$

$\ell$  = Loaded volume;  $\omega_{\ell}$  based on first equation.

Using this information, the following uncertainty limits (UL) were established:

#### Loaded Volume (ℓ)

Water, UL =  $\pm 0.28\%$

Isopropyl Alcohol, UL =  $\pm 0.65\%$

#### Expulsion Efficiency ( $\eta_e$ )

Water, UL =  $\pm 0.41\%$

Isopropyl Alcohol, UL =  $\pm 0.96\%$

A similar analysis was made for the flow rates with the following results:

Assuming a  $\omega_T = \pm 0.2$  seconds for the time measurement,

Water flow rate, UL =  $\pm 0.72\%$

Isopropyl flowrate, UL =  $\pm 0.93\%$

In addition, because two sets of data were taken for each test--a set based on volume and a set based on weight--an analysis of the differences between the two sets was made to determine if one set differed significantly from the other. Using standard statistical tests, the differences between the two sets of data for the isopropyl alcohol test were not significant at the 90% confidence level.

#### 6. Centrifuge Tests

Centrifuge testing was conducted to verify the selected design capability during high-g maneuvers such as reentry and abort modes. During these periods, large flow rate demands may be made on the system. Since these g-levels are positive and tend to settle liquid in a manner that aids expulsion, the ability of the system to perform its required function, gas-free liquid expulsion, should not be affected. However, experimental verification of this capability was required.

a) Objective - The objective of the centrifuge tests was to demonstrate the ability of the selected design to perform the required functions during the abort and reentry phases of the RCS mission. This required demonstration of gas-free liquid expulsion at flow rates and g-levels defined in the following subsection.

b) Approach - The 1/3-scale model with transparent tank was mounted on the centrifuge in the required positions to obtain the liquid orientations of interest at the test acceleration. Upon reaching the test conditions, the system was outflowed to the desired level at the required flow rates. Film documentation of the tank and transparent outflow line established system performance.

The g-levels and flowrates required of the RCS system during reentry and abort modes are defined by the environmental and performance requirements defined in Chapter II. The RTLS abort mode presented worst-case conditions compared to the AOA flight sequence. This is because of the lower flow rates required during AOA to deplete to the same minimum propellant load. The criteria, as defined for RTLS and reentry for the aft RCS oxidizer tanks, are shown in Table V-15. Only  $N_2O_4$  criteria are shown because a more stringent design requirement is imposed on the system by oxidizer propellant.

Table V-15 RCS Oxidizer Tank Requirements during RTLS and Reentry

Mission	Maximum G-Level	Outflow Rate, kg/s (lbm/s)	Depletion Level	Acceleration Vector
RTLS	3.3	12.0 (26.2)	34.5% of Tank Volume	8.6° from +X Axis in +Z Direction
Reentry	2.2	8.9 (19.7)	Terminal Drain	18° from -Z Axis in -X Direction

Verification of the subscale model with referee fluids for high-g operation required geometric and dynamic scaling to account for differences in fluid properties and tank sizes. The scaling analysis was performed as discussed previously. Results are shown in Table V-16. Freon TF was the test liquid.

Table V-16 Centrifuge Scaling Results

Mission Phase	Propellant	Test G-Level	Test Flowrate, l/s (in. <sup>3</sup> /s)
RTLS	$N_2O_4$	6.6	0.45 (27)
Reentry	$N_2O_4$	4.4	
Hi Mode			0.33 (20)
Low Mode			0.13 (8.1)

c) Apparatus and Procedure - Test configurations for the RTLS and reentry simulations are shown in Figure V-38 and V-39, respectively. Other than tank orientation, each system was basically the same. Main components were the subscale model, pressurization source, receiver tank, 16-mm movie camera, and mounting device to properly orient the tank. Both pressurization and outflow valves were of the solenoid type for remote actuation. The pressurization line contained a relief valve and regulator for varying tank pressure and flow rate.

Figure V-38

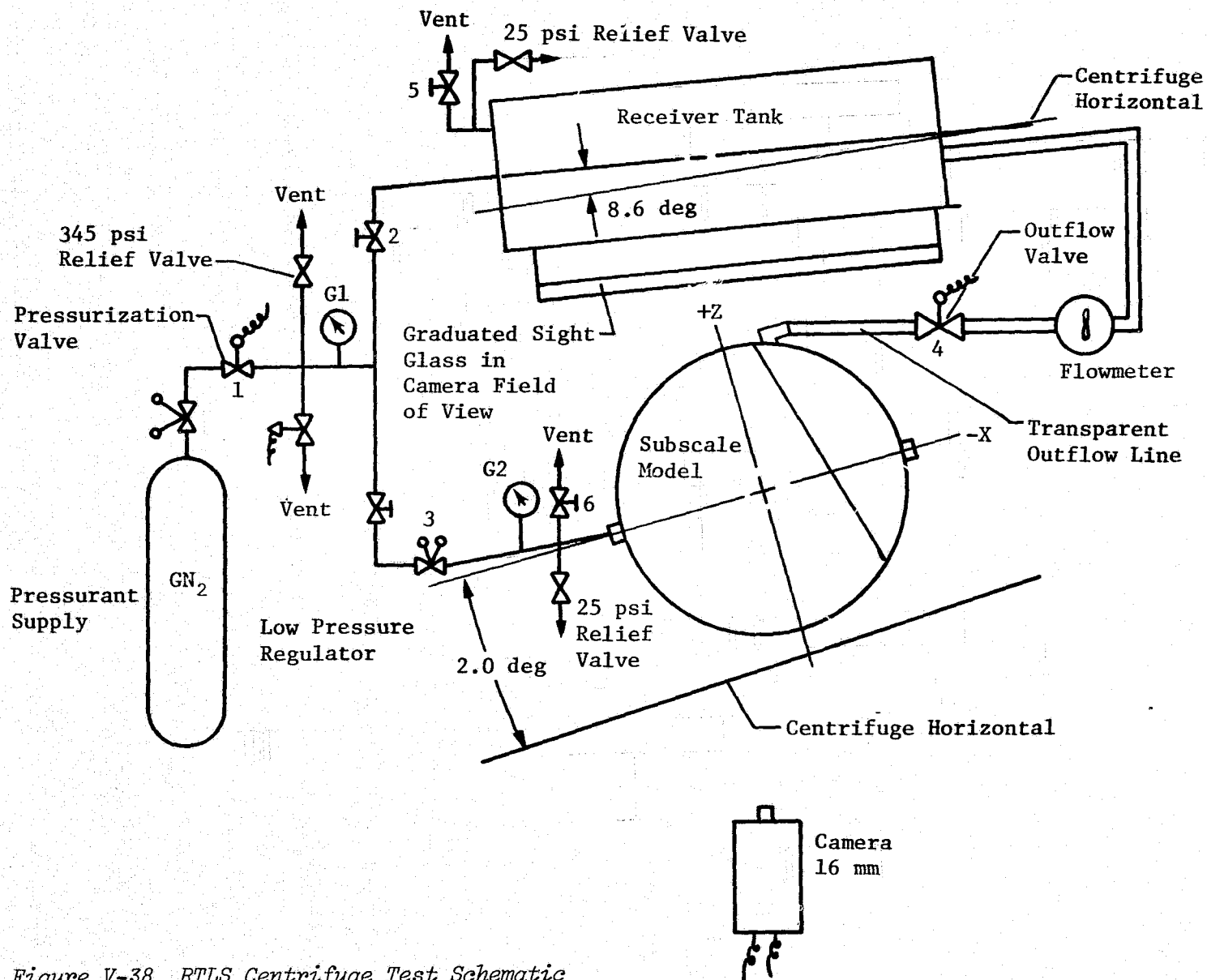
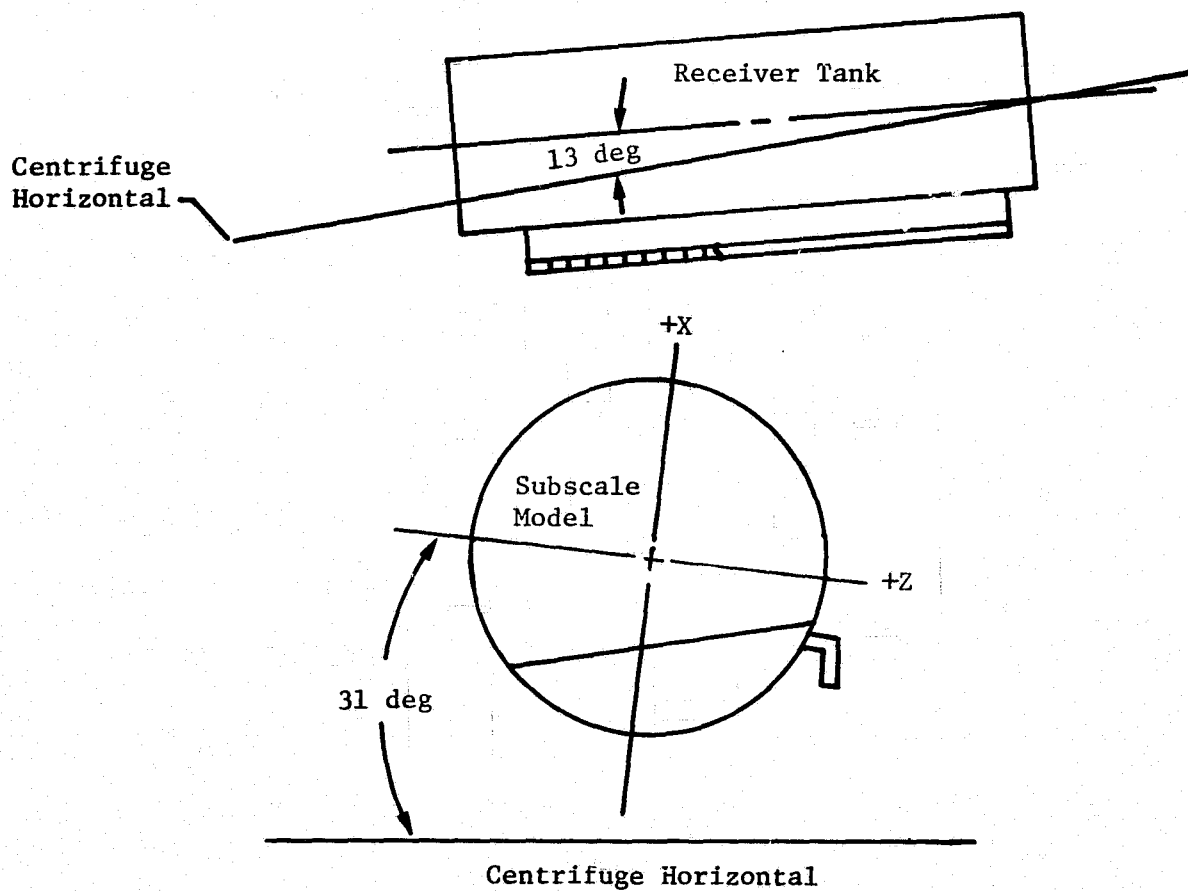


Figure V-38 RPLS Centrifuge Test Schematic





*Figure V-39 Tank Orientation for Reentry Simulation*

Key test items were a transparent portion of the outflow line and a scale mounted perpendicular to the liquid interface; both were in the camera field of view. These enabled determination of gas in the outflow line, flow rate, and expulsion efficiency. Also of importance was the mounting of the attachment fixture to achieve the proper angle. The respective angles for test tank and receiver tank orientation are shown in the schematics.

The 16-mm camera was mounted so the tank, outflow line, and graduated sight glass were in the field of view. It was remotely controlled so activation and deactivation could be achieved during centrifuge operation.

A photograph of the test system is shown in Figure V-40. All components are visible including the outflow sight glass, pneumatic ball valve, and graduated glass tube. The pressurant was ambient  $\text{GN}_2$  and the test fluid Freon TF at  $21^\circ\text{C}$  ( $70^\circ\text{F}$ ).

Reentry and RTLS tests were conducted in a similar manner to the prior tests although orientation of the tanks was somewhat different. The test article was loaded by detaching it from the test pallet and rotating it with the +Z axis higher than the -Z axis so that gas could be purged from the bottom compartment. At completion of filling, the tank was reattached to the test pallet and outflowed to purge gas from the system. The tank was then pressurized to the test level and the centrifuge rate of rotation increased to obtain the desired g-level. The camera was turned on before outflow was initiated and turned off after outflow was terminated. Test time was based on calculation of the time to outflow the desired amount of liquid. After camera deactivation, the centrifuge was stopped and visual observations of the tank made and recorded.

Ten tests were conducted at various flowrates, g-levels, and initial tank conditions to simulate RTLS and reentry mission events. These tests are listed in Table V-17. Three different initial tank pressures were used for each tank attitude. Initial tank levels of 100% and 50% were used to determine any effect of off-loading on system performance.

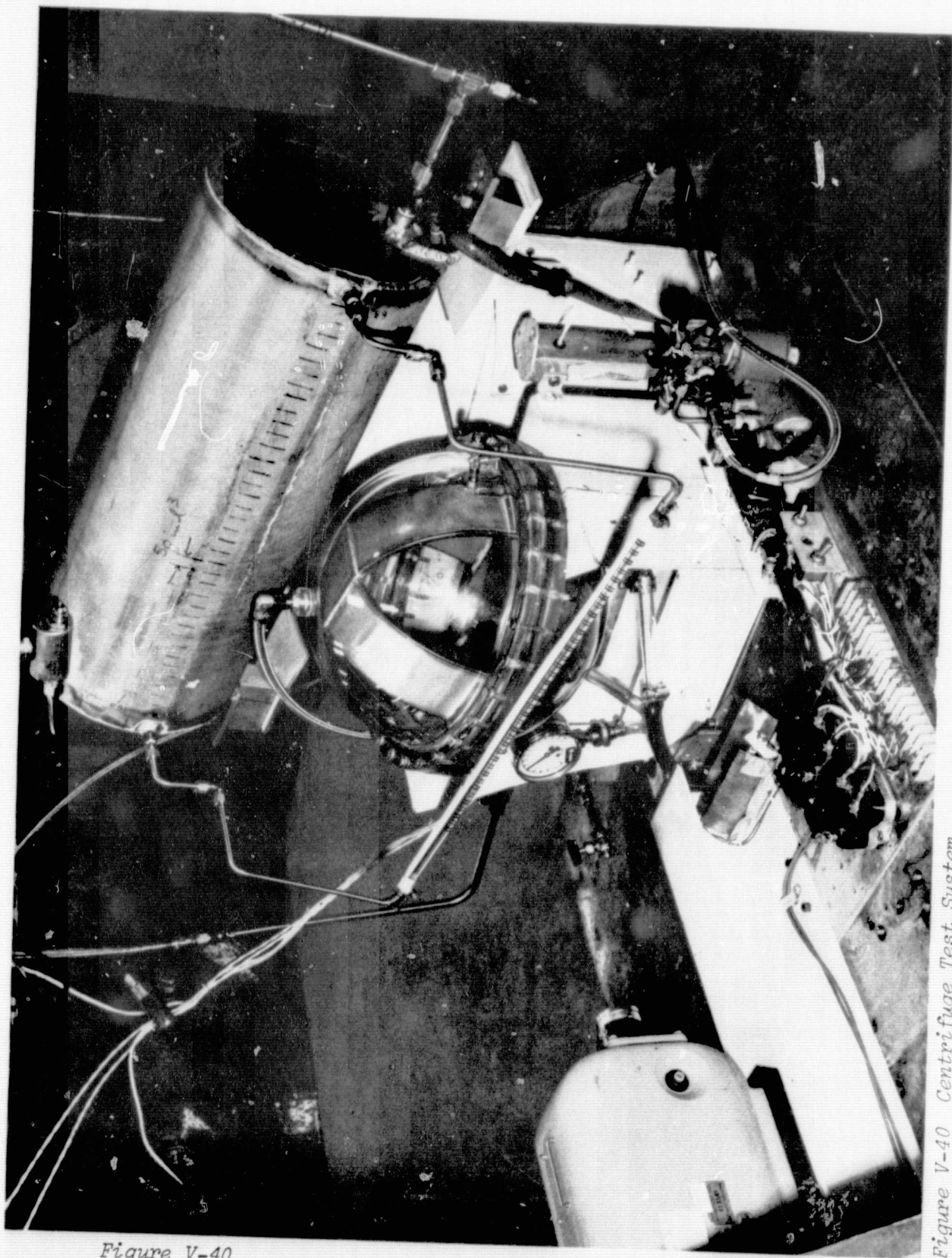


*Figure V-40*

V-88

*Figure V-40 Centrifuge Test System*

Table V-17 Centrifuge Test Matrix

Test No.	Mission Simulation	Tank Liquid Level		Tank Acceleration, g	Centrifuge Acceleration, g	Pressure N/cm <sup>2</sup> (psig)
		Initial, %	Final, %			
1	RTLS	Full	34.5	6.67	6.59	13.8 (20)
2	RTLS	Full	34.5	6.67	6.59	13.8 (20)
3	RTLS	Full	34.5	6.67	6.59	10.3 (15)
4	RTLS	Full	34.5	6.67	6.59	6.9 (10)
5	Reentry	Full	Depletion	4.44	4.33	13.8 (20)
6	Reentry	Full	↓	4.44	4.33	13.8 (20)
7	Reentry	Full		4.44	4.33	13.8 (20)
8	Reentry	50		4.44	4.33	13.8 (20)
9	Reentry	50		4.44	4.33	6.9 (10)
10	Reentry	50	Depletion	4.44	4.33	3.4 (5)

d) Data and Results - Flow rate and expulsion efficiency (or percent residual) for each test were determined from analysis of the film data. Test results, plotted in Figure V-41, show a reentry expulsion efficiency of approximately 90% during low mode operation and 84% during high mode operation. These performance numbers indicate the occurrence of screen dry out in the upper and lower compartments. The film data showed significant amounts of liquid were left in both compartments. Performance during RTLS testing indicated screen dryout was not pronounced as during reentry tests. Liquid in the top compartment was successfully drained until the manifold window was uncovered. Draining of the bottom compartment continued until final breakdown occurred. Results indicate that a 38% residual (based on loadable propellant) would be left during RTLS burn. This was short of the original design requirement of 34.5% by 3.5%, but it indicates a capability that far exceeds the revised 65% level requirement.

e) Conclusions - Test results indicated that the required expulsion efficiency of 98% could not be met during reentry. This was due primarily to dry out of the screens in the upper and lower compartments and subsequent pull-through of gas into the device. This was evident at all flowrates tested and required design modification to assure necessary performance.

V-90

Figure V-41

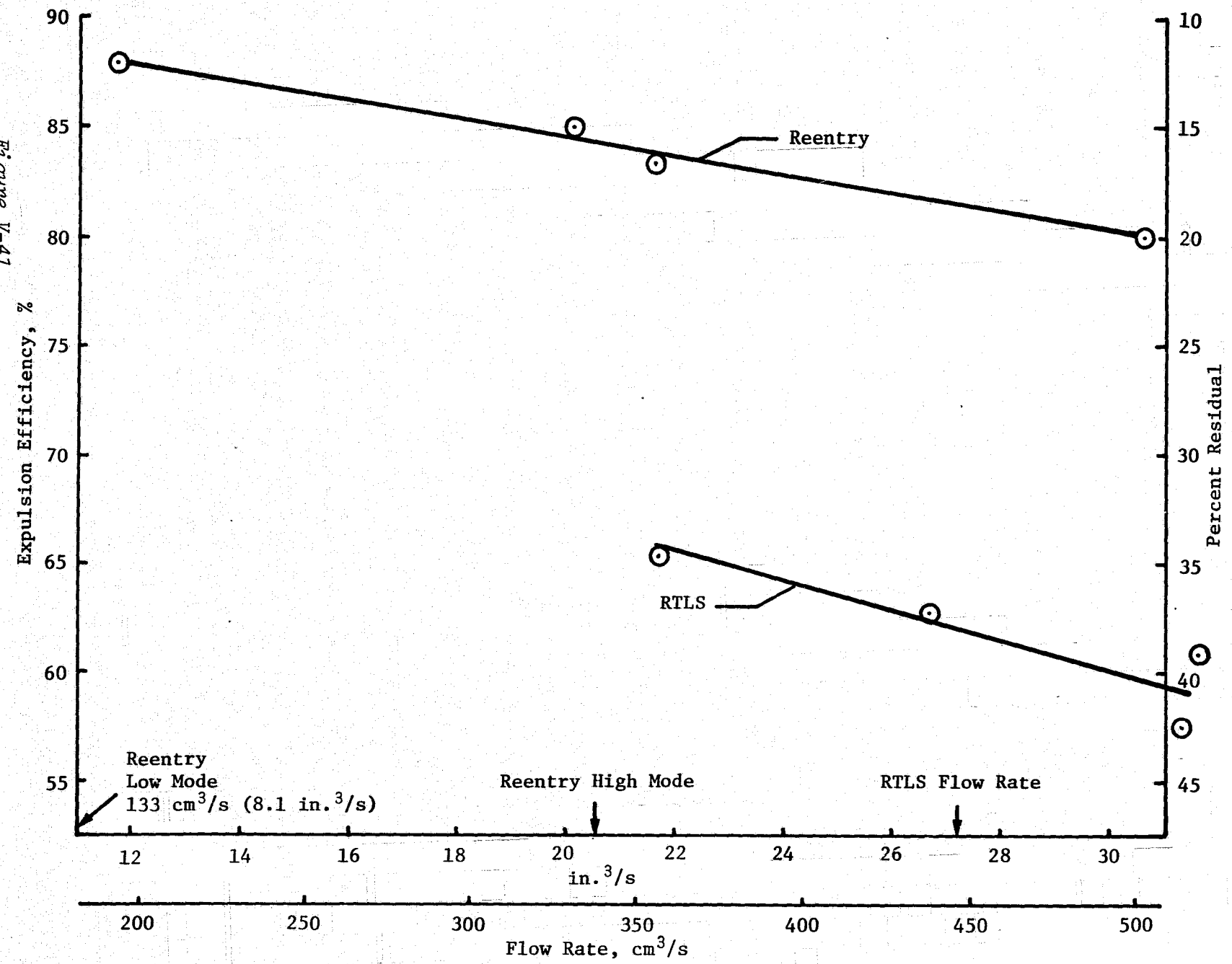


Figure V-41 Third Scale Model Centrifuge Test Results

Screen dry out was not as pronounced during RTLS expulsion, enabling the device to drain to the 38% residual level at the scaled RTLS flowrate for  $N_2O_4$ . Although this performance does not meet the original design criteria, it does meet the revised 65% level requirement. Because the performance capability exceeded the latest requirements by 20%, design modifications for RTLS were not required.

7) Vibration Tests - A significant amount of work had been performed to determine the effect of vibration on capillary screen devices at the time these subscale tests were initiated. In particular, two Martin Marietta programs have been completed and results published (Ref V-2 and V-9). During these programs, the effects of sine and random vibration on a dual-screen-liner system, and different types of fine-mesh screen and screen-channel configurations were evaluated. Results indicated that the effect was hydrostatic. As a result, an extensive investigation of vibration effects was not performed during this test program; instead the impact of vibration on the RCS subscale model was assessed.

a) Test Objective - The objective was to determine the effect of the RCS flight vibrational environment on the performance of the 1/3-scale model. Only the on-orbit vibration environment was of interest.

b) Approach - The subscale RCS tank system was mounted on the shaker table with the barrier horizontal and was subjected to random vibration in the vertical axis. This orientation facilitated mounting of the tank to the shaker table by the flanges for maximum transmissibility and also provided a close simulation of OMS roll control liquid-tank geometry. This mission event is of particular concern because the increased hydrostatic heads caused by vibration must be supported while maintaining gas-free liquid expulsion. The on-orbit random vibration level of importance to the RCS tanks results from OMS engine firing and is shown in Figure V-42. The rms value is 1.93 g. Two modes of OMS operation are of concern from a vibrational standpoint for the RCS. The first is the pure hydrostatic effect during firing of both OMS engines with no RCS outflow required. The second case is an OMS engine-out condition in which one OMS engine is firing and up to four RCS thrusters may be required to fire for roll control. These cases are summarized in Table V-18.

V-92

Figure V-42

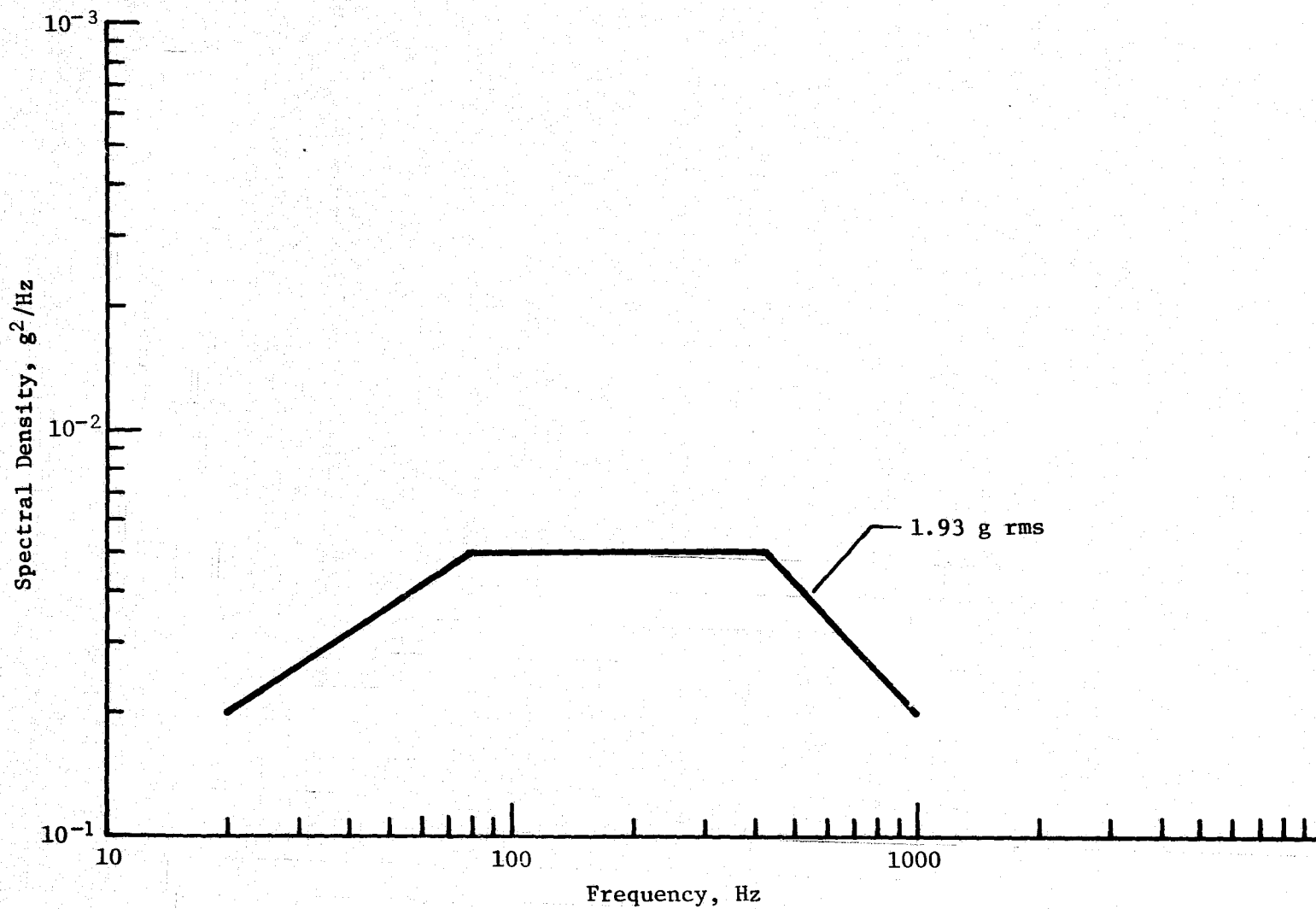


Figure V-42 On-Orbit Vibration Level for RCS Aft Tanks

Table V-18 RCS Requirements during On-Orbit Vibration

Number of OMS Engines Firing	N <sub>2</sub> O <sub>4</sub> Flowrate, kg/s (lbm/s)	Number of RCS Thrusters Firing	OMS Acceleration, g	Vibration, g rms	Total Acceleration on System, g
2	0	0	0.077	1.93	2.01
1	4.0 (8.8)	4	0.039	1.93	1.97

Scaling as defined by Equation [V-12] was used to simulate full-scale hydrostatic capability. Substituting appropriate values for the test fluid, Freon TF, and actual propellant, N<sub>2</sub>O<sub>4</sub>, into the equation for a 1/3-scale model ( $l_p/l_m = 3$ ), results in a test acceleration level of 4.1 g. Considering the contribution of gravity, the net random input required was 3.1 g rms.

Random vibration tests were run to verify the model's capability to withstand the design environment and to determine its operational capability. This was accomplished by running both outflow and nonoutflow tests. The nonoutflow tests were intended to correlate data on a purely hydrostatic basis, without the introduction of variables associated with flow. Outflow tests were run to simulate the OMS roll control maneuver previously described. The scaling of flowrate was analyzed as discussed at the beginning of this section. A full-scale flowrate of 40 kg/s (8.8 lbm/s) scales to a flow rate of 0.16 l/sec (10 in.<sup>3</sup>/s) in the model.

c) Apparatus and Procedure - A schematic of the vibration test system is shown in Figure V-43. The basic components of the system included a GN<sub>2</sub> pressurization source, the test article, and the receiver tank with graduated sight glass. The tank was mounted on the shaker table by the attachment fixture and supported at the tank flanges. This oriented the tank so that the barrier was horizontal and the +X axis was 16 deg from vertical. The test article was connected to the receiver tank by 1.27 cm ( $\frac{1}{2}$ -in.) Tygon tubing up to the 1.9-cm (0.75-in.) hand-operated ball valve. Stainless steel tubing was used to connect the ball valve to the receiver tank. The test fluid was Freon TF.

The actual test setup is shown in Figures V-44 and V-45. The aluminum attachment fixture is shown in both photographs, as are the five accelerometers that were used for monitoring the shaker input to the test device. The attachment fixture obstructed viewing the tank bottom hemisphere and restricted visual confirmation of the liquid test level. A hole in the attachment fixture allowed penetration of the outflow line and partial inspection of the enclosed section of the tank for leaks and residual test fluid.



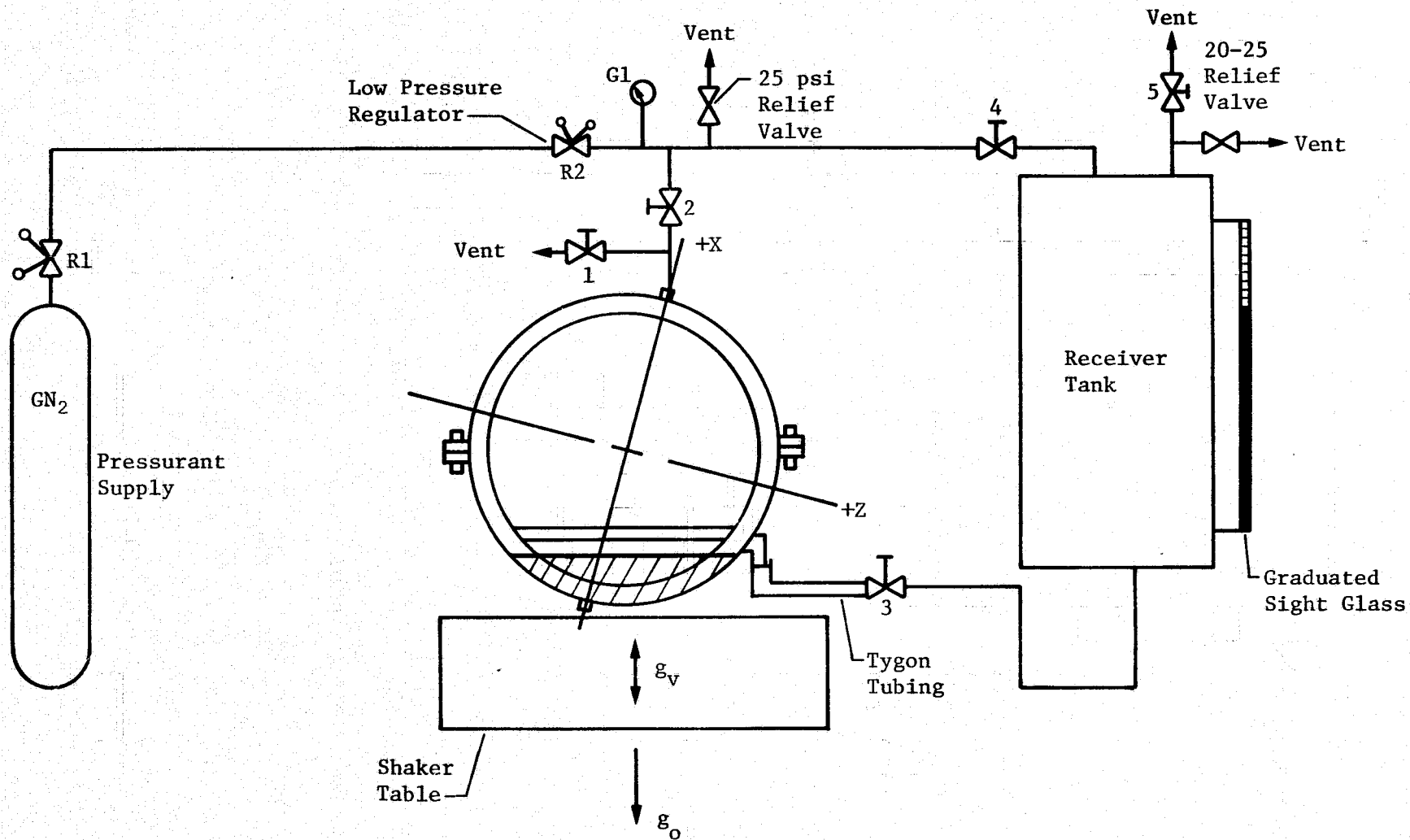
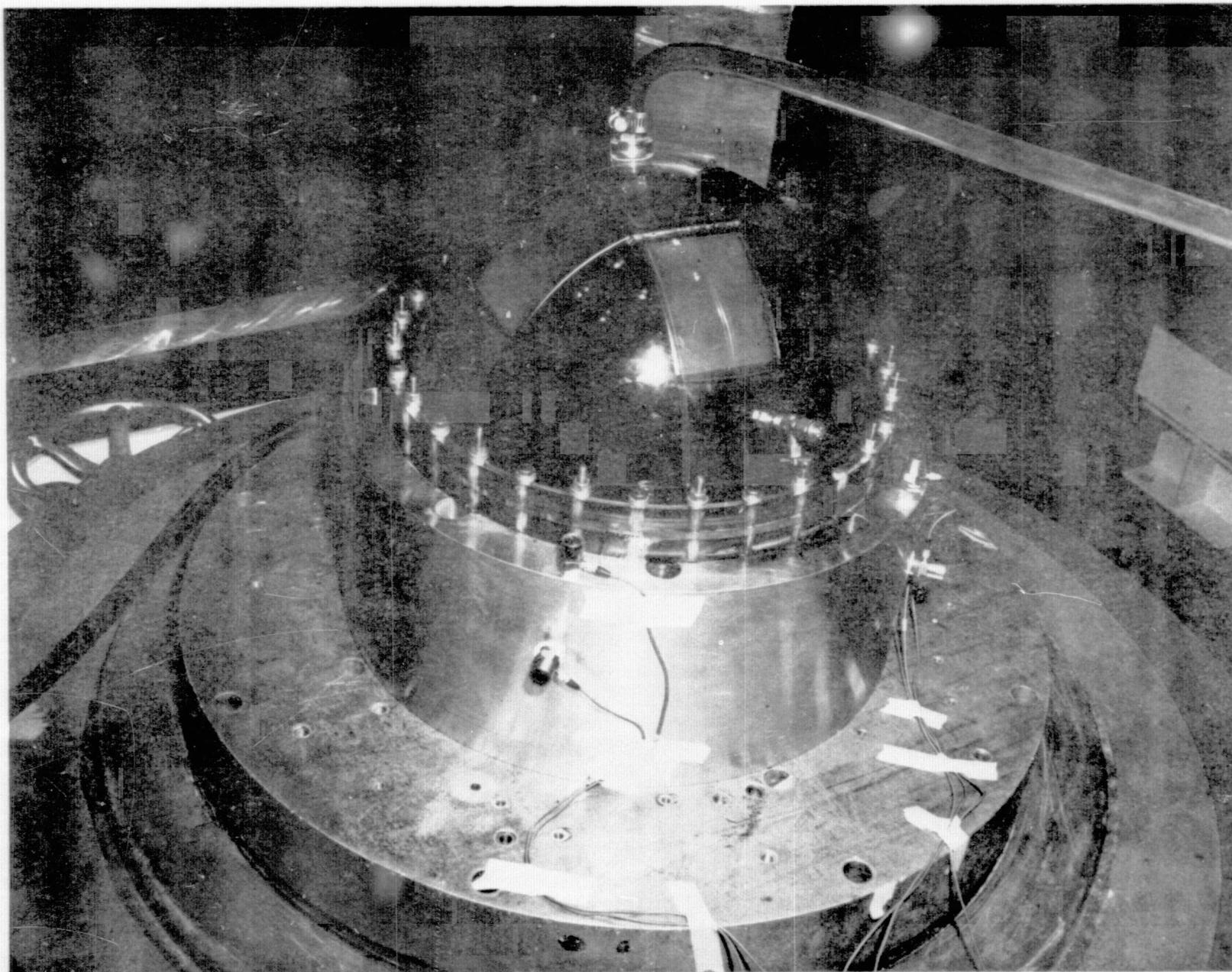


Figure V-43 Vibration Test Schematic

Figure V-44



V-95

Figure V-44 Subscale Model Vibration Attachment Fixture

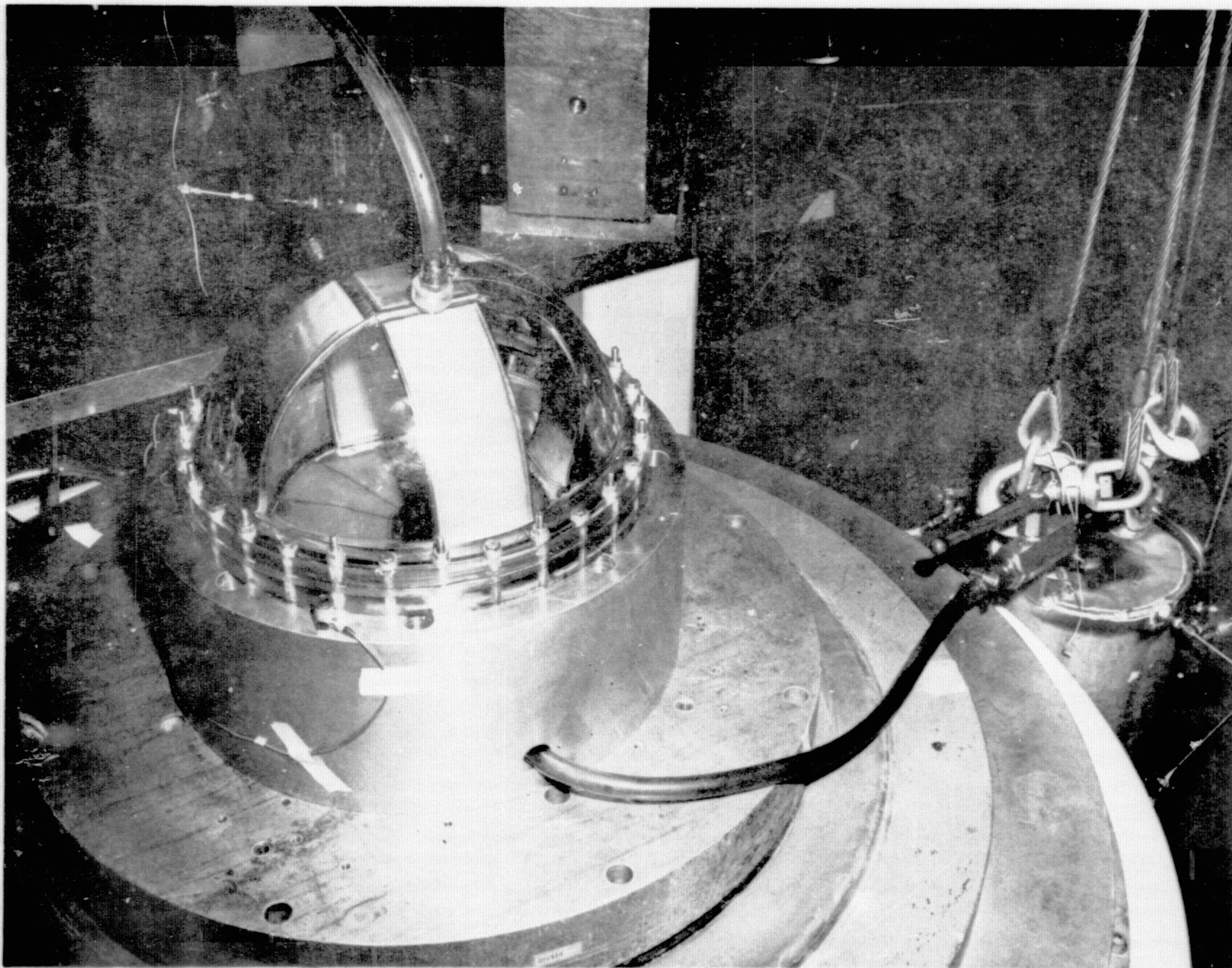


Figure V-45 Vibration Test Setup

Hydrostatic tests were run to determine the height of liquid that could be supported by the system at various vibration inputs. Outflow tests were run to determine the expulsion efficiency of the system when subjected to various levels of random vibration input in the vertical axis. The procedure for each of these test series was somewhat different.

Hydrostatic testing was conducted by filling the tank to a 100% loaded condition and recording the level in the receiver tank. The test article was then outflowed to the desired test level determined by the final graduated sight glass reading. This procedure assured the bottom compartment screens were wet and purged any gas that might have been trapped in the bottom compartment channel system. The system was pressurized to  $1.4 \text{ n/cm}^2$  (2 psig) and vibrated at the appropriate test levels for approximately 1 minute. After vibration was terminated, the outflow valve was opened and the Tygon section of the line monitored for immediate presence of gas. If gas was not present until final breakdown of the system, then the system remained stable during the test. Six different tests were performed in this manner--three random and three sinusoidal. The liquid levels and accelerations tested are shown in the vibration test matrix of Table V-19.

For the outflow tests, the tank was filled in the manner described previously and outflowed to the initial test level to purge gas from the system. The receiver tank reading was recorded and the tanks pressurized. When the induced vibration reached the test level, outflow was initiated until two-phase flow appeared in the outflow line.

Outflow and vibration were stopped and the receiver tank reading taken. The data allowed calculation of expulsion efficiency for the twelve outflow tests denoted in Table V-19. Outflow tests were also conducted in +1g before the vibration tests were started and periodically between vibration tests to accomplish the following objectives: (1) to acquire baseline data to which the performance of the model during vibration could be compared, and (2) to monitor performance of the system to determine if any structural damage had occurred.

d) Data and Results - Results of the hydrostatic tests are shown in Table V-20. Eight runs were made for the six test conditions. The column marked "Fill Level Hydrostatic Head" represents the length of screen channel exposed to ullage during the test, and consequently the liquid column height, which must be supported for channel stability. "Supportable Height", as defined in Table V-20, is the height of liquid that can be supported by a stable screen channel based on hydrostatic theory, i.e.,  $\Delta p = \rho gh$ . The g acceleration is a combination of the random rms input and earth gravity environment. Comparing these two columns, the supportable height based on a hydrostatic analysis is always greater, indicating

Table V-19 Vibration Test Matrix

Test Number	Vibration Type and Axis	Test Type	Initial Tank Level, %	Final Tank Level, %	Tank Pressure, N/cm <sup>2</sup> (psig)	Tank Design, G-level	Vibration Input
1	Random Vertical	Hydrostatic	4.6	4.6	1.4 (2)	4.1	6.0
2	↓	↓	5.0	4.6	1.4 (2)	4.1	7.0
3	↓	↓	4.6	4.6	1.4 (2)	4.1	7.5
4	Sinusoidal Vertical	↓	10.0	10.0	1.4 (2)	4.1	3.1
5	↓	↓	13.0	13.0	1.4 (2)	4.1	3.1
6	↓	↓	6.0	6.0	1.4 (2)	4.1	3.1
7	Random Vertical	Outflow	10.0	Level At Breakdown	1.4 (2)	4.1	3.1
8	↓	↓	10.0	↓	1.4 (2)	4.1	3.1
9	↓	↓	12.0	↓	1.4 (2)	4.1	3.1
10	↓	↓	12.0	↓	1.4 (2)	4.1	3.1
11	↓	↓	12.0	↓	0.7 (1)	4.1	3.1
12	↓	↓	12.0	↓	0.7 (1)	4.1	3.1
13	↓	↓	10.0	↓	1.4 (2)	4.1	5.0
14	↓	↓	10.0	↓	1.4 (2)	4.1	5.0
15	↓	↓	10.0	↓	2.8 (4)	4.1	3.1
16	↓	↓	10.0	↓	2.8 (4)	4.1	3.1
17	↓	↓	12.0	↓	2.8 (4)	4.1	3.1
18	Random Vertical	Outflow	12.0	Level At Breakdown	2.8 (4)	4.1	3.1

Table V-20 Hydrostatic Test Results

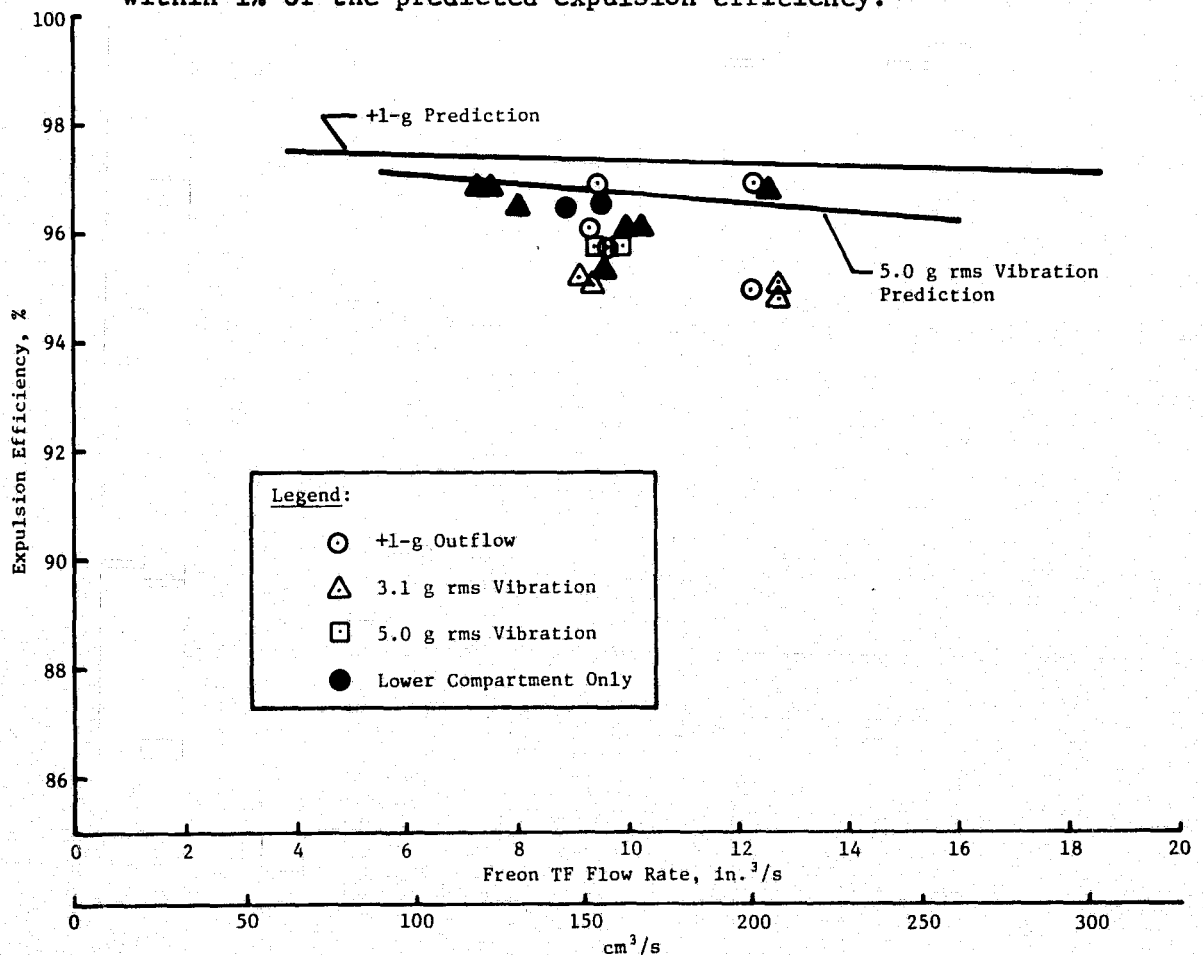
Run No.	Test No.	Fill Level Hydrostatic Head, cm (in.)	Supportable Height, cm (in.)	Gas in Outflow	Correlation
1	1	3.3 (1.3)	4.8 (1.9)	No	Yes
2	1	3.3 (1.3)	4.8 (1.9)	No	Yes
3	2	3.05 (1.2)	4.1 (1.6)	Yes	No
4	2	3.05 (1.2)	4.1 (1.6)	No	Yes
5	3	3.3 (1.3)	3.8 (1.5)	Yes	No
6	4	1.0 (0.4)	8.1 (3.2)	No	Yes
7	5	0 (0)	8.1 (3.2)	No	Yes
8	6	2.54 (1.0)	8.1 (3.2)	No	Yes



breakdown should never have occurred. However, gas was noted at the start of outflow in two cases. Considering the method used for measuring the ullage height in the tank and possible error in determining gas in the outflow line, these results are not surprising. Indeed, the data presented here tend to support the present hydrostatic treatment of vibration.

Outflow test results are shown in Figure V-46. Expulsion efficiency is plotted as a function of Freon TF flowrate. Computer predictions consider only the bottom compartment of the acquisition/expulsion system and are comparable to test data represented by solid symbols. Test data is plotted for 3.1 and 5.1 g rms vibration for both full tank and lower compartment expulsions.

Outflow from the lower compartment only may yield slightly higher expulsion efficiency, although data scatter is such that no definite trends are evident. The scaled g-level for OMS roll control of 3.1 g rms appears to have little effect on system operation when compared to the other test data. Also, the test data are generally within 1% of the predicted expulsion efficiency.



e) Conclusions - The data show no unexpected effects caused by vibration. Hydrostatic tests, although inconclusive, indicated that the surface tension device performed as expected based on hydrostatic theory. The two sets of data that deviated from theoretical capability were well within the accuracy of the test.

Outflow tests indicated little difference between steady 1-g expulsions and random vibration tests. For oxidizer scaled conditions, 3.1 g rms and 0.16 l/s (10 in.<sup>3</sup>/s), the expulsion efficiency of the device was 95.2% for full tank depletion, and 96.3% for lower compartment depletion. This indicates more than sufficient design capability because the minimum depletion level for the aft tanks during OMS roll-control is 13% (87% expulsion).

8) Slosh Tests - The barrier of the surface tension device provides some control of the bulk propellant within the tank. Any perturbation acting on the orbiter will produce motion of the propellant within each compartment. If the perturbations are periodic and near the harmonic frequency of the propellant, significant slosh can be induced. As far as the effect of the slosh on the performance of the surface tension device, slosh is considered to be a form of vibration. The effect of vibration on the device is considered in detail elsewhere in this report. The possible interaction of the propellant slosh and the orbiter guidance and control system is the problem being considered here.

Attitude corrections made by the RCS are the most likely source of periodic perturbations that could produce significant propellant slosh. Because RCS operates at some established frequency, a situation in which each attitude correction produces larger amplitude liquid motion, that requires a larger attitude correction is possible. Such a situation would reduce effectiveness of the RCS in maintaining the correct attitude and would result in excessive use of RCS propellant.

The usual approach to reducing the dynamic coupling between the propellant slosh and the attitude control system is to add slosh baffles to the propellant tank to damp the induced liquid motion. In addition, an attitude control operating frequency that is not near the harmonic frequency of the propellant can be selected.

The objective of these tests was to determine the basic slosh characteristics of the RCS tank/surface tension device system. The harmonic frequencies of the slosh, the damping provided by the surface tension device and the force of the liquid on the tank were measured. From these results an evaluation of the effect of the propellant slosh on the orbiter was accomplished.

*a. Apparatus and Procedure*

The subscale model of the RCS device, installed in a transparent tank, was tested using Martin Marietta's slosh test apparatus. Propellant slosh will be most significant when the liquid is positioned against the tank wall and the perturbations are acting parallel to the liquid surface. It is assumed that the perturbations produce a sinusoidal motion of the tank and linear liquid motion results. Nonlinear motion (i.e., breaking waves and rotation) tends to damp the response of the liquid. The accelerations acting on the RCS tanks during the mission are large enough to eliminate the need to consider low-g slosh effects.

The "quick-stop" test technique was used as the method of slosh testing the tank/surface tension device system. It is a straightforward method of determining the basic slosh parameters of a system. The tank is oscillated at the desired frequency and amplitude, and is then abruptly stopped at the point where the velocity is zero (maximum displacement). After stopping the tank, the motion of the liquid continues and the force required to hold the tank stationary is measured. This measured force is equal to the force the liquid applies to the tank. The harmonic slosh frequencies can be determined by observing the liquid slosh as the tank is being driven. The damping coefficient can be calculated from the decay in the force of the liquid on the tank after the tank is stopped.

The tank is shown mounted on the test fixture with the barrier oriented horizontally (Figure V-47) and vertically (Figure V-48). These two orientations are the extremes in the position of the device with respect to the liquid. Ball bearings suspend the slider on the rails and a hydraulic actuator is used to oscillate the tank. A rigid linkage, incorporating a load cell, connects the actuator to the tank.

The actuator is controlled electrically. A signal generator delivers a sinewave to the servo valve of the actuator. The frequency and amplitude of the sinewave can be varied to obtain the desired tank oscillation. The actuator was stopped by enabling a logic circuit that monitors the actuator travel (sensed with a potentiometer in the actuator) and compares it with a preset level representing the maximum travel. At the peak in the travel, the input to the actuator is transferred from the sinewave to a



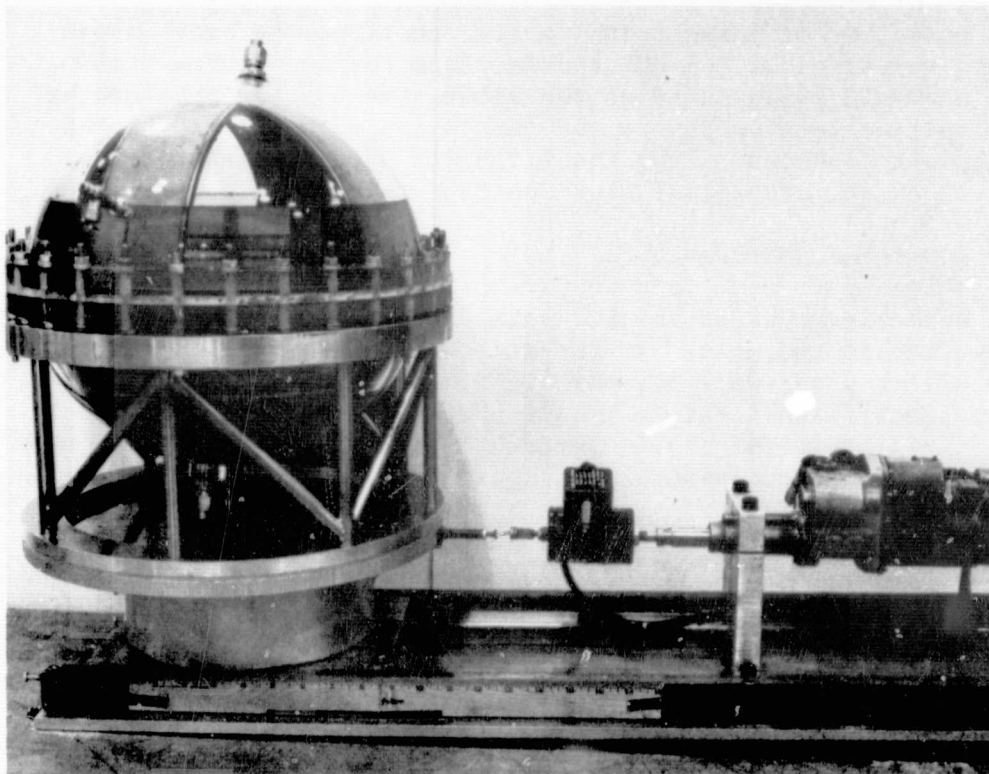


*Figure V-47  
Tank Mounted on Slosh Test Apparatus with Barrier Horizontal*

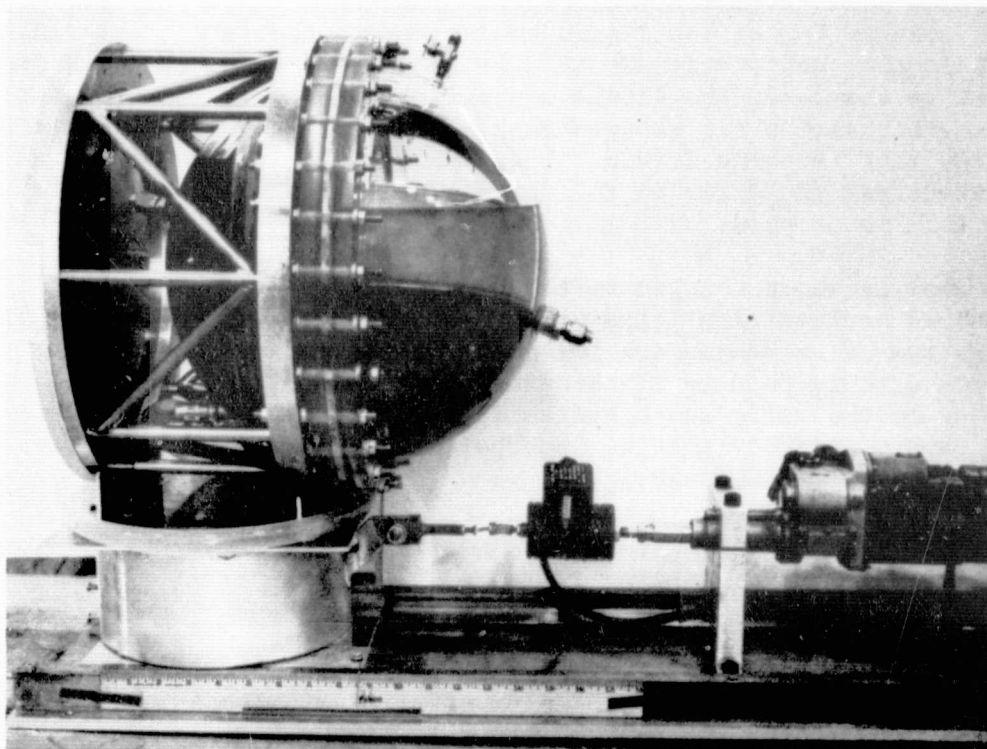


*Figure V-48  
Tank Mounted on Slosh Test Apparatus with Barrier Vertical*

DC bias voltage, abruptly stopping the actuator and holding it in that position. The actuator travel and the output of the load cell are monitored on a chart recorder.

Isopropyl alcohol was used as the referee test liquid. The volume of liquid in the tank was varied from 10 to 90%, in increments of 10%, for each tank orientation. A matrix of the test conditions is shown in Table V-21. For each test condition, the frequency of the first three harmonic modes of oscillation was determined. At the first mode frequency, the tank was quick-stopped so that the damping ratio could be measured. The decay of the force of the liquid on the tank is only clearly defined at the first mode frequency. All tests were accomplished using 1.6-mm (1/16-in.) oscillation amplitude or 3.2-mm (1/8-in.) peak-to-peak amplitude.

Table V-21 Slosh Test Matrix

Test Number	Liquid Volume (Percent of Tank Volume)	Device Barrier Orientation
1	10	Vertical
2	20	Vertical
3	30	Vertical
4	40	Vertical
5	50	Vertical
6	60	Vertical
7	70	Vertical
8	80	Vertical
9	90	Vertical
10	10	Horizontal
11	20	Horizontal
12	30	Horizontal
13	40	Horizontal
14	50	Horizontal
15	60	Horizontal
16	70	Horizontal
17	80	Horizontal
18	90	Horizontal

## b. Results

The basic slosh parameters of the tank/surface tension device system were determined. The harmonic frequency for the first three slosh modes was measured as a function of liquid volume. At each volume, the damping ratio was determined. The force of the liquid on the tank was also measured. From these basic parameters, the effects of the propellant slosh can be evaluated.

The slosh frequency is placed in dimensionless form using the following relation:

$$[V-33] \quad \bar{\omega} = \omega \sqrt{\frac{r}{a}}$$

where

$\bar{\omega}$  = dimensionless frequency parameter

$\omega$  = frequency, radian/second

$r$  = tank radius

$a$  = acceleration

Frequency can be scaled to another system based upon the geometry and the acceleration, independent of the liquid properties. The test data was placed in dimensionless form and is presented in Figures V-49 and V-50 for the horizontal and vertical barrier conditions.

With the barrier horizontal, the harmonic frequencies are similar to those for a bare spherical tank, which have also been plotted on Figure V-49 for comparison purposes. The differences between the two are caused by the surface tension device. A slight effect on frequency can be seen at large liquid volumes because of the channels of the device. When the liquid surface is near the barrier of the device it has a significant effect on frequency, especially at the first mode.

As the liquid volume is reduced below 40%, the liquid surface reaches the barrier and then liquid drains from the channels in the pressurization compartment. Not until the liquid volume reaches 10% is there again a free surface so that slosh can be observed. At 10% the harmonic frequencies again correspond with those of a bare spherical tank. The values of the harmonic frequency for a 96.5-cm (38-in.) diameter tank and accelerations of 0.01 g and 0.1 g have also been added to Figure V-49.

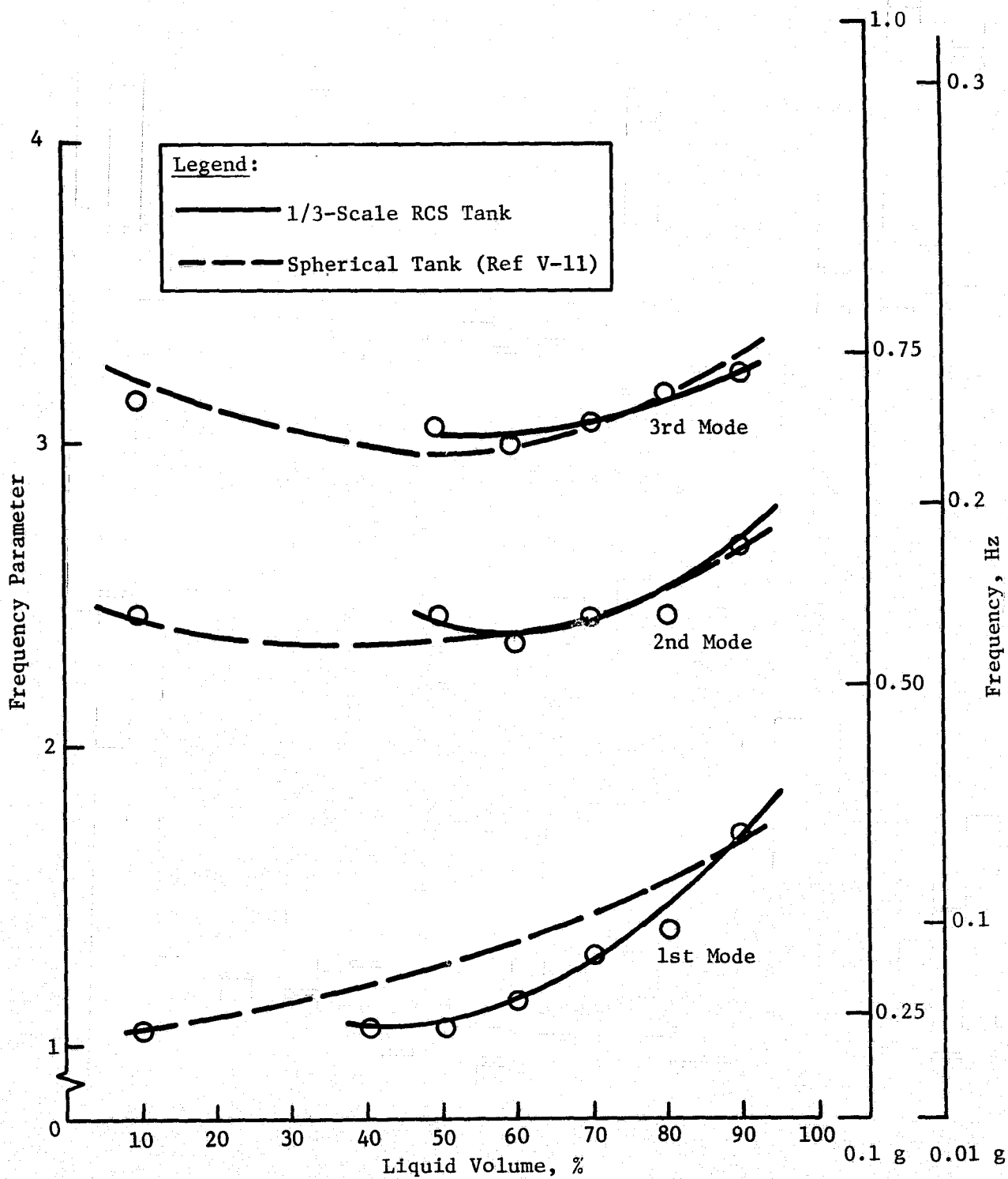


Figure V-49 Harmonic Frequencies, Barrier Horizontal

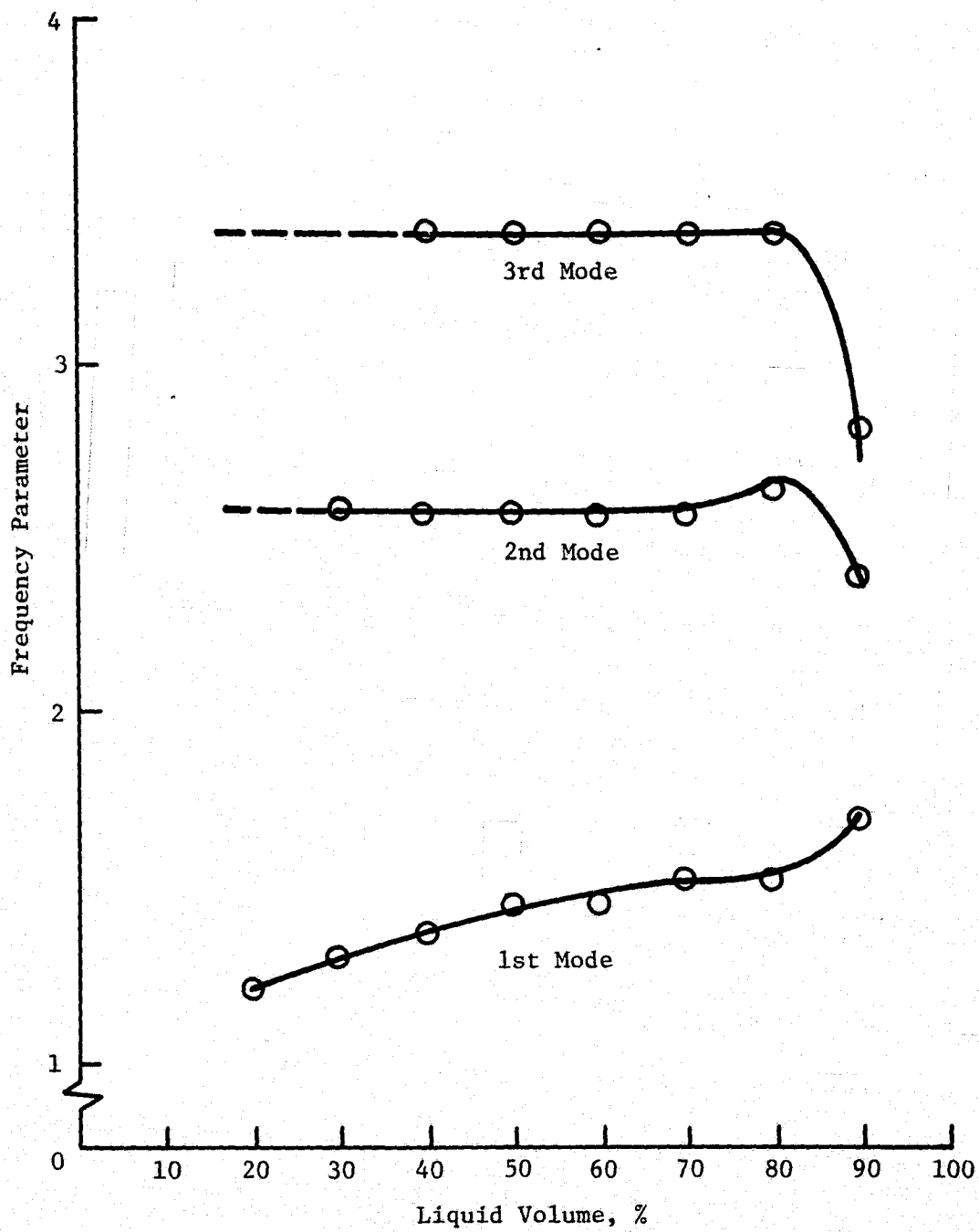


Figure V-50 Harmonic Frequencies, Barrier Vertical

When the barrier is vertical, the harmonic frequencies are of essentially the same magnitude as the barrier horizontal case. There are some differences in the way the frequency changes with liquid volume, as shown in Figure V-50. The slosh is not significant when the surface is in the lower compartment and frequencies for that condition are not shown.

When using the "quick-stop" test method, the damping ratio is determined by measuring the rate at which the force of the liquid on the tank decays. Based upon an exponential change in the force

$$[V-34] \quad F = F_o e^{-2\pi n \gamma}$$

where

$F_o$  = force at the 0th cycle

$F$  = force at the nth cycle

$n$  = number of cycles

$\gamma$  = damping ratio

or solving for the damping ratio

$$[V-35] \quad \gamma = \frac{1}{2\pi n} \ln \frac{F_o}{F}$$

Therefore, by measuring the maximum force at any two points during its decay, the damping ratio can be calculated.

A nondimensional form of the damping ratio is obtained by using the following relation:

$$[V-36] \quad \gamma = K \frac{\nu^{1/2}}{r^{3/4} a^{1/4}}$$

where

$K$  = damping ratio coefficient

$\nu$  = kinematic viscosity

$r$  = tank radius

$a$  = acceleration

The damping ratio coefficient is a function of only the geometric configuration of the tank. Knowing K, the damping ratio for a given tank size, liquid and acceleration can be calculated. The value of K versus liquid volume for the tank/surface tension device system with the barrier horizontal is plotted in Figure V-51. Values of K for a bare tank are also plotted so that the effect of the surface tension device can be seen. Effects of both the channels and the barrier are evident. Damping is increased by at least a factor of 5, over that of the bare tank.

When the barrier is vertical, there are abrupt changes in the damping ratio coefficient as the liquid volume changes (Fig. V-52) because of the location of the liquid surface with respect to the channels. At 30 and 60% volume the surface is between channels, so there is very little interaction of the slosh with the channels. At 50% and volumes greater than 70%, the surface is interacting with the channels. At volumes less than 30%, the barrier influences the damping.

Damping ratios for the full-size system can be calculated from the data. With MMH as the liquid and an acceleration of 0.1 g, the minimum damping ratio for the system ( $K = 5$ ) is 0.009. Using  $N_2O_4$  as the liquid, the minimum damping ratio is 0.0047.

The force of the liquid on the tank was determined by using the peak force that occurs immediately after stopping the tank. Before stopping the tank, the measured force includes the inertia of the tank and effects of the slider, so it is not a valid measure of the liquid force. The force is placed in dimensionless form with the following relation:

$$[V-37] \quad \bar{F} = \frac{F}{\rho g d^3 \left( \frac{x}{d} \right)}$$

where

$\bar{F}$  = dimensionless force

F = measured force of liquid

$\rho$  = liquid density

g = acceleration  $\left( a/g_c \right)$

d = tank diameter

x = amplitude of oscillation

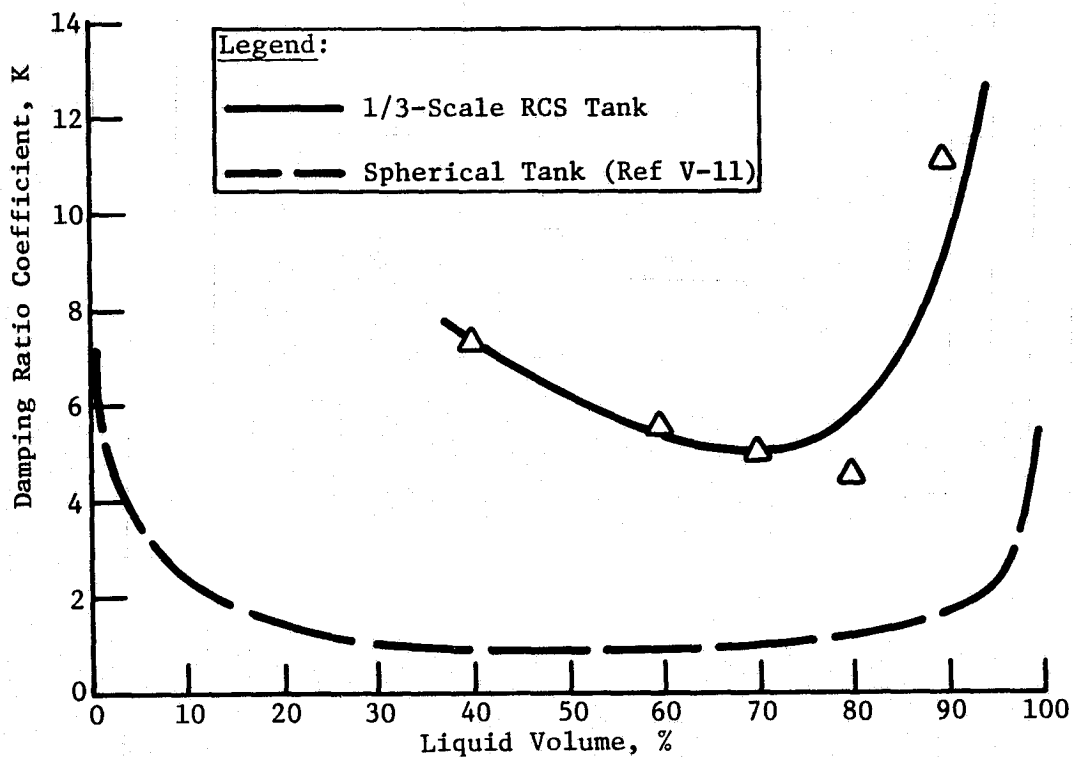


Figure V-51 Damping Ratio, Barrier Horizontal

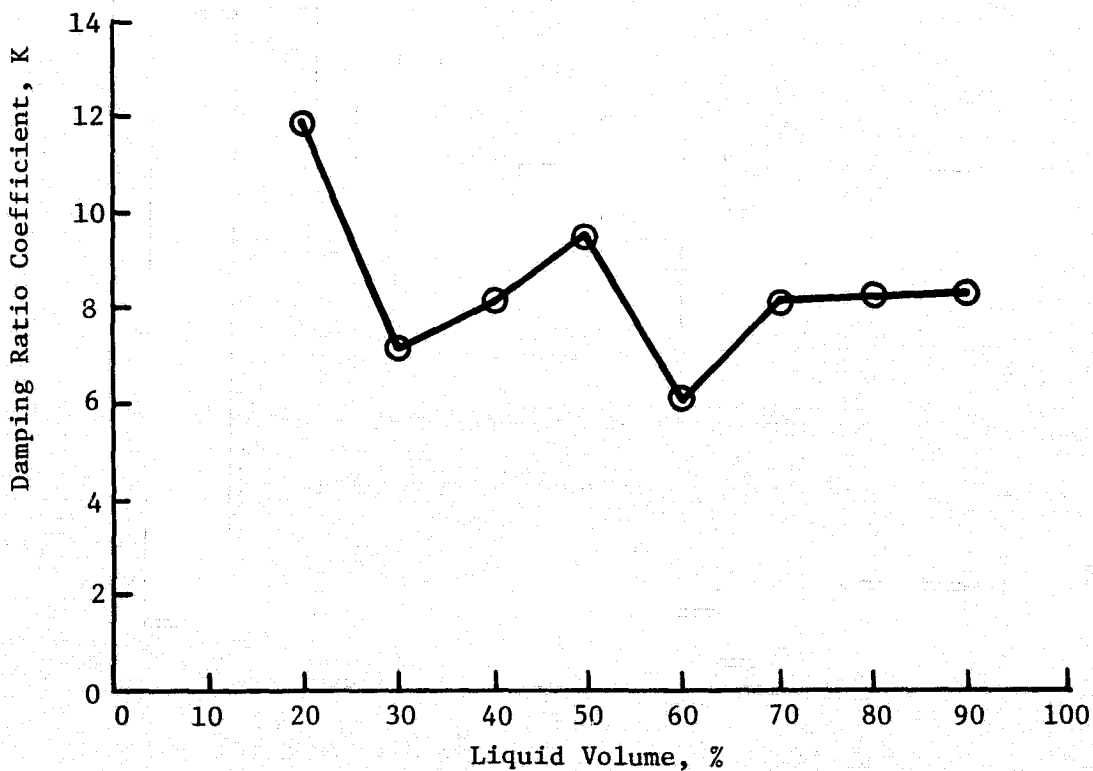


Figure V-52 Damping Ratio, Barrier Vertical



This dimensionless force is plotted versus liquid volume in Figure V-53 for both barrier horizontal and vertical cases. This force was always measured at the first mode natural frequency, when the slosh is the most significant.

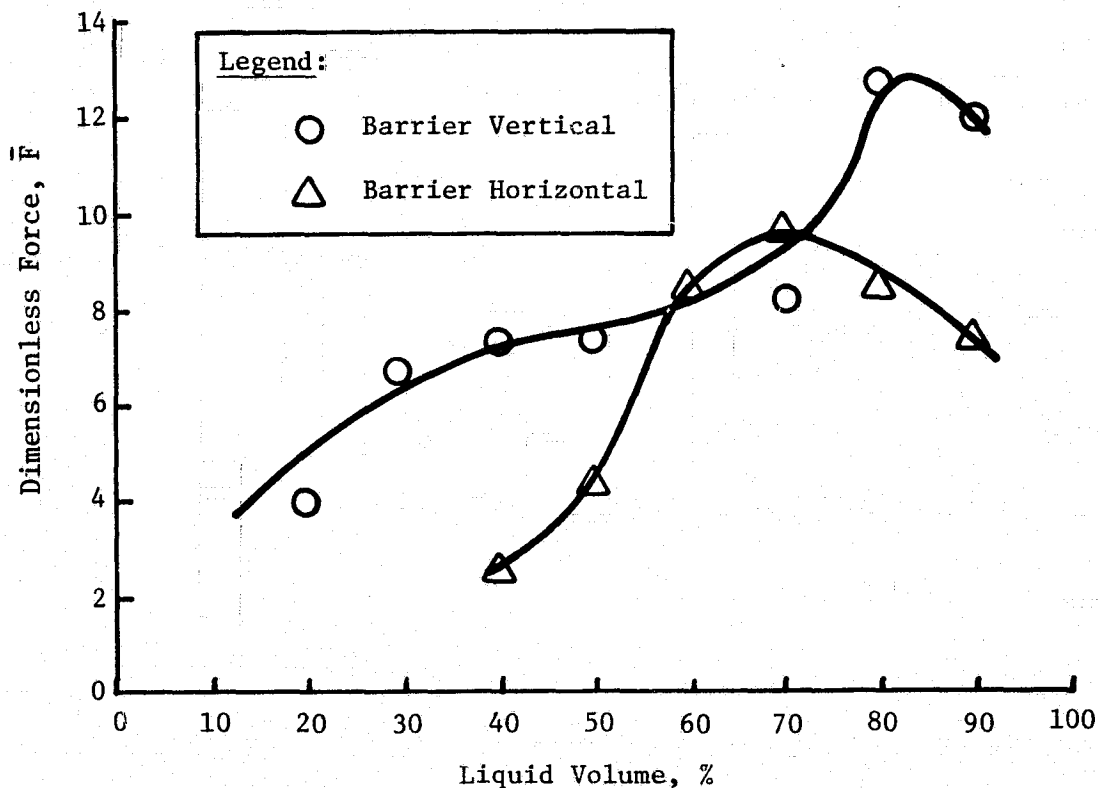


Figure V-53 Force Response

The force data are consistent with the damping data. The maximum forces occur when the damping is at a minimum. The largest slosh forces occur when the liquid volume is around 70 to 80%. At these volumes, the motion of the liquid is the least constrained by the surface tension device and tank walls. In addition, the mass of liquid that is in motion due to the slosh is a maximum. Applying the results of the actual propellants and tank size, the maximum forces listed in Table V-22 are obtained. An input driving amplitude of 1.6 mm (1/16 in.) was used in the calculations.

Table V-22 Force Response for Actual Propellants

Barrier Position	Force of Liquid on Tank, N (lbf)	
	N <sub>2</sub> O <sub>4</sub>	MMH
Horizontal	18.2 (4.1)	11.1 (2.5)
Vertical	26.7 (6.0)	16.5 (3.7)

c. Conclusions

This test program considered the possible effects of propellant slosh within a single RCS tank, including its surface tension device. The evaluation was accomplished by creating conditions under which the slosh was most significant. The liquid was always oriented against one side of the tank and the perturbations producing the slosh were parallel to the surface. First mode slosh frequencies were always used when determining the force the liquid could apply to the tank. The actual conditions that could occur in a Space Shuttle RCS tank must be considered with respect to the test conditions in applying the results of the tests.

The prime source of perturbations that could induce propellant slosh is the firing of the RCS thrusters. Firing of the RCS can occur at the harmonic slosh frequencies, so harmonic slosh of the propellants is possible. The evaluation of the effects of the slosh must then consider forces that would act on the Shuttle because of the slosh.

The surface tension device acts as a slosh baffle, damping the induced propellant slosh. It has been shown that a screen surface can actually increase the damping in comparison to a solid baffle of the same shape (Ref. V-12). When the volume of liquid is large (greater than 80%) or small (less than 30%), significant damping is provided by the device. At other volumes, the device still provides some damping. Damping ratios that were a factor of 5 greater than the damping of a bare spherical tank were measured.

Force of the liquid on the tank reached a maximum with liquid volumes around 70 to 80%. Applying the results to the actual tank yielded maximum forces due to slosh on the order of 15 N (3.4 lbf) to 25 N (5.6 lbf). These forces do not appear to be significant in comparison to the total mass of the Space Shuttle. These results, however, should be evaluated with respect to the dynamics of the Space Shuttle guidance and control system.

## DESIGN IMPACT

The two problem areas identified in the test program require modification of the design. Gas trapped during fill tests with dry wicking barriers was minimal, less than 0.6%. However, as much as 4% of the tank volume could be trapped if the screens are wet. Wicking barriers could not be relied on to assure gas-free filling of the tank. As a result, vent tubes were required in areas where gas could be trapped in the device during vertical loading.

The inability of the model to provide 98% expulsion efficiency during reentry was due to screen dry out and gas pull-through in the upper and lower compartment channels. The major design changes required to solve this problem were the addition of two bubble filters, one at the outlet of the lower compartment channels and the other at the outlet of the upper compartment manifold into the lower compartment. Also, a redesign of the upper compartment barrier manifold was indicated to maximize screen area while holding device volume small. This would increase the flow area and lower entrance losses to help prevent gas pullthrough during RTLS and reentry.

These are the only design changes that resulted from the subscale tests. They were incorporated into the design effort discussed in Chapter VI.

## VI. FULL-SCALE TANKAGE

---

A detailed design of the selected compartmented tank surface tension device was developed, fabricated, and tested in the final task of this program (Task V, Full-Scale Tankage). The design approach, fabrication details, and test results are presented in this chapter.

### A. SYSTEM DESIGN

The detailed design of the propellant acquisition system was based upon the preliminary design produced in Task IV and the results of the similitude tests. The new requirements of a major revision in the design criteria, which took place at this time, were incorporated. An in-depth analysis was performed to properly size and configure the concept to satisfy all mission requirements.

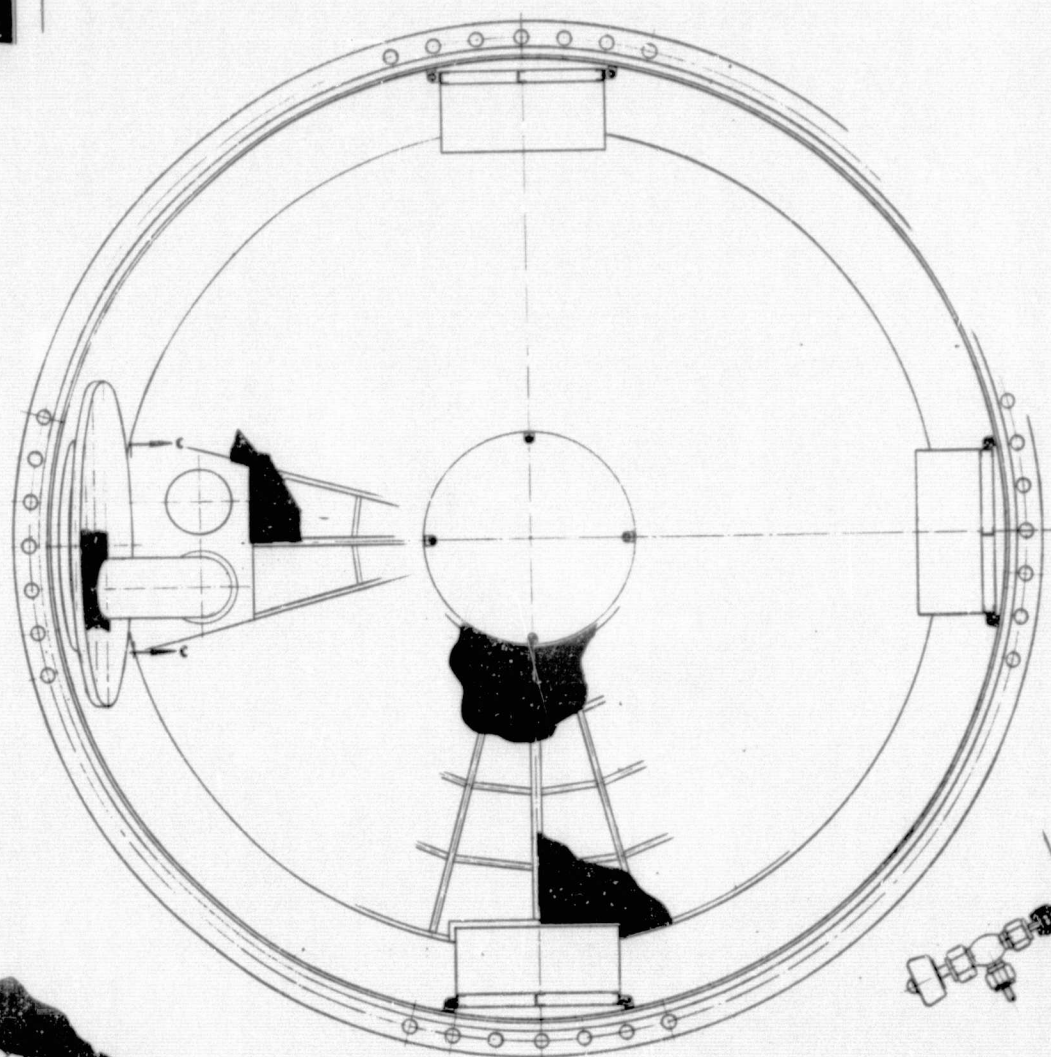
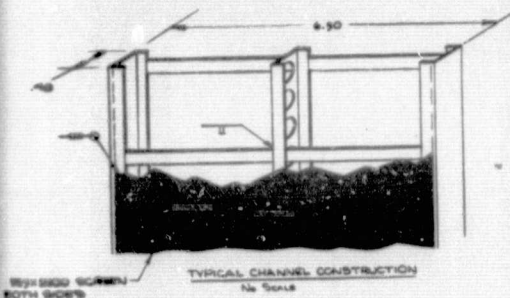
Drawings of the detailed design are presented in Figure VI-1. This figure shows the device and tank as built for the test program, using a thick walled tank. This system is a prototype for an actual flightweight acquisition system. It was built for the prime purpose of verifying the ground operations and checkout procedures for the acquisition system. A flightweight tank for

#### 1. Acquisition System Description

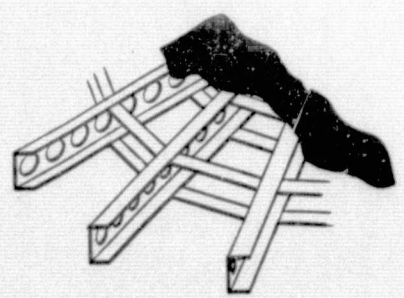
A simplified schematic of the detailed design is shown in Figure VI-3. Basically, it is a refinement of the preliminary design produced in the previous task. The major differences are the sizes of the channels, the addition of bubble filters, and a reentry collector and sump. The changes in the concept configuration followed results of the similitude testing and revisions to the design criteria.

##### *a. Physical Description*

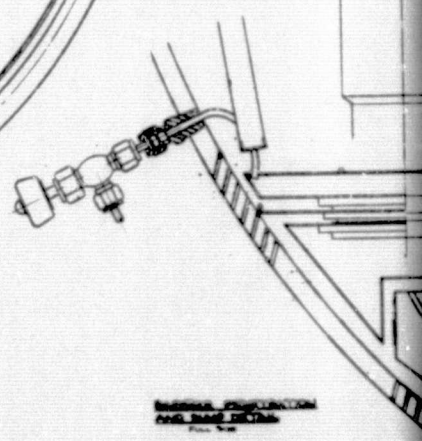
The screen acquisition system consists of two basic components: the upper compartment channel system and the lower compartment channel system. The tank is divided into two internal compartments by means of a solid barrier parallel to the tank parting plane. The volume below (on the outlet side) the barrier is 13.6% of the tank volume; the remaining 86.4% of the volume is above (on the pressurization port side) the barrier.



SECTION A-A

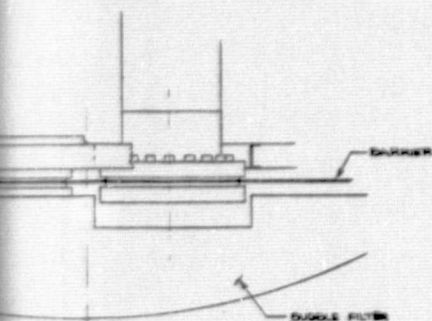


CROSS SECTION OF UPPER COMPARTMENT  
RING MANIFOLD  
No Scale

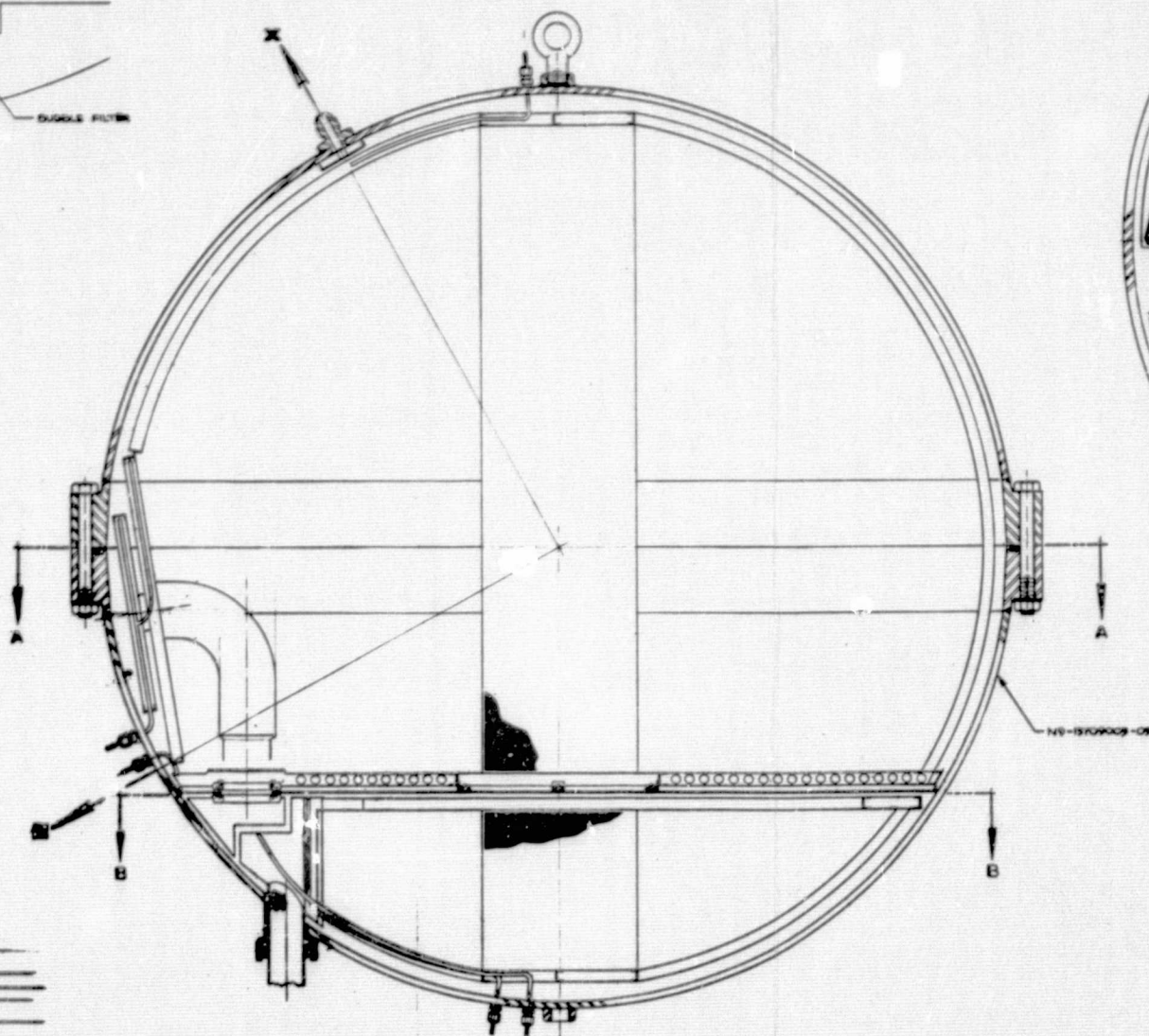


FOLDOUT FRAME PRECEDING PAGE  
PRECEDING PAGE BLANK NOT FILMED





VIEW C-C



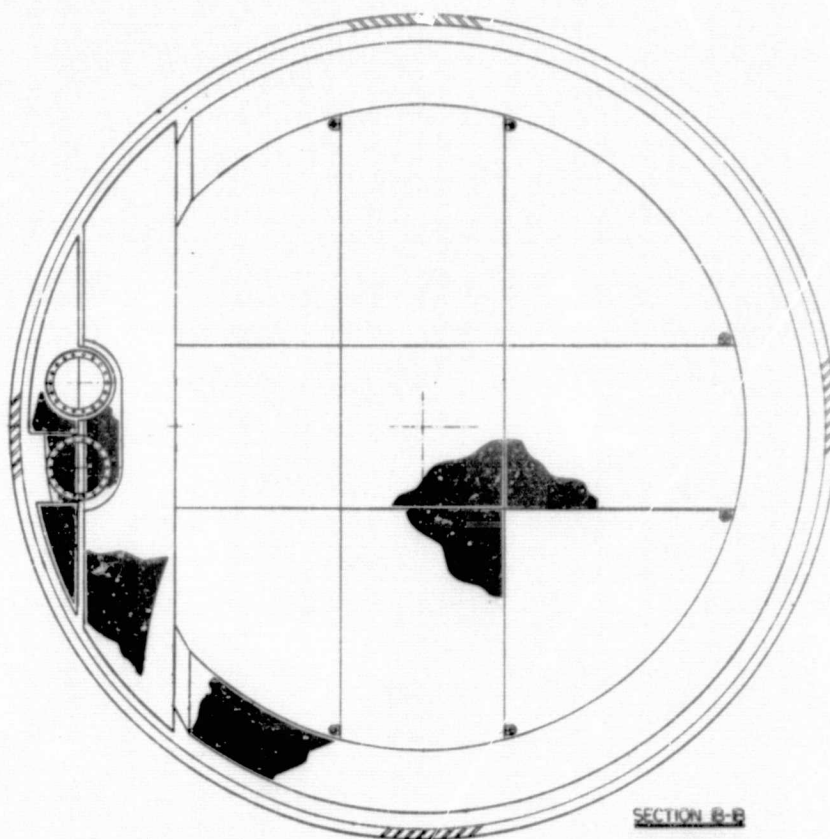
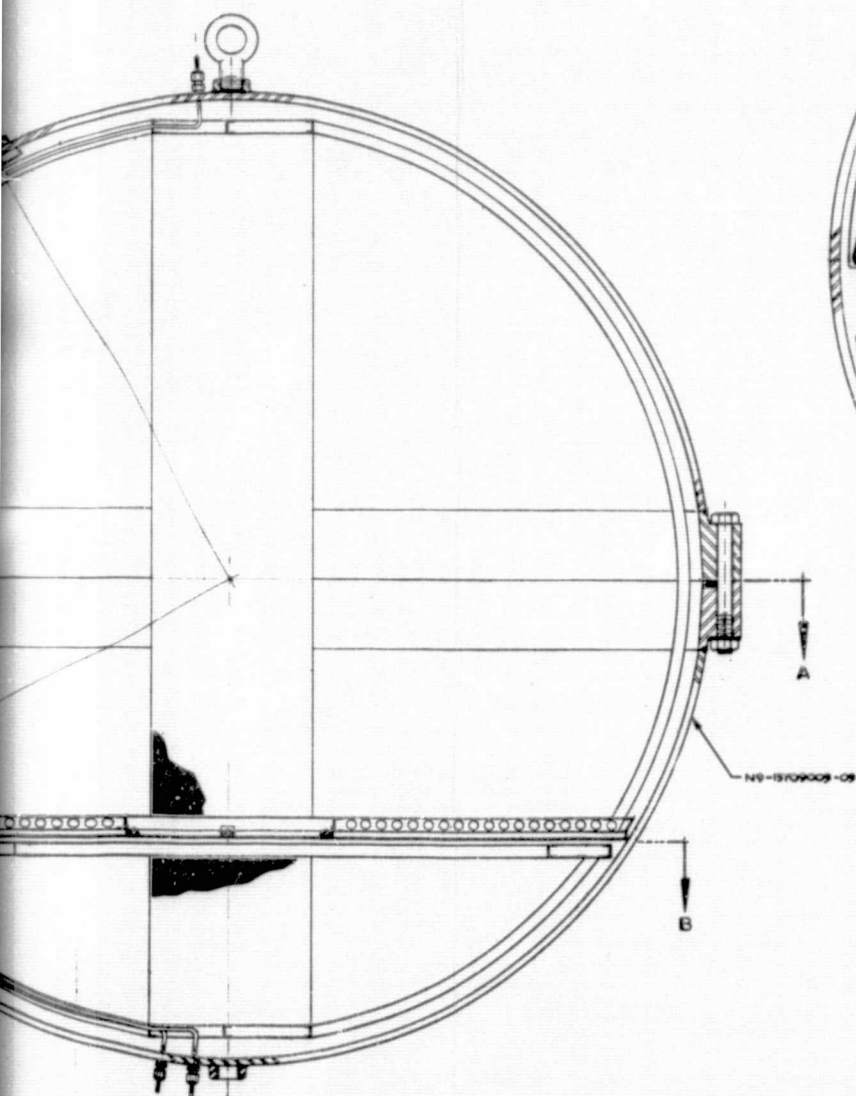
-009

NOTE: All dimensions are in inches; to convert to centimeters multiply by 2.54

Figure VI-1 SS/RCS Prop

FOLDOUT

FOLDOUT FRAME



-009

e in inches; to  
eters multiply

Figure VI-1 SS/RCS Property Acquisition Device Design Detail

VI-3 and VI-4

**FOLDOUT**

Figure VI-2

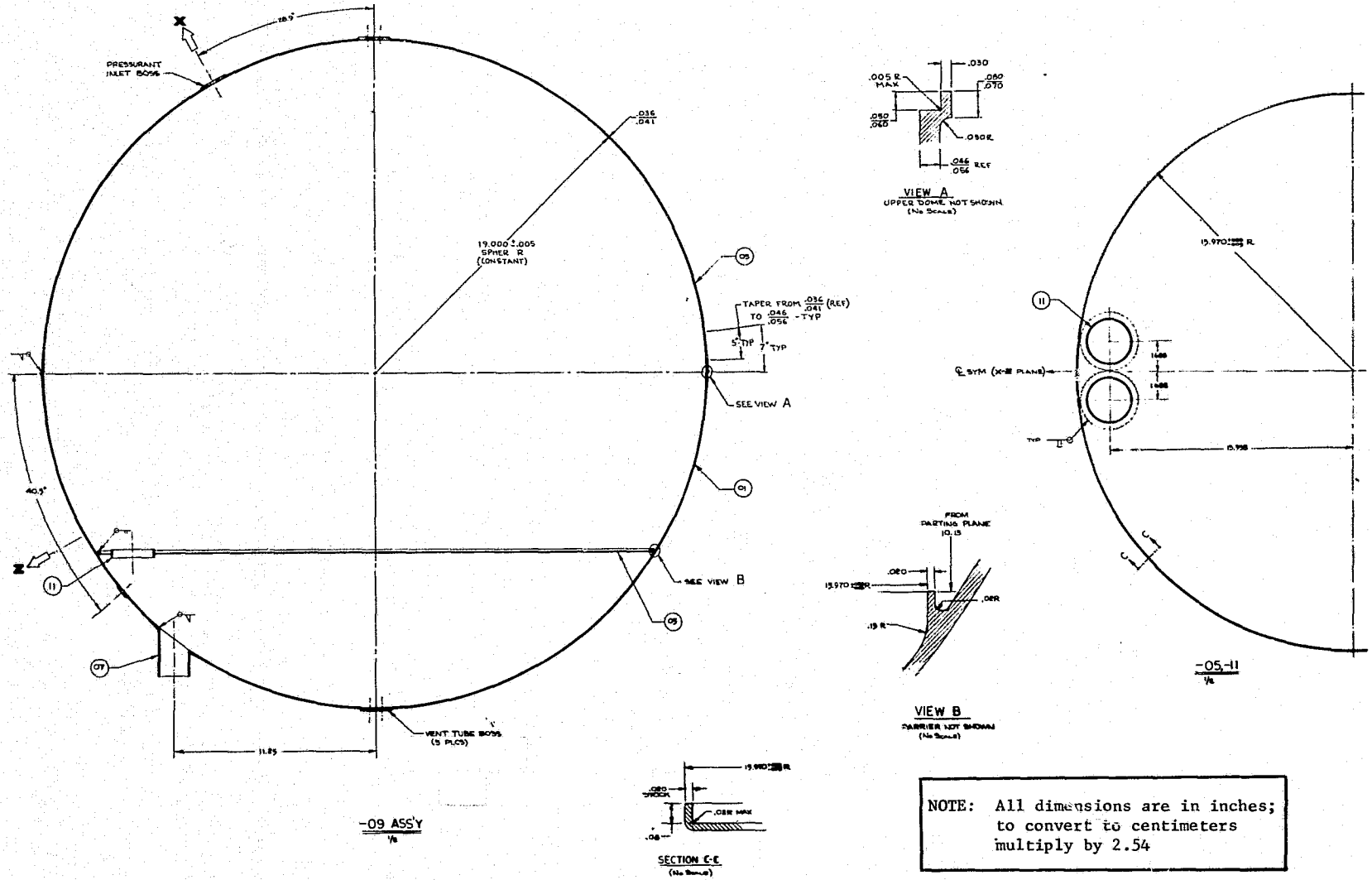
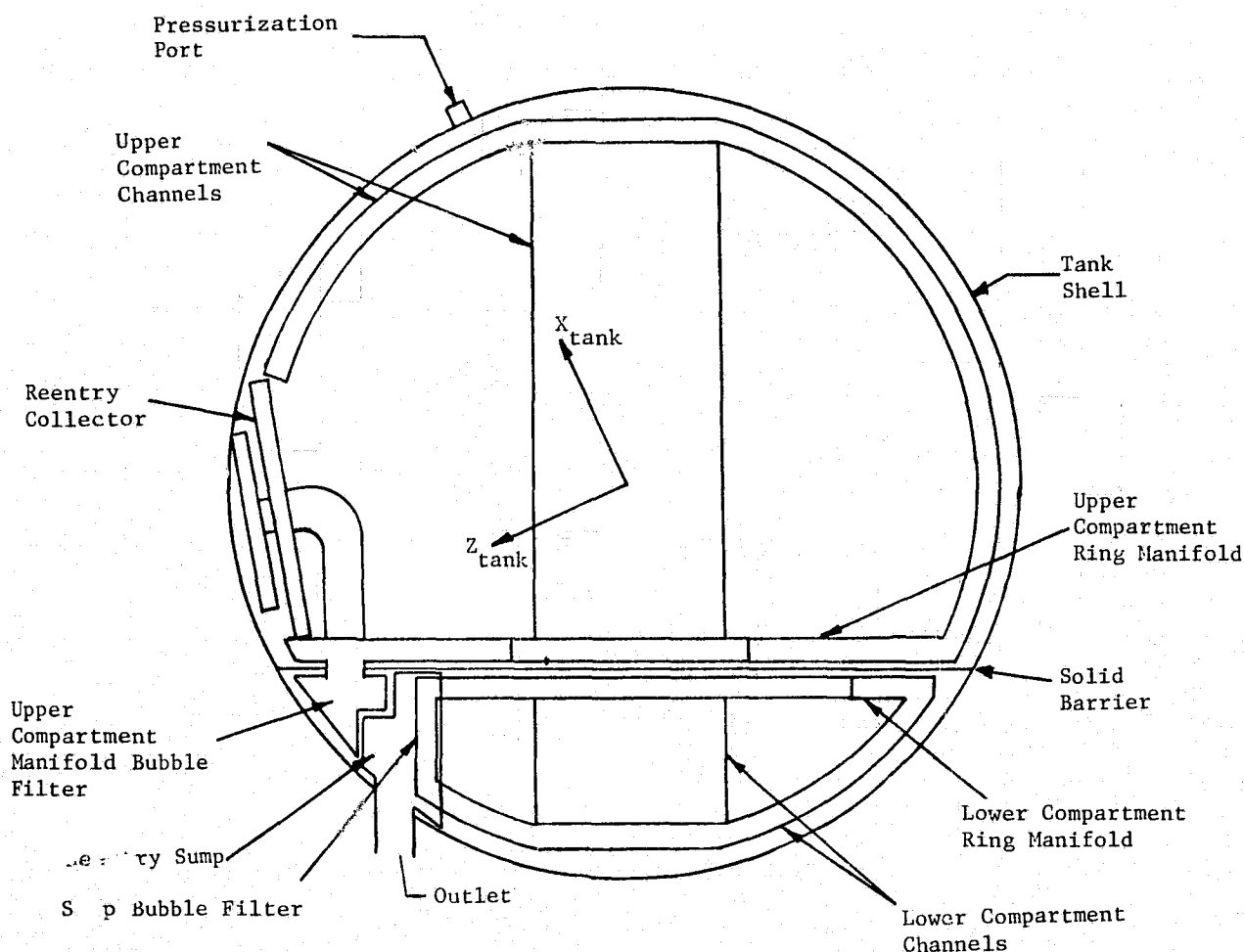


Figure VI-2 Flightweight Tank Design





*Figure VI-3 Surface Tension Device, Schematic*

The lower compartment contains a four-channel system composed of 325 x 2300 Dutch-twill weave screen. The channel cross-sectional dimensions are 16.5 cm (6.5-in.) x 1.22 cm (0.48-in.) and they cross at the center of the compartment to form a manifold. The channels are manifolded at their other ends into a ring manifold with cross-sectional dimensions of 6.4 cm (2.5-in.) x 1.27 cm (0.5-in.) and are covered with 325 x 2300 screen. The ring manifold and one of the four channels feed into a sump bubble filter in the interior of a reentry sump. The bubble filter is covered with 165 x 800 screen; the reentry sump with 325 x 2300 screen. Adjacent to the reentry sump is the upper compartment manifold bubble filter, also constructed of 165 x 800 screen.

The upper compartment channels are of 325 x 2300 screen with 16.5 cm (6.5-in.) x 1.22 cm (0.48-in.) cross-sectional dimensions. Four of these channels manifold together at the center of the upper compartment and into the upper compartment ring in three places. The fourth channel terminates at a reentry collector so that there is no communication between these two component parts. The upper compartment ring manifold is positioned off the barrier so that the 325 x 2300 screen can be used on both sides. The cross-sectional dimension of the ring is 30.5 cm (12-in.) x 1.27 cm (0.5-in.). A penetration through the solid barrier connects the upper compartment ring manifold with the manifold bubble filter below the barrier. The barrier penetration is a 5.1-cm (2-in.) circular hole.

The remaining component is the reentry collector. This collector extends between the short upper compartment channel and the barrier. The upper portion of the collector is formed of two parallel disks with 325 x 2300 screen on both sides (four screen sides - Fig. VI-3). These collectors are ducted in series into a 5.1-cm (2-in.) diameter solid tube that penetrates the solid barrier and upper compartment manifold adjacent to the upper manifold bubble strainer. The penetration is through a 5.1-cm (2-in.) circular hole that connects the reentry collector channel directly with the lower compartment bulk region.

The acquisition system contains nine vent and pressure monitoring ports located at the high points (tank X-axis vertical) of the various screen components. These ports are used only during ground and test operations. They were added to this prototype device so that the need for such ports could be evaluated during the test program.

#### *b. Operational Description*

The screen system is designed to deliver gas-free liquid propellant to the tank outlet under all Space Shuttle mission requirements. The design, consisting of a compartmented tank, supplies propellant in a series arrangement, with the upper compartment feeding propellant to the lower compartment, and the lower compartment feeding the tank outlet. The solid barrier separating the upper compartment from the lower compartment is actually located at an angle of 61.1 deg with the true tank centerline.

When the tank is filled, the lower compartment is completely filled and the upper compartment is filled to the desired level. During the filling of tanks, gas trapped in any of the screen components is vented through the vent tubes. After the tank reaches orbit, it is assumed that the upper channels are at least partially filled with gas because of breakdown of the channels during boost. This trapped gas will be purged into the lower compartment during the first orbital maneuvers. For the

on-orbit phase of the mission, the liquid is resupplied to the lower compartment as it is withdrawn from the tank so that no additional gas volume is added to the lower compartment. The flow path for the liquid is either into the upper channels or manifold, through the barrier and bubble filter and into the lower compartment, or through the reentry collector and directly into the lower compartment. Once in the lower compartment the liquid can either go directly into the sump and out of the tank, or go into the lower channels or manifold through the sump filter and then out of the tank.

The upper channels are designed so that for any orbital maneuver, even if only one or two channels are in contact with the bulk liquid, the mission requirements can be satisfied. In addition, if the liquid is settled between two channels, but in contact with the ring manifold, expulsion will still be possible.

For the forward tank application, liquid will continue to be expelled after the upper compartment has been exhausted. When the liquid in the upper compartment has been depleted, expulsion continues from the lower compartment bulk liquid through the lower compartment channels into the sump and out of the tank. The ring manifold of the lower compartment channels serves the same purpose as the ring manifold in the upper compartment; i.e., it provides a flow path to the sump even when the channels are not in contact with the liquid. The ring manifold serves the additional purpose of splitting the flow among the channels, thus reducing the dynamic pressure losses the fluid experiences. When the bulk liquid in the lower compartment has been expelled, flow will stop and the liquid still in the lower channel system remains in the tank and is charged against expulsion efficiency. A condition where only fluid remains in the lower compartment channel network or system represents expulsion efficiency in excess of 98%.

During the RTLS abort maneuver, the tanks are drained to a 65% propellant level. This is a high-g maneuver that exposes and breaks down the upper channels and the reentry collector channel. The collector channel screen must remain wet to prevent passage of gas into the lower compartment during the RTLS event.

During the high-g reentry maneuver, the liquid is settled over the reentry collector. The high-g acceleration causes the upper channels to break down if any liquid remains in them. That liquid will also settle over the reentry collector. The manifold bubble filter prevents gas from being pulled through into the lower compartment before the upper compartment is drained down to a 1% level, coinciding with the level of the reentry collector upper screen surface. At that point, the lower compartment begins to drain and the sump filter prevents gas ingested into the lower channel assembly, due to the simultaneous high-g and the flow,

from entering the sump and being delivered into the outflow line until a 1% level is reached in the lower compartment. The minimum residual quantity for the reentry maneuver is thus 2%, or an expulsion efficiency of 98%. Once the orbiter has returned to earth, any residual propellant remaining in the RCS tanks can be drained in either the vertical or horizontal tank attitudes. If a screen integrity checkout is required, the vent tubes can be used in the measurement of the bubble point of the screen surfaces.

## 2. Design Analysis

An in-depth analysis of the compartmented tank concept was performed to establish the full-scale detailed design. Results of a detailed design analysis were presented in a separate report (Ref VI-1); only the basic analytical approach will be summarized here.

### *a. Screen Selection*

Four Dutch-twill weave screen meshes were considered for the channels of the acquisition system: 325 x 2300, 250 x 1370, 200 x 1400, and 165 x 800. These are the finest stainless steel wire mesh sizes that are readily available. The retention capability, or bubble point, of these screens with both propellants is listed in Table VI-1. Bubble point values with and without a safety factor of 1.15 are shown. The 1.15 safety factor, used for all full-scale design activity, resulted from the new mission criteria adopted at the start of the Task V effort. (See revised criteria, Chapter II.) The bubble point values shown in Table VI-1 were calculated from minimum acceptance level bubble point values measured in methanol at 20°C (68°F). These minimum values also presented in Table VI-1, represent a minimum bubble point, that can still be obtained after degradation due to fabrication of screen components. Establishment of these minimum values was based on out extensive experience in fabricating screen acquisition systems. To calculate the propellant bubble points presented in Table VI-1, the standard conversion equation presented in Chapter IV (Equation IV-1) was used. The results of the supporting test phase of the program (Task III) clearly indicated the validity of using this technique to calculate bubble points for  $N_2O_4$  and MMH. (See Chapter IV.) The values of  $N_2O_4$  and MMH surface tension used for calculations were obtained from Figure IV-14 in Chapter IV. These surface tension values were selected, based on the results of Task III.

As can be seen from the bubble point values listed in Table VI-1, the 325 x 2300 screen has the greatest retention capability, so the pressure losses in the acquisition system can be larger with 325 x 2300 screen and usually the expulsion efficiency will be the greatest. However, one source of pressure loss is the flow through the screen. When the area of screen in contact with the propellant is small, this entrance loss becomes very significant.

Table VI-1 Screen Bubble Point

Screen Mesh (Bubble Point)	Propellant	Temperature °C (°F)	Bubble Point N/cm <sup>2</sup> (psi)	Bubble Point with 1.15 Safety Factor N/cm <sup>2</sup> (psi)	
325 x 2300  [61 cm water (24 in. water)] *	N <sub>2</sub> O <sub>4</sub>	4.4 ( 40)	0.79 (1.14)	0.67 (0.99)	
		20.0 ( 68)	0.70 (1.02)	0.62 (0.89)	
		51.7 (125)	0.56 (0.81)	0.48 (0.70)	
	MMH	4.4 ( 40)	0.95 (1.38)	0.83 (1.20)	
		20.0 ( 68)	0.90 (1.31)	0.79 (1.14)	
		51.7 (125)	0.81 (1.18)	0.71 (1.03)	
	250 x 1370  [51 cm water (20 in. water)] *	N <sub>2</sub> O <sub>4</sub>	4.4 ( 40)	0.65 (0.95)	0.58 (0.83)
			20.0 ( 68)	0.59 (0.85)	0.51 (0.74)
			51.7 (125)	0.47 (0.68)	0.41 (0.59)
MMH		4.4 ( 40)	0.79 (1.15)	0.69 (1.00)	
		20.0 ( 68)	0.75 (1.09)	0.66 (0.95)	
		51.7 (125)	0.68 (0.98)	0.59 (0.85)	
200 x 1400  [41 cm water (16 in. water)] *		N <sub>2</sub> O <sub>4</sub>	4.4 ( 40)	0.52 (0.76)	0.46 (0.66)
			20.0 ( 68)	0.47 (0.68)	0.41 (0.59)
			51.7 (125)	0.37 (0.54)	0.33 (0.47)
	MMH	4.4 ( 40)	0.63 (0.92)	0.55 (0.80)	
		20.0 ( 68)	0.60 (0.87)	0.53 (0.76)	
		51.7 (125)	0.54 (0.79)	0.48 (0.69)	
	165 x 800  [19 cm water (7.5 in. water)] *	N <sub>2</sub> O <sub>4</sub>	4.4 ( 40)	0.25 (0.36)	0.21 (0.31)
			20.0 ( 68)	0.22 (0.32)	0.19 (0.28)
			51.7 (125)	0.17 (0.25)	0.15 (0.22)
MMH		4.4 ( 40)	0.30 (0.43)	0.26 (0.37)	
		20.0 ( 68)	0.28 (0.41)	0.25 (0.36)	
		51.7 (125)	0.26 (0.37)	0.22 (0.32)	
*Minimum acceptance level bubble point measured in methanol at 20°C (68°F)					

The ratio of the entrance loss to the bubble point of the screen was determined for each of the screens as a function of the flow-rate per unit area (Fig. VI-4). Comparison of the screens shows that the 165 x 800 has the smallest entrance loss in comparison to its bubble point. The 325 x 2300 screen is the next best, followed by the others. If all other sources of pressure differentials in the flow channels (hydrostatic head and friction and velocity flow losses) were always insignificant, 165 x 800 would be the preferred screen mesh.

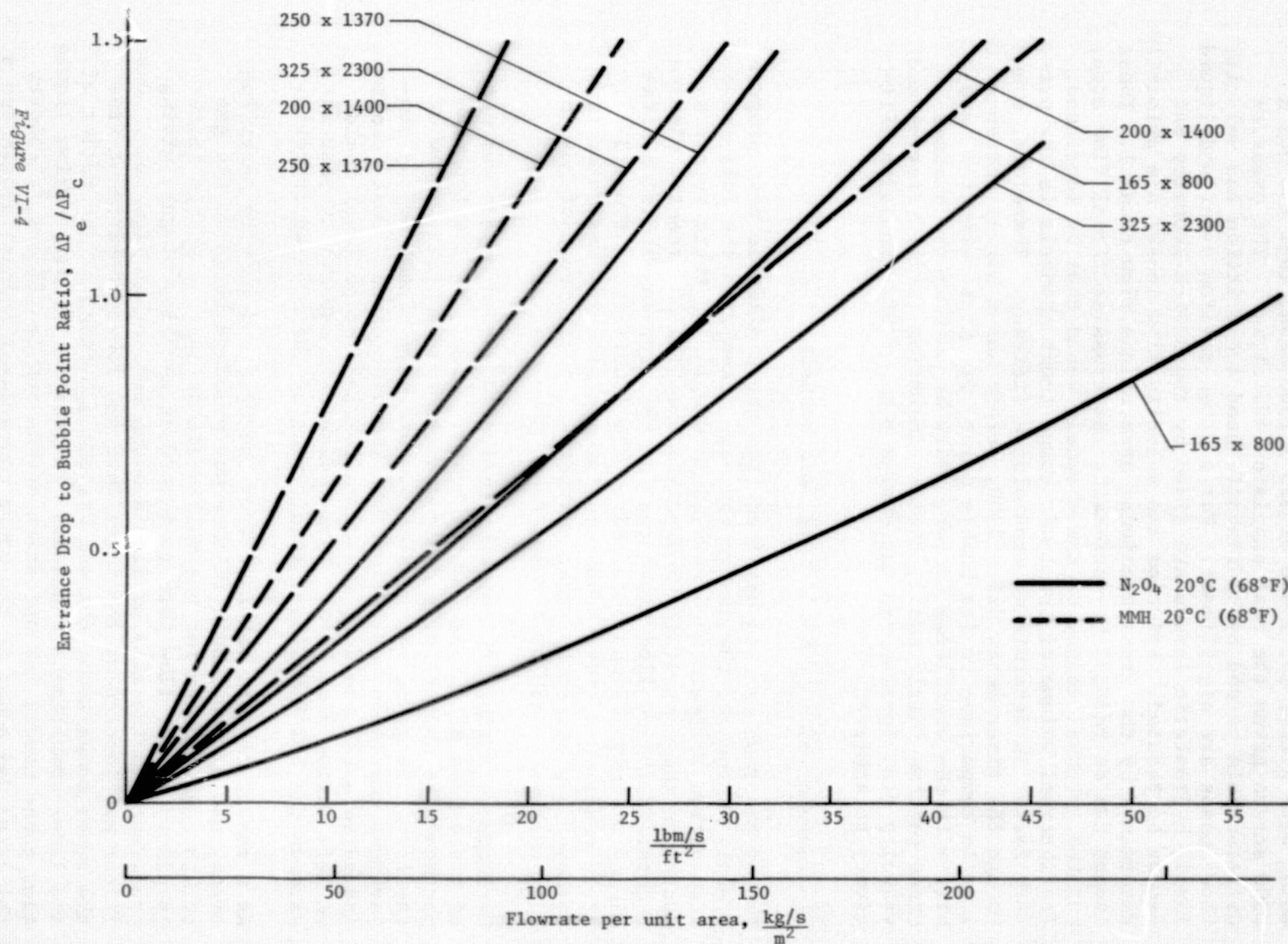


Figure VI-4  
Entrance Loss Ratio as a Function of Propellant Flowrate per Unit Area

It was found in the analysis of the surface tension device, operating with either 165 x 800 or 325 x 2300 mesh, that the 325 x 2300 screen gives the best expulsion efficiency. The pressure differentials caused by hydrostatic head and friction and velocity flow losses are significant. For a given mission event and liquid level, hydrostatic losses are fixed by the device geometry and cannot be reduced. Friction and velocity flow losses are primarily determined by the cross-sectional area of the flow channel. These losses can be reduced by increasing the cross-sectional flow area, but the internal volume of the channels would thus be increased. The internal volume of the lower compartment channels is the primary factor in determining expulsion efficiency. Therefore, even though the finer mesh, 325 x 2300, screen has a higher entrance loss in comparison to its bubble point, its high retention capability is the overriding factor. Only by keeping the channel cross section fairly small, thereby incurring larger friction and velocity flow losses, can the design goal of 98% expulsion efficiency be achieved.

#### *b. Incorporation of Similitude Test Results*

Two of the test results obtained from the similitude test program greatly influenced the design approach taken with the full-scale acquisition system. As discussed in Chapter V, tests were conducted on the centrifuge to simulate the RTLS and reentry mission events. Using scaled flowrates for reentry, an expulsion efficiency of only 90% was obtained.. The inability of the 1/3-scale model to achieve a 98% expulsion efficiency was determined to have been caused by screen dryout and pullthrough of gas in both the upper and lower compartment channels.

Performance during RTLS testing indicated screen dryout was not as pronounced as during reentry tests. Liquid in the top compartment was successfully drained until the manifold window of the 1/3-scale model was uncovered. Draining of the bottom compartment continued until final breakdown occurred. Test results indicated a 38% residual (based on loadable propellant) would be left during RTLS burn. This indicates a capability that far exceeds the 65% RTLS level requirement of the updated criteria.

As a result of data obtained from the RTLS and reentry centrifuge tests, use of two bubble filters was proposed to solve the gas pullthrough problem for the full-scale design. A bubble filter is placed in the flow path to interrupt the flow of gas, giving preference to the flow of liquid along some other flow path. One filter was located at the inlet into the lower compartment from the upper compartment channel system; the other at the outlet of the lower compartment channels. To provide the alternative liquid flow paths needed for operation of the bubble filters, a reentry collector was added to the upper compartment channel system and a reentry sump was added to the lower compartment channel system. The design analysis of the two filters, the sump, and the collector

will be discussed in detail in subsection 2d.) of this Chapter. In addition to the incorporation of the bubble filters and re-entry collector and sump, a redesign of the upper compartment barrier manifold, to give maximum screen area and thereby reduce entrance losses, was proposed to help prevent gas pullthrough during RTLS.

The second result from the similitude tests that influenced design of the full-scale device came from subscale fill and drain tests. Relatively large quantities of gas were trapped within the model during tank filling. Screen devices are designed to exclude gas from the expelled propellant; therefore, gas trapped in the device during the fill sequence can present problems. Because the Dutch-twill screens used in the RCS designs contain a great number of capillary paths, they will wick liquid in advance of the actual liquid level. Moreover, from an operational standpoint, the RCS tanks may be refilled without ever having undergone complete draining during which the screens could be dried. Thus, the tanks could be either reloaded with wet screens, or the screens could wick over during the fill process even if the system was initially dry. In either case, the potential for the entrapment of gas in the screen device exists. In some components of the screen system, such as the upper compartment channels, the entrapment of gas may be tolerated because of breakdown during boost. However, the entrapment of gas is either highly undesirable in the lower compartment channels, or totally unacceptable in the reentry sump. The subscale model had no provisions to vent any trapped gas. The device, however, was equipped with anti-wicking barriers across the screen, but these barriers did not adequately prevent the entrapment of gas. Therefore, vent ports were added to all the screen components of the full-scale device that could entrap gas.

#### *c. Propellant Property Considerations*

An assessment was made, as part of the design activity, to determine the propellant and temperature that would constitute the worst-case operating condition. Test cases (a low-mode and a high-mode mission event) were analyzed with the computer program by varying the propellant temperature for both  $N_2O_4$  and MMH with a fixed capillary system geometry. The results clearly showed that MMH at  $4.4^\circ C$  ( $40^\circ F$ ) was the worst case.

The reason that MMH yields the worst case for this application is indicated by the properties of the two propellants (Fig. IV-12, IV-13, and IV-14 of Chapter IV). Based on surface tension and density,  $N_2O_4$  appears to be the worst case. MMH has a higher surface tension than  $N_2O_4$ , so the retention capability of any given screen will be almost 30% higher with MMH than it is with  $N_2O_4$ . Moreover,  $N_2O_4$  has a density 65% greater than that of MMH, so for a given acceleration environment the hydrostatic pressures will be larger with  $N_2O_4$ .



Flow losses are a dominant factor in this acquisition system. Mass flow rates are large and the channel cross section has to be kept to a minimum to reduce the propellant residuals. Frictional losses caused by flow along the channels and the loss due to flow through the screen are both functions of viscosity. Therefore, even when temperature effects are considered, viscosity becomes the most important propellant property. The viscosity of MMH is over 100% greater than that of  $N_2O_4$ , based on the values at  $20^\circ C$  ( $68^\circ F$ ). The viscosity of MMH changes by a factor of three over the temperature range of interest, with its largest value at the minimum temperature of  $4.4^\circ C$  ( $40^\circ F$ ). At  $4.4^\circ C$  ( $40^\circ F$ ), the difference in viscosity between MMH and  $N_2O_4$  has increased over what it was at  $20^\circ C$  ( $68^\circ F$ ). MMH has a viscosity 140% greater than  $N_2O_4$  at that temperature.

One of the more significant flow losses, the entrance loss, is shown as a function of temperature for 325 x 2300 screen in Figure VI-5. With MMH, there is a significant variation in the entrance loss with temperature, showing the influence of viscosity.

#### *d. Design Analysis*

The full-scale SS/RCS acquisition system was designed by analyzing each of the critical design mission events (Chapter II) to assure that the acquisition device could satisfy the requirements of these events. Figure VI-6 shows the liquid orientations for each of the critical mission events analyzed. The magnitudes of flowrates and acceleration levels for these mission events are listed in Table II-4 in Chapter II. How these various critical mission events influenced the design of the full-scale system is summarized in Table VI-2. The design process can not concentrate on a single component at a time because the components of the acquisition device do interact with one another. More than one mission event can influence the design of a component, so compromises are involved.

1) Solid Barrier Location - As can be seen from Table VI-2, two mission events (RTLS and reentry) influenced where the solid barrier that compartments the tank was located. During the RTLS, the penetrations of the barrier that feed liquid from the upper compartment to the lower compartment must always remain submerged down to the 65% level. If this were not the case, gas contained in the channel system of the upper compartment, which breaks down under the high accelerations of the RTLS maneuver, would enter the lower compartment before the 65% level was reached. The lower channel system cannot remain stable during RTLS if too much gas enters the lower compartment.

Figure VI-5

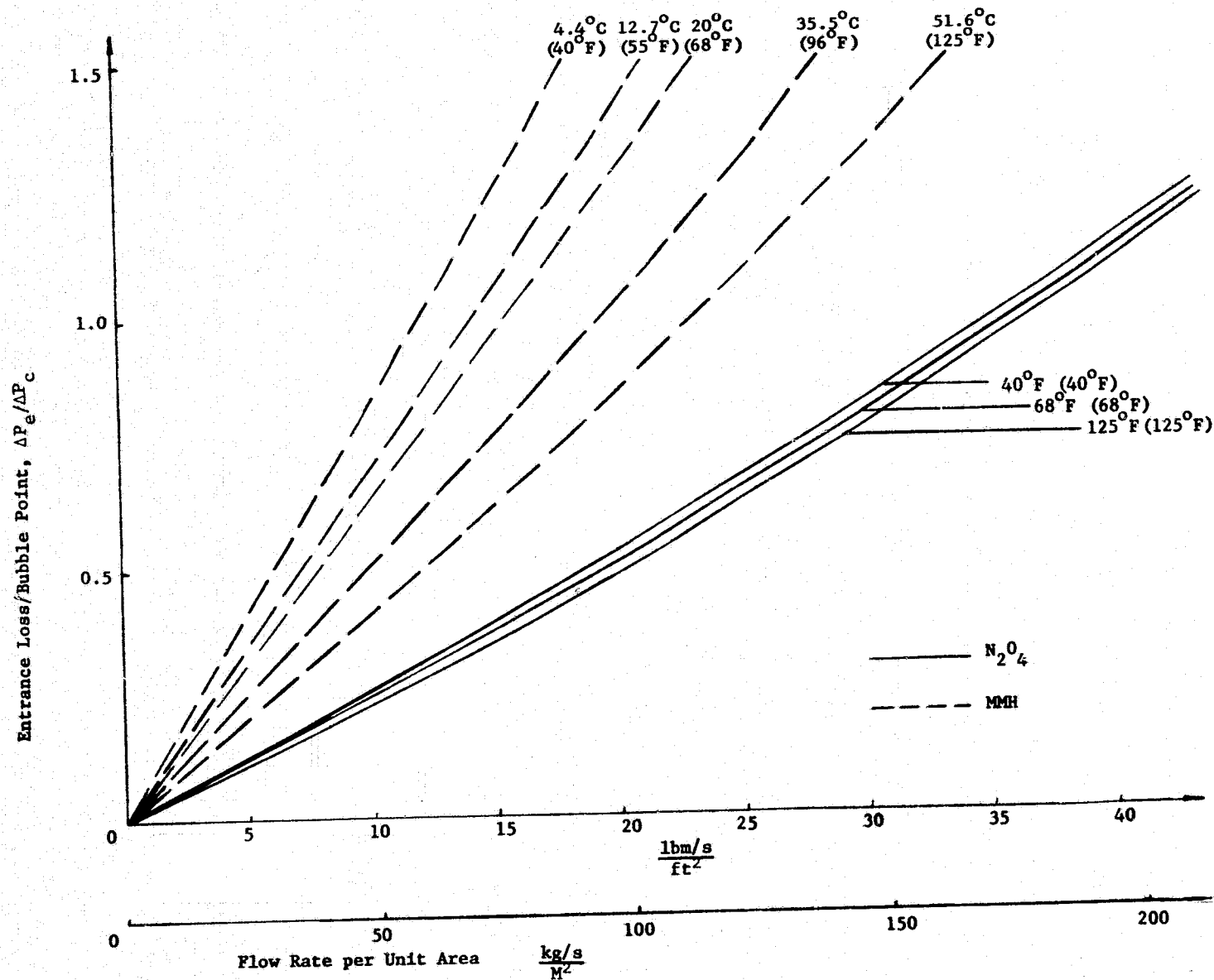


Figure VI-5 Effect of Temperature on Entrance Loss for 325 x 2300 Screen

Figure VI-6

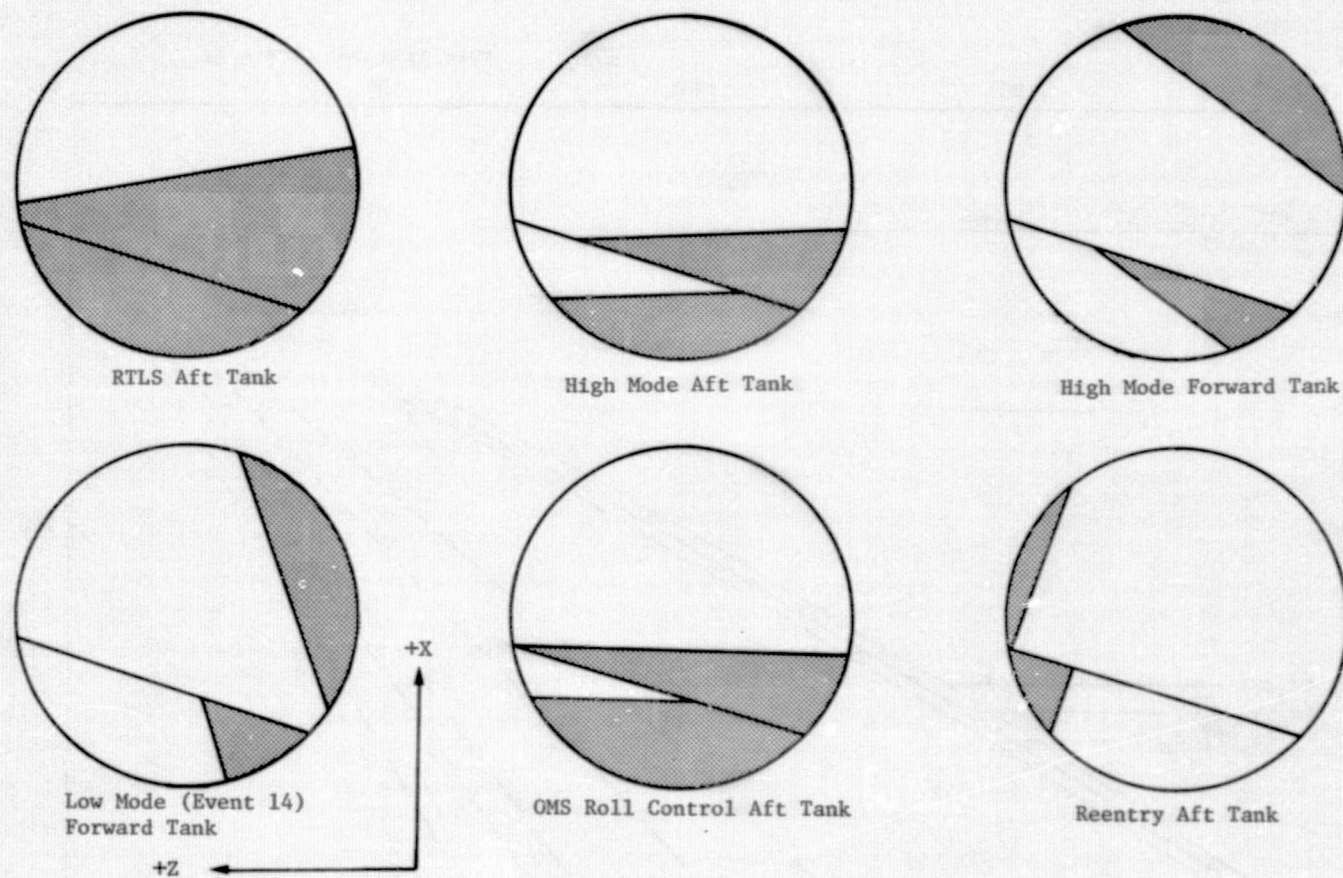


Figure VI-6 Critical Mission Event Liquid Orientation

Table VI-2  
Influences of Critical Mission Events on Full Scale Design

Critical Mission Event	Primary Influences	Secondary Influences
On-orbit Low-Mode (Event 14)	Channel Sizing Size of Lower Compartment Screen Mesh	Sizing of Reentry Sump and Bubble Filter
On-orbit High-Mode (including OMS Roll Control)	Location of Barrier Tank	Channel Sizing Lower Compartment Size Upper Compartment Ring Manifold Sizing Screen Mesh
RTLS Abort	Location of Barrier/Tank Attachment Point on +Z Axis Sizing of Upper Compartment Ring Manifold	Reentry Collector Design Manifold Bubble Filter Design
Reentry	Reentry Collector Design Manifold Bubble Filter Design Reentry Sump Design Sump Bubble Filter Design Location of Barrier Tank Attachment Point on +Z Axis	

During reentry, the liquid is positioned up to 119 degrees from its position during RTLS. A bubble filter prevents gas pull-through into the lower compartment during reentry. It is desirable to keep this filter in contact with the reentry puddle until it is as small as 2% of the loaded propellant. If this reentry filter stands out away from the puddle, an adverse hydrostatic head would have to be supported, thus reducing its capability of keeping gas out of the lower compartment. (The details of the design of this filter are presented later in this section.)

The factors influencing the barrier location are depicted in Figure VI-7. To maintain the barrier penetration and the upper compartment bubble filter below the minimum reentry puddle level and still maintain the barrier penetration submerged during RTLS, the bubble filter would have to fit into the shaded space shown. A filter of this size would adversely impact the design of the reentry collector for operation during RTLS, as will be discussed later.

The approach was to locate the +Z axis attachment point of the solid barrier as far into the 2% reentry puddle as possible, keeping the barrier below the 65% RTLS cutoff level. The barrier penetrations were submerged during RTLS, and the adverse hydrostatic head the upper compartment bubble filter supported during reentry was minimized. The resulting barrier location is shown in Figure VI-1.

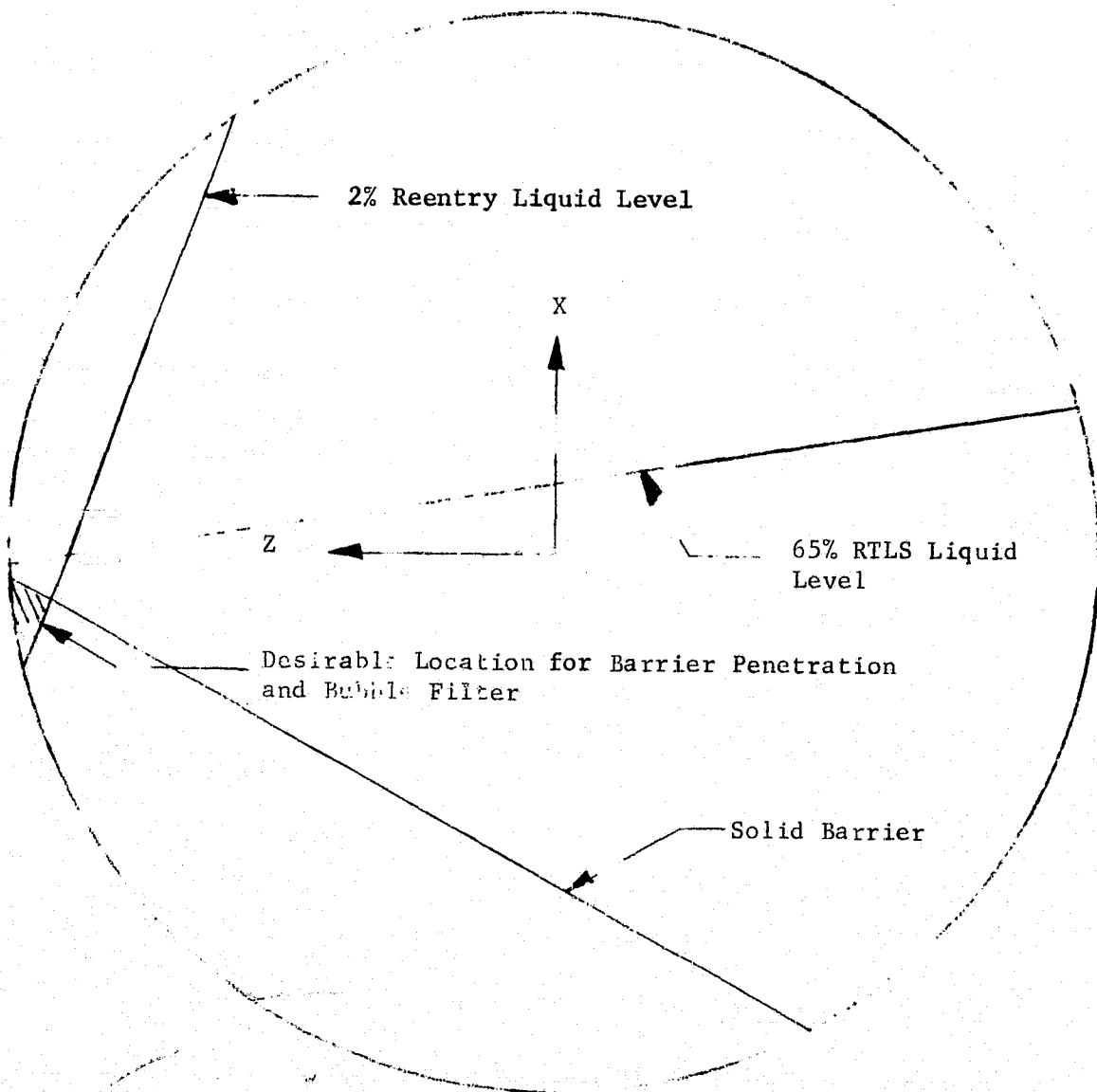


Figure VI-7 Reentry and RTLS Minimum Volume Puddle Locations

2) Sizing of Lower Compartment and Flow Channels - For the final design, the primary influence on sizing both the flow channels and the lower compartment came from the worst-case, low-mode, on-orbit mission event (event 14). During this low-mode maneuver, the forward RCS tanks must be capable of a 98% expulsion efficiency. Therefore, the size of the lower compartment channel system, including bubble filters, ring manifold, and reentry sump, must be less than 2% of the loadable propellant volume. It is assumed that the upper compartment will be empty before terminal expulsion of the forward tanks. As long as the size of the lower compartment is not too small, this assumption was shown to be credible under the Tasks II and IV analyses, presented in Chapters

III and V, respectively. Therefore, it is desirable to maximize the lower compartment volume and still obtain 98% expulsion efficiency during the terminal expulsion.

The desirability of having a large lower compartment and keeping the lower compartment channel system small enough to obtain a 98% expulsion efficiency, directly oppose one another. To design the optimum system, the computer program developed during Task II was used to analyze various lower compartment volumes and channel system geometries. To change the size of the lower compartment, the solid barrier was rotated about its +Z axis attachment point, which was fixed by the RTLS and reentry requirements. At each barrier angle, the geometry of the lower compartment channels and manifold were changed to yield a minimum of 98% expulsion efficiency. This process was continued until the largest possible lower compartment volume that still gave a 98% expulsion efficiency was obtained. This resulting lower compartment is 64.0 l (2.26 ft<sup>3</sup>) in volume (13.6% of the tank volume) located 25.9 cm (10.21 in.) below the tank centerline and at an angle of 28.9 deg to the tank -Z axis. The channels are 16.5 cm (6.5 in.) x 1.2 cm (0.48 in.) in cross section, with a ring manifold located just below the barrier, 6.4 cm (2.5 in.) x 1.2 cm (0.48 in.) in cross section.

To ensure that the low-mode events define the lower compartment configuration, the device was analyzed for the high-mode events using the computer model. Because high-mode events terminate before the 13% propellant level is reached, it was found that gas free expulsion of liquid could be maintained during those events. The amounts of residuals at breakdown in the lower compartment during the on-orbit mission events are presented in Table IV-3. The 13% and 2% requirements of the high-mode and OMS maneuvers, and the low-mode event 14 are easily met. The detail calculations are contained in Reference VI-1.

A concern during the OMS roll control and the de-orbit burn maneuvers was the 1.93 g rms vibration level under which the aft RCS tanks had to operate. The power spectral density that produces this 1.93 g rms level is shown in Figure VI-8.

Under another NASA contract (Ref VI-2) performed by Martin Marietta, test results showed that the rms value of a random acceleration can be sensed by the liquid at the screen. In those tests, the screen was attached to the supporting structure so that its surface was taut. The screen was supported by a perforated plate so the total structure was relatively stiff, having a natural frequency between 60 and 80 Hz.

CB

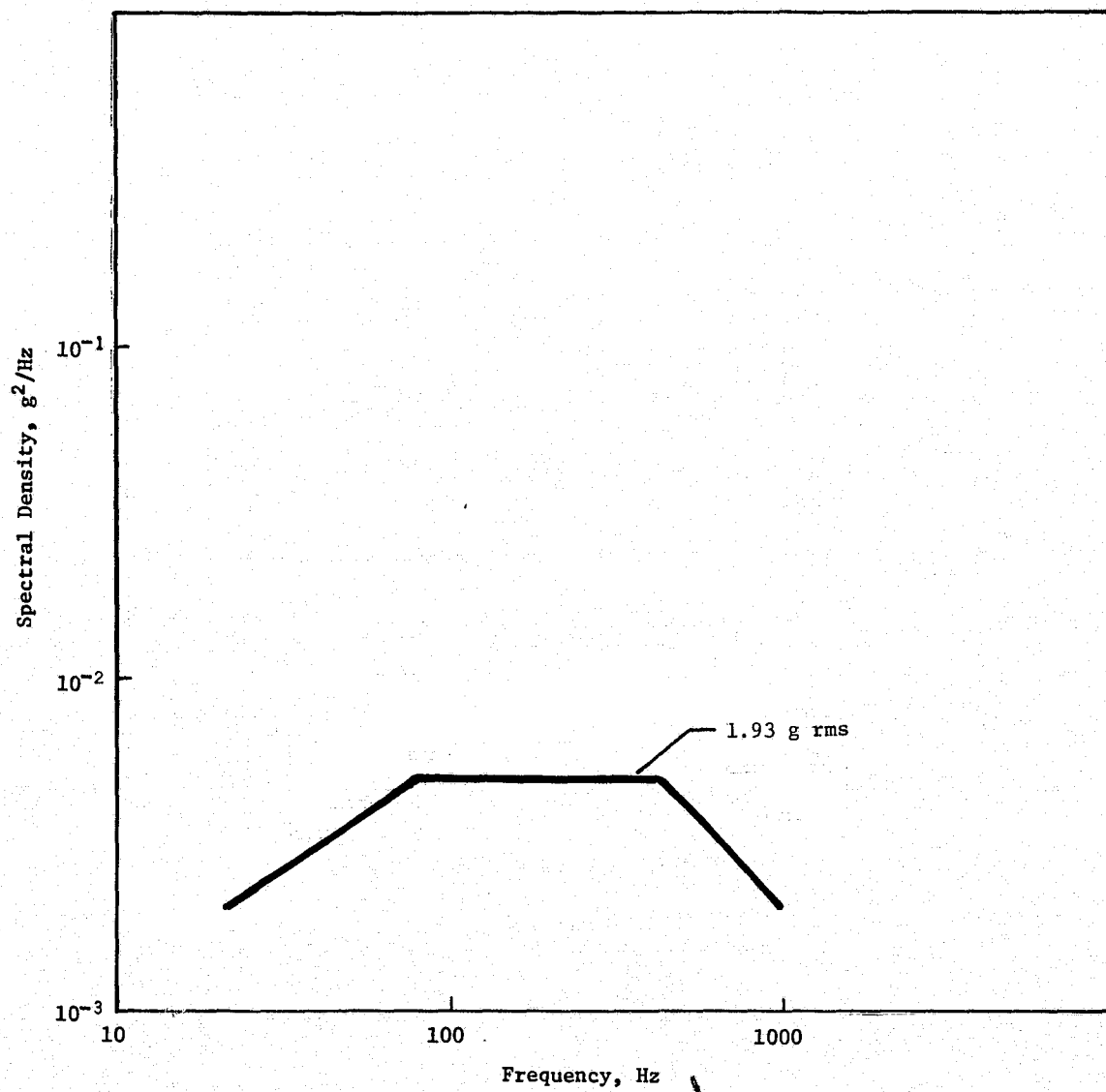


Figure VI-8 On-Orbit Vibration Level for RCS Aft Tanks

Table VI-3 Lower Compartment Residuals

Critical Mission Event	Propellant	Puddle Residual, % of Load	Total Residual, % of Load (includes lower components device volume)
Low-Mode Event	N <sub>2</sub> O <sub>4</sub>	~ 0	2.0
14 Forward Tank	MMH	0.1	2.0
High-Mode	N <sub>2</sub> O <sub>4</sub>	0.2	2.2
9 Thrusters			
Forward Tank	MMH	1.8	3.7
High-Mode	N <sub>2</sub> O <sub>4</sub>	1.8	3.8
8 Thrusters			
Aft Tank	MMH	1.8	3.7
OMS Roll Control	N <sub>2</sub> O <sub>4</sub>	~ 0	2.0
Aft Tank	MMH	~ 0	1.9
De-orbit Burn	N <sub>2</sub> O <sub>4</sub>	~ 0	2.0
Aft Tank	MMH	~ 0	1.9
<p>Lower Compartment:</p> <p>Volume = 15.6% N<sub>2</sub>O<sub>4</sub>  = 15.0% MMH</p> <p>Lower Device Volume = 2.0% N<sub>2</sub>O<sub>4</sub>  = 1.9% MMH</p> <p>Based upon propellant densities at 4.4°C (40°F)</p>			

The supporting perforated plate was not used for the full-scale RCS acquisition device and the screens were not taut but relatively loose. Therefore, the device had a much lower natural frequency; predicted below 20 Hz. With the loose screens, sufficient slack can exist so that when the structure vibrates the screens never become taut. This means that the screen does not move through or away from the liquid in the channels, no hydrostatic g-loads result, and liquid is retained without gas ingestion.

To assess the extent of screen motion, a RMS displacement value,  $X_{rms}$ , was determined by using a variation of Mile's equation:

$$[VI-1] \quad X_{rms} = \sqrt{\frac{\pi}{2} f Q DSD_f}$$



where

$f$  = frequency, Hz

$Q$  = amplification factor, dimensionless

$DSD_f$  = displacement spectral density at  $f$ ,  $cm^2/Hz$  ( $in.^2/Hz$ )

$X_{rms}$  = rms displacement, cm (in.)

The displacement spectral density is determined from the power spectral density (Fig. VI-8) using an expression relating acceleration to displacement.

Starting with the sinusoidal expression relating displacement to frequency and amplitude ( $A$ ) as a function of time,

$$[VI-2] \quad X = A \sin (2\pi f)t$$

If this above expression is differentiated twice, the following relationship results for acceleration ( $a$ ):

$$[VI-3] \quad a = -(2\pi f)^2 A \sin (2\pi f)t$$

Substituting Equation [VI-2] into [VI-3] yields

$$[VI-4] \quad X = \frac{a}{(2\pi f)^2}$$

The displacement spectral density is defined as the square of the displacement divided by frequency and the power spectral density (PSD) is the acceleration squared divided by frequency, so

$$[VI-5] \quad DSD_f = PSD_f \frac{(980)^2}{(2\pi f)^4} \text{ with } DSD_f \text{ in } cm^2/Hz \text{ and } PSD_f \text{ in } g^2/Hz$$

or

$$[VI-6] \quad DSD_f = PSD_f \frac{(386)^2}{(2\pi f)^4}$$

where

$DSD_f$  is in  $in.^2/Hz$  and  $PSD_f$  is in  $g^2/Hz$ .

Because the  $DSD_f$  varies inversely with  $f^4$ , the largest rms displacement will be obtained at the lowest frequency (worst-case assumption). Using the minimum frequency of 20 Hz and the corresponding  $PSD_f$  of  $0.002 g^2/Hz$ , from Figure VI-8, with a

conservative Q of 10, results in an  $X_{rms}$  of 0.49 mm (0.0194 in.). Considering a 3 $\sigma$  variation increases this to 1.47 mm (0.058 in.).

For the full-scale design, the amount of screen slack should be on the order of 2.5 mm (0.1 in.). Since the  $X_{rms}$  is at least half this value, the random on-orbit vibration should not affect the performance of the acquisition system. Therefore, the OMS roll control on-orbit vibration was not a primary concern in sizing the lower compartment.

A computer analysis of the upper compartment channels showed that the channels could be the same size as those in the lower compartment, simplifying fabrication because the same tooling can be used to make all the channels. The results of the upper channel analysis are summarized in Table IV-4. This analysis was based upon gas-free expulsion of the upper compartment. The residuals listed in the table can continue to be transferred to the lower compartment as two-phase flow.

Table VI-4 Upper Compartment Residuals

Critical Mission Event	Propellant	Puddle Residual, % of Load	Total Residual, % of Load
Low-Mode Event 14 Forward Tank	N <sub>2</sub> O <sub>4</sub>	~ 0	4.0
	MMH	~ 0	3.8
High-Mode 9 Thrusters Forward Tank	N <sub>2</sub> O <sub>4</sub>	3.7	7.7
	MMH	5.4	9.2
High-Mode 8 Thrusters Aft Tank	N <sub>2</sub> O <sub>4</sub>	4.6	8.6
	MMH	5.9	9.7
OMS Roll Control Aft Tank	N <sub>2</sub> O <sub>4</sub>	1.0	5.0
	MMH	2.2	6.0
Upper Device Volume = 4.0% N <sub>2</sub> O <sub>4</sub> = 3.8% MMH			
Based upon propellant densities at 4.4°C (40°F)			

Adding the residuals for the high-mode and OMS roll control maneuvers for the lower compartment (Table VI-3) and the upper compartment (Table VI-4) gives a total residual of approximately 13%. This indicates that the full-scale device is capable of satisfying the 13% cutoff requirement for these maneuvers even with continuous expulsion from a full tank.

3) Sizing of Upper Compartment Ring Manifold - Design of the upper compartment ring manifold is influenced primarily by the RTLS. Based on preliminary design work in Task IV, a manifold on the barrier, into which the upper compartment channels could feed, was deemed necessary. During RTLS this manifold is totally submerged. Therefore, it is the primary path for liquid transfer from the upper compartment to the lower compartment. The more screen area on this manifold, the lower the pressure drop in the liquid between the upper and lower compartment.

During RTLS, the reentry collector (The collector design will be covered in more detail later in this section.) breaks down because of extremely high-g levels. Since this collector is an extension of the bulk region of the lower compartment, it senses all of the pressure drops the liquid experiences traveling from the upper to the lower compartment. To prevent gas pullthrough from occurring in the collector, these pressure drops must be as low as possible. Therefore, the amount of screen area on the manifold was maximized to reduce the screen entrance loss during RTLS. This was accomplished by placing screen on the top and bottom of the manifold without making the size of the manifold excessive. The manifold is spaced off the barrier enough to allow an adequate flow passage for liquid to enter both the bottom and top of the manifold.

The large ring manifold helps to improve performance of the device during other mission events. OMS roll control and one of the high-mode mission events position liquid in the vicinity of the ring manifold.

4) Sizing of Reentry Collector, Sump, Manifold Bubble Filter, and Sump Bubble Filter - The design efforts for these four components were not independent activities. The functions of the components are interdependent. Therefore, a change in the size or position of one component had an effect on the size or position of one or more of the other components. The design activity was, therefore, analogous to solving a set of simultaneous equations.

The reentry maneuver is the primary influence on the design of the reentry collector, sump, and bubble filters. During reentry the channel network of the upper compartment is assumed to break down and dry out. Therefore, gas can be pulled through the channel network in preference to liquid entering the channels. When flowing through a screen, the gas does not sustain as high a

pressure drop as does the liquid. To prevent this gas from entering the lower compartment until the proper amount of liquid has been expelled from the upper compartment, the manifold bubble filter was added. The filter is located at the exit of the barrier penetraion connecting the bulk region of the lower compartment to the upper compartment ring manifold. Therefore, any gas that enters the channel network will be trapped in this filter.

Because the filter will prevent passage of gas, another flow path for liquid was required. If another flow path were not provided, the liquid coming from the upper compartment would also have to pass through the filter. The filter would simultaneously have to prevent gas from entering the lower compartment and at the same time allow the passage of liquid. Liquid crossing the filter would sustain a pressure loss, lowering the pressure on the downstream side of the filter. As more gas is held by the filter, the amount of available screen area for liquid flow would be reduced. Eventually the liquid flow screen area would be reduced to a point where the pressure loss sustained by the liquid crossing the filter would equal the filter bubble point. When this point was reached, the gas being held by the filter could be ingested into the lower compartment.

To provide the separate flow path to the lower compartment, a reentry collector was added to feed liquid directly into the lower compartment during reentry.

The design of the manifold bubble filter must also consider the other mission events. By far the worst conditions among these other mission events are imposed by RTLS. As was pointed out in the discussion of the upper compartment ring manifold design, the pressure loss experienced by the fluid being transferred from the upper compartment to the lower compartment must be low enough to prevent gas from being pulled through the reentry collector. Because the manifold bubble filter is in the flow path of the liquid during the RTLS event, minimizing the pressure loss across it was a design consideration.

For both the reentry collector and the manifold bubble filter to operate properly during reentry, screen entrance loss caused by the liquid entering the collector had to be less than the screen retention capability of the manifold bubble filter, less any hydrostatic pressure differential experienced by the filter because of its location above the liquid level in the upper compartment, i.e.,

$$\Delta P_{e_{\text{collector}}} < \left[ \Delta P_{c_{\text{filter}}} - \Delta P_h \right]$$

The hydrostatic term was discussed perviously as a factor in locating the compartment barrier. The above relationship was used to simultaneously size collector and the manifold bubble filter. The equation shows that a filter of minimum size and maximum retention capability would best satisfy this criterion. However, this criterion imposes design constraints that are in opposition to those imposed by the RTLS requirements discussed previously.

Finally, the position and size of the manifold bubble filter and the reentry collector are also related to the location and size of the sump in the lower compartment, and the design of all three components is constrained further by the 98% on-orbit and reentry expulsion efficiency.

As is the case for the upper channel network, the lower channel network also breaks down and dries out during reentry. Therefore, a filter is also required in the lower compartment to prevent gas pullthrough into the tank outlet. This filter is located at the exits of the lower compartment ring manifold and the +Z axis channel and, as was the case for the ring manifold bubble filter, a separate flow path for liquid is required when there is only gas on the upstream side of the bubble filter. This separate path is provided by the reentry sump.

For the sump and filter to operate properly during reentry, the following relationship must be satisfied until a 98% expulsion efficiency is achieved:

$$\Delta P_{e_{\text{sump}}} \leq \Delta P_{c_{\text{filter}}}$$

where:

$\Delta P_c$  = bubble point

$\Delta P_e$  = entrance loss

This expression states that the retention capability of the filter must always be greater than the entrance loss of the liquid entering the sump. Therefore, enough screen area must be provided on the sump to maintain this condition. However, the size of the sump is also constrained by the 98% expulsion efficiency requirement. During the reentry maneuver, the combined sump and reentry collector volumes are jointly constrained so that they remained submerged below the residual 2% puddle allowing a 98% expulsion efficiency. Therefore, the criterion for designing the sump was to maximize the screen area while satisfying the 98% expulsion efficiency requirement.

To accomplish this task required a decision on how the residuals during reentry should be divided between the upper and lower compartments. This was required so that the sump could be designed for maximum efficiency. For the sump to operate at maximum efficiency it must remain totally submerged in the residual puddle so that all the screen area is used and no hydrostatic head is imposed on the screen.

Analysis determined that a division of the residuals with 1% puddles in both the lower and upper compartments at breakdown during reentry was acceptable. Therefore, the sump was designed so that it remained submerged in a 1% puddle in the lower compartment during reentry and the collector was designed to remain submerged in a 1% puddle in the upper compartment. The sump was designed so that its volume, when added to the volume of the lower channel system was less than 2% and the 98% on-orbit expulsion efficiency requirement could be met.

Adequate sump screen area, with minimum sump volume, was obtained by using a compact sump in the form of a section of a frustum of a cone. With this configuration, a 1% residual will remain in the lower compartment when the reentry sump breaks down ( $\Delta P_e > \Delta P_c$ ).

For the design of the sump bubble filter, 165 x 800 mesh screen was selected. This mesh provides enough retention capability so that excessive screen area on the sump was not required. It is important that the pressure loss caused by flow of liquid through the sump bubble filter be held to a minimum. During the on-orbit events, the surface of the sump can be exposed to gas, so the entrance loss due to the filter influences the retention capability of the screen on the sump.

For the screen on the manifold bubble filter, 165 x 800 screen was selected. This screen allows a minimum flow pressure loss but still has sufficient retention capability to satisfy its other criteria. This filter was designed so that the hydrostatic head it experienced during reentry was minimized.

The reentry collector, reentry sump, and upper and lower channel networks were all designed with 325 x 2300 screen.

Throughout most of the RTLS abort the reentry collector is submerged, but for a short period of time before reaching the 65% cutoff level, it is exposed to gas. After sufficient height of the collector is exposed, it breaks down allowing gas to enter. Wicking of liquid acts to refill the pores of the screen that break down, so the screen continues to resist the flow of gas into the collector. This resistance should be sufficient to keep the other flow path, through the manifold and into the

lower compartment, a preferential path for liquid. Any gas that enters the collector should not be transferred to the lower compartment. However, as breakdown of the collector continues, complete dry out of a portion of the screen is possible. If dry out occurs the screen loses most of its resistance to gas flow and then gas will be transferred to the lower compartment in preference to liquid. The key factor as to whether dry out occurs is the period of time the screen is broken down during RTLS.

Based on results of the subscale test program, there did not seem to be a dry out problem for RTLS. Subsequent testing of the full-scale device, however, did indicate that premature gas ingestion into the lower compartment did occur for a constant 1-g simulated RTLS maneuver; but that liquid continued to flow into the lower compartment through the preferential flow path (through manifold into manifold bubble filter). A detailed discussion of this simulated RTLS test is presented later in this chapter under the full-scale test program.

### 3. Reliability Analysis

The reliability of many active systems and components has been analyzed, verified with functional tests, and reduced to a mean time between failure prediction. On the other hand, passive systems that have no moving parts do not always lend themselves to such an analytical or experimental approach. The RCS surface tension propellant acquisition device is such a passive system, consisting of screen material supported by a structure. Because the design of surface tension systems requires knowledge of the operating environment, the system's reliability primarily depends on how well the operating environment is understood.

The RCS full-scale capillary device has a primary single failure that occurs when operation of the device has been sufficiently degraded that gas enters the feedline. The possible failure modes that can lead to gas entering the engine are shown in Figure VI-9. The right-hand column of the figure lists possible basic causes of failure of the surface tension device. These causes are the result of unexpected or excessively severe environmental conditions. If the loads acting on the device exceed those expected, failure of the structure might occur. If the accelerations acting on the spacecraft exceed those expected, the capillary screens may not be able to retain the liquid. Thermal environment, corrosion, contamination, and fluid behavior are additional environmental factors that could cause failure of the device.

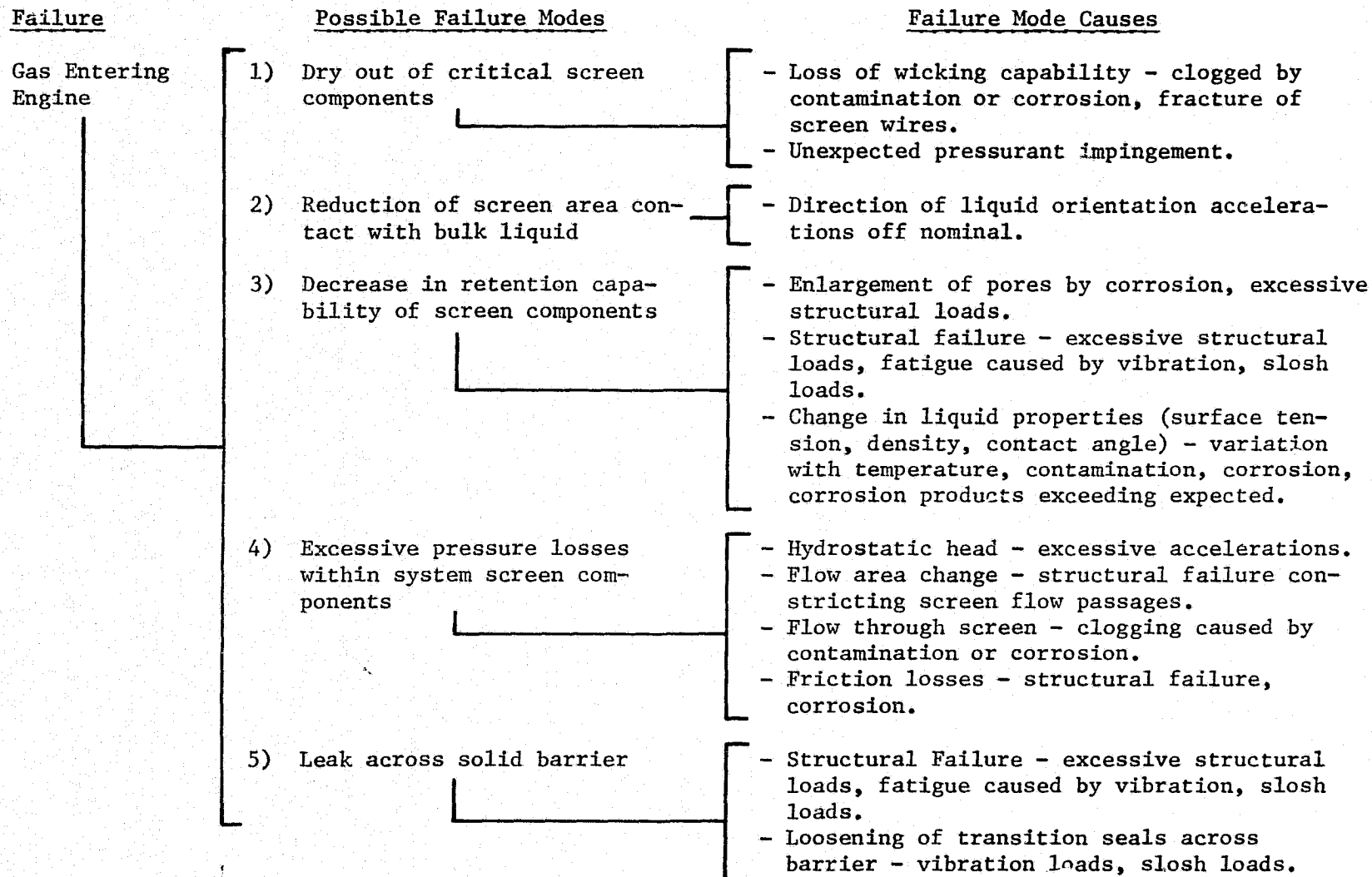


Figure VI-9 Failure Modes of Surface Tension Devices



For failure modes 2, 3, and 4, listed in Figure VI-9, the occurrence of these failures does not necessarily mean that gas will enter the engine. The magnitude of the failure mode is critical to whether or not a performance degradation of the capillary component being considered occurs. In designing the full-scale RCS system, a safety factor on screen bubble point was used, allowing a marginal regime in which the RCS device can operate off its design point without causing a performance degradation. Therefore, the amount of reduction of screen area (failure mode 2), the amount of decrease in screen retention capability (failure mode 3), and the magnitude of the excessive pressure losses (failure mode 4) must be great enough to overcome the design safety margin provided before performance degradation could occur.

As in the case for failure modes 2, 3, and 4, failure mode 5, a leak across the solid barrier, may not cause gas ingestion into the engine. The magnitude of the leak is critical to whether or not a performance degradation of the SS/RCS device can occur. If the leak occurs at a  $\Delta P$  above the bubble point of the screen components in the upper compartment, no degradation of performance will result. However, if this leak occurs below the upper compartment screen components retention capability, then a performance degradation is possible.

The block diagram of Figure VI-10 shows how the full-scale propellant acquisition device fits into the RCS propulsion system and how it functions. The diagram illustrates the primary function of the device to provide gas-free liquid to the spacecraft engine on demand during the various mission events. The full-scale RCS capillary device has six basic screen components or elements: two located within the upper compartment and four in the lower compartment, plus the solid barrier equipped with two penetrations. The two upper compartment elements consist of the flow channel network, including the large ring manifold, and the reentry collector. Liquid entering the collector goes directly into the bulk region of the lower compartment through one of the penetrations of the solid barrier. Liquid entering the channel network must pass through the manifold bubble filter before going into the bulk region of the lower compartment. The fluid entering the lower compartment does not have to be gas free for all of the mission events. The primary purpose of the upper channels and collector is to provide a path for liquid of some quality to the lower compartment during on-orbit operations. The lower compartment capillary system supplies gas-free liquid to the engine. However, if the overall liquid quality entering the bulk region of the lower compartment for a number of on-orbit mission events is too low, excessive usage of liquid from the lower compartment, in lieu of liquid from the upper compartment, will result. This could lead to premature depletion of the lower compartment causing gas ingestion into the engine.

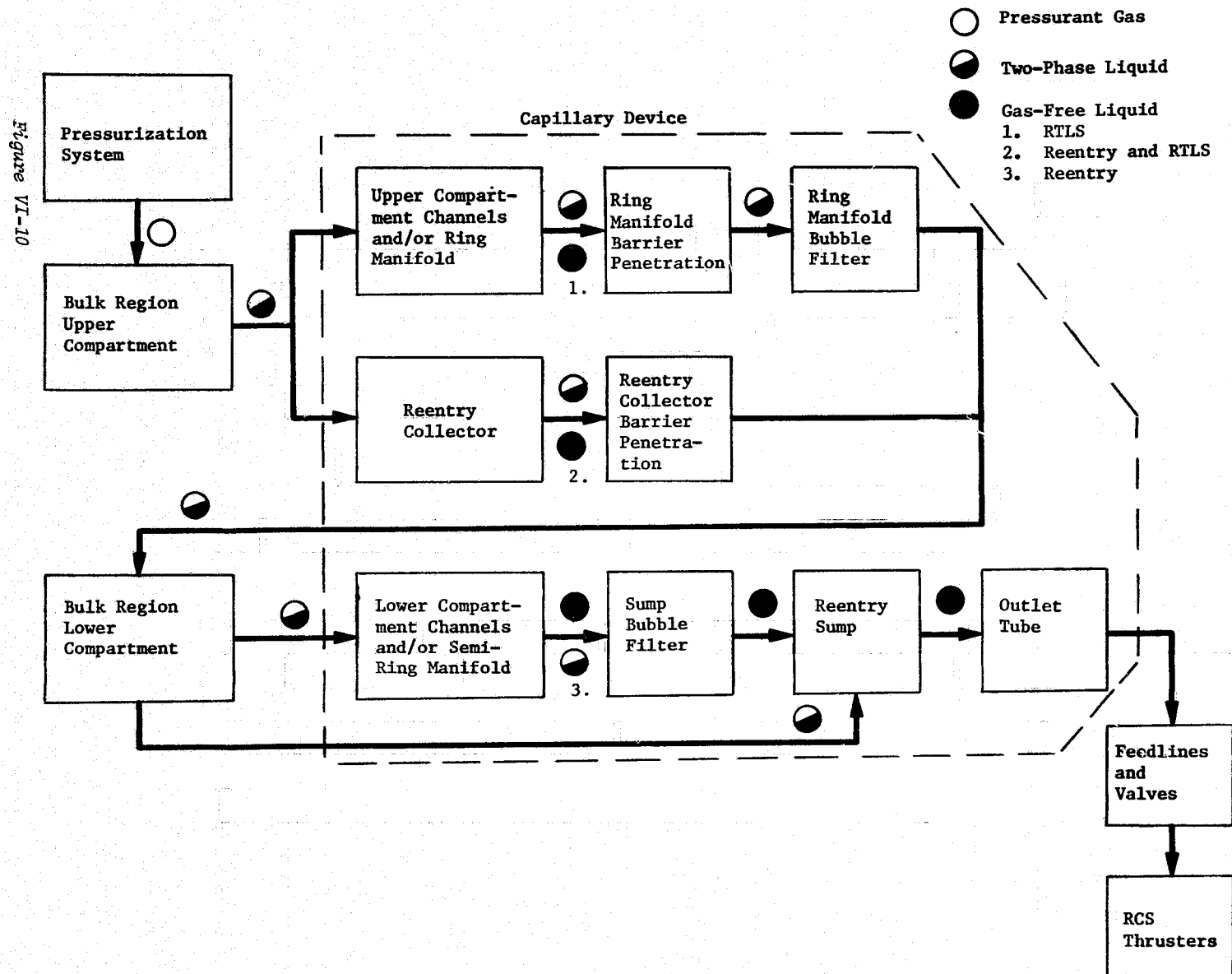


Figure VI-10 Acquisition System Block Diagram

The primary factor that affects the overall quality of the liquid entering the lower compartment is the order in which the various on-orbit mission events occur during any particular Space Shuttle mission (mission duty cycle). Therefore, a degradation in the performance capability of the upper compartment capillary system during one or many of the on-orbit mission events may or may not cause a failure (gas ingestion into engine). Whether a failure occurs depends upon how the overall quality of liquid entering the lower compartment is affected by this upper compartment capillary system degradation for any particular Space Shuttle mission.

Similarly, a leak across the solid barrier, assuming the leak occurs at a  $\Delta P$  below the retention capability of the upper compartment screen components, can change the overall quality of liquid entering the lower compartment. If a leak exists, either gas or liquid could be transferred to the lower compartment, depending on whether or not liquid is puddled over the barrier (a function of the mission events). If the mission duty cycle is such that gas enters the lower compartment more often than liquid (liquid quality reduced) excessive usage of the lower compartment liquid instead of the upper compartment liquid will result, and this could lead to gas ingestion into the engine.

For two of the mission events, RTLS and reentry, the liquid quality entering the lower compartment must be 100%. Very little gas can be tolerated in the lower compartment during RTLS. For reentry, 100% liquid quality must be maintained until only 1% of the load remains in the upper compartment. After this point, two-phase flow can occur.

The lower compartment elements of the RCS capillary system consist of a channel network, including the semi-ring manifold, the reentry sump, and the bubble filters that prevent gas pull-through during the reentry phase of the mission (premature gas ingestion into the lower compartment for the manifold bubble filter and premature gas ingestion into the sump for the sump bubble filter). During all other mission events, the two bubble filters are not essential to the operation of the device. However, since flow must go through the filters and therefore sustain a pressure drop, the filters have an impact on the operation of the capillary device during the mission events other than reentry. A failure that could cause an excessive pressure loss across these two filters could affect the performance of the entire capillary system during the other mission events such as event 14.

A failure modes effects analysis (FMEA) for the full-scale RCS capillary system is presented in Table VI-5. Each acquisition device element or component of the capillary system was analyzed. For each component, the effect of a possible failure mode on the operation of the RCS acquisition system was assessed. In addition, Table VI-5 lists possible consequences of these failure effects on the performance of the acquisition device. Because of the complex operational requirements of the SS/RCS capillary acquisition system, the FMEA was conducted for each critical mission event used in design of the system. These mission events are listed at the end of the table.

All of the possible failure modes listed in Figure VI-9 were analyzed. The effect of each of these failure modes on the operation of each of the screen components of the acquisition device was analyzed with exception of failure mode 5. Because this mode only applies to the barrier it was not evaluated for the other screen components. The solid barrier evaluation with respect to failure mode 5 is presented last in Table VI-5.

As can be seen by the FMEA presented in Table VI-5, the effect of each failure is highly dependent on mission event. For many of the components analyzed, degradation of the acquisition system performance for any particular failure mode would only occur for a certain mission event. For the other mission events considered, no effect on the performance would result. In addition, whether the possible consequences of the failure effects happen or not is dependent upon the mission duty cycle for a particular Space Shuttle mission. Therefore, the listed consequences may not occur even though the failure effect for a particular mission event has occurred.

Table VI-5 Failure Mode Effects of SS/RCS Capillary Propellant System Components

Component	Failure Mode (Fig. VI-9)	Critical Mission Event Which Could Be Affected*	Effect of Failure during Mission Event	Possible Consequences of Failure Effect during Mission Event
Upper Compartment Channel Network Including Ring Manifold	1	(A)	No effect	None
		(B)	Dry out highly improbable if channel network wet before initiation of mission event.	None
		(C)	Dry out highly improbable if channel network wet before initiation of mission event.	None
		(D)	No effect	None
		(E)	No effect - system designed for dry screens	None
	2	(A)	Premature breakdown of upper compartment - ingestion of gas into lower compartment if there is insufficient screen area in contact with liquid.	Excessive usage of lower compartment liquid in lieu of upper compartment liquid - could lead to premature depletion of lower compartment and gas ingestion into engine.
		(B)	Premature breakdown of upper compartment - ingestion of gas into lower compartment if there is insufficient screen area in contact with liquid.	Excessive usage of lower compartment liquid in lieu of upper compartment liquid - could lead to premature depletion of lower compartment and gas ingestion into engine.
		(C)	Premature breakdown of upper compartment - ingestion of gas into lower compartment if there is insufficient screen area in contact with liquid.	Excessive usage of lower compartment liquid in lieu of upper compartment liquid - could lead to premature depletion of lower compartment and gas ingestion into engine.
		(D)	Premature gas ingestion into lower compartment through ring manifold if liquid orientation uncovers barrier penetration prematurely.	Will lead to premature gas ingestion into engine.
		(E)	No effect	None
	3	(A)	If retention capability drops below margin given by safety factor-premature gas ingestion into lower compartment.	Same as for failure mode 2.
		(B)	If retention capability drops below margin given by safety factor-premature gas ingestion into lower compartment.	Same as for failure mode 2.
		(C)	If retention capability drops below margin given by safety factor-premature gas ingestion into lower compartment.	Same as for failure mode 2.

Table VI-5 (cont)

Component	Failure Mode (Fig. VI-9)	Critical Mission Event Which Could Be Affected*	Effect of Failure during Mission Event	Possible Consequences of Failure Effect during Mission Event
Reentry Collector	4	(D)	No effect	None
		(E)	No effect	None
		(A)	If losses become large enough to overcome margin given by safety factor--premature gas ingestion into lower compartment.	Same as for failure mode 2.
		(B)	If losses become large enough to overcome margin given by safety factor--premature gas ingestion into lower compartment.	Same as for failure mode 2.
		(C)	If losses become large enough to overcome margin given by safety factor--premature gas ingestion into lower compartment.	Same as for failure mode 2.
		(D)	Depending on magnitude of pressure losses, gas pull-through in entry collector could occur--would result in premature gas ingestion into lower compartment.	Same as for failure mode 2.
	1	(E)	No effect: if manifold losses become excessive all flow will go into collector.	None
		(A)	Dry out highly improbable if collector wet before mission event initiation.	None
		(B)	No effect	None
		(C)	No effect	None
		(D)	Premature gas ingestion into lower compartment through collector due to gas pull-through	Same as for failure mode 2 for upper compartment channels and ring manifold network.
		(E)	Impossible to dry out since collector totally submerged in liquid.	None
	2	(A)	No effect	None
		(B)	No effect - enough screen area on channels to pick up liquid.	None
		(C)	No effect - enough screen area on channels to pick up liquid.	None
		(D)	Higher probability of drying out collector if liquid oriented so that less of it is in contact with collector screen.	If dry out occurs: premature gas ingestion into engine will occur.
		(E)	If collector not completely covered, gas pull-through into lower compartment will prematurely occur.	Inability to achieve $\eta_e = 98\%$ .

Table VI-5 (cont)

Component	Failure Mode (Fig. VI-9)	Critical Mission Event Which Could Be Affected	Effect of Failure during Mission Event	Possible Consequences of Failure Effect during Mission Event
Ring Manifold Bubble Filter	3	(A)	Same effect as for upper compartment channel network for failure mode 3.	Same consequences as for upper compartment channel network.
		(B)	Same effect as for upper compartment channel network for failure mode 3.	Same consequences as for upper compartment channel network.
		(C)	Same effect as for upper compartment channel network for failure mode 3.	Same consequences as for upper compartment channel network.
		(D)	Increases probability of drying out collector.	Same as for failure mode 2.
		(E)	No effect - Collector covered.	None
	4	(A)	Minor effect - liquid not required to feed into the collector during event. Excessive hydrostatic heads may cause premature collector breakdown if safety margin exceeded.	Premature gas ingestion into lower compartment.
		(B)	Minor effect - liquid not required to feed into the collector during event. Excessive hydrostatic heads may cause premature collector breakdown if safety margin exceeded.	Premature gas ingestion into lower compartment.
		(C)	Minor, as above, since collector not fed during event 14. Excessive hydrostatic head a problem.	Premature gas ingestion into lower compartment if safety margin overcome.
		(D)	Same as for upper channel network for failure mode 4.	Same as for upper channel network for failure mode 4.
		(E)	Depending on magnitude of losses, gas breakthrough into lower compartment could occur (manifold bubble filter breaks down).	Inability to obtain $\eta_e = 98\%$ .
	1	(A)	No effect	None
		(B)	No effect	None
		(C)	No effect	None
		(D)	No effect	None
		(E)	Impossible to dry out since filter will be completely full of liquid until upper compartment is drained (Filter no longer required after that point).	None
	2	(A)	No effect	None
		(B)	No effect	None
		(C)	No effect	None
		(D)	No effect	None

Table VI-5 (cont)

Component	Failure Mode (Fig. VI-9)	Critical Mission Event Which Could Be Affected*	Effect of Failure during Mission Event	Possible Consequences of Failure Effect during Mission Event
Lower Compartment Channel Network and Semi-Ring Manifold	3	(E)	Possibility of 165 x 800 drying out if liquid not in contact with bubble filter.	If dry out occurs while > 1% of load in upper compartment (assuming gas on both sides of screen); inability to reach 98% $\eta_e$ .
		(A)	No effect	None
		(B)	No effect	None
		(C)	No effect	None
		(D)	No effect	None
	4	(E)	Premature gas breakthrough into lower compartment if safety margin overcome.	Inability to reach 98% $\eta_e$ .
		(A)	For flow losses across bubble filter screen - same comments as for upper channel network failure mode 4.	Same as for upper channel network failure mode 4.
		(B)	For flow losses across bubble filter screen - same comments as for upper channel network failure mode 4.	Same as for upper channel network failure mode 4.
		(C)	For flow losses across bubble filter screen - same comments as for upper channel network failure mode 4.	Same as for upper channel network failure mode 4.
		(D)	For flow losses across bubble filter screen - same comments as for upper channel network failure mode 4.	Same as for upper channel network failure mode 4.
	1	(E)	No flow through filter but excessive hydrostatic head could cause filter to break down if design safety margin exceeded.	Same as for failure mode 3 above.
		(A)	Dry out impossible - all of network filled by liquid.	None
		(B)	Dry out impossible - channel network full before initiation of mission event.	None
		(C)	Dry out impossible - channel network full before initiation of mission event.	None
		(D)	Same as (A) above.	None
		(E)	No effect - system designed to dry out.	None



Table VI-5 (cont)

Component	Failure Mode (Fig. VI-9)	Critical Mission Event Which Could Be Affected*	Effect of Failure during Mission Event	Possible Consequences of Failure Effect during Mission Event
	2	(A)	No effect as long as sump remains covered.	None
		(B)	Premature breakdown of channel network if a large amount of screen loses contact with the bulk liquid.	Premature gas ingestion into engine.
		(C)	Premature breakdown of channel network if a large amount of screen loses contact with the bulk liquid.	Premature gas ingestion into engine.
		(D)	No effect - lower compartment should be full.	Premature gas ingestion into engine.
		(E)	No effect	Premature gas ingestion into engine.
	3	(A)	If retention capability degraded below safety margin; premature breakdown of channel network.	Premature gas ingestion into engine.
		(B)	If retention capability degraded below safety margin; premature breakdown of channel network.	Premature gas ingestion into engine.
		(C)	If retention capability degraded below safety margin; premature breakdown of channel network.	Premature gas ingestion into engine.
		(D)	No effect - lower compartment full.	None
		(E)	No effect	None
	4	(A)	If losses become large enough to overcome safety margin - premature breakdown of channel network or sump will result.	Premature gas ingestion into engine.
		(B)	If losses become large enough to overcome safety margin - premature breakdown of channel network or sump will result.	Premature gas ingestion into engine.
		(C)	If losses become large enough to overcome safety margin - premature breakdown of channel network or sump will result.	Premature gas ingestion into engine.
		(D)	No effect	None
		(E)	No effect - if channel losses become excessive all flow will go directly into sump.	None

Figure VI-5 (cont)

Component	Failure Mode (Fig. VI-9)	Critical Mission Event Which Could Be Affected*	Effect of Failure during Mission Event	Possible Consequences of Failure Effect during Mission Event
Sump	1	(A)	Dry out impossible since sump is full of liquid at all times.	None
		(B)	Dry out impossible since sump is full of liquid at all times.	None
		(C)	Dry out impossible since sump is full of liquid at all times.	None
		(D)	Dry out impossible since sump is full of liquid at all times.	None
		(E)	Dry out impossible since sump is full of liquid at all times.	None
	2	(A)	No effect - sump screen not required for OMS roll control.	None
		(B)	Depending on which high mode mission event is being considered, premature breakdown could occur if sump is not submerged and flow losses through lower compartment channel network become excessive.	Premature gas ingestion into engine.
		(C)	No effect - sump screen area not required for event 14.	None
		(D)	No effect - lower compartment full.	None
		(E)	If too much of the sump becomes uncovered, premature breakdown will occur when design safety margin exceeded.	Inability to obtain 98% $\eta_e$ .
	3	(A)	If design safety margin is not enough to handle retention degradation - premature breakdown of sump will occur.	Premature gas ingestion into engine.
		(B)	If design safety margin is not enough to handle retention degradation - premature breakdown of sump will occur.	Premature gas ingestion into engine.
		(C)	If design safety margin is not enough to handle retention degradation - premature breakdown of sump will occur.	Premature gas ingestion into engine.
		(D)	No effect - sump submerged.	None
		(E)	No effect - sump submerged.	None

Table VI-5 (cont)

Component	Failure Mode (Fig. VI-9)	Critical Mission Event Which Could Be Affected*	Effect of Failure During Mission Event	Possible Consequences of Failure Effect during Mission Event
Sump Bubble Filter	4	(A)	Depending on magnitude of losses could cause premature breakdown of sump.	Premature gas ingestion into engine.
		(B)	Depending on magnitude of losses could cause premature breakdown of sump.	Premature gas ingestion into engine.
		(C)	Depending on magnitude of losses could cause premature breakdown of sump.	Premature gas ingestion into engine.
		(D)	No effect - lower compartment full.	None
		(E)	If losses become too high, could cause gas pull-through (sump bubble filter breaks down).	Same as (A) above. Inability to obtain 98% $\eta_e$ .
	1	(A)	Dry out impossible since filter always submerged.	None
		(B)	Dry out impossible since filter always submerged.	None
		(C)	Dry out impossible since filter always submerged.	None
		(D)	Dry out impossible since filter always submerged.	None
		(E)	Dry out impossible since filter always submerged.	None
	2	(A)	No effect - filter always covered by liquid.	None
		(B)	No effect - filter always covered by liquid.	None
		(C)	No effect - filter always covered by liquid.	None
		(D)	No effect - filter always covered by liquid.	None
		(E)	No effect - filter always covered by liquid.	None
	3	(A)	No effect - pressure retention of screen not required.	None
		(B)	No effect - pressure retention of screen not required.	None
		(C)	No effect - pressure retention of screen not required.	None
		(D)	No effect - pressure retention of screen not required.	None
		(E)	Premature gas breakthrough into sump if retention degradation overcomes design safety margin.	Inability to obtain 98% $\eta_e$ .

Table VI-5 (concl)

Component	Failure Mode (Fig. VI-9)	Critical Mission Event Which Could Be Affected*	Effect of Failure during Mission Event	Possible Consequences of Failure Effect during Mission Event
Solid Barrier**	4	(A)	Same effect as for sump failure mode 4.	Same consequences for all sump failure mode 4.
		(B)	Same effect as for sump failure mode 4.	Same consequences for all sump failure mode 4.
		(C)	Same effect as for sump failure mode 4.	Same consequences for all sump failure mode 4.
		(D)	Same effect as for sump failure mode 4.	Same consequences for all sump failure mode 4.
		(E)	Same effect as for sump failure mode 4.	Same consequences for all sump failure mode 4.
	5	(A)	Direct transfer of liquid from upper to lower compartment.	None
		(B)	Direct ingestion of gas into lower compartment for forward tank high mode only. For aft tank high mode same effect and consequence as (A) above.	Excessive usage of lower compartment liquid in lieu of upper compartment liquid - could lead to premature depletion of lower compartment and gas ingestion into engine.
		(C)	Direct ingestion of gas into lower compartment.	Excessive usage of lower compartment liquid in lieu of upper compartment liquid - could lead to premature depletion of lower compartment and gas ingestion into engine.
		(D)	Same as (A) above.	None
		(E)	Premature gas ingestion into lower compartment through leak depending on location of leak (leak covered by liquid or not).	Inability to obtain 98% $\eta_e$ .

- \*(A) OMS Roll Control  
 (B) High-Mode, On-Orbit Operations (worst case FWD TNK and AFT TNK cases)  
 (C) On-Orbit Low Mode (Event 14)  
 (D) RTLS  
 (E) Reentry

\*\*For this evaluation it is assumed that the leak across the barrier occurs at a  $\Delta P <$  bubble point of the upper compartment channel network and reentry collector.

## B. SYSTEM FABRICATION

Based on the design analysis a detailed design of a full-size acquisition system was accomplished. The design approach and details of the fabrication methods are described here. Figure VI-1 shows the most significant fabrication details of the device, and a complete set of drawings are part of Reference VI-1.

### 1. Design Approach

The general approach with regard to fabrication of the full-scale SS/RCS acquisition system, was to design a prototype flight-weight device capable of insertion into either a heavy-weight ground test tank or a flight-weight tank. In this way, fabrication approaches for the flight-weight device could be verified as the device was fabricated for ground testing.

The primary attachment of the acquisition device to the tank is between the barrier and the tank wall. Welding was selected as the means of making this joint, as opposed to mechanical attachment, brazing, or soldering. Previous technology studies (Ref VI-4) have shown that the all-welded approach is the most desirable. However, because the flightweight tank is titanium (6Al-4V) and the screen is stainless steel (304L), a transition joint is required. The 325 x 2300 screen mesh is available only in stainless steel, so the structure of the device is also stainless steel permitting reliable attachment of the screen to the plate. The transition from stainless to titanium could either have been made where the barrier is attached to the tank wall or by fabricating the barrier of titanium, welding it to the tank and making the mechanical transition at the two penetration points in the barrier. From the standpoint of providing a reliable seal across the barrier, the latter approach was considered the proper choice. The larger the diameter of a bolt ring type of seal, the greater the amount of force required (greater number and larger size of bolts) to provide a good seal. By requiring only two small [5.1-mm (2-in.) diameter] bolt ring seals at the collector transfer tube penetration and the ring manifold/manifold filter penetration, a more reliable system would result. In addition, the tank bosses required on the tank wall to bolt the entire solid barrier to the tank and the necessary bolts, would cause a significant increase in the tank weight.

To make the full-scale acquisition system as light as possible, 0.69-mm (0.027-in.) sheet metal was used for all of the solid structure of the device. Construction of the various components of the acquisition device--channels, ring manifolds, sump, filters, and collector--consisted of cutting, forming, and welding this sheet metal into a frame support structure. The screen was then attached to these various support structures to form the completed components of the device. The components were

A consideration in the spacing of the channel cross members was the maximum allowable unsupported screen area that could be permitted without incurring structural damage to the screen because of excessive screen deflection. Fine mesh screen, when subjected to a differential pressure, deflects like a thin membrane and builds up stresses within its wires. If the unsupported area is too large, plastic deformation can result in the screen wires. In addition, the screen deflection can become severe enough to reduce the flow area in the channels (pressure differential from outside to inside of channel). Under a previous technology study, the structural characteristics of fine mesh screen were extensively investigated and a mathematical structural model for screen was developed (Refs VI-5 and VI-6). The use of the 7.6 x 7.6 mm (3 x 3 in.) unsupported screen areas for the full-scale device channels was determined using this screen mathematical model. (See Reference VI-1 for detail calculations.) This unsupported area represents the largest area that could have been used, giving the least amount of support structure, and therefore lowest weight, without either reaching the elastic limit of the screen wire or obtaining too much flow constriction because of screen deflection.

*b. Barrier and Upper Compartment Ring Manifold*

The large upper compartment ring manifold was fabricated in the same manner as the channels. The frame structure for the manifold is shown in Figure VI-12. The component in the bottom of the picture is the manifold bubble filter. As can be seen, additional sheet metal was provided in the areas where the three upper compartment channels weld into the manifold. This was done to structurally strengthen these junction points and provide material for the welding operation. The radial support members of the manifold are perforated in order to provide a flow path to the manifold bubble filter. The completed ring manifold with screen attached is shown in Figure VI-13.

The solid barrier that compartments the RCS tank must be capable of withstanding numerous structural loads. These loads arise from hydrostatic forces, propellant slosh, and propellant settling. To withstand these loads and yet be as lightweight as possible, the barrier was designed as shown in Figure VI-1. It derives its structural strength from the way it is attached to the tank. Around the outer perimeter, the barrier is welded to the tank wall. Near its center it is attached to the ring manifold at four tab locations. Since the ring manifold is extremely rigid, due to its frame support structure, enough rigidity is transferred to the barrier to increase its strength. The manifold/channel network system attaches to the tank wall by means of tabs located near the tank parting plane. (See Figure VI-1.)

*c. Sump, Sump Bubble Filter, Manifold Bubble Filter, and Reentry Collector*

For fabrication of these four screen components, the same frame support approach used on the channels was again used. A rear view of the semi-completed reentry sump is shown in Figure VI-14; the front of the sump is shown in Figure VI-15. In both views, the sump front face (not yet attached) is shown beside the sump. The rectangular cutout for the +Z axis channel, which connects into the sump bubble filter, can be seen in this front face. The sump bubble filter is located just behind the front face of the sump. The cut out area at the top and back of the sump was provided to allow proper clearance for the connection of the manifold bubble filter to the barrier penetration, and enough flow space for incoming liquid from the reentry collector. The hole provided in the bottom of the sump connects into the outlet tube of the tank.

The completed manifold bubble filter, which is located just behind the reentry sump, is shown in the three views in Figure VI-16. The solid ring located on its front face mates with the barrier penetration connecting this filter with the upper compartment ring manifold. The details of this penetration seal will be discussed later in this section. This ring fixture fits into the cutout area of the sump discussed previously. The cutout area in the top of the filter provides flow space for the incoming liquid from the reentry collector so that it is distributed properly when entering the bulk region of the lower compartment.

The collector consists of two screen channel disks manifolded together. This disk approach was used to obtain enough screen area for the collector. The disks then connect into a solid transfer tube which penetrates, but does not connect into, the upper compartment ring manifold (the right penetration in manifold of Figure VI-13) and mates with the penetration in the solid barrier. The frame support structure of the two collector disks and a section of the solid transfer tube, are shown in Figure VI-17. The radial support members are perforated to provide a flow path inside the disks. The semi-completed reentry collector back and front face is shown in Figure VI-18. The connecting aperture to the solid transfer tube can be seen.

*d. Barrier Penetration Seals*

The attachment between (1) the reentry collector and the bulk region of the lower compartment through the solid barrier, and (2) the upper compartment ring manifold and the manifold bubble filter through the barrier, was accomplished with mechanical seals.

Between the manifold filter and the large ring manifold, the mechanical joint used consisted of two bolt flanges that seal against a metal crush ring. This ring is part of the barrier and consists of an upper and lower half. One bolt flange is welded to the outlet of the ring manifold (left hole in Figure VI-13); the other flange is part of the filter. The upper half of the crush ring fits into a recess in the flange on the manifold, while the lower half fits into the mating flange on the filter (Fig. VI-16). The tightening bolts fit through the top of the manifold flange and are internally located in the lower flange on the filter. Once the bolts are tightened crushing the ring, the only path for liquid in the manifold is through the barrier penetration and manifold filter.

The mechanical seal for attachment of the reentry collector to the barrier is basically the same. The upper sealing flange is welded to the collector transfer tube. The lower flange is not welded to the barrier or any other component and is secured by the tightening bolts.

These mechanical seals were proposed for the flightweight design and used on the all-stainless ground test system. Teflon seal rings were used in place of the metal crush rings, however, because of cost.

#### *e. Tank Design*

Two types of tank shells were designed for the full-scale acquisition device: a flightweight shell and a heavyweight ground test tank shell. Only the ground test tank was fabricated for the full-scale tankage test program. The completed heavyweight tank is shown in Figure VI-19. The weld lips for the solid barrier and the outlet tube can be seen in the bottom half of the tank. The tank shell was fabricated from 0.95 cm (3/8 in.) thick 304L stainless steel stock. Since the tank was stainless steel, the barrier was also made of stainless steel for the prototype, while in an actual flight system the barrier would be titanium. The tank weighs 293 kg (646 lbm) minus the bolts.

The design of the flightweight shell is presented in Figure VI-2. The tank halves would be welded together, unlike the ground test tank that must have the capability of being reopened.

#### *f. Device Installation and Assembly Details*

Each of the various screen components was welded together to form the major subassemblies, which could then be installed into the tank. The assembly steps for the lower compartment channel sub-assembly are depicted in Figures VI-20 through VI-22. Figure VI-20 shows the four lower compartment channel, semi-ring manifold, and sump bubble filter welded together. The square shaped channel



manifold has, as yet, not been welded in place. The completed lower compartment channel subassembly (except for the attachment of the outflow line) is shown in Figures VI-21 and VI-22. Figure VI-21 presents a bottom view while Figure VI-22 presents a top view. As can be seen, the reentry sump is welded in place so as to have the sump bubble filter positioned just behind its front face.

The completed upper compartment channel network subassembly is shown in Figure VI-23. The three long upper compartment channels have been welded in place into the large ring manifold. The space between the short or stub channel is for the reentry collector.

To install the completed subassemblies into the propellant tank, the following procedure was used.

- 1) Insert lower compartment channel subassembly into lower half of tank, mating the outlet tube with tank outlet.
- 2) Attach lower channel assembly to tank wall using attachment tabs.
- 3) Position manifold bubble filter into the tank behind reentry sump.
- 4) Place lower reentry collector joint flange on top of reentry sump.
- 5) Position solid barrier on tank weld lip, aligning the barrier penetrations properly, and complete closure weld on barrier.
- 6) Position upper compartment channel network on top of barrier and align penetrations properly.
- 7) Complete mechanical seal of the ring manifold and its bubble filter.
- 8) Weld into position the manifold cover plate. (This cover-plate is required in order to seal the top opening of the manifold. This top opening provides a means of access into the manifold to reach the bolts of the manifold seal. (See Figure VI-13.)
- 9) Position and align the reentry collector and seal the collector transfer tube to the solid barrier, using the lower joint flange positioned below the barrier previously.
- 10) Attach the collector and the upper compartment channel network subassembly to the tank by use of attachment tabs.

number of these tubes was put into the system to assess the proper number of tubes or bleed lines a flight system would require. The vent tubes installed in the lower channel system can be seen in Figures VI-21 and VI-22. These same tubes can also be seen in Figure VI-24 coming out of the tank along with the upper compartment vent tubes.

During the entire assembly and installation of the full scale system, precautions were taken to maintain cleanliness. Before welding of the screens on the fabricated frame structures of the various device components, all frame structures were exposed to a mild HF bath to remove any contaminant. The screens, themselves, were ultrasonically cleaned before welding. After screen attachment, the completed components were kept free of foreign particles by placing them in clean polyethylene bags. During welding of the components into the subassemblies, care was exercised to prevent any dirt or contamination from contacting these assemblies.

Methyl alcohol, which was used to check the bubble point of the screens during the fabrication and assembly operations, was the only fluid to which the screen components were exposed during fabrication. These bubble point checks were performed at the component level (completed channel, filter, etc), subassembly level (upper channel network, etc) and after the device had been installed in the tank. This bubble point testing showed no severe degradation in bubble point during fabrication and assembly processes (always met the 24 in. of  $H_2O$  bubble point acceptance level with 325 x 2300, or 7.5 in. of  $H_2O$  with 165 x 800 as measured in methanol).

After the acquisition system had been installed into the test tank, a proof pressure test was conducted to verify the integrity of the ground test tank. Using filtered demineralized water, the tank was pressurized to  $261 \text{ N/cm}^2$  (379 psig) and held for three minutes.

## C. TEST PROGRAM

The overall objective of the full-scale ground tests was to verify the performance of the fuel and oxidizer tankage systems against Space Shuttle criteria and to compare performance with predictions. Specifically, the test objectives were to verify fill and drain procedures, checkout procedures, and conduct representative outflow tests for comparison with predictions. The specific objectives, as well as the detail descriptions of the specific tests conducted, will be presented later in this section. A general description of the ground test fixture follows.

The test tank consists of a flanged 96.5-cm (38-in.) I.D. 304L stainless steel tank with 9.5-mm (3/8-in.) wall thickness. The tank flanges are sealed with an O-ring and secured with 72 14.3-mm (9/16-in.) bolts. The pressurization port is a 9.5-mm (3/8-in.) AN fitting positioned at an angle of 61.1 deg with the tank parting plane. The tank outlet is positioned with its center at an angle of 53.3 deg from the parting plane in the hemisphere opposite the pressurization port. The outlet port is not positioned radially; its centerline is perpendicular to the tank parting plane. The outlet tube is stainless steel tubing, 3.8-cm (1.5-in.) O.D. with a 1.24-mm (0.049-in.) wall thickness. Nine additional tank penetrations of 3.2-mm (1/8-in.) tubes are provided to vent and pressure monitor various internal screen compartments and provide a reference pressure tap as shown in Figure VI-25. The nine pressure monitoring tubes are connected to the screen components as follows: 1, reentry sump; 2, A&B, sump bubble strainer; 3, upper compartment ring manifold; 4, upper compartment channels; 5, A&B, reentry collector channel; 6, upper compartment bulk propellant region; and 7, lower compartment bulk propellant region.

The tank is mounted in a mobile support stand (Fig. VI-26) by means of two trunnions bolted to the flanges with their centerlines coincident with the y-axis of the tank. This allows the tank to be rotated or positioned through 360 deg around the Y axis. The support stand is provided with four casters so that the entire assembly can be moved freely.

For all of the full-scale tests conducted (fill and drain, check-out, and outflow), the test fixture shown schematically in Figure VI-27 was employed. This fixture includes a fluid loading and outflow system, a pressurization system, a load cell system to determine loaded weight, and the necessary instrumentation for conducting all of the tests required. The tank support stand was mounted on a single load cell, as shown, for monitoring fluid weight during fill and outflow of the tank. All instrumentation and valving to the nine tank test ports was mounted on the tank, which allowed tank rotation without having to remove these systems. The outflow and pressurization lines were flexible to permit tank rotation. The screen checkout tests were conducted through the hand valve system shown. Both the pressurant and fluid inlets were fitted with filters to maintain tank cleanliness and a sample port was included to obtain fluid samples to check cleanliness. An orifice was used to obtain the proper fluid flow rate for each of the outflow tests. A listing of the instrumentation used during the test program is presented in Table VI-6. Two views of the full-scale RCS tankage test system are presented in Figure VI-28, a front view of the test system, and in Figure VI-29, a view from the right side.  $\Delta P_3$ ,  $\Delta P_4$ , and  $\Delta P_5$  can be seen attached to the tank flange in Figure VI-28.  $\Delta P_1$  and  $\Delta P_2$  can be seen in Figure VI-29.

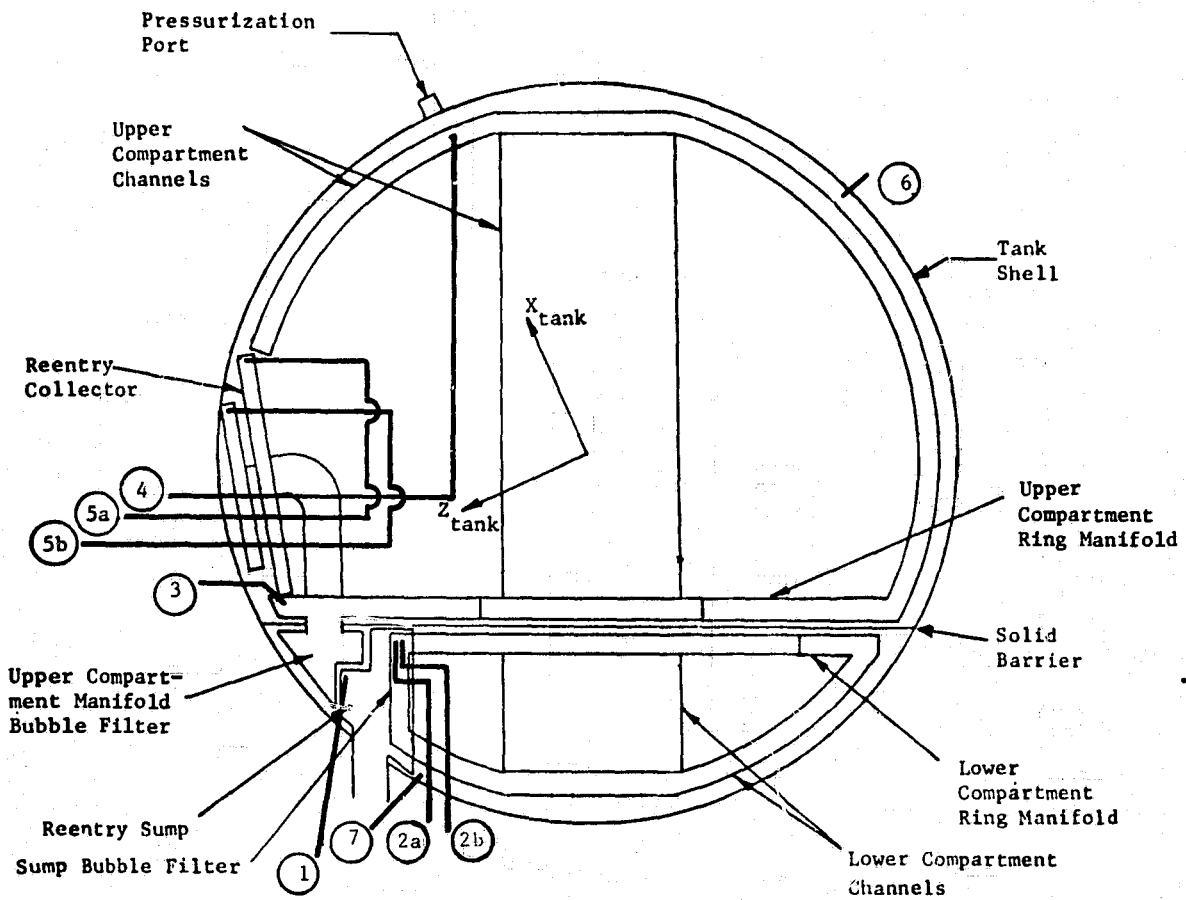


Figure VI-25 Full-Scale Acquisition Test Device, Schematic

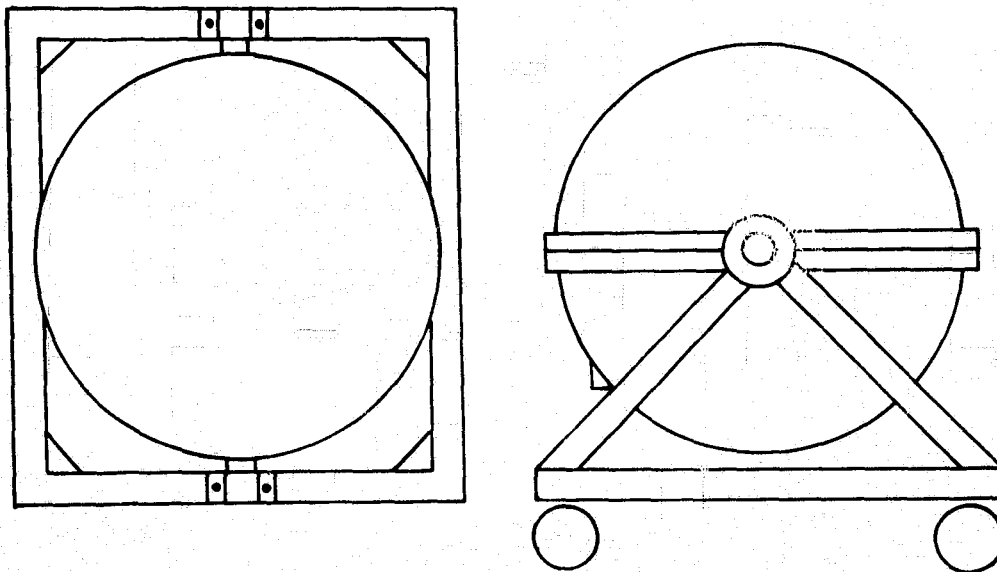


Figure VI-26 Full-Scale RCS Tank Support Stand

Figure VI-27

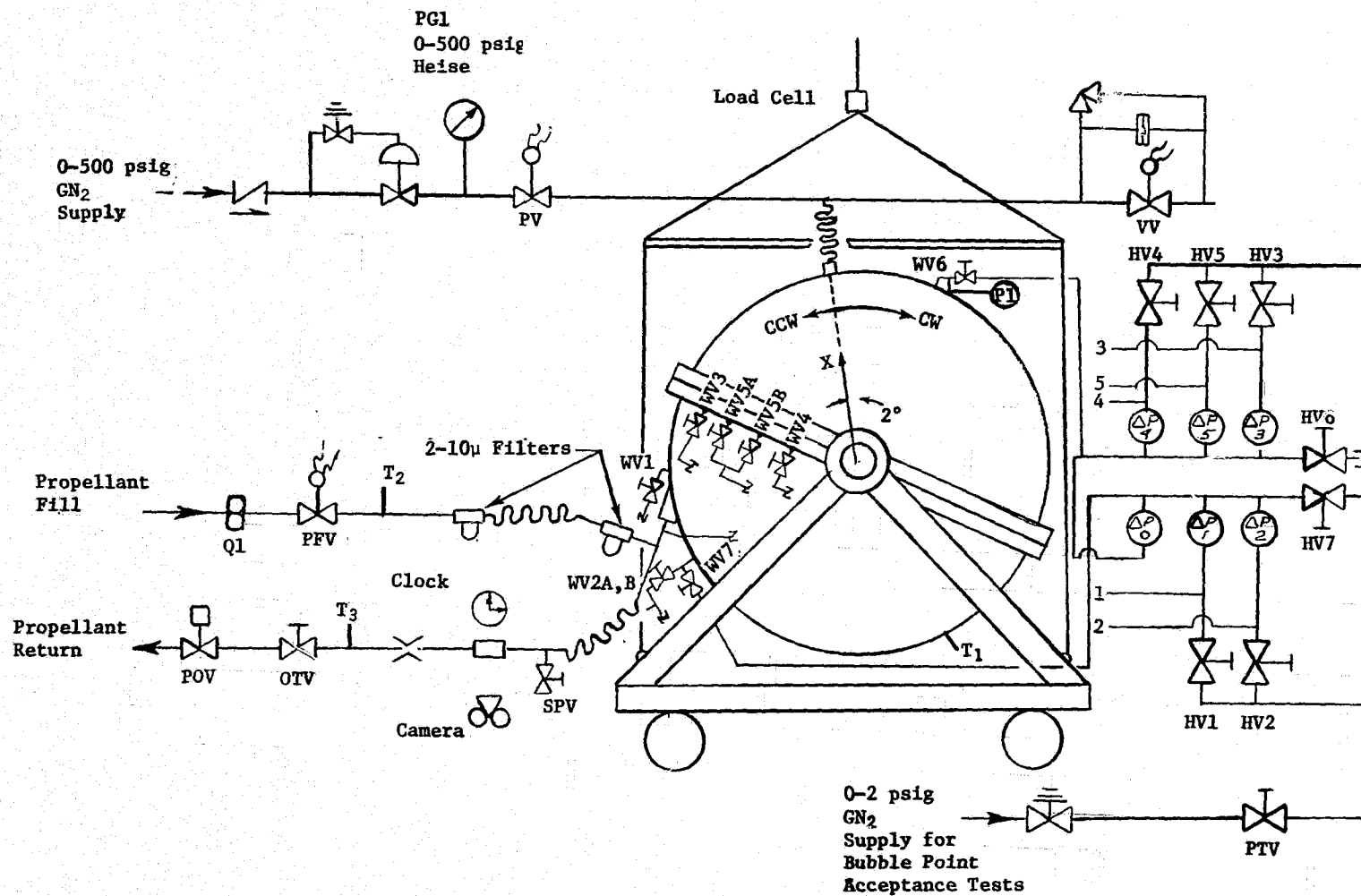


Figure VI-27 General Test Installation Schematic

Table VI-6 RCS Tank Test Instrumentation List

Measurement	Type	Range	Accuracy %	Response, Hz
PG1	Pressure Gage	0-500 psig	$\pm 1$	1
P1	Pressure Transducer	0-300 psig	$\pm 1$	10
T1, T2, & T3	Temperature Thermocouple	0-100°F	$\pm 2$	1
$\Delta P_1$ through $\Delta P_5$ and $\Delta P_0$	Delta Pressure Transducers	$\pm 5.0$ psid	$\pm 1$	10
Q1	Liquid Flow Meter	0-150 gpm	$\pm 1$	1
LC	Load Cell	700-2200 lbs	$\pm 0.25$	10
Camera	16 mm Movie Camera	100 fps		

The six pressure transducers shown in Figure VI-27 were included in the test system to monitor the pressure difference between the inside of the various capillary components of the device and the ullage regions. For the outflow tests, the  $\Delta P$ s were required to determine the breakdown point of the various components during expulsion. For the checkout tests, these  $\Delta P$ s were necessary to obtain bubble points for the screens. To provide the pressure differential connections between the various screen compartments and the bulk regions, nine vent tube and pressure monitoring ports schematically shown in Figure VI-27 were used. For  $\Delta P_3$  and  $\Delta P_4$ , vent lines 3 and 4 were connected to one side of the transducer. For  $\Delta P_5$ , vent lines 5A and 5B were first manifolded together and then connected to the transducer. The other sides of  $\Delta P_3$ ,  $\Delta P_4$ , and  $\Delta P_5$  were connected to pressure monitoring port 6. With this arrangement, the pressure differential between the reentry collector, the upper compartment channels, and ring manifold, and the bulk region of the upper compartment could be monitored during the various tests conducted. For monitoring of the pressure differential between the reentry sump and the lower compartment bulk region,  $\Delta P_1$  was connected between vent line 1 and pressure monitoring port 7;  $\Delta P_2$  was connected using vent lines 2A and 2B and pressure monitoring port 7;  $\Delta P_0$  was connected between the lower compartment bulk region and the outflow line.

## 1. Fill and Drain Tests

### *a. Objectives*

The fill and drain tests were conducted for two primary reasons. The first was to determine the minimum number of vent tubes required to obtain a reliable fill. Results of the subscale test program demonstrated the need for vent tubes for tank filling to obtain a gas-free fill of all of the capillary compartments of the device. The full-scale device was, therefore, equipped with vent tubes, located at all of the high points of the various screen components, to enable any gas trapped in these components to be vented during or after the fill operation. To assess the minimum number of tubes required, the amount of gas trapped in each of the screen components was measured during tank filling. This then determined which of the vent tubes were necessary and which were not.

The second objective of the fill and drain tests was to determine how much propellant could be removed from the tank in either the horizontal or vertical position. The vertical attitude corresponds to a drain of the RCS tanks when the Shuttle orbiter is in the launch position. The horizontal attitude corresponds to a drain of the RCS tanks after the orbiter has landed and is in the horizontal position. The full-scale SS/RCS acquisition system must be capable of being drained in either orientation. It was not required, however, to accomplish these drains in a gas-free expulsion manner, two-phase flow being permissible.

### *b. Test Approach*

To accomplish measurement of the trapped gas, a water displacement procedure was adopted. This procedure simply consisted of venting the trapped gas into a graduated glass cylinder filled with water and inverted in a water bath. The trapped gas displacing the water in the cylinder could then be easily measured.

To accomplish the objectives of the two drain tests, the full-scale RCS tank was outflowed in the two orientations specified. A normal outflow consisted of operating the tank in the gas-free expulsion mode, i.e., pressurizing the tank through its pressurization port. However, because of the fact that these drain tests had as their objective the maximum removal of propellant from the RCS tank, not necessarily gas-free, outflow was not terminated when the lower channel system broke down (two-phase flow in outflow line). Outflow was continued until no more liquid could be seen exiting the tank. The drains were conducted at very low flowrates [38 lpm (10 gpm)] to minimize screen breakdown so that the maximum amount of propellant could be outflowed.

Isopropyl alcohol (IPA) was used as the test liquid in all the fill and drain tests to simplify the tests conducted and minimize test hazards.

*c. Test Description and Results*

Three trapped gas measurements were made during the fill and drain tests: two were performed with the screen system dry before tank filling; the third assessed the amount of trapped gas for a fill with the screens wet before filling.

1) Trapped Gas Determination during Tank Filling - To assess the amount of trapped gas in the full-scale acquisition device screen compartments, the following procedure was used. Before tank filling, all of the valves connected to the vent lines were closed so that no gas could be vented during the fill operation (WV valves of Fig. VI-27). The tank was then filled at a slow rate until the desired tank load was obtained. Tank loading consisted of filling through the outlet with the tank in the vertical orientation to simulate loading on the launch pad. At the completion of tank filling a pad pressure of 3.4 to 6.9 N/cm<sup>2</sup> (5 to 10 psig) was applied. The valves on each of the vent ports were then individually opened to expel any trapped gas through clear plastic tubing into the graduated cylinder.

The amount of gas trapped in each of the device components is listed in Table VI-7. The dry screen assessments were conducted to simulate an initial fill. The wet assessment was conducted to simulate a tank loading immediately after the Shuttle orbiter has returned from orbit and is being readied for another flight. The amounts of trapped gas listed in Table VI-7 clearly indicate that the reentry sump traps a large amount of gas during tank filling whether the screens are dry or wet before the fill operation. For the other screen components, relatively small amounts of gas were trapped unless the screens were wet before filling. For the upper compartment channels, effectively no gas was trapped regardless of whether the screens were wet or dry. It is interesting to note that the 2440 cc (149 in.<sup>3</sup>) of gas trapped by the reentry collector during the wet screen fill test exceeds the volume of the reentry collector. This gas must have come from the lower compartment bulk region because the collector is effectively an extension of that region. Likewise, the amount of trapped gas contained in the reentry sump is larger than the volume of the sump. Therefore, this gas must have either come from the lower compartment channels or was trapped in the outflow line.



Table VI-7 Trapped Gas Quantities during IPA\* Tank Fills

Trapped Gas Region	Screens Dry before Filling, cc (in. <sup>3</sup> )		Screens Wet before Filling, cc (in. <sup>3</sup> )
	Run 1	Run 2	
Sump	1750 (107)	2064 (126)	4721 (288)
Lower Compartment Channel Network Including Sump Filter	43 (2.6)	60 (3.7)	969 (59)
Upper Compartment Ring Manifold Including Manifold Bubble Filter	38 (2.3)	49 (3.0)	239 (14.6)
Reentry Collector and Lower Compartment Bulk Region	51 (3.1)	50 (3.1)	2440 (149)
Upper Compartment Channels	**	6 (0.4)	5 (.03)
<p>* Isopropyl Alcohol</p> <p>**During this run, the tank was not completely filled. Upon venting the upper channels, it was found that the top portion of the channels was not wet and pressurant gas was being vented.</p>			

(There was gas in the line before filling.) Since the filter screen should have been wet before filling, it does not seem likely that the gas came from the channels. (Gas would have passed through the sump bubble filter to get into the sump.) It is more likely, therefore, that gas was trapped in the fill line.

The data presented in Table VI-7 show that filling with wet screens definitely increases the amounts of gas trapped in the device compared to filling a dry system. In addition, with wet screens the tank would only fill at 18.9 lpm (5 gpm) with the IPA supply tank at 31 N/cm<sup>2</sup> (45 psig) and with the throttle valve fully open. During all other IPA tank fills 38 lpm (10 gpm) or more could easily be attained with a supply tank pressure of only 17 N/cm<sup>2</sup> (25 psig).

The trapped gas data obtained under the IPA fill and drain tests indicate that all but one of the vent ports are needed for a flight-type system. The amount of gas trapped in the upper compartment channels was so small, whether the screens were dry or wet before loading, that vent tube number 4 is not required. For the other screen compartments, however, the amount of gas trapped when loading with wet screens was large enough to warrant vent tubes for these components on a flight system.

2) IPA Drain Tests - To accomplish the horizontal and vertical drains, the tank was first pressurized to  $21 \text{ N/cm}^2$  (30 psig) and then outflowed at approximately 38 lpm (10 gpm) until no more liquid could be expelled from the test tank. These two outflow tests, from start of outflow up to lower compartment channel breakdown, are covered in more detail, from the standpoint of verifying the performance of the full-scale acquisition system, under the outflow test discussion presented later in this section. Of importance here is the portion of the test from system breakdown to end of obtained flow. For the vertical drain test, gas-free expulsion was obtained down to 11.8 kg (26 lbm) remaining in the test tank. From that point on, an additional 5 kg (11 lbm) was removed from the tank as two-phase flow until no change in weight was indicated by the load cell. This left as residual liquid in the test tank 6.8 kg (15 lbm) of IPA or only 2% of a maximum tank load [ $0.44 \text{ m}^3$  ( $15.4 \text{ ft}^3$ ) based on a 609-kg (1343-lbm) load of  $\text{N}_2\text{O}_4$  at  $37.8^\circ\text{C}$  ( $100^\circ\text{F}$ )].

For the horizontal drain, performance was even better. System breakdown occurred when only 7.7 kg (17 lbm) of IPA was left in the tank. At the end of liquid flow, the residual liquid measured 3.4 kg (7.5 lbm) of IPA or 1% of maximum propellant load.

Results of the two drain tests indicate that a continued expulsion (flow not terminated at system breakdown) at low flowrate can probably be used to accomplish vertical and horizontal drain of the RCS tankage. When using such an expulsion, the acquisition system was capable of draining down to 98% of the load in the vertical attitude and 99% in the horizontal attitude using IPA. Based on results of the  $\text{N}_2\text{O}_4$  reentry 1-g simulation tests, discussed in detail later in this section, it is believed that the 99% drain capability in the horizontal attitude also applies to  $\text{N}_2\text{O}_4$ . The reentry attitude is very close to that of the horizontal drain and the  $\text{N}_2\text{O}_4$  reentry tests obtained expulsion efficiencies of 98.4 to 98.9% for gas-free expulsions. In addition it is felt that the full-scale SS/RCS tankage can obtain an  $\eta_e$  of 98% for an  $\text{N}_2\text{O}_4$  vertical drain. However, greater  $\text{N}_2\text{O}_4$  screen dry out potential might present problems not seen with IPA. Further testing is required in this area.

During the drain tests, samples of IPA were taken to evaluate the cleanliness approach used during fabrication of the full-scale acquisition device. Based on a particle count of these samples, the cleaning approaches used during fabrication were deemed adequate.

## 2. Checkout Tests

### *a. Objective*

The prime objective of the checkout tests was to develop a procedure by which the full-scale RCS acquisition system could be remotely (tank not opened) inspected to verify that its operational capability had not been degraded by use.

### *b. Approach*

The operational capability of the system can, in theory, be remotely determined in two ways. The first approach is to perform a remote bubble point test on all of the screen components of the device. In this way, the integrity of the screens of the acquisition system can be assessed. To accomplish such a bubble point test, a pressure differential equal to the screen bubble point must be imposed across the wetted screens of the device components and monitored remotely. This approach requires the screens to be wetted before the test and kept wet during the bubble point measurement. It has the advantage of being able to test all of the screen area of either the upper or lower compartment at one time.

The other method available is to conduct a number of tank expulsions in various orientations and record the breakdown residuals of these tests. By monitoring the pressure differentials across the different screen components of the device, the point at which the various components break down can be determined. A detail discussion of this  $\Delta P$  monitoring technique is presented under the outflow test section, where it was employed to help assess the performance of the full-scale device. Also, residual propellant quantities can be compared to computer predictions or previously established measurements to see if the acquisition system performed as it should have, thus assessing whether or not the operational integrity of the device has been degraded. A number of expulsions in different orientations are required so that all of the screens can be uncovered during an outflow. The screen that breaks down is the screen exposed to the pressurant gas. The screen that is submerged in liquid is not tested during the expulsion. This checkout procedure suffers from the disadvantage of being only an indirect measure of screen integrity. With the bubble point approach, a direct measure of screen integrity is made.

By considering the advantages and disadvantages of the two checkout techniques, the bubble point approach was adopted as the primary technique to be investigated during the checkout tests. To wet the screens before bubble pointing, it was decided to conduct a fill and drain test on the tank just before testing the screens. The details of how the bubble point fill and drains were accomplished is discussed later under the test description of the bubble point tests. To accomplish pressurization in the different screen compartments of the full-scale device, the vent tube or bleed line system was employed.

Because of the nature of the full-scale device design, direct pressurization of one screen component would not necessarily bubble point only that component, since bubble filters of coarser screen mesh are included in the system. Consider the upper compartment. If the upper compartment channel network is pressurized (channels plus ring manifold) through either vent port 3 and/or 4 (Fig. VI-22 and VI-24), the manifold bubble filter will also be pressurized. Because this filter use 165 x 800 screen compared to the channel network 325 x 2300 screen, the filter will break down first. If the lower compartment bulk region is being vented along with the upper compartment bulk region, the upper channel network will never reach its bubble point, since all the pressurizing gas will pass through the filter and be vented. To prevent this from occurring, both the reentry collector and/or the lower compartment bulk region (collector is an extension of lower bulk region) and the upper compartment channel network were pressurized simultaneously. In this way, the manifold bubble filter was short circuited during the pressurization process (no  $\Delta P$  across filter). However, the reentry collector was then tested along with the upper channel network. With this approach, there was no way of determining which screen component (collector or channel network) broke down first. This was considered acceptable. To obtain the bubble point of just the manifold filter, pressurization of only the upper channel network while venting the upper and lower bulk regions was employed, as previously discussed.

For the lower compartment, a similar situation exists because of the presence of the sump bubble filter located between the channel network and the reentry sump. Therefore, to obtain the bubble point of the lower channel network, it was necessary to pressurize the reentry sump and channel network simultaneously while venting the lower bulk region. To test the sump bubble filter, the lower channel network was pressurized while venting both the reentry sump and lower bulk region.

To develop a bubble point procedure, isopropyl alcohol (IPA) and  $N_2O_4$  were used as test liquids.  $N_2O_4$  was chosen as the propellant for this verification because of its high vapor pressure and the greater potential for screen dry out.

### *c. Test Description and Results*

Five bubble point tests were conducted using IPA and one was conducted using  $N_2O_4$ . In addition, an expulsion checkout test was conducted using  $N_2O_4$ . For all of the bubble point tests, the test tank was oriented so that the solid barrier was horizontal. The tank was filled in the normal vertical position.

1) IPA Tests - For the first IPA bubble point test, the screens were wetted by first filling the test tank completely full (All trapped gas was vented using the vent lines so that a complete fill was obtained.) and then draining completely. To drain the tank, a modified gravity drain procedure was used. This procedure consisted of using gravity to drain the liquid from the tank by suspending the tank above the IPA return tank. The low capacity pressurization system (Fig. VI-27) was used to replace the IPA with  $\text{GN}_2$  that had been bubbled up through a small tank filled with IPA. In this way, the incoming  $\text{GN}_2$  would become saturated with IPA so that the potential of having the IPA vaporize off the screens during the drain would be either eliminated or reduced. The speed at which the tank drained, therefore, was dependent on the  $\text{GN}_2$  flowrate through the low capacity pressurization system. The entire tank was drained in approximately an hour and a half.

During the tank drain, the bleed or vent tube ports were opened to allow the  $\text{GN}_2$  to enter the inside of the different screen components of the device. This was done to prevent a pressure differential from building up across the screens and breaking down the device during the drain. The IPA should have drained from the inside of the screen compartments and bulk regions together, leaving the screens wet but not broken down.

Once the entire tank had been drained, an upper compartment bubble point was performed. The low capacity pressurization system was used to pressurize (using the saturated  $\text{GN}_2$ ) the upper channel network and the reentry collector simultaneously. The upper compartment bulk region was vented to the atmosphere so that the bubble point of these two screen components could be measured. The  $\Delta P$  traces for these two components indicated that very little pressure was building up in them, even though the supply pressure was more than adequate. It was concluded that either the upper channels or the collector had dried out and that the pressurizing gas was simply flowing across dry screen. An attempt to bubble point the manifold bubble filter, reentry sump, lower channels, and sump filter produced the same result. From results of the first IPA bubble point attempt, it was concluded that the screen dry out resulted from the extremely long tank drain time.

The second bubble point attempt concentrated on the lower compartment because it could be drained in a fairly short time. Only the lower compartment was filled; draining required only 15 minutes.

By pressurizing the lower compartment channel network and reentry sump simultaneously, while venting the lower compartment bulk region, a good bubble point was obtained. The value recorded for  $\Delta P_1$  and  $\Delta P_2$  was 58 cm (23 in.)  $\text{H}_2\text{O}$  measured in IPA

which corresponds to the 61 cm (24 in.) H<sub>2</sub>O acceptance level for 325 x 2300 screen as measured in methanol at 20°C (68°F). The bubble point trace obtained for  $\Delta P_2$  is shown in Figure VI-30. The sump bubble filter was tested next by pressurizing the lower channel network and venting the sump and lower compartment bulk region. Again, a good bubble point corresponding to 20.3 cm (8 in.) H<sub>2</sub>O, if measured in methanol at 20°C (68°F), was obtained. This value is slightly higher than the minimum acceptance level set for 165 x 800 screen during the fabrication of the full-scale device.

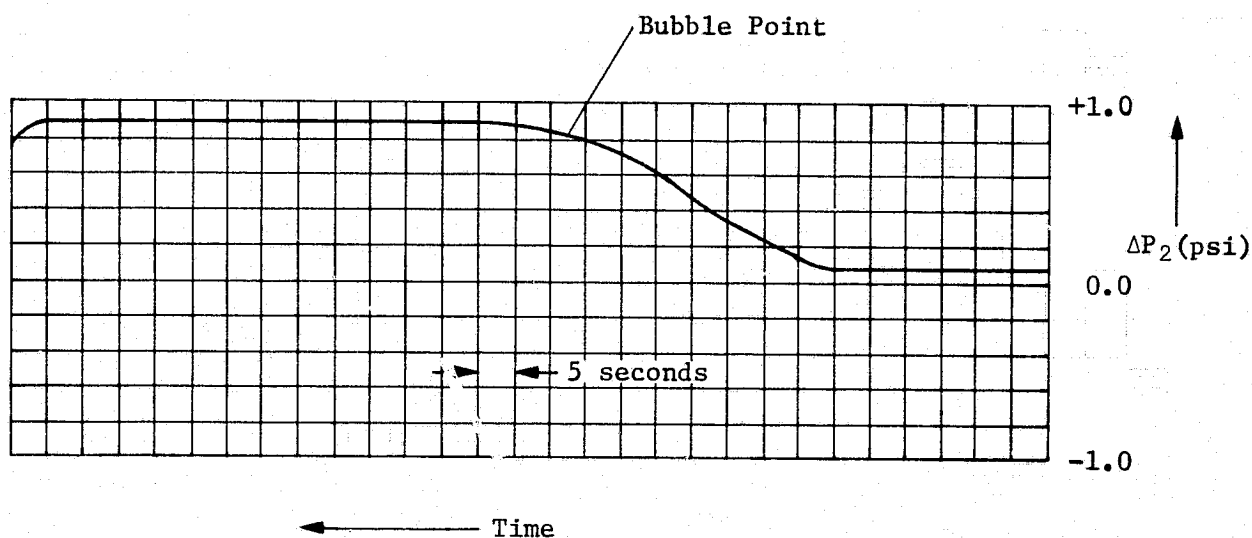


Figure VI-30 IPA Bubble Point Trace for Lower Channel System ( $\Delta P_2$ )

Since the second IPA bubble point attempt demonstrated that a successful bubble point could be obtained using the modified gravity drain technique, another attempt was made to bubble point the upper compartment. The test tank was drained in a little under one hour. Pressurization of the upper compartment channel network and reentry collector failed to yield a successful bubble point. After closing the pressurization valve, the pressure decreased indicating that the screens were dry.

For the fourth test, a normal expulsion (gas-free liquid expulsion) was used as the means of draining the tank. The upper compartment was slowly outflowed to a point at which it still remained stable. At this point, the channels and collector were still full of liquid and could not have dried out. The amount of liquid that remained in the upper compartment, corresponding to this stability point, amounted to about 11 kg (25 lbm) or about 8 to 10 cm (3 to 4 in.) of liquid depth above the solid barrier. The reentry collector and upper channel system were then pressurized simultaneously

while the upper bulk region was vented. This pressurization should have (1) emptied all the liquid from the collector and channel network by forcing it into the bulk region, and (2) created a  $\Delta P$  across the screens for bubble pointing. During this pressurization,  $\Delta P_4$  (delta between upper channels and bulk region) increased until it seemingly indicated a bubble point near the proper value (relatively sharp change in slope of  $\Delta P$  trace (Fig. VI-30 as typical). However,  $\Delta P_5$  (delta between collector and bulk region) always lagged  $\Delta P_4$  and did not reach a bubble point. Upon further examination of the data, the lagging of  $\Delta P_5$  was believed to have been caused by the conditions. When the collector was pressurized, the pressurant gas rather than pressurizing the collector simply transferred liquid from the lower compartment (collector is an extension of the lower compartment) up to the upper compartment by way of the manifold bubble filter and upper compartment ring manifold (ring manifold is submerged). This process would have continued until the manifold bubble filter became completely uncovered. However, before this occurred, the pressure in the upper channels reached a point that broke down the screens.

Based on this hypothesis, it was proposed for the fifth IPA bubble point test to expel in the same manner as in the fourth test, but to terminate the expulsion when the liquid level was in the lower compartment and was below the manifold bubble filter. In this way, there would be no liquid path from the lower bulk region back to the upper compartment, and the re-entry collector could be pressurized. However, to expel down into the lower compartment would require the breakdown of either the collector or the upper channel network. It was hoped that when gas broke through the screens, they would still remain wet.

The fifth IPA bubble point attempt was also unsuccessful.  $\Delta P_4$  showed a breakdown point far below the expected value when the collector and upper channel network were pressurized. Upon repeating the pressurization sequence two more times ( $\Delta P$  was dropped almost to zero to reseal screens and then increased to bubble point), the breakdown  $\Delta P$  became lower and lower with each new attempt. These data indicated that the upper channel screens never resealed after they were initially broken down during the expulsion.

The fifth attempt was the last bubble point attempt using IPA. Although no set bubble point procedure was developed from the IPA tests, data that were applied to a remote bubble point procedure for the  $N_2O_4$  testing were obtained.

2)  $N_2O_4$  Tests - Two checkout tests were conducted using  $N_2O_4$ . The first test consisted of an expulsion to measure directly the breakdown  $\Delta P$  of the screen components. As previously discussed, this type of checkout test consists of simply running a normal expulsion while monitoring screen  $\Delta P$ . The test was conducted in the reentry orientation to try to obtain a good breakdown  $\Delta P$  for

the reentry collector, which was never successfully bubble pointed using IPA. The vent tube pressure monitoring ports are located so that if the expulsion were run in the reentry configuration, the breakdown  $\Delta P$  of the top screen surface of the collector (rest of collector submerged in reentry paddle) would be obtained.

To conduct the  $N_2O_4$  expulsion checkout, the tank was first completely filled (venting out all trapped gas) and then expelled very slowly [(111 lpm (3 gpm))] maintaining the tank pressure near  $62 \text{ N/cm}^2$  (90 psig) to subcool the  $N_2O_4$  to prevent boiling. As predicted  $\Delta P_5$  and  $\Delta P_1$  (reentry collector and sump) showed a distinct  $\Delta P$  indicating screen breakdown. (See outflow tests for discussion of breakdown  $\Delta P$  traces.) No other useful  $\Delta P$  data were obtained. For instance,  $\Delta P_4$  (upper compartment channels referenced to upper bulk region) showed only a gradual low magnitude rise and decrease throughout the expulsion. The point at which the  $\Delta P$  trace slope changed, however, did seem to correspond to where the upper channels should have broken down. However, vent port 4 was not at the breakdown location of the upper channels in the reentry configuration but submerged in liquid. It, therefore, did not record the breakdown of the upper channels.

The  $\Delta P$  magnitudes recorded for  $\Delta P_5$  and  $\Delta P_1$ , were  $0.62 \text{ N/cm}^2$  (0.9 psi) and  $0.69 \text{ N/cm}^2$  (1.0 psi), respectively, at breakdown. At the temperature [ $20^\circ\text{C}$  ( $68^\circ\text{F}$ )] the expulsion was conducted,  $325 \times 2300$  screen should have a bubble point of  $0.70 \text{ N/cm}^2$  (1.02 psi), corresponding to the minimum acceptance bubble point standard set during manufacturing, 61 cm (24 in.)  $H_2O$  measured in methanol at  $20^\circ\text{C}$  ( $68^\circ\text{F}$ ).

Due to the fact that the  $N_2O_4$  checkout expulsion test was able to check only a small amount of screen, a  $N_2O_4$  bubble point test similar to the ones conducted with IPA was performed.

The last IPA bubble point test clearly showed that once the screens of the upper compartment broke down, they did not reseat. Therefore, any bubble point procedure should not contain a drain or expulsion procedure that breaks down the screens before bubble pointing. The data from the IPA tests indicated that retaining bulk liquid in contact with the screen components can cause problems. In addition, the first three IPA bubble point tests showed that a modified gravity drain technique was not applicable to the upper compartment because of the long drain time and associated screen dry out problem.



For  $\text{N}_2\text{O}_4$ , a worse dry out problem exists due to the much higher vapor pressure. On the basis of the conclusions drawn from the IPA bubble point tests, it was decided to use a pressurized expulsion procedure to empty the tank before bubble point testing. The tank was completely loaded in the vertical position and slowly pressurized to  $69 \text{ N/cm}^2$  (100 psi) to subcool the  $\text{N}_2\text{O}_4$ . The pressurant was  $\text{GN}_2$  bubbled through a  $\text{N}_2\text{O}_4$  reservoir to saturate it with  $\text{N}_2\text{O}_4$  vapor and minimize screen dry out. The tank was then expelled with the barrier in the horizontal position at about 11 lpm (3 gpm), maintaining the  $69 \text{ N/cm}^2$  (100 psig) pressure on the tank, down to the point where the screens of the upper compartment were about to break down. At this point, the vent tube ports of the tank were opened to allow pressurant gas to enter both the inside of the collector and upper channel network as well as the upper bulk region. In this way, the  $\text{N}_2\text{O}_4$  could in theory be outflowed from the upper compartment without breaking down the screens. Expulsion then continued until the load cell indicated that the  $\text{N}_2\text{O}_4$  liquid level was in the lower compartment and below the manifold bubble filter. At this point, the outflow was terminated and the tank locked up. The pressure in the reentry collector and upper channel network was then increased simultaneously and monitored relative to the upper bulk region by use of  $\Delta P_5$  and  $\Delta P_4$  (collector and upper channel network were pressurized through ports 7 and 3, respectively). No increase was measured on  $\Delta P_4$  and  $\Delta P_5$  even though the pressurant gas was definitely going into the channels and collector. This indicated that the screens in the collector and/or channels had dried out. A check of the manifold bubble filter was attempted next with the same result.

After these attempts, the expulsion of the tank was continued bleeding in pressurant gas into the sump, and lower channel network, and lower bulk region, until the tank was empty. A bubble point check was then accomplished in the lower compartment.  $\Delta P_1$  and  $\Delta P_2$  measured a breakdown  $\Delta P$  of about  $0.76 \text{ N/cm}^2$  (1.1 psi) (Fig. VI-31) indicating acceptable screens on the reentry sump and lower channel network. However, a bubble point was not obtained for the sump bubble filter. Indications were that the screens of the lower channel network had dried out or never resealed as a result of the bubble point just performed.

Upon examination of the  $\Delta P$  traces obtained during the pressurized expulsion of the upper compartment, a breakdown  $\Delta P$  was indicated for both the ring manifold and reentry collector (referenced to upper bulk region). These occurred at the point where the upper compartment depleted.

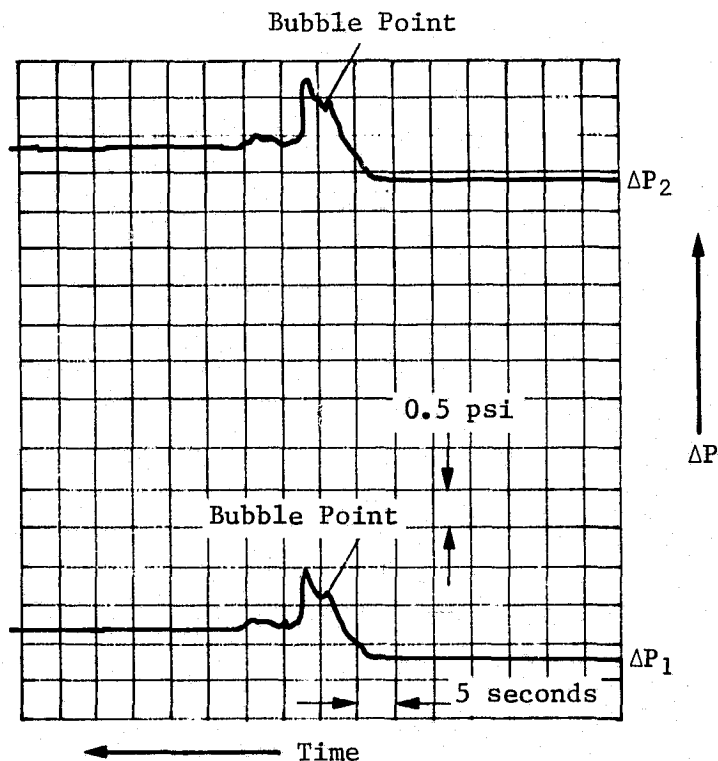


Figure VI-31  
 $N_2O_4$  Bubble Point Trace for Lower Channel System ( $\Delta P_2$ ) and  
 Reentry Sump ( $\Delta P_1$ )

As stated earlier, pressurant gas was bled into the channels and collector during the expulsion to prevent these components from developing a pressure differential across their screens. However, as indicated by the  $\Delta P$  traces, a pressure differential large enough to cause screen breakdown was imposed. This was probably due to the pressurization lines (in this case, the vent tubes) being only 3.2-mm (1/8-in.) diameter tubing. The pressurization port of the RCS test tank is a 9.5-mm (3/8-in.) fitting. Therefore, the preferred pressurant flow path was into the upper bulk region rather than into the channels or reentry collector. The pressurant supplied into the collector and ring manifold was probably not sufficient to keep up with the increase in  $\Delta P$  due to the liquid crossing the ever decreasing screen area near the depletion of the upper compartment. From examination of the data, none of the problems encountered could have been due to liquid in the vent lines used for pressurizing.

For both the IPA and  $N_2O_4$  checkout tests, difficulty was encountered in obtaining good screen integrity data. These difficulties were, in the case of the bubble point tests, directly attributable to the procedures used to wet the screens, and were not a result of the actual bubble pointing process itself. For the one checkout expulsion conducted, the opposite was true. As a result of the checkout expulsion process, only certain screen compartments of the full-scale device could be checked and even these compartments were not checked completely. (Much of collector and sump were submerged when breakdown occurred.) Therefore, the bubble point approach still seems to be the best method for device checkout. What is required is a reliable means of wetting the screens. The pressurized expulsion procedure that was used to empty the tank for the  $N_2O_4$  bubble point test, seemed to be the best method for keeping the screens wet. If adequate provisions were made so that the bleed in pressurization could have been kept uniform, a successful upper compartment bubble point could probably have been measured.

### 3. Outflow Tests

#### *a. Objectives*

Three test fluids, isopropyl alcohol, MMH, and  $N_2O_4$ , were used in the outflow tests. The objectives were to conduct representative tests of the expulsion capability of the test tank based on Shuttle criteria, to verify the tank performance and compare performance with prediction.

#### *b. Approach*

The outflow test program was structured to conduct tests that closely simulated mission events. With one exception, simulation was limited to those events that could be reasonably modeled under a 1-g environment. The exception was the +Z orbital expulsion conducted with  $N_2O_4$ . Because the acceleration environment of 1-g was more than an order of magnitude greater than any anticipated on-orbit acceleration, the test was more qualitative than quantitative.

In instances where tests were not repeated with both propellants, the propellant that presented the worst case for that particular test was usually selected. The initial expulsion tests were performed with isopropyl alcohol. This served the dual purpose of eliminating hazard during the initial system familiarization process, and providing data with a test fluid with which considerable prior test experience had been gained.

### *c. Data Acquisition*

The test system and instrumentation was described previously. Primary data for all outflow tests were provided by the load cell from which the tank was suspended, the venturi flow meter, the thermocouples mounted on the tank and in the flow lines, and the tank pressure transducers. These data were recorded on strip charts. All expulsion tests were documented further by filming a sight glass in the outflow line with 16mm color motion pictures. In addition, pressure differentials across the various screen compartments were measured during the actual expulsion tests. An explanation of these data follows.

### *d. Data Interpretation*

While the tank weight, propellant flowrate, pressurization level, and propellant temperature (all as a function of time) comprised the numerical data of the tests, much of the interpretation resulted from correlation with the differential pressure transducer data. Because the sight glass in the flow line was a considerable distance from the tank, the appearance of bubbles did not coincide with the actual breakdown of the reentry sump, but occurred after a time lag. By inspecting the  $\Delta P$  trace for the reentry sump, the exact point in time when the sump broke down could be ascertained. To illustrate, observe Figure VI-32. This data is taken from the later stages of the first  $N_2O_4$  reentry test. Shown are the  $\Delta P$  traces for the reentry sump ( $\Delta P_1$ ) and the lower compartment channel assembly ( $\Delta P_2$ ). The  $\Delta P$  traces show that a relatively steady condition existed until 166 seconds into the test. At that time, the reentry collector depleted the liquid in the upper compartment and began ingesting gas. This ingestion of gas into the lower compartment caused slight fluctuations in the compartment pressure; because the sump and the lower channel  $\Delta P$  measurements are referenced to the lower compartment pressure, they began to reflect this pressure fluctuation also. Expulsion continued, with pressurization gas entering the lower compartment through the reentry collector until the sharp rise in the  $\Delta P$  caused by the greatly decreased screen entrance area to the channels and sump, indicated the near depletion of the compartment. The sharp peak in the  $\Delta P_2$  trace and the flattening of the  $\Delta P_1$  trace at 187 seconds indicate breakdown. By correlating this information with the tank weight trace, it was determined that 11.9 kg (26.3 lbm) of  $N_2O_4$  remained in the tank, representing a 98.04% expulsion efficiency of loadable propellant 609 kg (343 lbm).

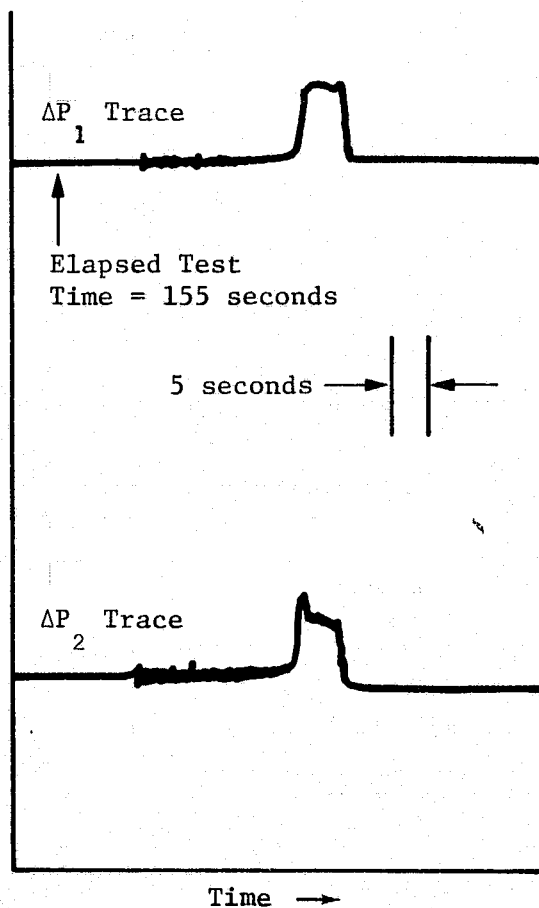


Figure VI-32  
 Typical  $\Delta P$  History for Lower Channels  
 and Sump during Outflow

*e. Test Descriptions and Results*

Eight expulsion tests were run with the three test fluids, three with isopropyl alcohol, two with MMH, and three with  $N_2O_4$ . These outflow tests are listed in Table VI-8 in the order in which they were performed during the test program. The tests are discussed here by function rather than strictly by groupings of test fluids or by chronology.

Table VI-8 Outflow Test Sequence

Test Sequence	Test Type	Fluid	Fluid Flowrate	Tank X-Axis Orientation, deg **	Comments
1	Vertical Drain	IPA*	37.9 lpm (10 gpm)	-2.0	Aft tank worst case drain
2	Horizontal Drain	IPA	37.9 lpm (10 gpm)	-104.0	Forward tank worst case drain
3	Reentry Outflow	IPA	50.2 lpm (13.25 gpm)	-110.2	Scaled to MMH at 4.4°C (40°F)
4	RTLS Outflow	MMH	6.8 kg/s (15 lbm/s)	+8.8	Partial outflow to 247.7 kg (546 lbm) remaining
5	Reentry Outflow	MMH	2.3 kg/s (5.0 lbm/s)	-110.2	
6	Reentry Outflow	N <sub>2</sub> O <sub>4</sub>	3.6 kg/s (8.0 lbm/s)	-110.2	Continuous Outflow
7	+Z Orbital Maneuver	N <sub>2</sub> O <sub>4</sub>	3.6 kg/s (8.0 lbm/s)	+82.0	Flow to screen breakdown
8	Reentry Outflow	N <sub>2</sub> O <sub>4</sub>	3.6 kg/s (8.0 lbm/s)	-72.0	Continue expulsion conducting an off-nominal reentry

\* Isopropyl Alcohol

\*\*The angle reference is with respect to a vertical plumb line. A (-) angle is counterclockwise and a (+) angle is clockwise from the vertical. The tank reference line is toward the pressurization port.

1) Vertical Expulsion - The objective of the vertical expulsion test was to assess the capability of the tank to be outflowed in an attitude simulating that which would occur in the launch attitude. Results of the portion of the test in which the tank is completely drained, with no intention of obtaining gas-free liquid, were discussed previously. The drain event was analyzed from an expulsion point of view to acquire some initial data regarding expulsion, and these data are discussed here.

The approach taken on the vertical expulsion test was to simulate the worst case with regard to tank orientation. The tank orientation selected, -2 deg from vertical, simulates a drain of the aft tanks in the launch attitude. The -2 deg attitude reduces the amount of barrier tilt or inclination the least. The larger the tilt angle of the barrier, the greater the potential for trapping liquid in the upper compartment. The forward tank is at -8

deg in the launch attitude. A flowrate of 37.9 lpm (10 gpm) was selected since this flowrate is not high enough to cause premature breakdown of the upper compartment screens, yet high enough to allow expulsion in a relatively short amount of time (13 minutes). Premature breakdown of the upper compartment screens was a concern because of the barrier tilt.

Results of the test are presented in Figure VI-33. This figure shows the total remaining alcohol load as a function of time. The test required 735 seconds until breakdown of the reentry sump and lower channels were noted on the  $\Delta P$  strip chart. At this point 11.8 kg (26 lbm) of alcohol remained in the tank representing an  $\eta_e = 96.6\%$  based on the corresponding loaded volume

for  $N_2O_4$ . As noted on Figure VI-33, the upper compartment manifold pressure tap ( $\Delta P_3$ ) indicated gas ingestion at 643 seconds. Figure VI-33 shows that the corresponding total alcohol load remaining at this time was approximately 56.7 kg (125 lbm). Since the lower compartment holds 49.9 kg (110 lbm) of IPA, only 6.8 kg (15 lbm) remained in the upper compartment when the indication of gas ingestion in the ring manifold occurred. Subtracting from the 11.8 kg (26 lbm) residual, existing at the time of lower channel system breakdown, the weight of IPA corresponding to the volume of the lower channels and reentry sump [5.8 kg (12.8 lbm)], the difference obtained [6 kg (13.2 lbm)] is less than the 6.8 kg (15 lbm) left in the upper compartment when  $\Delta P_3$  indicated gas ingestion. This indicates that (1) at least 0.82 kg (1.8 lbm) of two-phase flow was transferred to the lower compartment after the upper compartment broke down, and (2) essentially all of the IPA was expelled from the bulk region of the lower compartment before lower channel system breakdown.

2) Horizontal Expulsion - The objective of the horizontal expulsion test was to assess the ability of the tank to be expelled in the attitude the Shuttle would assume when resting on its landing gear. As with the vertical expulsion test, this test was basically a slow expulsion until the time of lower channel and sump breakdown, and the data relating to that portion of the test is discussed here.

The approach was again to select the worst case tank orientation. For the horizontal expulsion, the worst case is presented by the forward tank, which is positioned at -104 deg in the horizontal attitude. An outflow rate of 37.9 lpm (10 gpm) was again picked based on the same reasoning used for the vertical drain test.

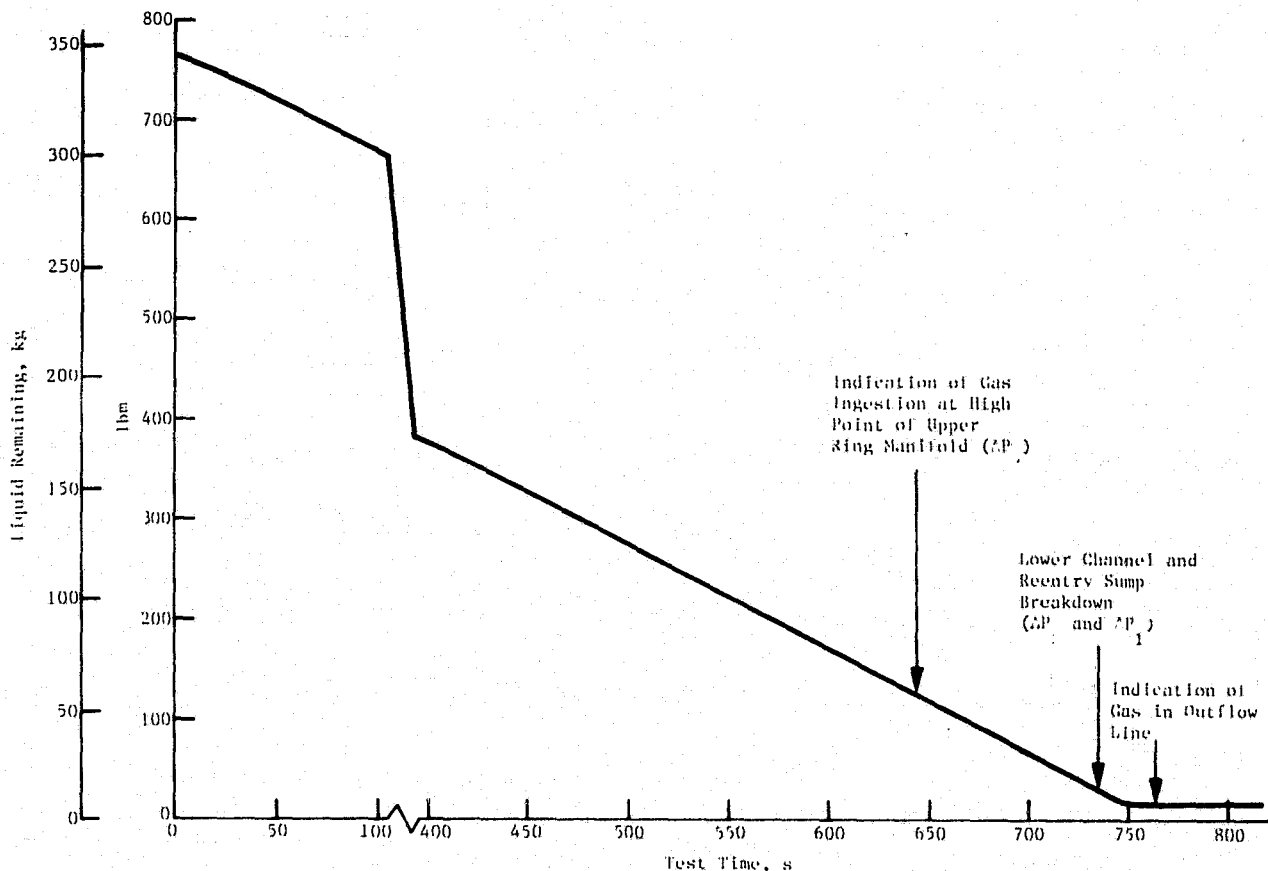


Figure VI-33

*Vertical Expulsion with Isopropyl Alcohol, Liquid Remaining*

The IPA load history is shown in Figure VI-34. Correlation with the  $\Delta P$  transducer data showed that the upper channel system broke down with approximately 62.6 kg (138 lbm) remaining in the tank as indicated on Figure VI-34. This corresponds to 49.9 kg (110 lbm) in the lower compartment and 12.7 kg (28 lbm) in the upper compartment. This 12.7 kg (28 lbm) corresponds to the capacity of the upper channels and collector and suggests that the upper bulk region was near depletion when the screen broke down. The upper manifold registered gas ingestion at 653 seconds. Since the manifold sensor ( $\Delta P_3$  pressure tap) was at the bottom in the orientation, the manifold would be empty when this occurred. At 653 seconds, Figure VI-34 indicates that 54.4 kg (120 lbm) was left in the tank, corresponding to the lower compartment volume and indicating that the upper compartment was completely expelled except for approximately 4.5 kg (10 lbm). The reentry sump showed breakdown at 753 seconds with 7.7 kg (17 lbm) remaining in the tank. This is the point at which the sump became uncovered. However, as was discussed in the drain results, the tank continued to flow until gas was ingested in the outflow line. The expulsion efficiency represented by 7.7 kg (17 lbm) is 97.8% based on the corresponding loaded volume for  $N_2O_4$ . This indicates that the drain efficiency was slightly better in the horizontal attitude than in the vertical attitude.



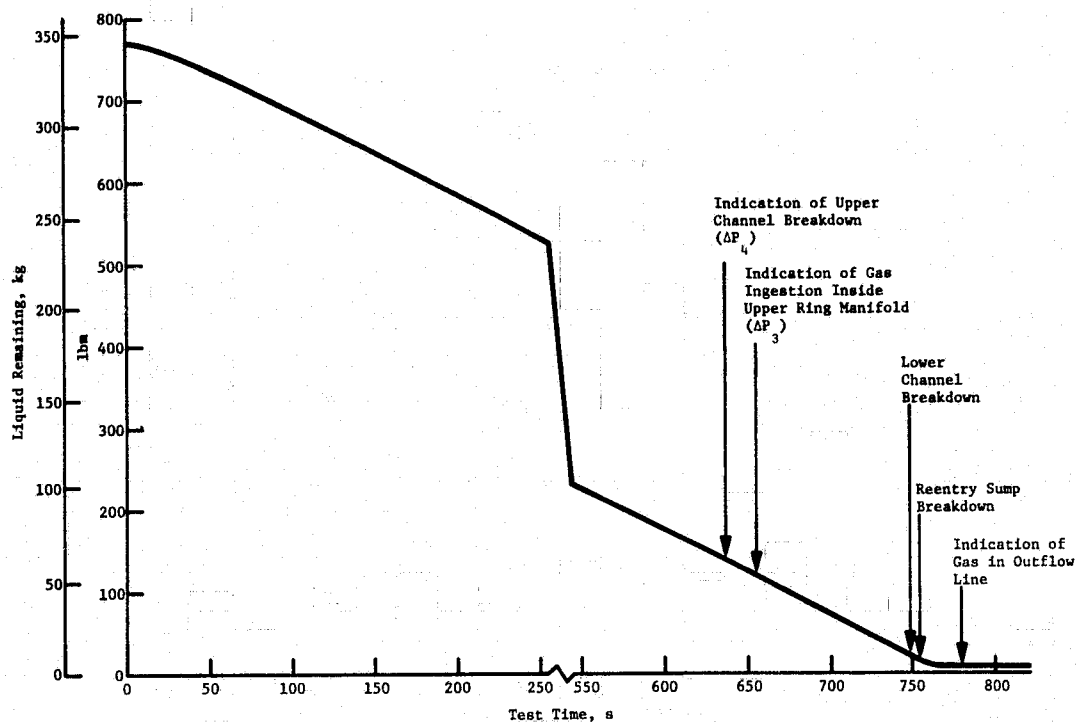


Figure VI-34

Horizontal Expulsion with Isopropyl Alcohol, Liquid Remaining

3) RTLS Expulsion - The objective of this test was to verify the performance of the device during a simulated RTLS expulsion.

The approach was to use MMH as the test propellant and to orient the tank so that the gravity vector was in the same orientation as the RTLS acceleration. This was accomplished by rotating the tank 8 deg clockwise from vertical. The test flowrate to be used was the actual MMH RTLS flowrate of 6.8 kg/s (15 lbm/s), and the tank was to be expelled to the final RTLS propellant level of 65%.

During all other expulsion tests, the flow was controlled with a manual throttling valve in the test cell. However, because of the greatly increased flowrate involved with the MMH RTLS test and as a result of personnel safety considerations, the decision was made to attempt to remotely control the flowrate with the tank pressure. The impact of this decision on the test is discussed in the following paragraphs.

Results of the test are presented in the propellant flowrate history in Figure VI-35 and in the propellant mass history in Figure VI-36. Figure VI-35 shows that the desired flowrate of 6.8 kg/s (15 lbm/s) was not maintained after being initially achieved. Figure VI-37 shows the test tank pressure history and reveals the cause of the low flowrate. The pressure curve drops rapidly at the start of the test and never regains the initial level of 152 N/cm<sup>2</sup> (220 psig) even though the system was operating at full capacity. Inspection shows that the shapes of the pressure and flowrate curves are essentially the same. Therefore, due to the insufficient capability of the pressurization system, the desired flowrate could not be maintained, and the actual flowrate stabilized at approximately 4.0 kg/s (9 lbm/s).

From examination of the  $\Delta P$  strip chart data obtained, the reentry collector had a peak pressure differential (referenced to the ullage pressure of the upper compartment) at 28 seconds, which was maintained until 32 seconds as indicated in Figure VI-36. While the pressure differential trace of the reentry collector did not exhibit a characteristic breakdown profile (Fig. VI-32 and VI-38 for comparison), a gradual increase in the pressure differentials in the lower channels and sump, beginning at 32 seconds, suggests that gas was in fact being ingested through the reentry collector into the lower compartment. Therefore, it is estimated that 252 kg (555 lbm) of MMH remained at the time that gas began passing into the lower compartment (32-s mark). The target RTLS termination level was 248 kg (546 lbm).

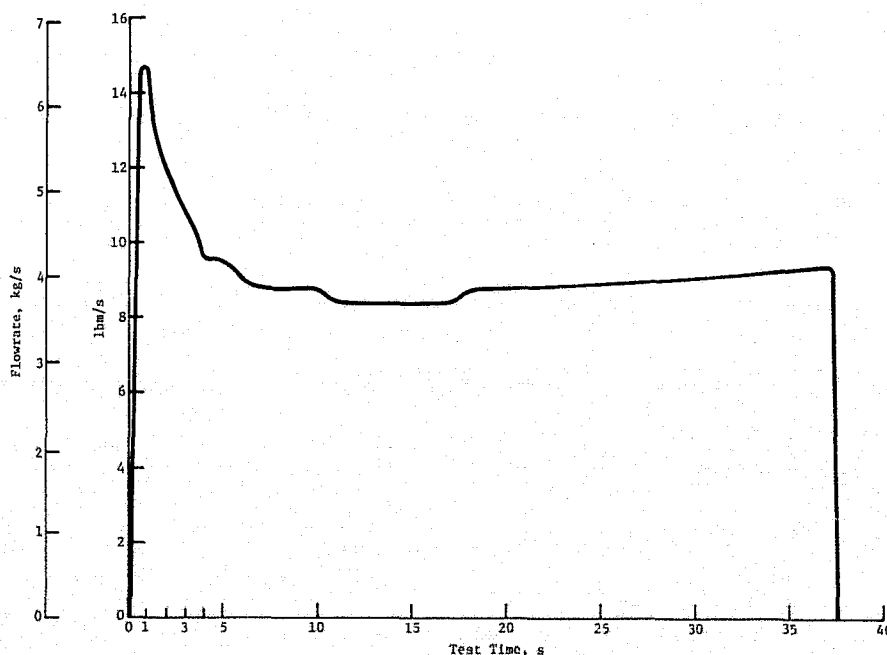


Figure VI-35 Mass Flow History for MMH RTLS Expulsion Test

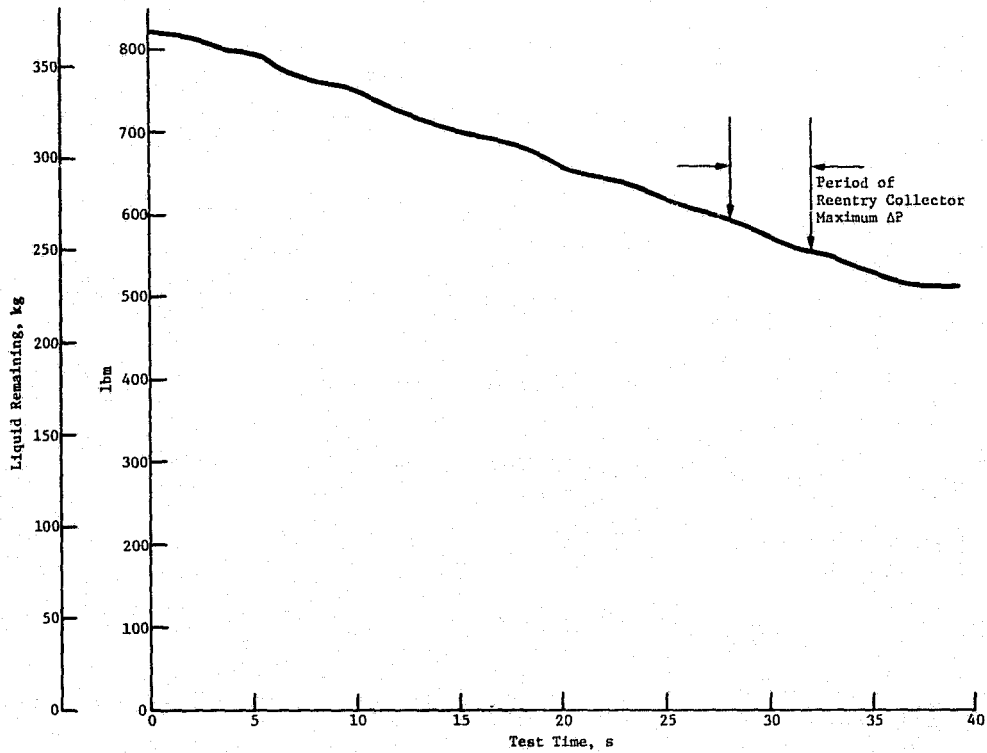


Figure VI-36 Mass History for MMH RTLS Expulsion Test

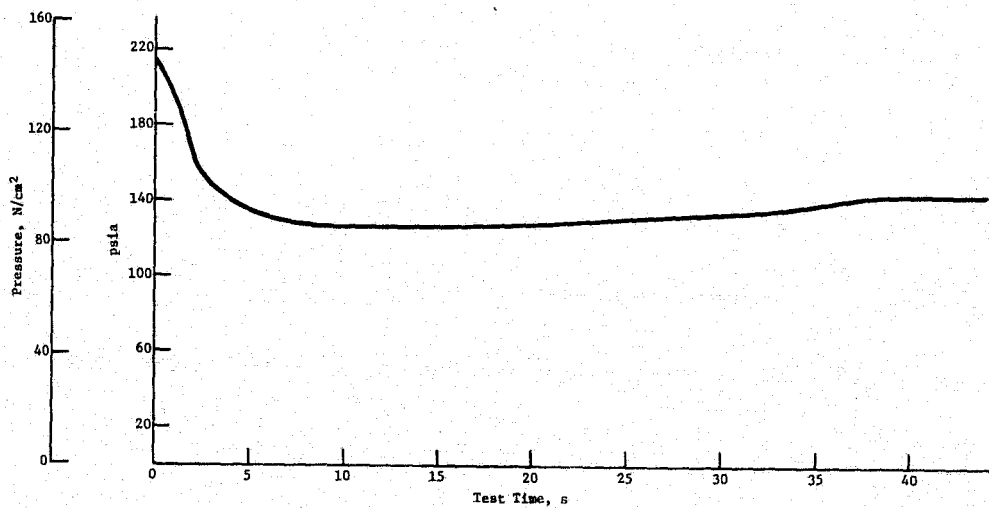


Figure VI-37 Pressure History for MMH RTLS Expulsion Test

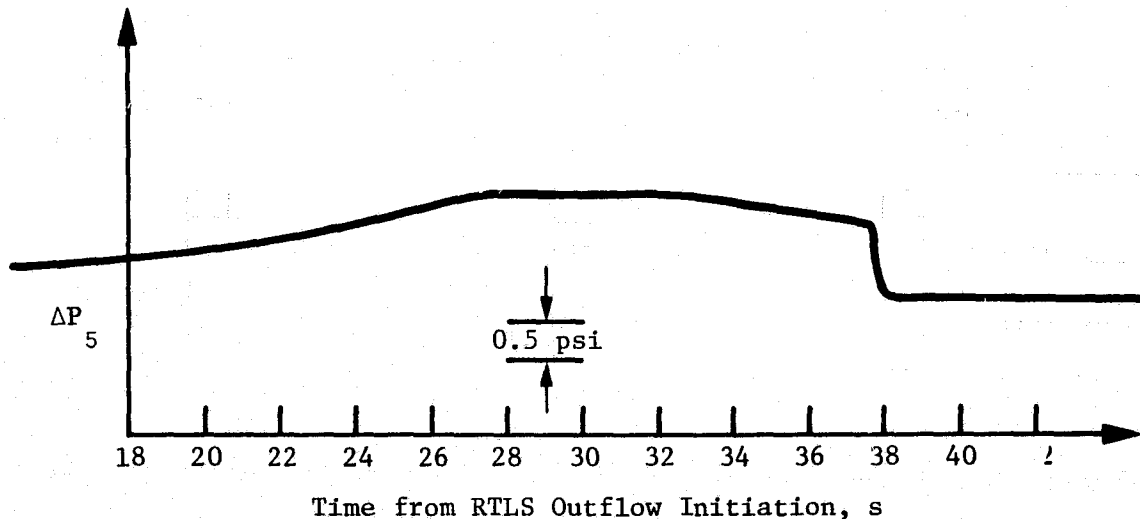


Figure VI-38  
Reentry Collector  $\Delta P$  Trace for MMH RTLS Expulsion Test

As can be seen from Figure VI-35, the test was inadvertently continued beyond the 65% level and was ultimately terminated with an indicated load of 231 kg (510 lbm). However, during this extended RTLS expulsion, the lower compartment continued to deliver propellant, the system did not break down, and gas was not ingested into the outflow line even though the volume of gas transferred to the lower compartment could be as much as 40% of that compartment volume.

The reasons for the ingestion of gas into the lower compartment at the 252 kg (555 lbm) level instead of at the 248 kg (546 lbm) level is not clear and conclusions based on the results of one test are premature. More testing is required. However, results do indicate that the RTLS requirement of allowing no gas to be transferred to the lower compartment may be unnecessarily restrictive because the device continued to deliver gas free liquid despite ingestion of gas into the lower compartment. However, the actual 2.47g RTLS acceleration environment would be more restrictive. Finally, because the test flowrate was not as high as desired, the reentry collector had a longer amount of time in which to dry out after it broke down - compared to the actual flight case. This may explain the premature gas ingestion.

4) +Z Orbital Maneuver - The objective of the +Z orbital test was to verify the performance of the device with the gravity vector in the same orientation as a vehicle +Z-axis acceleration vector in an orbital environment.

The approach was to use  $N_2O_4$  and to rotate the tank 82 deg clockwise to simulate the attitude of the forward tank during a +Z

orbital acceleration. The test flowrate was established at 3.5 kg (8 lbm/s), the equivalent of four thrusters firing. The 1-g test environment was not representative of the orbital environment, but the approach was to compare the results with computer predictions to verify performance.

$N_2O_4$  mass history for the test is shown in Figure VI-39. Table VI-9 summarizes the computer predictions for this test. The initial  $N_2O_4$  load was 656 kg (1446 lbm). The expulsion test continued for 64.5 seconds at which time gas was noted in the transparent window of the outflow line and the test was terminated. At this time the weight of  $N_2O_4$  remaining in the tank was 476 kg (1050 lbm). This was substantially larger than the residual that had been predicted (Table VI-9). Subsequent inspection of the data revealed the cause of the premature breakdown and suggested a remedy for an apparent slight design deficiency.

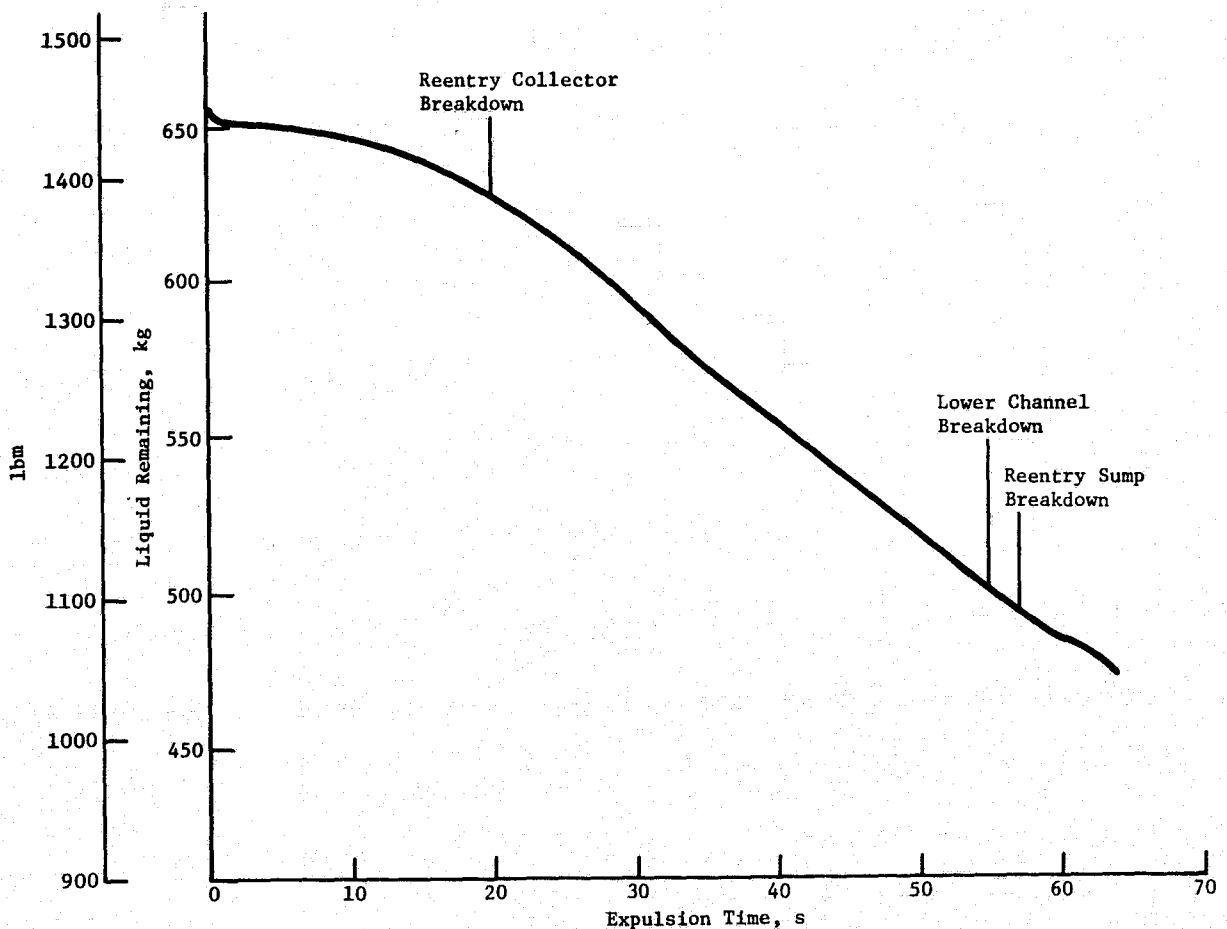


Figure VI-39 Mass History for  $N_2O_4$  +Z Orbital Maneuver Test

Table VI-9 +Z Orbital Maneuver Test Predictions

Events	Liquid Remaining, kg (lbm)
Initial Load	609 (1343)
Reentry Collector Breakdown, gas ingested into lower compartment, 365 kg (804 lbm) residual in upper compartment	456 (1006)
Reentry Sump Breakdown, 43 kg (94 lbm) in lower compartment	407 (898)*
*Assumes no two-phase flow from upper to lower compartment - sum of upper and lower compart- ment residuals.	

From analysis of the differential pressure transducer data it was observed that the reentry collector broke down prematurely, causing gas to flow from the upper to the lower compartment before the upper compartment channels had broken down. The cause of this breakdown is apparently the result of an unstable condition existing in the reentry collector tube. The tube has no screen or other capillary material across the bottom where it enters the lower compartment. Because of its size, the tube would not be stable in 1-g if the exit into the lower compartment were exposed to a pocket of gas. The tube would have a tendency to drain, with the gas moving into the tube and displacing the liquid.

The situation described was very likely the case in the minus 1-g test and the reentry collector did not function as intended. During the venting of trapped gas just after tank filling, the test personnel were unable to ascertain for certain whether or not all of the trapped gas had been removed. Because of safety reasons, only a very small pad pressure [2 to 3.5 N/cm<sup>2</sup> (3-5 psi)] was put into the tank for the trapped gas venting operation. The N<sub>2</sub>O<sub>4</sub> was at an absolute pressure (for Denver, Colorado) very close to its boiling point. Therefore, when the vent ports were opened, N<sub>2</sub>O<sub>4</sub> vapor was immediately released into the test area. For this reason, the vent ports were not left open as long as desired. In general, the ports were closed as soon as some liquid, not necessarily gas-free liquid, appeared in the vent line. A good possibility exists, therefore, that some inert gas was still left below the barrier, and this gas displaced the liquid inside the reentry collector before test initiation. A potential solution to this displacement problem is discussed at the end of this chapter.

The data presented in Figure VI-39 show that a total of 488 kg (1075 lbm) remained in the tank at the time the sump broke down and that 628 kg (1385 lbm) remained when the reentry collector broke down. The difference between these two numbers of 141 kg (310 lbm) is greater by more than 45 kg (100 lbm) the capacity of the lower compartment [92 kg (202 lbm)]. Since the lower channel system could not have expelled all of its bulk liquid before its breakdown, the above weight comparison shows that at least 45 kg (100 lbm) was transferred as two-phase flow from the upper to the lower compartment after the reentry collector broke down. Considering the predicted lower compartment breakdown residual listed in Table VI-9, 43 kg (94 lbm), the amount of two-phase flow transferred was probably more on the order of 91 kg (200 lbm) rather than 45 kg (100 lbm).

Because of the premature breakdown of the reentry collector, no definite conclusions can be reached on the performance of the upper and lower channels. They appeared, however, to function as predicted, but supportive data on their exact performance is not available. The impact of the ingested gas in the lower compartment on the ability of the system to perform an off-nominal reentry is discussed in the reentry test section. The continued transfer of oxidizer into the lower compartment, by means of the upper channel and manifold system, despite the collector malfunction is important. It demonstrates that failure of a component of the system does not instantly render the system inoperable, and it demonstrates the concept of an average fluid quality being transferred across the barrier.

5) Reentry Expulsion - A reentry expulsion was run with each of the three test fluids. In addition, an off-nominal reentry test was run with  $N_2O_4$ . The objective of the three nominal tests was to verify the performance of the system in the reentry attitude. The objective of the one off-nominal test was to determine the performance flexibility of the full-scale SS/RCS acquisition system in the reentry attitude.

The approach, except for the off-nominal reentry test, was to expel in the reentry attitude, that is, with the gravity vector in the same direction as the actual reentry acceleration vector, using the actual mission flow rates [3.6 kg/sec (8 lbm/s) for  $N_2O_4$  and 2.3 kg/s (5 lbm/s) for MMH] for each propellant. The ground test environment provided a test acceleration of slightly less than half the actual reentry value of 2.2 g. The correct acceleration vector was achieved by rotating the tank to an attitude -100.2 deg from vertical for the three nominal tests and -72 deg for the off-nominal  $N_2O_4$  test rotated counterclockwise. For the alcohol test, the approach was to use a scaled flowrate to approximate the MMH case. The MMH case was scaled because its density is close to the value of alcohol. The scaling was done on the basis of entrance loss considerations for the reentry collector. (See Chapter V, Scaling Analysis.)

Contrary to intuitive expectation, the reduced level of acceleration does not enhance the reentry test conditions. During actual reentry conditions the screen channels of the upper and lower compartments would break down sooner because of the 2.2 g acceleration. Thus, a 1-g test causes the liquid to be held in the channels longer, ultimately creating the possibility that their contents may be more difficult to expel.

Two  $N_2O_4$  reentry tests were conducted, one from a full tank load of 656 kg (1446 lbm) (nominal test); the second from a load of approximately 454 kg (1000 lbm) which was the load remaining after the +Z orbital maneuver outflow test (off-nominal test). The  $N_2O_4$  load histories for these two tests are presented in Figures VI-40 and VI-41. Indicated on each curve, as before, are significant events that took place during the screen system tests. The various pressure transducer traces indicate that the  $N_2O_4$  tests behaved in a similar manner as did the isopropyl alcohol tests discussed later.

Some differences between the two  $N_2O_4$  reentry tests do exist. After the initial flow transients, the flow rate for the nominal test remained relatively constant at slightly less than 3.6 kg/s (8 lbm/s). As indicated in Figure VI-40, ingestion of gas into the lower compartment occurred at 166 seconds into the outflow with the remaining  $N_2O_4$  load of 99 kg (219 lbm). Comparing this to the capacity of the lower compartment [92 kg (202 lbm)], 1.3% of the load remained in the upper compartment when the reentry collector ingested gas. Breakdown of the sump in the lower compartment occurred at 187 seconds with a remaining load of 9.1 kg (20 lbm) giving an expulsion efficiency of 98.4% for the nominal reentry maneuver.

The off-nominal  $N_2O_4$  reentry test followed the +Z orbital maneuver test without refilling the tank. The flowrate during this expulsion was approximately 3.4 kg/s (7.5 lbm/s). The sump in the lower compartment broke down at 159 seconds at a remaining load of 7.0 kg (15.4 lbm). The expulsion efficiency was therefore 98.9% for the off-nominal reentry test. These results clearly indicate that the performance of the full-scale device was not degraded by orienting the reentry outflow in an off-nominal attitude. The device, therefore, seems to be flexible enough to handle reentry orientations which do not exactly puddle the liquid directly over the reentry collector or sump.



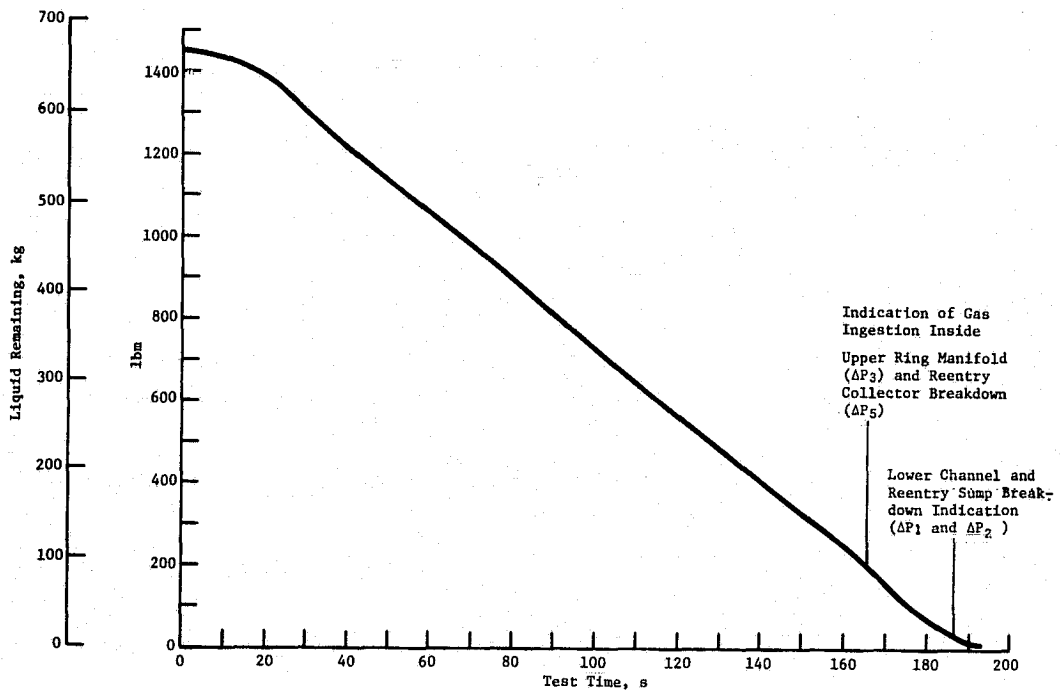


Figure VI-40 Mass History for  $N_2O_4$  Nominal Reentry Expulsion Test

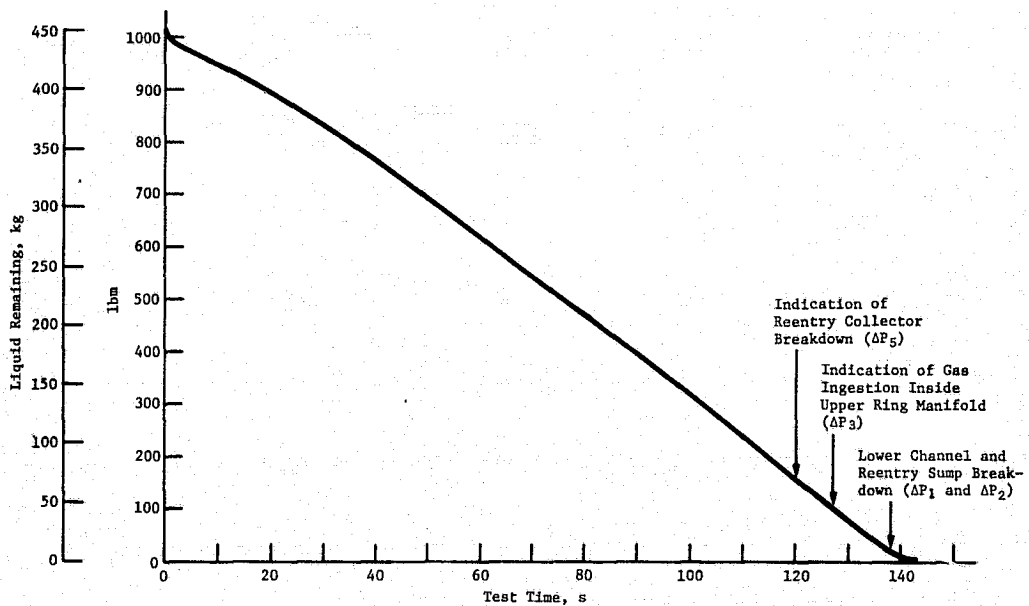


Figure VI-41 Mass History for  $N_2O_4$  Off-Nominal Reentry Expulsion Test

Comparing the weights of the loads for the two  $N_2O_4$  reentry tests, when the upper compartments were depleted (Figures VI-40 and VI-41), the difference in weights is due to the breakdown of the reentry collector in the +Z orbital test that immediately preceded the off-nominal reentry test. This breakdown caused gas to be ingested into the lower compartment where it remained at the beginning of the reentry test. Therefore when the upper compartment was depleted in the off-nominal test, the lower compartment contained a significant volume of gas. The data indicates this volume could be as much as  $0.02 \text{ m}^3$  ( $2/3 \text{ ft}^3$ ). Despite this volume of gas in the lower compartment and the fact that the system broke down during the +Z orbital test, the reentry test was completed without problems and satisfactory results were obtained.

The flowrate for the isopropyl alcohol reentry test was scaled at 50.2 lpm (13.25 gpm) or 0.66 kg/s (1.45 lbm/s) based on entrance loss considerations for the reentry collector. The alcohol reentry test began with a total load of 308 kg (680 lbm) and was expelled at essentially a constant flowrate through the entire test. The tank load history during expulsion is shown in Figure VI-42. The weight data show that the reentry collector began ingesting gas when the remaining tank load was approximately 54 kg (120 lbm). This is equivalent to the capacity of the lower compartment [50 kg (110 lbm)] plus some upper compartment residual. Gas was ingested into the reentry sump at 514 seconds with 7.5 kg (16.5 lbm) of alcohol remaining. This remaining IPA residual is equivalent to an expulsion efficiency of 97.8% based on a comparative MMH load volume.

Results of the MMH reentry test are shown in Figures VI-43 and VI-44 for the flowrate history and load history, respectively. As in the previous MMH test (RTLS), the flowrate was controlled by tank pressurization and the pressure history curve is presented in Figure VI-45. Figure VI-43 shows that the MMH reentry flowrate of 2.3 kg/s (5 lbm/s) was maintained through the entire expulsion. The differential pressure transducer data indicated that depletion of the upper compartment, signified by the breakdown of the reentry collector, occurred at 90 seconds with 37.4 kg (82.5 lbm) of MMH remaining in the tank. Because the capacity of the lower compartment is 56 kg (124 lbm) of MMH, this demonstrates that a substantial volume of gas was present in the lower compartment at the initiation of the reentry expulsion. The sump broke down at 101 seconds with a remaining propellant load of 13.8 kg (30.5 lbm), or an expulsion efficiency of 96.4%.

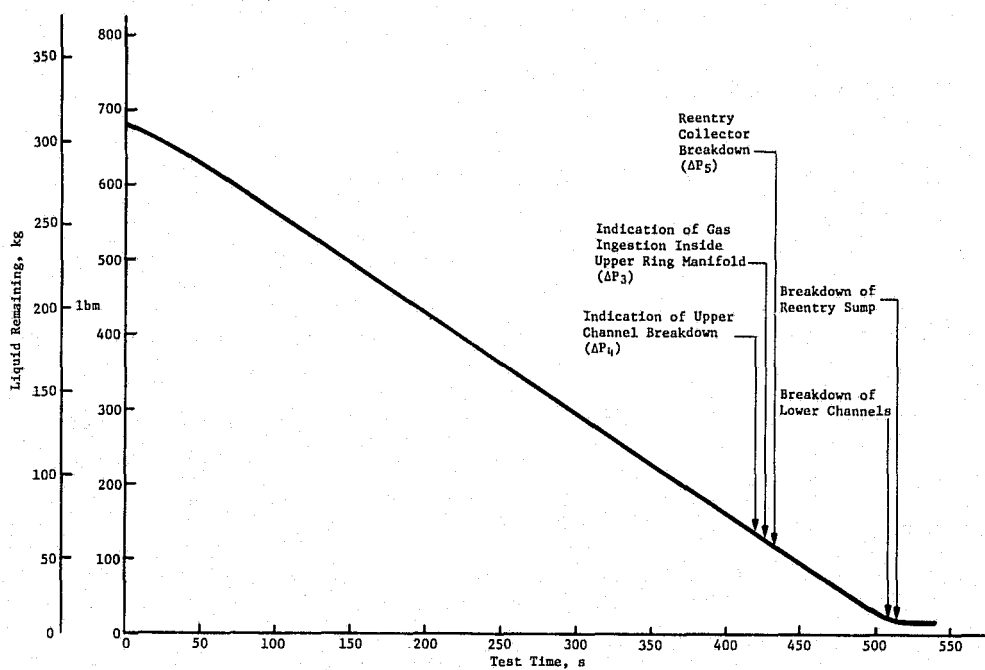


Figure VI-42 Mass History for IPA, Reentry Expulsion Test

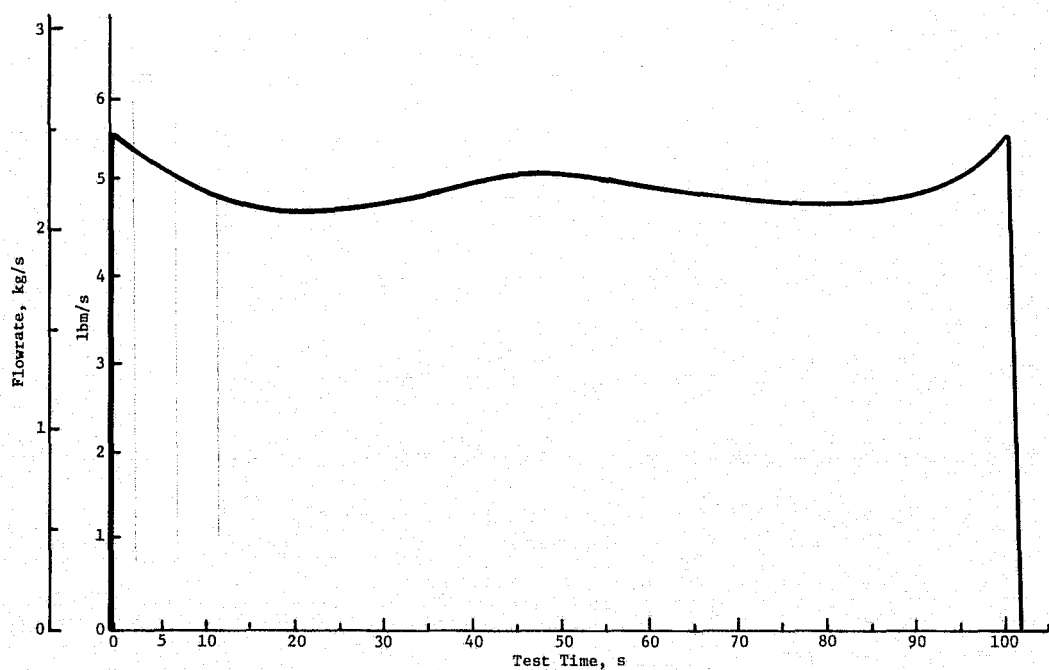


Figure VI-43 Mass Flow History for MMH Reentry Expulsion Test

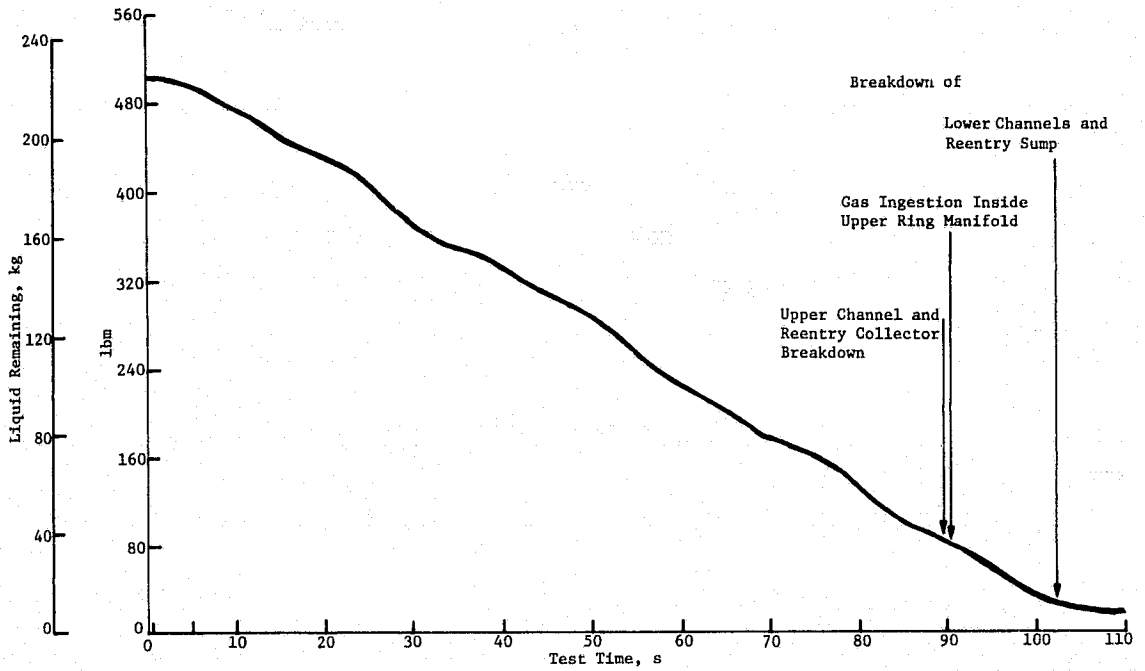


Figure VI-44 Mass History for MMH Reentry Expulsion Test

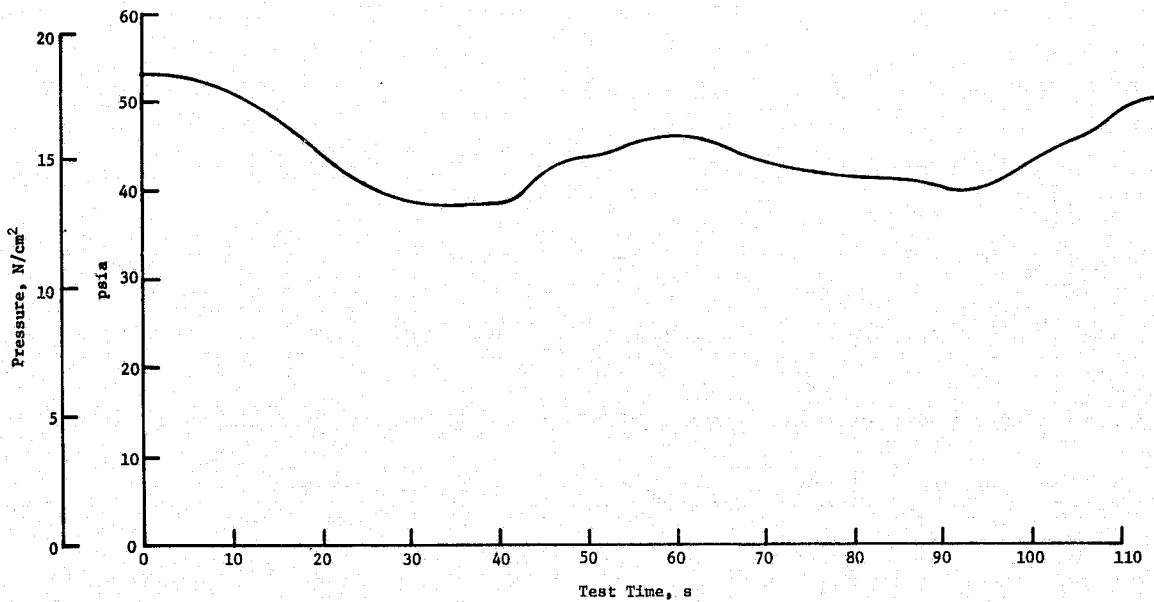


Figure VI-45 Pressure History for MMH Reentry Expulsion Test

The expulsion efficiency of the MMH reentry test was clearly adversely affected by the 1-g environment of the test, compared to the 2.2 g of the actual reentry. The hydrostatically stable height of MMH with the 325 x 2300 screens used in the upper channels and manifold network is 104 cm (41 in.), exceeding by 7.5 cm (3 in.) the diameter of the tank. Of the three fluids tested in the reentry attitude, the MMH is the only one having a stable height greater than the tank diameter. Inspection of the differential pressure transducer traces during the test showed that the MMH test traces differed significantly from those of the alcohol or  $N_2O_4$ . In the alcohol and  $N_2O_4$  tests, the upper channels broke down soon enough before the end of the test leaving sufficient time for the liquid they contained to be slowly drained and transferred to the lower compartment. Because the channels were hydrostatically stable for much longer in the MMH tests, this liquid was not able to drain out and be transferred to the lower compartment before the lower compartment was depleted. This would not have been the case in the normal 2.2-g reentry environment and the 98% expulsion efficiency would have been achieved.

In conclusion, the capability of the system to perform the reentry maneuver was demonstrated for all test liquids despite the presence of substantial quantities of gas in the lower compartment for two of the tests, and the fact that the system had actually broken down immediately before one of the tests. The initial condition of having the lower channel systems broken down was more severe than originally planned, and demonstrates the broad range of initial conditions under which reentry can still be accomplished.

#### 4. Recommended Changes to the Full-Scale Design

Based upon the limited number of tests conducted in the test program, certain design changes in the full-scale acquisition system were felt necessary. A discussion of these design changes is presented in this section. Further testing at NASA/JSC will be required to determine whether or not these changes are truly needed for a flight system.

##### *a. Fill and Drain Tests*

The results of the fill and drain tests clearly indicated that a vent tube system is required for a flight system to prevent gas entrapment during tank filling. These results also showed that at least one vent tube must be located in each of the many screen compartments of the full-scale device. The only exception is the upper compartment channels which do not require gas venting because of the low amount of gas trapped in the upper channels during filling. Therefore, no design changes are recommended with regard to tank filling of the device, except for the elimination of the vent tube located in the upper channels.

With regard to ability of the full-scale device to drain in both the vertical and horizontal attitudes, the test results clearly showed that the acquisition system could successfully accomplish these drains and no design changes are recommended.

#### *b. Checkout Tests*

Overall, the IPA and  $N_2O_4$  bubble point tests were fairly successful. The direct pressurization bubble point technique was shown to be a valid means of checking the retention capability of the screens, as demonstrated by the successful bubble points obtained in the lower compartment. If the screens could not be maintained wetted, difficulties were encountered during the testing. Therefore, it is recommended that a spray system that could wet the screen with propellant as required be incorporated into the device. This system could be incorporated either into the inside of the various screen compartments or be located in the bulk regions. Such a system (bulk region system) was designed under a previous technology study (Ref VI-4) for an OMS screen acquisition system. In addition, an internal spray bar system (bars located inside of screen channels) was designed and demonstrated successfully in a subscale RCS cylindrical tank model (Ref V-8).

#### *c. Outflow Tests*

From the limited number of outflow tests conducted, the overall performance capability of the full-scale acquisition system was verified. However, some problems were encountered during the RTLS and -lg expulsions. As previously discussed, the full-scale system did not perform as predicted during RTLS. Gas was ingested into the lower compartment near the end of the RTLS outflow. However, the device was able to satisfy the RTLS requirement of gas-free expulsion down to 65% remaining in the tank. More important, the device demonstrated that it could successfully go into reentry even though gas had been ingested into the lower compartment. On the basis of these test results, therefore, it is believed that the full-scale design will satisfy the RTLS requirements for an actual flight case. Based on this, no design changes are recommended for the RTLS. However, further testing in this area is required.

For the -lg outflow test (+Z orbital maneuver), the full-scale device did not perform as predicted. Breakdown of the reentry collector occurred much too soon during outflow, forcing liquid to be expelled from the lower compartment prematurely. The cause of the premature collector breakdown was postulated to have resulted from a gas pocket existing below the barrier before expulsion. Since the 5.1-cm (2-in.) diameter barrier penetration from the transfer tube of the collector is unstable under lg, the liquid in the collector would have drained into the lower compartment if a gas pocket existed below the barrier. The evacuated collector would then have dried out, causing its premature breakdown.

The -lg expulsion is not a case that the full-scale device will ever encounter during on-orbit operations. However, upon examination of the 5.1-cm (2-in.) diameter transfer tube penetration on the barrier, it was found that this hole would be unstable during the worst-case, on-orbit operations. Therefore, a similar situation to the one encountered during the -lg expulsion could develop during one of the on-orbit maneuvers.

To correct this situation, the following design change is recommended for a flight system. Across the barrier penetration from the collector transfer tube, a piece of 100 x 100 mesh screen should be positioned. This screen mesh has an insignificant pressure drop due to flow, so that its inclusion in the design will not affect the performance of the device during reentry. This mesh is, however, fine enough to be stable under the worst-case, on-orbit g levels.

## VII. CONCLUSIONS AND RECOMMENDATIONS

---

### A. CONCLUSIONS

Through a combination of analysis, subscale testing, and computer program predictions, a design of the preferred surface tension propellant acquisition/expulsion system was developed for the Shuttle orbiter RCS tanks. A full-scale tank system was fabricated per this design and ground verification testing was conducted. In general, it was found that the fine-mesh screen, compartmented tank system provides the performance, flexibility, reusability, and other numerous characteristics required by the omnidirectional thrusting, pulsed-flow RCS system. The acquisition system is capable of performing both the high-g and low-g mission operations; however, 98% expulsion for on-orbit conditions has not been proven with the full-scale system. Additional analysis and testing are required to translate the results of this program into a fully-developed flight system. The program results provide an excellent technology base for this very purpose. Specific conclusions drawn from this program follow.

1. A tank divided into a larger forward compartment and a smaller aft compartment by a solid barrier is preferred. Pressurant enters the forward compartment and propellant feeds from this compartment through a total communication-type channel network into the bulk region of the aft compartment. From there, the propellant flows into and through another channel network to the tank outlet located in the aft compartment. The design accommodates two-phase flow from the forward compartment while assuring only liquid feed to the outlet. This study has resulted in the solid barrier, tilted toward the +Z axis, with penetrations confined to the +Z side of the barrier, allowing the outlet to be positioned in the aft compartment in the reentry puddle under the barrier.

2. The physical property data, presented in Chapter IV, are adequate for designing surface tension acquisition systems for MMH,  $N_2O_4$ , and  $N_2H_4$ .

3. No contact angle problems are encountered with the RCS propellants, MMH and  $N_2O_4$ . These liquids readily wet titanium, aluminum, and stainless steel materials cleaned according to standard aerospace industry procedures. Just the opposite was encountered with  $N_2H_4$ . Finite contact angles were repeatedly experienced; these degrade the theoretical capillary retention capability of screen materials with  $N_2H_4$ . Standard cleaning

**PRECEDING PAGE BLANK NOT FILLED**



procedures either did not remove or were the source of a contaminant/film to which the problem was attributed. Two stringent cleaning approaches for minimizing  $N_2H_4$  contact angle were identified.

4. Dissolved pressurant and other minor impurities have negligible impact on propellant surface tension/screen retention capability, and little change occurs with pressure level. Surface tension/retention capability decreases with increasing temperature according to previously known and well established relationships, reaching zero at the critical point of the fluid.

5. System performance agrees well with predictions. The computer program models the system well and can be used with confidence.

6. The performance is scalable based on known dimensionless relationships. Model testing can be reliably scaled to full-size system performance.

7. In subscale tests, the system demonstrated good high-g and low-g slosh damping. Low-g liquid reorientation was accomplished with liquid always remaining in communication (contact) with the channels in both compartments.

8. Pulsed-flow had little impact on system performance over the flowrate range of interest.

9. The need for bubble filters to prevent premature gas pull-through during reentry was demonstrated. This necessitates a separate reentry collector, however, to feed from the forward to the aft compartment.

10. Low-g, on-orbit depletion of the forward compartment was evaluated analytically only; no KC-135 testing was conducted. Depletion of the forward compartment entails a feed of two-phase fluid at some average quality after breakdown of the channels (between gas ingestion and final depletion). Experimental verification of this facet of the performance is required.

11. Fabrication of the full-scale device was demonstrated. The combination of a welded tank/barrier assembly together with a mechanical seal between the penetrations and the barrier was shown feasible. This approach allows both the tank and the barrier to be constructed of titanium with the screens, channels, and barrier penetrations made of stainless steel. The simplicity and reliability of the Martin Marietta technique for joining screen to plate was shown.

12. Use of the bubble point technique for acceptance testing of as-received screen, parts, subassemblies, and the total assembled acquisition system was demonstrated during the fabrication process, but before tank closure.

13. Particulate count from effluent samples taken during assembled tank flush operations showed that the necessary cleanliness level can be provided using reasonable care during fabrication.

14. High-point bleed lines are needed for tank filling to eliminate trapped gas from the various capillary components. With this approach, satisfactory fill was demonstrated in the vertical orientation.

15. Tank draining was successfully accomplished in both the vertical (98% expulsion) and horizontal (99% expulsion) orientations with IPA.

16. Inspection of the surface tension tankage was accomplished by tank draining and by bubble point. These tests were performed with IPA and with  $N_2O_4$ . Problems were encountered in getting to the proper wetted screen starting condition for bubble point measurement without breaking the system down. This precluded measurement of the bubble point of the upper compartment components. The approach was successful for the outlet compartment components, however. The problem was aggravated with  $N_2O_4$  because of its high vapor pressure. Spray bars to allow spray wetting are probably required to provide and maintain wetted screens for bubble point inspection tests.

17. The high-point bleed lines serve a double purpose. They are also useful for measuring  $\Delta P$  across the various screen components during bubble point testing.

18. Performance appears satisfactory for the RTLS abort operation, based on limited testing. Some gas ingestion into the aft compartment during RTLS is probably acceptable.

19. Demonstration of 98% expulsion efficiency for reentry was performed in the 1-g environment. The capability of reestablishing single phase outflow to greater than 98% expulsion efficiency, after previously breaking down in a prior orientation, was demonstrated with  $N_2O_4$ .

20. Further evaluation of the combined effects of vibration and acceleration on the full-scale device performance is required.

## B. RECOMMENDATIONS

The results of this program should be used to the maximum extent possible in the RCS flight tankage program.

It is recommended that additional ground testing be conducted with the full-scale tankage system delivered to NASA-JSC. In particular, further evaluation of system inspection or checkout should be conducted and testing should be performed under the mission vibration and acceleration environments. Simulations should include RTLS, OMS roll control, and reentry operations.

Subscale KC-135 testing should also be conducted to evaluate low-g depletion characteristics of the system.

Further assessment of cleaning techniques and their impact on the contact angle between aerospace construction materials and  $N_2H_4$  should be performed.

A test program should be conducted to evaluate the mechanism, magnitude and extent of screen dryout with  $N_2O_4$  and the potential impact on RCS tankage performance.

## VIII. REFERENCES

---

- I-1. D. A. Fester et al: *Acquisition/Expulsion System for Earth Orbital Propulsion System Study, Final Report, Volume V - Earth Storable Design*. MCR-73-97 (Vol V). Martin Marietta Corporation, Denver, Colorado, October 1973.
- I-2. R. N. Eberhardt: *Capillary Propellant Storage and Feed System Analysis*. D-74-48766-001. Martin Marietta Corporation, Denver, Colorado, December 1974.
- I-3. J. D. Carpenter: *Surface Tension Tankage Computer Program Manual*. MCR-74-478. Martin Marietta Corporation, Denver, Colorado, March 1975.
- I-4. P. E. Uney: *Hydrazine Interfacial Phenomena*. D-74-48714-001. Martin Marietta Corporation, Denver, Colorado, July 1974.
- I-5. P. E. Uney: *SS/RCS Surface Tension Propellant Acquisition/Expulsion Tankage Technology Program, Interim Report - Task III Supporting Tests*. MCR-74-278. Martin Marietta Corporation, Denver, Colorado, August 1974.
- I-6. D. A. Fester: *SS/RCS Surface Tension Propellant Acquisition/Expulsion Tankage Technology Program, Minutes of the First Program Review*. MCR-74-149. Martin Marietta Corporation, Denver, Colorado, April 1974.
- I-7. D. A. Fester et al: *SS/RCS Surface Tension Propellant Acquisition/Expulsion Tankage Technology Program, Verification Test Plan*. MCR-74-162. Martin Marietta Corporation, Denver, Colorado, 20 May 1974.
- I-8. *Tank, Propellant-Reaction Control Subsystem*. Specification Number MC282-0061, Revision B. Rockwell International, Downey, California, 10 July 1974.
- RCS Propellant Tank - Impending Procurement Specification Changes*. Subcontractor Engineering Memorandum MMC-005. Rockwell International, Downey, California, 9 September 1974.
- I-9. D. A. Fester: *SS/RCS Surface Tension Propellant Acquisition/Expulsion Tankage Technology Program, Minutes of the Program Review and Full-Scale Tankage Design Review*. MCR-74-463. Martin Marietta Corporation, Denver, Colorado, November 1974.

I-10. P. E. Uney: *SS/RCS Surface Tension Propellant Acquisition/Expulsion Tankage Technology Program, Hardware Design Document*. MCR-75-15. Martin Marietta Corporation, Denver, Colorado, January 1975.

I-11. K. C. Lunden and C. E. Lynch: *SS/RCS Surface Tension Propellant Acquisition/Expulsion Tankage Technology Program, Full-Scale Tankage Test Plan*. MCR-74-477. Martin Marietta Corporation, Denver, Colorado, December 1974.

I-12. J. R. Butz: *SS/RCS Surface Tension Propellant Acquisition/Expulsion Tankage Technology Program, Full-Scale Tankage Maintenance and Operations Manual*. MCR-75-174. Martin Marietta Corporation, Denver, Colorado, April 1975.

II-1. Letter from D. L. Connelly, NASA Lyndon B. Johnson Space Center, Houston, Texas, to D. A. Fester, Martin Marietta Corporation, Denver, Colorado, dated 7 December 1973, Subject: Design Definition Data for Contract NAS9-13709, *SS/RCS Surface Tension Propellant Acquisition/Expulsion Tankage Technology Program*.

II-2. *Tank, Propellant-Reaction Control Subsystem. Specification Number MC282-0061, Revision B*. Rockwell International, Downey, California, 10 July 1974.

II-3. *RCS Propellant Tank - Impending Procurement Specification Changes*. Subcontractor Engineering Memorandum MMC-005. Rockwell International, Downey, California, 9 September 1974.

III-1. J. D. Carpenter: *Surface Tension Tankage Computer Program Manual*. MCR-74-478. Martin Marietta Corporation, Denver, Colorado, March 1975.

III-2. *Viking Orbiter 1975 Propellant Management Device - Final Report*. Report No. SE010-47-01. Martin Marietta Corporation, Denver, Colorado, May 1973.

III-3. G. R. Page et al: *Acquisition/Expulsion System for Earth Orbital Propulsion System Study, Final Report, Volume III - Cryogenic Tests*. MCR-73-97 (Vol III). Martin Marietta Corporation, Denver, Colorado, October 1973.

III-4. H. L. Paynter et al: *Capillary Screen System for Liquid/Gas Separation, Final Report, Volume I - Analysis and Design*. MCR-73-181. Martin Marietta Corporation, Denver, Colorado, August 1973 (Restricted).

III-5. H. L. Paynter, et al: *Investigation of Space Storable Propellant Acquisition Devices, Final Report, Volume I - Evaluation*. MCR-70-171, Vol I. Martin Marietta Corporation, Denver, Colorado, October 1970.

- III-6. D. A. Fester, et al: *Space Storable Propellant Acquisition System*. NASA CR 114493. Martin Marietta Corporation, Denver, Colorado, October 1972.
- IV-1. P. E. Uney: *SS/RCS Surface Tension Propellant Acquisition/Expulsion Tankage Technology Program, Interim Report - Task III Supporting Tests*. MCR-74-278. Martin Marietta Corporation, Denver, Colorado, August 1974.
- IV-2. *Engineering Property Data on Rocket Propellants (U)*. AFRPL-TR-68-100. Rocketdyne Division, North American Rockwell Corporation, Canoga Park, California, May 1968 (Confidential).
- IV-3. *Liquid Propellant Manual (U)*. CPIA/M4. Chemical Propulsion Information Agency, Johns Hopkins University, Silver Spring, Maryland, December 1966 (Confidential).
- IV-4. L. R. Krumland: *Propellant Properties Manual for Hydrazine, Hydrazine Nitrate, and Water Mixtures*. 66-0750. The Garrett Corporation, Los Angeles, California, March 1967.
- IV-5. *Performance and Properties of Liquid Propellants, Revision A*. 8610-6S Aerojet General Corporation, Sacramento, California June 1961.
- IV-6. *Handbook of Astronautical Engineering*. The McGraw-Hill Book Company, New York, New York, 1961.
- IV-7. *PBPS Propellant Characteristics Report*. C5-1988/319. Autonetics Division, North American Aviation, November 1965.
- IV-8. R. R. Liberto: *Titan II Storable Propellant Handbook*. Report 8182-93004. Bell Aerosystems Company, Buffalo, New York, March 1962.
- IV-9. W. R. Fish, et al: *Storable Liquid Propellants for Titan II*. LPR198. Aerojet General Corporation, Sacramento, California, September 1960.
- IV-10. R. H. Seale, et al: *Properties and Performance of Nitrogen Tetroxide and Unsymmetrical Dimethylhydrazine*. D5-14077. The Boeing Company, Michoud, Louisiana, February 1969.
- IV-11. N. A. Gokcen, et al: *Effect of Water on the Density of  $N_2O_4$* . TDR-669(6116-30)-1. Aerospace Corporation, El Segundo, California, December 1965.

IV-12. L. A. Schluter and I. D. Smith: "Density and Viscosity Measurement of Live and Referee Propellants (U)," *Analytical Chemistry Working Group 33rd Meeting Bulletin (U)*. CPIA Publication No. 152. Martin Company, Denver, Colorado, August 23-25, 1966 (Confidential).

IV-13. D. A. Fester et al: *Acquisition/Expulsion System for Earth Orbital Propulsion System Study, Final Report, Volume V - Earth Storable Design*. MCR-73-97 (Vol V). Martin Marietta Corporation, Denver, Colorado, October 1973.

IV-14. R. Razouk: "Surface Tension of Propellants," *JPL Quarterly Technical Review*. Vol. 2, No. 1, April 1972, pp 123-134.

IV-15. P. E. Uney: *Hydrazine Interfacial Phenomena*. D-74-48714-001. Martin Marietta Corporation, Denver, Colorado, July 1974.

V-1. G. R. Page, et al: *Acquisition/Expulsion System for Earth Orbital Propulsion System Study, Final Report, Volume II - Cryogenic Design*. MCR-73-97 (Vol II). Martin Marietta Corporation, Denver, Colorado, October 1973.

V-2. G. R. Page, et al: *Acquisition/Expulsion System for Earth Orbital Propulsion System Study, Final Report, Volume III - Cryogenic Tests*. MCR-73-97 (Vol III). Martin Marietta Corporation, Denver, Colorado, October 1973.

V-3. R. L. Berry and J. R. Tegart: *Experimental Study of Transient Liquid Motion in Orbiting Spacecraft*. MCR-75-4. Martin Marietta Corporation, Denver, Colorado, January 1975.

V-4. T. A. Coney: *Surface Tension, Viscosity, and Density Measurements of Two Fluorocarbon Solvents, FC-43 and FC-78*. NASA TM X-1862. Lewis Research Center, Cleveland, Ohio, August 1969.

V-5. J. A. Salzman and W. J. Masica: *Experimental Investigation of Liquid Propellant Reorientation*. NASA TND-3789. Lewis Research Center, Cleveland, Ohio, January 1967.

V-6. T. E. Bowman, B. K. Larkin, and J. L. McGrew: *Criteria for Cryogenic Liquid Experiments in Orbit*. MCR-65-25. Martin Marietta Corporation, Denver, Colorado, October 1965.

V-7. T. E. Bowman: *Response of the Free Surface of a Cylindrically Contained Liquid to Off-Axis Accelerations*. Proceedings of the 1966 Heat Transfer and Fluid Mechanics Institute, Stanford University Press, 1966.

V-8. Eberhardt, R. N.: *Capillary Propellant Storage and Feed System Analysis*. D-74-48766-001. Martin Marietta Corporation, Denver, Colorado, December 1974.

- V-9. R. P. Warren: *Acquisition System Environmental Effects Study*. MCR-75-21. Martin Marietta Corporation, Denver, Colorado, May 1975.
- V-10. S. J. Kline and F. A. McClintock: "Describing Uncertainties in Single-Sample Experiments." *Mechanical Engineering*, January 1953.
- V-11. H. N. Abramson, Editor: *The Dynamic Behavior of Liquids in Moving Containers*. NASA SP-106. National Aeronautics and Space Administration, Washington, D. C., 1966.
- V-12 J. R. Tegart: *Slosh Damping of Screen Surfaces*. R-74-48602-002. Martin Marietta Corporation, Denver, Colorado, December 1974.
- VI-1. P. E. Uney: *SS/RCS Surface Tension Propellant Acquisition/Expulsion Tankage Technology Program, Hardware Design Document*. MCR-75-15. Martin Marietta Corporation, Denver, Colorado, January 1975.
- VI-2. R. P. Warren: *Acquisition System Environmental Effects Study*. MCR-75-21. Martin Marietta Corporation, Denver, Colorado, May 1975.
- VI-3. *Liquid Propellant Manual (U)*. CPIA/M4. Chemical Propulsion Information Agency, Johns Hopkins University, Silver Spring, Maryland, December 1966 (Confidential).
- VI-4. D. A. Fester, et al: *Acquisition/Expulsion System for Earth Orbital Propulsion System Study, Final Report, Volume V - Earth Storable Design*. MCR-73-97 (Vol V). Martin Marietta Corporation, Denver, Colorado, October 1973.
- VI-5. G. R. Page, et al: *Acquisition/Expulsion System for Earth Orbital Propulsion System Study, Final Report, Volume II - Cryogenic Design*. MCR-73-97 (Vol II). Martin Marietta Corporation, Denver, Colorado, October 1973.
- VI-6. G. R. Page, et al: *Acquisition/Expulsion System for Earth Orbital Propulsion System Study, Final Report, Volume III - Cryogenic Tests*. MCR-73-97 (Vol III). Martin Marietta Corporation, Denver, Colorado, October 1973.



# APPENDIX--TANK PRESSURE AND FLUID EXPOSURE LOG

Date	Test	Fluid	Maximum Tank Pressure	
			N/cm <sup>2</sup>	(psig)
2/19/75	Proof Pressure	Demineralized Water	261	(378)
2/26/75	Loading for Bubble Point	Isopropyl Alcohol (IPA)	-	-
2/27/75	Gravity Drain for Bubble Point	IPA	-	-
2/28/75	Load and Drain (twice) for Bubble Point	IPA	-	-
3/6/75	Leak Check	Methanol	-	-
3/7/75	Load and Drain for Bubble Point	IPA	-	-
3/8/75	Load and Drain for Bubble Point	IPA	-	-
3/11/75	Load for Vertical Drain	IPA	-	-
3/12/75	Vertical Drain	IPA	21	(30)
	Horizontal Drain	IPA	21	(30)
3/13/75	Reentry Outflow	IPA	27	(39)
3/14/75	RTLS Outflow	MMH	148	(215)
	Reentry Outflow	MMH	37	(54)
3/17/75 thru 3/19/75	System Flushes (3)	Demineralized Water	-	-
3/21/75	System Passivation	N <sub>2</sub> O <sub>4</sub> Vapor	3	(5)
3/24/75	Reentry Outflow	N <sub>2</sub> O <sub>4</sub>	85	(123)
3/25/75	Minus one G expulsion	N <sub>2</sub> O <sub>4</sub>	83	(121)
	Reentry Outflow	N <sub>2</sub> O <sub>4</sub>	57	(82)
3/26/75	Check-Out Drain	N <sub>2</sub> O <sub>4</sub>	66	(95)
3/31/75	Bubble Point	N <sub>2</sub> O <sub>4</sub>	66	(95)
4/9/75	Bubble Point (Open Tank)	IPA	-	-